Synthesis and Reactivity of Pt^{II} Complexes with Secondary Sphere N-H Moieties

Braden A. Zahora

A dissertation submitted in partial
fulfillment of the requirements for the degree of

Doctor of Philosophy

University of Washington

2019

Reading Committee:
Karen I. Goldberg, Chair
D. Michael Heinekey
Forrest E. Michael

Program Authorized to Offer Degree:

Department of Chemistry

University of Washington

Abstract

Synthesis and Reactivity of Pt^{II} Complexes with Secondary Sphere N-H Moieties

Braden A. Zahora

Chairperson of the Supervisory Committee:
Professor Karen I. Goldberg
Department of Chemistry

Direct transformations of abundant hydrocarbons into higher valued products would circumvent energy intensive processes, reforming the chemical industry. Late transition metals, particularly platinum, are known to selectively convert alkanes into functionalized products. However, a practical method with an economically viable oxidant has yet to be discovered. New methods for alkane activation may yield further advances towards this goal. This dissertation focuses on how platinum methyl complexes with ligand-based protons can form methane, the microscopic reverse of methane activation. Chapter 1 provides an introduction on the need to develop new methods to functionalize hydrocarbons. Furthermore, a survey of the literature with respect to how late metal complexes can undergo productive reactivity with substrates which are deemed necessary for practical alkane partial oxidation is presented.

Chapter 2 focuses on the synthesis and reactivity of 5-(6-methyl-2-pyridyl)-3-*tert*-butylpyrazolate (NN^{Me}) and 2-(5-*tert*-butylpyrazol-3-yl)-6 (diethylaminomethyl)pyridine (NNN^{Et}) ligated Pt^{II} complexes. Once formed, conditions necessary for methane formation were found and

it was determined that the ligand-based N-H was not involved in methane formation. Chapter 3 explores synthesis and reactivity of 5-*tert*-butyl-1,3-bis(pyrazol-3-yl)pyridine (NNN) and 5-*tert*-butyl-1,3-bis(pyrazol-3-yl)benzene (NCN) ligated Pt^{II}-alkyl complexes with electrophilic reagents. It was found that tridentate ligated pyrazolate Pt^{II}-R systems can undergo protonation at the ligand if there is a weak pyridine *trans* donor (vs strong phenyl *trans* donor) to the Pt^{II}-R moiety. However, reactivity with methyl iodide occurred at the metal first, with further ligand methylation spectroscopically observed for the NNN ligated Pt-CH_3 complex. Chapter 4 discusses the synthesis and characterization of bis(phosphino)amine ligated Pt^{II} complexes, which contained a ligand-based N-H. Taking advantage of unfavorable steric congestion of bulky Ph groups on the ligand, methane formation was observed from thermolysis reactions of a bis(phosphino)amine ligated $Pt(CH_3)_2$. Although additional characterization of the resulting metal-containing product is required, it appears that methane was formed through cooperation of the ligand-based N-H moiety and the Pt-CH_3 ligand.

Table of Contents

List of Figures

List of Schemes

List of Tables

Glossary

Å	angstrom
Ac	acetate
Ar	aryl
BDE	bond dissociation energy
bdmimp	3,5-bis(2,6-dimethylphenyliminoacetyl)-4-methylpyrazole
bpym	bipyrimidine
CENTC	center for enabling new technologies through catalysis
CMD	cyclometallation deprotonation
COE	cyclooctene
DCM	dichloromethane
DFT	density functional theory
DMEP	dimethyl((pyridinylmethylene)amino)ethylamine
DMPP	dimethyl((pyridinylmethylene)amino)propylamine
DMSO	dimethylsulfoxide
dppbz	Bis(diphenylphosphino)benzene
dppe	1,2 bis(diphenylphosphino)ethane
ESI-MS	electrospray ionization mass spectroscopy
Et	ethyl
fac	facial
ft^3	cubic feet
$^{H}NCN^{H}$	5-*tert*-butyl-1,3-bis(pyrazol-3-yl)benzene
$^{H}NNN^{H}$	5-*tert*-butyl-1,3-bis(pyrazol-3-yl)pyridine
HOMO	highest occupied molecular orbital
Hz	hertz
Inc	incorporated
IS	internal standard
kcal/mol	kilocalorie per mole
KIE	kinetic isotope effect

LUMO	lowest unoccupied molecular orbital
m^3	cubic meters
Me	methyl
MeOH	methanol
MLC	metal ligand cooperation
NMR	nuclear magnetic resonance
NN^H	5-(2-pyridyl)-3-*tert*-butylpyrazolate
NN^{Me}	5-(6-methyl-2-pyridyl)-3-*tert*-butylpyrazolate
NNN^{Et}	2-(5-*tert*-butylpyrazol-3-yl)-6 (diethylaminomethyl)pyridine
Pd	palladium
Ph	phenyl
PP	pyridinophane
ppm	parts per million
Pt	platinum
R-H	hydrocarbon
SQD	signal quality detector
TACN	1,4,7-triazonane
^{t}Bu	*tert*-butyl
THF	tetrahydrofuran
TON	turnover number
Tp	hydridotrispyrazolylborate
TUV	tunable ultra-violet
UPLC	ultra performance liquid chromatography

Compound Numbering Scheme

Pt(*NN)$_2$ (**B1**)

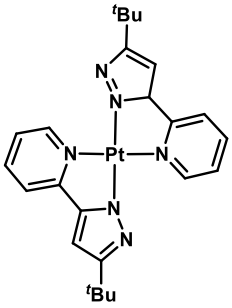

Pt(*NN)(S(CH$_3$)$_2$)(CH$_3$) **(B2a or B2b**)

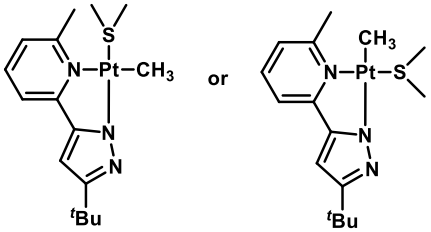

B2a **B2b**

Pt(*NN)^{Me}(PPh$_3$)(CH$_3$) (**B3**)

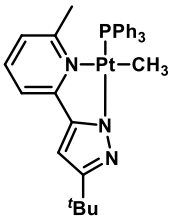

Pt(*NNN)^{Et}CH$_3$ **(B4a)**

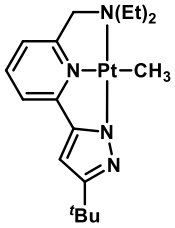

Pt(*NNN)^{Et}C$_6$H$_5$ **(B4b)**

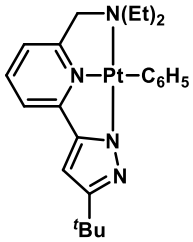

Pt(*NNN)^{Et}Cl **(B5)**

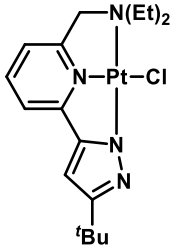

Synthesis of Pt(^{H}NNN)^{Et}Cl **(B5a)**

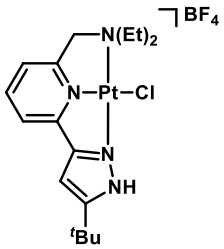

Pt(*NNN)^{Et}Cl **(B5b)**

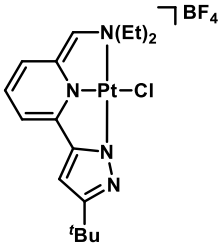

[Pt(^{H}NN)^{Me}(S(CH$_3$)$_2$)(CH$_3$)][BF$_4$]

(B6a/B6b)

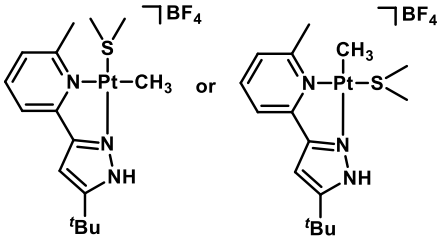

B6a **B6b**

Synthesis of [Pt(^{H}NNN)^{Et}CH$_3$][BF$_4$] **(B7)**.

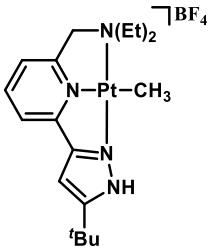

Pt(κ^1-*NNN)^{Et}(P(C$_5$H$_6$)$_3$)$_2$CH$_3$ **(B8a)**

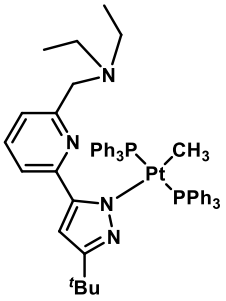

Pt(κ^1-*NNN)^{Et}(P(CH$_3$)$_3$)$_2$CH$_3$ **(B8b)**

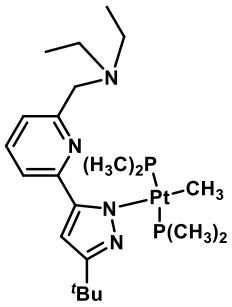

[Pt(^{H}NNN^{H})Cl][Cl] **(C1)**

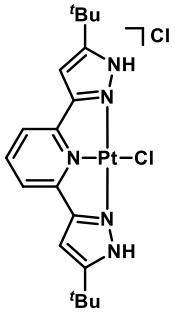

[Pt(^{H}NNN^{H})Cl][BF$_4$] **(C2)**

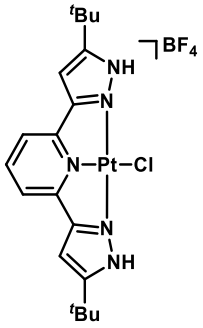

[Pt(^{H}NNN^{H})NCCH$_3$][(BF$_4$)$_2$] **(C3)**

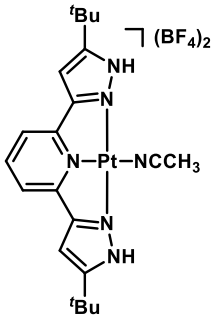

Pt(^{H}NCN^{H})^{H}Cl **(C4)**

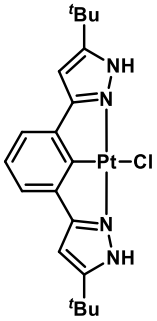

[Li(THF)$_2$]$_2$[Pt(*NCN*)^{tBu}Cl] (**C4A)**

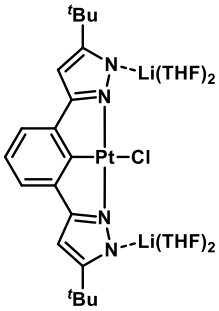

Pt(^{H}NCN^{H})^{tBu}Cl **(C5)**

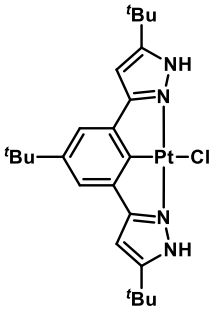

[Li(THF)$_2$]$_2$[Pt(*NCN*)^{tBu}Cl] **(C5A)**

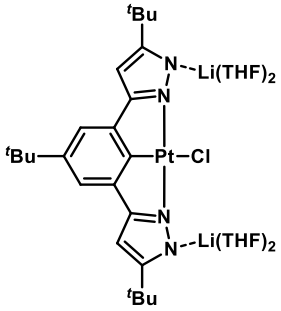

[Li$_2$Cl(THF)$_4$][Pt(*NNN*)CH$_3$] **(C6)**

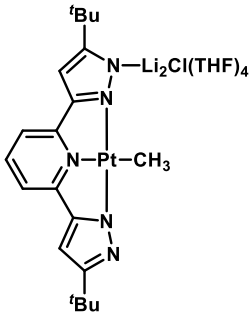

[Li(THF)]$_2$[Pt(*NNN)CH$_2$CN]$_2$ **(C7)**

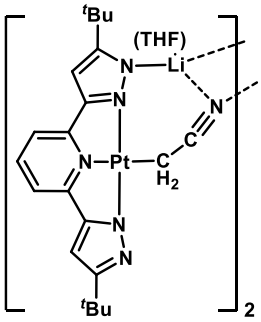

[PPN][Pt(*NNN*)CH_3] **(C8)**

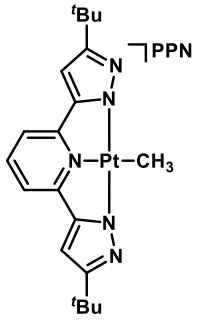

[Pt(^{H}NNN^{H})CH_3][Cl] **(C9)**

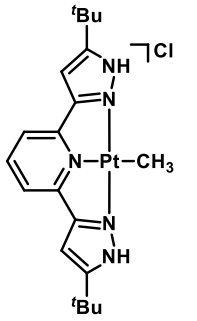

[Pt(^{H}NNN^{H})CH_3][BAr_F^{24}] **(C10)**

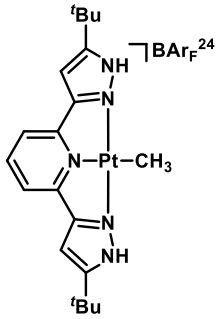

[$Li(THF)_2$]$_2$[Pt(*NCN*)^{H}(CH_3)] **(C11)**

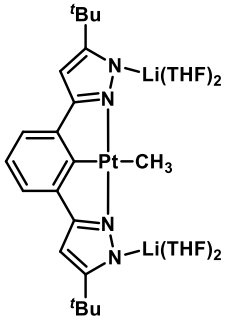

[$Li(THF)_2$]$_2$[Pt(*NCN*)^{tBu}(CH_3)] **(C12)**

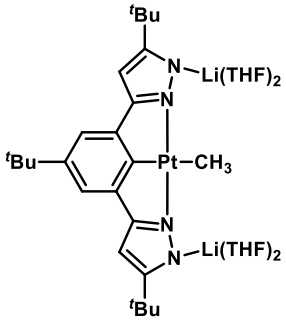

[Li]$_2$[Pt(*NCN*)^{tBu}(C_6H_5)] **(C13)**

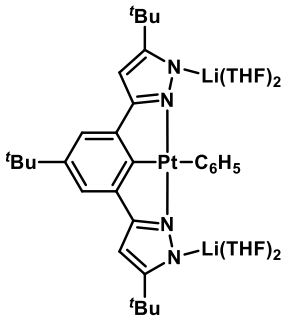

Pt(^{CH3}NNN*)$(CH_3)_2$(I) (**C15**)

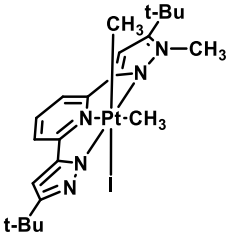

Pt(^{H}N(P$(C_6H_5)_2)_2)(CH_3)_2$ (**D1a**)

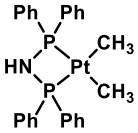

Pt(^{H}N(P(^{t}Bu$)_2)_2)(CH_3)_2$ (**D1b**)

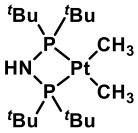

[Pt(^{H}N(P$(C_6H_5)_2)_2)_2$][BF_4]$_2$ (**D2)**

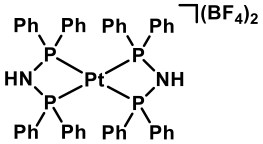

Pt(*N(P$(C_6H_5)_2)_2)_2$ (**D3**)

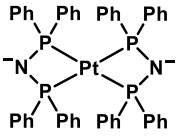

Pt(^{H}N(P(^{t}Bu$)_2)_2)(Cl)_2$ (**D4**)

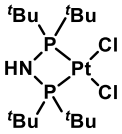

[Pt(^{H}N(P$(C_6H_5)_2)_2)(CH_3)$(pyr-d_5)][BF_4] (**D5**)

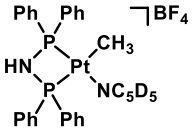

Pt$_2$(μ-*N(P$(C_6H_5)_2)_2$)(μ-CH_2)(pyr)$_2$ (**D6**)

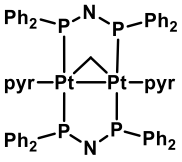

Acknowledgements

I would like to begin by thanking everyone who has helped me along my journey to complete my Ph.D. I have wanted this ever since I was a little kid and I am forever grateful for those who have contributed to helping make this possible.

To my 8th grade chemistry teacher Mr. Schreck at Queens Grant Community School, thank you for being the first teacher who established my love for chemistry. I hope to one day see you again and thank you in person for setting me on my path.

To my parents, Ingrid and Andy; my brother, Connor; and to the rest of my family I discussed my experiences with along the way, I love you all. Dad, you have inspired me ever since I was little. I have always looked up to you and have always wanted to be a Ph.D., just like you. Glad I could finally join the club! Mom, thank you for all your words of wisdom. When I was down and struggling, talking with you lifted me up and you gave me the strength to continue. You always set my mind right and encouraged me to see the brighter side. Connor, you have also always been there for me and you are so fun to hang around. You have become a fine man and I am so proud to call you my brother. To my grandma and nana who recently passed away. I love you both so much - you're often on my mind and I miss you both more than I can put into words. To the rest of my family: Karen and Mike, Rob and Janet, Ken, Bonnie and Mark and co., Nils and Consuelo and Jim and Karen; you all are so amazing and thank you all for providing a strong support for me to lean on.

Thank you, Karen Goldberg, for being a terrific mentor throughout my graduate career. The love and passion you show for solving complex chemistry problems first drew me to your lab and I was honored when I was given the opportunity to join. While moving the lab across the country had its challenging moments, I was happy to do it with you and the wonderful people in your lab. All in all, with your guidance, I grew into the scientist that I am today, and I am forever grateful. I learned so much from you; you are beyond an exceptional chemist and I wish you all the success in the world at UPenn.

To all my fellow scientists that I met along the way, thank you for making graduate school fun and providing an outlet from science. I met so many amazing people in both Seattle and in Philadelphia and while I can't mention everyone, you all mean so much to me. To the past and present Goldberg lab: Wilson, Cameron, Marie, Tyler, Zu, Karena, Irene, Jon, Ash, Tim, Magnus, Amy, Kelly, Hannah, Byongjoo, Sophie, Alex, Drew, Evan, Sabrine, Anant and Walter, thank you for your help not only in the lab but also your friendship – I'll never forget you all. To the now Dr. Michael Enright, you have been an amazing friend and I miss all the fun we had going on hikes, touring the city and just hanging out watching sports. I hope to see you soon and keep our friendship going for years to come. To Dr. Louise Guard and Dr. Jonathan Kuo, I cannot thank both of you enough for all that you did for me. You both are phenomenal chemists and friends and helped me succeed when I couldn't. I'll never forget you both.

And finally, to Jenn Lee, I am so lucky to have met you and am continuously falling more in love with you every day. While the long-distance relationship was tough while I was at UPenn, thank you for the love and support you showed me while I was thousands of miles away. It was tough and I missed you so much, but we made it! Now the real journey begins, and I couldn't think of a better person to share it with.

Chapter Contributions

Much of the work detailed in the following chapters would not have been possible without the valuable efforts of NMR and X-ray facility staff at the University of Washington and the University of Pennsylvania.

Chapter 2.

Sarah E. Flowers, Maike Blakely and Werner Kaminsky for the crystallographic characterization of **B4b** and **B5**

Michael Gau and Pat Carroll (Upenn) for the crystallographic characterization of **B4a**

Chapter 3

Sarah E. Flowers, Maike Blakely and Werner Kaminsky for the crystallographic characterization of **C5a**

Michael Gau and Pat Carroll (Upenn) for the crystallographic characterization of **C2**, **C3**, **C4**, (**Pt_4(*NCN*)(^{H}NCN^{H})$_3$**), **C6**, **C8**, **C9**, and **C11**

Chapter 4

Sarah E. Flowers, Maike Blakely and Werner Kaminsky for the crystallographic characterization of Pt(*N(P(^{t}Bu)$_2$)$_2$)$_2$

Michael Gau and Pat Carroll (Upenn) for the crystallographic characterization of **D3** and **D6**.

Chapter 1

Introduction

1.1 A Need to Reduce Hydrocarbon Flaring

Hydrocarbons are the main component of petroleum and natural gas. While petroleum is made up of a large array of saturated and unsaturated hydrocarbons, natural gas is primarily comprised of low molecular weight alkanes, mainly methane. These valuable resources supply over 90% of the carbon feedstocks to the chemical industry.[1] In fact, total world consumption of natural gas in 2018 was over 10 billion m^3/day and total world consumption of petroleum in 2018 was about 100 million barrels/day.[2,3] The Bakken formation in North Dakota is one of the largest contiguous deposits of oil and natural gas in the United States and contains a predicted 7.4 billion barrels and 6.7 trillion ft^3, respectively, of proven resources.[4] Respective crude oil and natural gas production for the Bakken region has increased to a record 1.5 million barrels/day and 2.2 million ft^3/day in October 2019.[5] Petroleum and natural gas are ever-present in the chemical industry economy and it is crucial to efficiently utilize these resources.

Petroleum and natural gas (or "associated gas") from oil fields such as the Bakken Formation are often extracted through a process known as hydraulic fracturing (or "fracking"). Here, a specially engineered fluid is injected down a well, which penetrates shale and forces the less dense oil and gas upwards towards the well site.[6] A lack of adequate natural gas storage and/or transportation infrastructure from the fracking well sites result in significant "flaring" or the controlled burning of associated gas to mitigate more serious environmental impacts.[7] In fact, oil extraction in March of 2019 through the Bakken region produced 560 million ft^3 of flared gases resulting in a wasted $6.7 million if extrapolated throughout the year (based on reported US price in March 2019 of $4.33/1000 ft^3).[8,9] Flaring occurs on such a large scale in North Dakota that it can even be seen from space (Figure 1.01).[10] Even though the North Dakota oil and natural gas extraction industry has spent billions of dollars on infrastructure already, gas liquification, storage

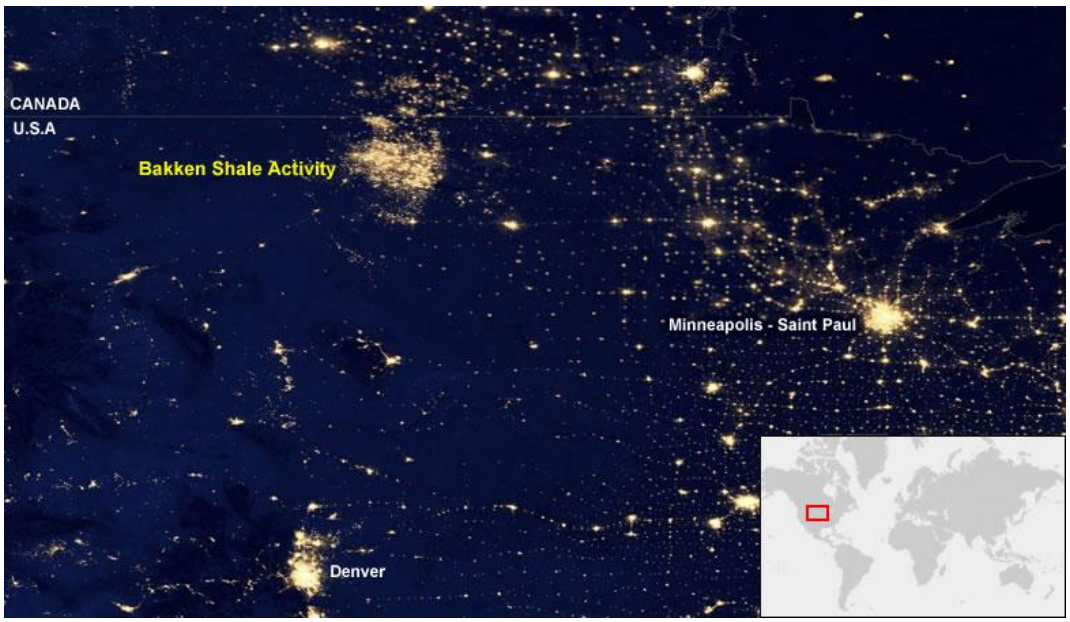

Figure 1.0 1 Image of light pollution across the central United States. Image was produced by NASA using data acquired in April and October 2012. Image downloaded from https://geology.com/articles/oil-fields-from-space/ in November 2019.

and transportation is expensive; there is little economic incentive to completely prevent flaring and keep up with the increasing gas production in the state.[7,11]

Current industrial methods of hydrocarbon functionalization require large amounts of energy. There is no industrially viable method for directly and selectively oxidizing methane, which could help provide an economic incentive. Currently, hydrocarbons are initially converted to syn-gas, a mixture of H_2 and CO. This process requires high temperatures (ca. > 800 °C) and often results in over-functionalization to CO_2.[12,13] A separate reaction (ca. > 170 °C) then transforms syn-gas to functionalized products, such as methanol.[14] In addition, hydrocarbon functionalization plants (or "gas-to-liquid" plants) require large initial costs. In 2018, ONEOK, Inc. company began the production of the Demicks Lake I and II natural gas processing plants (and associated infrastructure) in the Bakken region, which are expected to cost a total of $1.7 billion and add about 1.1 billion ft^3/day plant capacity.[15] While the production of plants like these help the flaring situation, natural gas production in the North Dakota Bakken region exceeded 2.4 billion ft^3/day in July 2018, and increased by about 8.7 % from July 2018 - December 2018.[15,16] New methods need to be developed to avoid this costly, atom inefficient and energy intensive procedure.

A highly desirable process would be the direct transformation of hydrocarbons like methane into valuable commodity chemicals in a single step. This is considered to be one of the "holy grail" reactions of catalysis and numerous organic functionalized compounds have been targeted such as methanol, formaldehyde, ethylene, benzene and others.[17,18] Perhaps most intriguing in this list is methanol, as it could be formed by methane partial oxidation from O_2 in the atmosphere. Heterogeneous catalysts offer practical aspects for use in industrial chemistry, such as ease of product and catalyst separation, and additionally have demonstrated stability at high temperatures and pressures. Recently reported heterogeneous catalysts have exhibited low conversion of methane

(~15 %) and good selectivity (> 60 %) for methanol (over such products as HCOOH, CH_3COOH and CO_2), and are still not efficient enough for industrial applications.[19,20] As reaction pathways can be difficult to study in heterogeneous systems, therefore often precluding rational catalyst design, we turn to homogeneous catalysis to improve selectivity and explore other potential routes for alkane partial oxidation.

1.2 Homogeneous Partial Oxidation of Methane, an Overview

Difficulties in methane functionalization originate from the inert nature of alkanes: high C-H bond strengths (c.a. 105 kcal/mol for methane), pK_as (c.a. 50 in DMSO for methane), and large orbital energy mismatches (no low energy empty orbitals or no high energy filled orbitals) all contribute.[21] Additionally, the functionalized products formed are often more reactive than the starting hydrocarbons (i.e. methanol C-H bond strength of 96 kcal[22] and CH_3O-H pK_a of 29 in DMSO.[23] Organometallic complexes allows us to address these challenges and successful homogeneous methane partial oxidation has been observed.[13,24]

Noble metal complexes have shown a great propensity to activate strong bonds, the first step in functionalization.[25] In the late 1970s, Shilov and coworkers were the first to describe a platinum complex which could catalytically functionalize methane to methanol and chloromethane under aqueous conditions, albeit with low conversion rates (Figure 1.02).[13] Here, methane C-H activation is achieved by a $Pt^{II}Cl_2(H_2O)_2$ catalyst to form HCl and a Pt^{II}-CH_3 complex. While there has been extensive experimental and computational evidence for R-H oxidative addition at Pt^{II} model complexes to generate Pt^{II}-R, the alternative electrophilic C-H activation for the Shilov system cannot be ruled out as operational in the Shilov catalyst system.[26] After formation of the Pt^{II}-CH_3 complex, an equivalent of added Pt^{IV} oxidizes the Pt^{II}-CH_3 to a Pt^{IV}-CH_3 complex. Nucleophilic

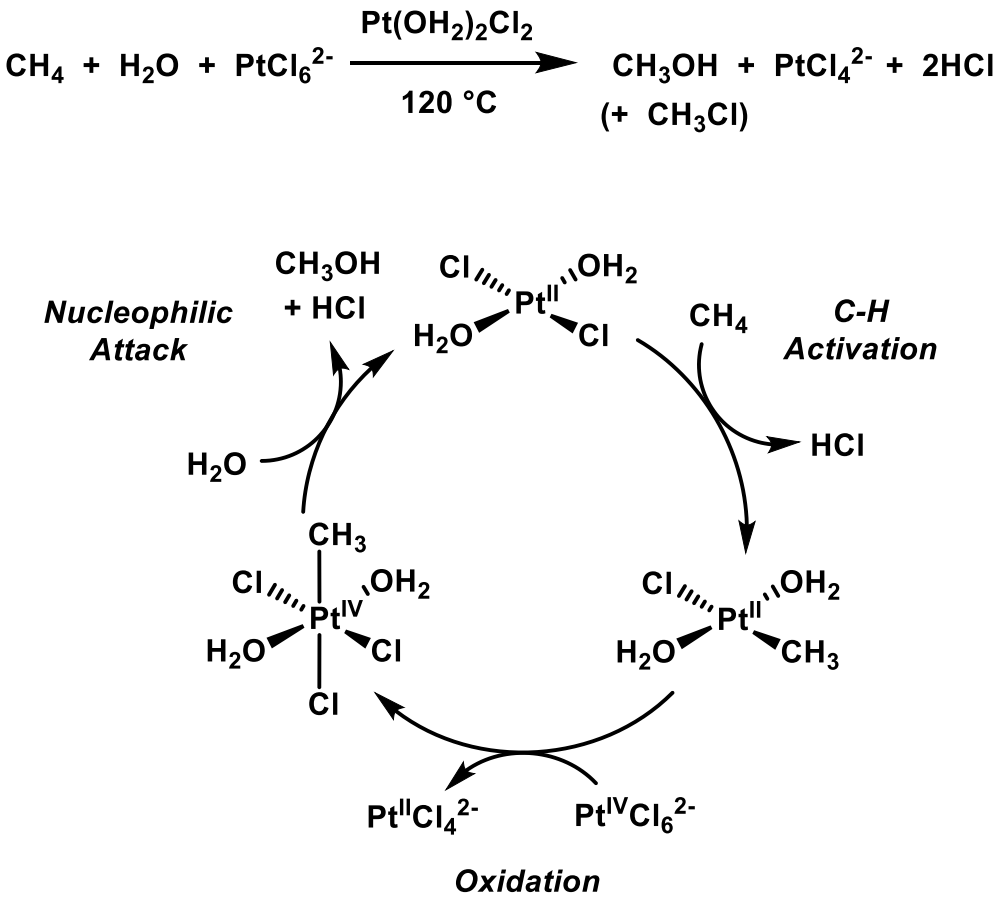

Figure 1.0 2 Catalytic system developed by the Shilov transforming methane to methanol (and chloromethane).

attack by water then generates methanol and regenerates the Pt^{II} catalyst. Through extensive isotopic labeling experiments, Bercaw and Labinger conclusively showed that Pt^{IV} acted as an external oxidant, indicating potential for use of other oxidants.[27] Additionally, conversion rates of methane to methanol were limited due to the poor thermal stability of Pt^{II} catalyst, which decomposed to metallic Pt at high temperatures. Heterogeneous metallic Pt is known to be an active but unselective catalyst for hydrocarbon oxidation.[28] Overall, even though this system was not practical, it demonstrated the potential for electrophilic methane activation by Pt^{II} and highlighted the need for the discovery of more practical oxidants.

To improve upon Shilov's seminal work, oxidants other than Pt^{IV} have been explored for alkane oxidation catalysis with Pt^{II} catalysts. While substituting Cl_2 or $S_2O_8^{2-}$ for Pt^{IV} in the Shilov system gave only a few turnovers, it did confirm that methane partial oxidation is not dependent on the presence of Pt^{IV}.[29,30] Furthermore, functionalization of ethanesulfonate (a hydrophilic alkane replacement) to 2-hydroxyethanesulfonic acid with stoichiometric amounts of $CuCl_2$ was shown using a $PtCl_4^{2-}$ catalyst and up to 43 turnovers were demonstrated.[31] A competition experiment in water between Pt^{IV} and $CuCl_2$ revealed the latter increases the rate of oxidation of $[Pt^{II}Cl_3(CH_3)]^{2-}$ to $[Pt^{IV}Cl_5(CH_3)]^{2-}$ by an order of magnitude (ca. $k_{oxidation}/k_{protonation}$ = 191 vs 20).[32] Unfortunately, even for these alternative oxidants, eventual formation of metallic Pt was observed, just as it was in the original Shilov system.

A significant advance in the electrophilic functionalization of methane was reported in 1993 by Periana and coworkers. Hg^{II} was found to catalyze methane oxidation to methylbisulfate in concentrated sulfuric acid, proceeding with 85 % selectivity and 50 % conversion.[33] An improvement on this system, based on, the Pt based Catalytica process, was also reported by the Periana group.[34] Like the Hg^{II} system, the Catalytica process converts methane to methyl bisulfate. In the Catalytica system, a bipyrimidine (bpym) ligated Pt^{II} precatalyst in concentrated sulfuric acid is employed (Scheme 1.01). An even higher conversion (> 70 %) of methane and similar selectivity

Scheme 1.01. Catalytica reaction

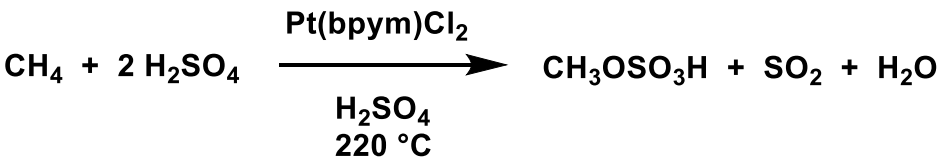

for methyl bisulfate (> 80 %) was achieved, resulting in an overall yield of 72 %. The methyl bisulfate product can then be extracted onto methanol by hydrolysis. A similar mechanism to the

Shilov system was proposed, where a primary difference is oxidation by sulfuric acid solvent, instead of Pt^{IV}. Additionally, while little experimental evidence has been disclosed, computational work supports electrophilic C-H activation proceeding through a Pt-(σ-CH_4) complex.[35] In all, the Catalytica system is the most efficient homogeneous methane functionalization effort to date. However, several problems have plagued it from being commercially relevant, such as high product separation cost and insufficient reaction rates. In addition, efficient methane functionalization only occurs in concentrated sulfuric acid. As water is generated during the reaction, there is a supplementary cost of re-concentrating sulfuric acid solvent.[36]

While previous systems have achieved the successful functionalization of methane, a practical method with an economically viable oxidant has yet to be discovered. For large scale applications, the most cost-effective choice is oxidation by O_2. O_2 is an inexpensive, abundant and environmentally benign oxidant. While there has been some limited success of methane oxidation with a Pt^{II} catalyst using either Cu^{II}/O_2 or Fe^{III}/O_2 combinations as oxidants, the catalyst deactivated after around 50 turnovers of methanol production.[36,37] Stoichiometric O_2 oxidation of a bis(dimethylpyrazolyl)acetate (NNO) or dipyridyl methanesulfonate (dpms) ligated Pt^{II}-CH_3 complex to a Pt^{IV}(NNO)(CH_3)$(OH)_2$ or Pt^{IV}(dpms)(CH_3)$(OH)_2$ complex, respectively, was demonstrated in H_2O solvent, with further release of methanol from Pt^{IV} at elevated temperatures in the latter example.[38,39] However, C-H activation of the resulting product to close a potential catalytic cycle was never demonstrated. A system which utilizes O_2 as a selective oxidant in methane functionalization remains a “holy grail”.

.

1.3 Designing A New System for Alkane Functionalization

The need for a new route to accomplish catalytic methane functionalization is apparent from analysis of the several known systems (Section 1.2). While the most efficient system to date, Catalytica, built upon Shilov's seminal work, choice of solvent/oxidant and low reaction rates precluded practical use. Partial oxidation by abundant, benign and inexpensive O_2 is desired and a productive pathway as described in Figure 1.03 can be envisioned. Here, a low valent M^n complex

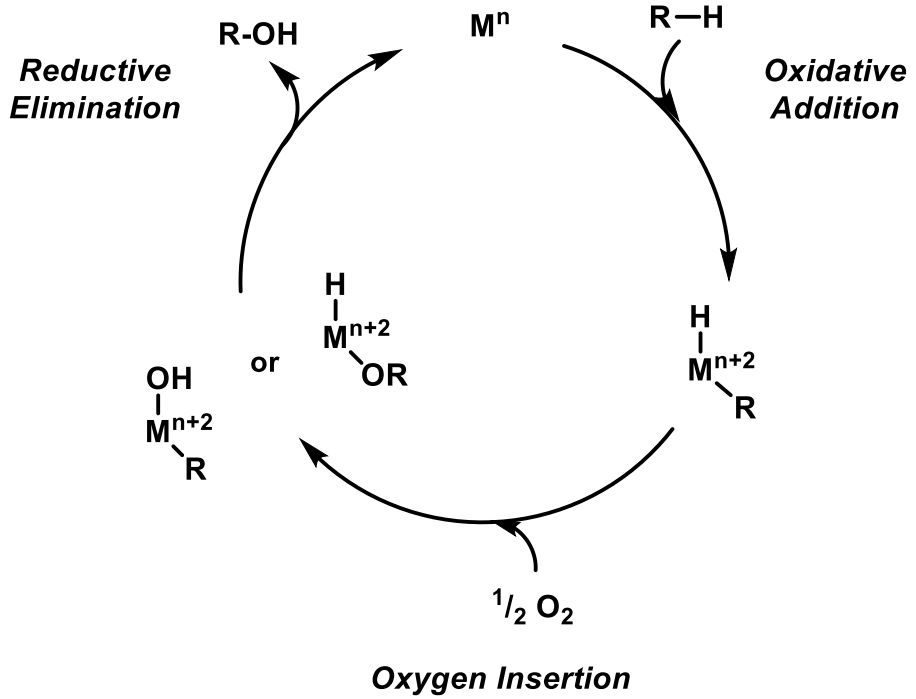

Figure 1.0 3 Proposed catalytic cycle for methane functionalization using O_2.

is proposed to activate an R-H substrate through oxidative addition, a step for which there is significant precedence.[24,25] The oxidized M^{n+2} complex undergoes oxygen insertion into the M^{n+2}-R or M^{n+2}-H bond to form a M^{n+2}-(OOR) or M^{n+2}-(OOH) complex. Oxygen insertion to Pt^{II}-CH_3 complexes have been described and form Pt^{II}-$OOCH_3$ complexes.[40,41] In addition to Pt^{II}, several examples of O_2 insertion into the Pt-H bond of higher valent Pt^{IV}-R_2H complexes to form Pt^{IV}-$(OOH)(R)_2$ have previously been described.[42,43] Decomposition of Pt^{IV}-$(OOH)(R)_2$ to form Pt^{IV}-

$(OH)(R)_2$ has also been reported.[42,43] The M^{n+2} oxygen insertion product would then reductively eliminate R-OH to reform the low valent M^n complex. Evidence of C-O reductive elimination from Pt^{IV} has previously been described; thermolysis of a 1,2-Bis(diphenylphosphino)ethane (dppe) or 1,2-Bis(diphenylphosphino)benzene (dppbz) ligated $Pt^{IV}(CH_3)_3(OR)$ (R = Aryl, Acetate) complexes form CH_3OR and Pt^{II}(dppe/dppbz)$(CH_3)_2$.[44,45] While there is precedence for all of the individual steps in this possible catalytic cycle, a full catalytic cycle has yet to be realized in practice.

The envisioned catalytic cycle (Figure 1.03) has potential, yet one major problem exists: the low valent metal complex. Low valent metals are often reactive towards other bonds present in the reaction mixture, apart from the desired C-H bond, such as the alcohol product, O_2, and N_2. To start, not only are functionalized C-H bonds weaker than unfunctionalized C-H bonds, but other reactive bonds are present.[34] O-H oxidative addition to low valent complexes have been postulated numerous times and direct observation has even been documented.[46,47] Oxidative addition of O_2 to low valent metals is also known and has been studied, leading to another unproductive side reaction for the targeted catalytic cycle.[48,49] If our goal is to develop aerobic oxidations of alkanes, we need to find a system that would be more tolerant of O_2, water, and the potential functionalized products. Pt^{II} complexes are an attractive target; they are often stable in solution and they are already known to functionalize methane C-H bonds at elevated temperatures (Section 1.2). While R-H is known to undergo oxidative addition reactions at Pt^{II}, does a pathway exist which might activate the C-H bond without undergoing a net oxidation state change at the metal?

To draw inspiration, we can turn to a CH_4 analog, H-H. Dihydrogen is a nonpolar small molecule and contains a similarly strong bond (ca. H-H BDE = 104 kcal/mol).[50] Additionally, it is known to initially react with transition metals to form dihydrogen complexes (M^n-(H_2)) through a σ interaction with the metal.[51,52] Once coordinated, homolytic cleavage to form a M^{n+2}-$(H)_2$ complex can occur through an oxidative addition route. However, heterolytic cleavage can also occur intermolecularly or intramolecularly, as M^n-(H_2) complexes are generally acidic.[51] The pK_a of Re(η-C_5Me_5)(CO)(NO)(η^2-H_2) was estimated to be around -2 in CH_2Cl_2, as it protonated diethyl ether.[53] Heterolytic cleavage by deprotonation of a dihydrogen complex is intriguing, as it circumvents formal oxidation at the metal. Furthermore, intramolecular dihydrogen cleavage at a benzoquinolate ligated Ir^{III} center was observed; the amine deprotonated the Ir^{III}-(H_2) moiety (Scheme 1.02a).[54] This example is powerful, as it demonstrates the power of the ligand to assist in deprotonating strong bonds. Intramolecular heterolytic H_2 activation by aminophosphine ligated Pt^{II} is also known (Scheme 1.02b).[55]

Scheme 1.02. Heterolytic cleavage of H_2 by an a) Ir^{III} complex and b) Pt^{II} complex

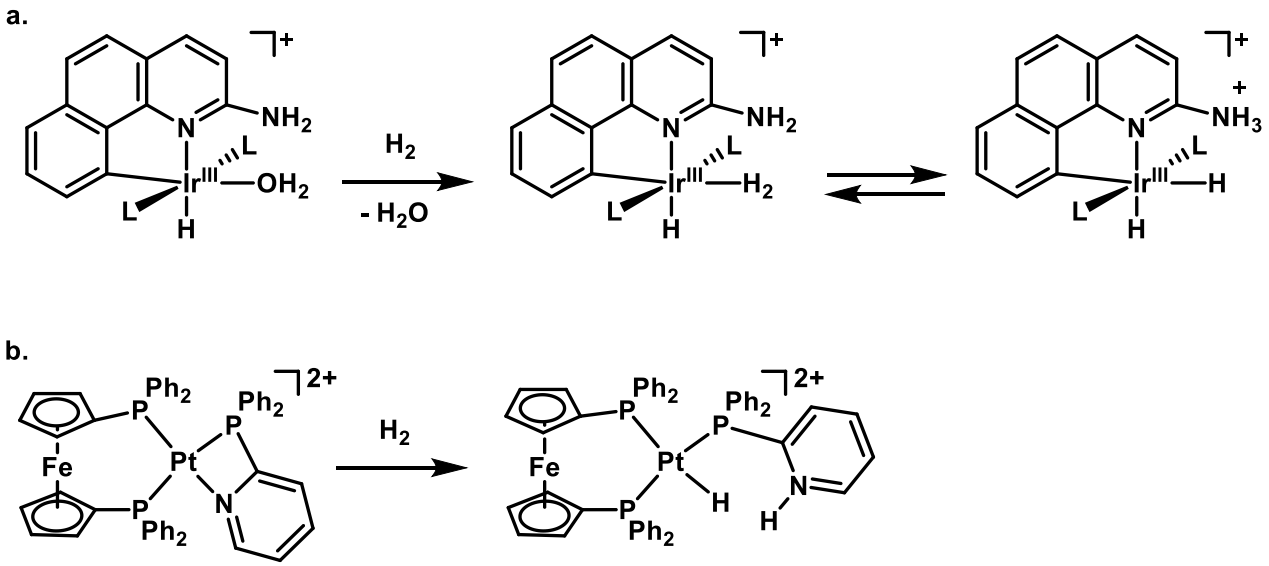

Nonpolar R-H bonds can also initially interact with metal centers like dihydrogen, forming a very reactive σ-alkane metal complex. The formation of σ-complex intermediates has been postulated from H-D scrambling experiments and inverse kinetic isotope effects in the reduction elimination reaction of higher valent metal alkyl hydrides.[25] The σ-alkane metal complex, $[Rh^{I}(PONOP)(CH_4)]^{+}$, was even observed and spectroscopically characterized at -110 °C.[56] Observance of this σ-methane complex, the simplest alkane analog to M-(H_2) complexes, provides further insight into initial reactivity of R-H with transition metals. Furthermore, hydrocarbon substrates could potentially react with transition metals in an analogous way to H_2. Here, the C-H bond of the σ-alkane complex could be deprotonated, either intermolecularly or intramolecularly (Figure 1.04). No net change in oxidation state in the metal center would additionally occur.

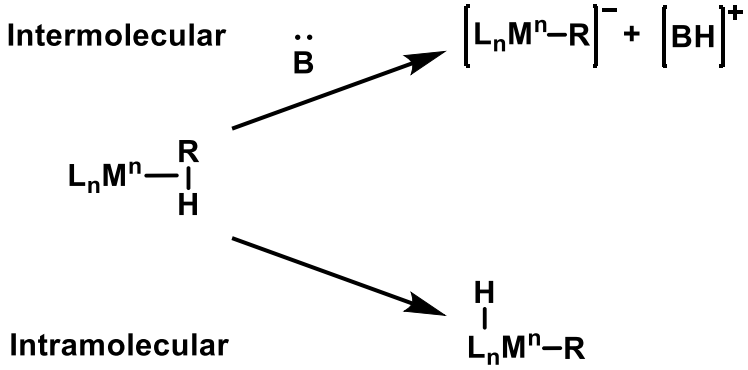

Figure 1.0 4 Activation of R-H substrate by an intermolecular (top) or intramolecular (bottom) pathway.

Intermolecular C-H activation with transition metals through an oxidative addition route has been extensively studied,[57–59] yet deprotonation of the sigma complex by an external base has yet to be directly observed (Figure 1.04, top pathway). However, electrophilic aromatic substitution of arene C-H moieties by transition metals is a similar process. Arene C-H substrates are activated by electrophilic metals, like Pt^{II}, and are postulated to initially form a metal substituted Wheland intermediate (Figure 1.05a).[60] The reactive metal-based Wheland intermediate has even been isolated and characterized at a Pd^{II} complex.[61] The intermediate is

subsequently deprotonated to rearomatize the arene. Such C-H activations have been postulated in the metalation of multidentate ligands.[62,63]

Intramolecular C-H activation has been observed as well, where noble metals are known to participate in concerted metalation deprotonation (CMD) reactions.[64,65] CMD, demonstrated in

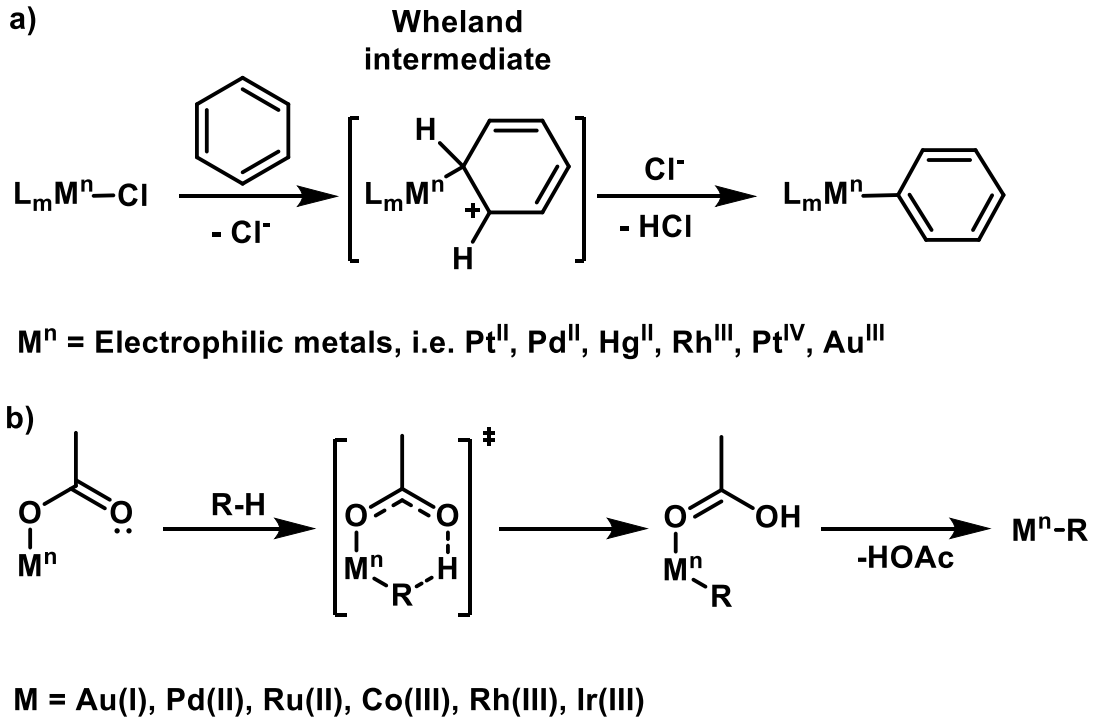

Figure 1.0 5 Activation of R-H substrate by an (a) electrophilic aromatic substitution pathway, and (b) concerted metalation deprotonation pathway.

Figure 1.05b, is a powerful type of C-H activation, where the metal and a basic ligand (typically a carboxylate) heterolytically cleave an R-H bond in a concerted manner without a formal metal oxidation state change.[66] The protonated weakly binding ligand then dissociates from the metal complex. If a basic site could be incorporated into the ligand backbone, then the protonated ligand could later transfer the acidic proton back to the substrate, either inter or intramolecularly.

Heterolytic activation of C-H substrates by a CMD route is attractive, yet dissociation of acidic ligand after C-H activation could hinder its utilization in future M-C functionalization reactions. Loss of ligand could be addressed by utilization of a ligand basic site, which would remain attached after C-H activation. Notably, the Milstein[67,68] and Huang[69] group have observed C-H activation of benzene substrate (Figure 1.06) by a relevant proposed pathway. In the Milstein group

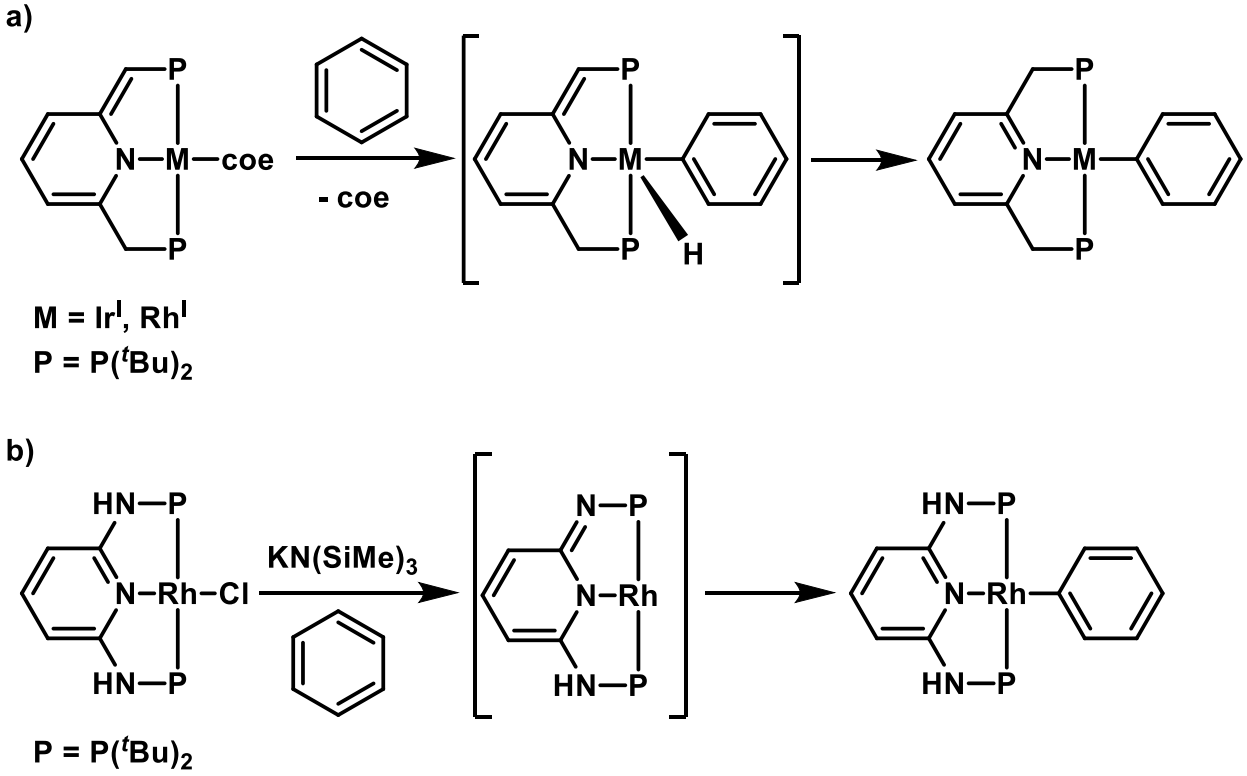

Figure 1.0 6 Activation of C_6H_6 substrate by (a) Ir^I/Rh^I(PNP) complexes, and by a (b) Rh^I(PNNNP) complex.

example, a bis-phosphinoethylpyridine (PNP) ligated Rh^I and Ir^I complexes activated benzene C-H substrate after ligand methylene CH_2 deprotonation (Figure 1.06a). Reduced temperatures (-78 °C) experiments indicate initial reactivity at the metal to form the Ir^{III} alkyl hydride, followed by intramolecular ligand protonation of the Ir-H at the deprotonated methylene site by ^{1}H NMR spectroscopy.[67] The ability of the ligand to aid in deprotonation was furthered by Huang, where a

basic N in a Rh^{I} species was proposed to aid in activation of the benzene C-H bond in a similar manner to that proposed by the Milstein group (Figure 1.06b).[69] C-H activation reactions by the Milstein and Huang group are proposed to be promoted by a dearomatization/aromatization reorganization within the system.

While previous examples have demonstrated that C-H bond activation by a ligand aided intramolecular route is possible with Ir^{I}/Rh^{I} complexes, similar transformations using Pt^{II} complexes have not been extensively explored. The premise of the following work would be to construct a Pt^{II} complex with a ligand based basic site which could be used to either deprotonate the Pt^{II}-(σ-(R-H)) moiety or the resulting Pt^{IV}-(R)(H). If such a C-H activation system is to be developed, it is reasonable to predict that a species which could activate a C-H bond might be quite reactive. To address this, we sought to examine the microscopic reverse reaction (or formation of C-H bonds) to gain an understanding into the forward reaction (C-H activation). Extensive studies have been performed on the protonation of Pt^{II}-R compounds (initially forming Pt^{IV}-(R)(H) species) and often eliminating R-H and the appropriate Pt^{II} complex through reductive elimination.[25] If a basic N site, is incorporated into the ligand, one can ask will similar reactivity be observed exclusively at the metal, or will the proton of the C-H substrate migrate to the ligand?

1.4 Dissertation Summary

The following chapters describe the syntheses, characterization, and reactivity studies of Pt^{II}-alkyl complexes with reactive N sites on the ligand, as shown in the bottom intramolecular pathway in Figure 1.04. The focus of this work is geared towards a greater understanding of C-H activation reactions by examining the microscopic reverse, or by what conditions Pt^{II}-alkyl species with an N-H proton in the ligand generate alkane (C-H formation). The findings from these studies expand the

scope of reactivity for Pt^{II}-alkyl systems which contain a ligand basic site. Specifically, pyrazolate (Chapter 2 and 3) ligated Pt^{II}-CH_3 and aminobisphosphine (Chapter 4) ligated Pt^{II}-$(CH_3)_2$ complexes were investigated.

Chapter 2 describes the synthesis and characterization of bidentate 5-(6-methyl-2-pyridyl)-3-*tert*-butylpyrazolate (NN^{Me}) and tridentate 2-(5-*tert*-butylpyrazol-3-yl)-6 (diethylaminomethyl)pyridine (NNN^{Et}) ligated Pt^{II}-Cl and Pt^{II}-R (R = CH_3 and C_6H_5) complexes. Once formed, protonation and thermolysis studies of (NN^{Me}) and (NNN^{Et}) ligated Pt^{II}-CH_3 complexes were performed to investigate parameters for alkane formation (microscopic reverse of C-H activation). Chapter 3 additionally examines the synthesis and characterization of 5-*tert*-butyl-1,3-bis(pyrazol-3-yl)pyridine (NNN) and 5-*tert*-butyl-1,3-bis(pyrazol-3-yl)benzene (NCN) ligated Pt^{II}-Cl and Pt^{II}-CH_3 complexes. The reactivity of Pt^{II}-CH_3 complexes was evaluated with Brønsted acids and the reactivity with electrophilic methyl iodide was additionally explored. Chapter 4 discusses synthesis and characterization of both known and novel bis(phosphino)amine ligated Pt^{II} complexes, taking advantage of steric congestion to promote productive reactivity. Successful methane elimination (C-H formation) was demonstrated from a ligand protonated bis(phosphino)amine $Pt(CH_3)_2$ species, however, the resulting paramagnetic complex could not be characterized and thus requires further investigation.

1.5 Notes for Chapter 1

(1) Weissermel, K.; Arpe, H.-J. *Industrial Organic Chemistry*, 4th ed.; Wiley-VCH: Weinheim; 2003.

(2) *Natural Gas Monthly*; U.S. Energy Information Administration, U.S. Governement Printing Office: Washington, D.C.; 2019.

(3) *Short-Term Energy Outlook (STEO)*; U.S. Energy Information Administration; U.S. Governement Printing Office: Washington, D.C.; 2018.

(4) How much oil and gas are actually in the Bakken Formation? https://www.usgs.gov/faqs/how-much-oil-and-gas-are-actually-bakken-formation?qt-news_science_products=3#qt-news_science_products (accessed Oct. 25, 2019)

(5) *Drilling Productivity Report.* U.S. Energy Information Administration; U.S. Governement Printing Office: Washington, D.C. 2019

(6) Boyd, G.; Burden, S.; Joffe, A. T.; Marker, D.; Sharkey, S.; Souders, S.; Tinsley, C.; Wiser, N. *Review of Well Operator Files for Hydraulically Fractured Oil and Gas Production Wells.*. Report for U.S. Envirnmental Protection Agency: Washinton, D.C., 2016.

(7) *NATRUAL GAS INFRASTRUCTURE, Appendix,B: Natural Gas*; U.S. Department of Energy, U.S. Government Printing Office: Washington, D.C. 2017.

(8) MacPherson, J. North Dakota Oil Producers are Wasting Billions of Cubic Feet of Natural Gas. *L.A. Times*. [Online] **2019**, https://www.latimes.com/business/la-fi-north-dakota-natural-gas-flaring-carbon-emissions-20190527-story.html (accessed Oct. 23, 2019).

(9) United States Natural Gas Industrial Price, https://www.eia.gov/dnav/ng/hist/n3035us3m.htm. (accessed Nov. 1, 2019)

(10) Oil Fields from Space at Night, https://geology.com/articles/oil-fields-from-space/(accessed Oct. 23, 2019).

(11) *Oil and Natural Gas Sector Hydraulically Fractured Oil Well Completions and Associated Gas during Ongoing Production*; U.S. EPA Office of Air Quality Planning and Standards 2014.

(12) Bergman, R. G. *Nature* **2007**, *446*, 391–393.

(13) Shilov, A. E.; Shul, G. B. *Chem. Rev.* **1997**, *2665*, 2879–2932.

(14) Rodríguez Vallejo, D. F.; De Klerk, A. *Energy and Fuels* **2013**, *27*, 3137–3147.

(15) Dalrymple, A. New Natural Gas Processing Plant Announced for Bakken *Bismarck Tribune*. (Online) **2018**, https://bismarcktribune.com/bakken/new-natural-gas-processing-plant-announced-for-bakken/article_d4004e1b-7b82-5d9b-9d7c-50310aa51056.html (accessed Nov 2, 2019)

(16) Monthly Crude Oil and Natural Gas Production. https://www.eia.gov/petroleum/production/ (accessed Nov 5, 2019)

(17) Horn, R.; Schlögl, R. *Catal. Letters* **2015**, *145*, 23–39.

(18) Goldberg, K. I.; Goldman, A. S. *Acc. Chem. Res.* **2017**, *50*, 620–626.

(19) Xie, J.; Jin, R.; Li, A.; Bi, Y.; Ruan, Q.; Deng, Y.; Zhang, Y.; Yao, S.; Sankar, G.; Ma, D.; Tang, J. *Nat. Catal.* **2018**, *1*, 889–896.

(20) Shan, J.; Li, M.; Allard, L. F.; Lee, S.; Flytzani-Stephanopoulos, M. *Nature* **2017**, *551*, 605–608.

(21) Tang, P.; Zhu, Q.; Wu, Z.; Ma, D. *Energy Environ. Sci.* **2014**, *7*, 2580–2591.

(22) Ruscic, B. *J. Phys. Chem. A* **2015**, *119*, 7810–7837.

(23) Gao, D. *J. Chem. Educ.* **2009**, *86*, 864–868.

(24) Labinger, J. A.; Bercaw, J. E. *Nature* **2002**, *417*, 507–514.

(25) Lersch, M.; Tilset, M. *Chem. Rev.* **2005**, *105*, 2471–2526.

(26) Goldman, A. S.; Goldberg, K. I. In *Activation and Functionalization of C-H Bonds*; 2004; pp 1–43.

(27) Luinstra, G. A.; Wang, L.; Stahl, S. S.; Labinger, J. A.; Bercaw, J. E. *J. Organomet. Chem.* **1995**, *504*, 75–91.

(28) Mallat, T.; Baiker, A. *Catal. Today* **1994**, *19*, 247–283.

(29) Horváth, I. T.; Cook, R. A.; Millar, J. M.; Kiss, G. *Organometallics* **1993**, *12*, 8–10.

(30) Basickes, N.; Hogan, T. E.; Sen, A. *J. Am. Chem. Soc.* **1996**, *118*, 13111–13112.

(31) Lin, M.; Shen, C.; Garcia-zayas, E. A.; Park, U. V; Pennsyl, V.; June, R. V. *J. Am. Chem. Soc.* **2001**, *6*, 1000–1001.

(32) Weinberg, D. R.; Labinger, J. A.; Bercaw, J. E. *Organometallics* **2007**, *26*, 167–172.

(33) Periana, R. A.; Taube, D. J.; Evitt, E. R.; Löffler, D. G.; Wentrcek, P. R.; Voss, G.; Masuda, T. *Science* **1993**, *259*, 340–343.

(34) Gunsalus, N. J.; Koppaka, A.; Park, S. H.; Bischof, S. M.; Hashiguchi, B. G.; Periana, R. A. *Chem. Rev.* **2017**, *117*, 8521–8573.

(35) Kua, J.; Xu, X.; Periana, R. A.; Goddard, W. A. *Organometallics* **2002**, *21*, 511–525.

(36) Labinger, J. A. In *Alkane C-H Activation by Single-Site Metal Catalysis,*; 2012; pp 17–71.

(37) Kreutz, J. E.; Shukhaev, A.; Du, W.; Druskin, S.; Daugulis, O.; Ismagilov, R. F. *J. Am. Chem. Soc.* **2010**, *132*, 3128–3132.

(38) Vedernikov, A. N.; Binfield, S. A.; Zavalij, P. Y.; Khusnutdinova, J. R. *J. Am. Chem. Soc.* **2006**, *128*, 82–83.

(39) Prantner, J. D.; Kaminsky, W.; Goldberg, K. I. *Organometallics* **2014**, *33*, 3227–3230.

(40) Scheuermann, M. L.; Goldberg, K. I. *Chem. - A Eur. J.* **2014**, *20*, 14556–14568.

(41) Zeitler, H. E.; Kaminsky, W. A.; Goldberg, K. I. *Organometallics* **2018**, *37*, 3644–3648.

(42) Wick, D. D.; Goldberg, K. I. *Organometallics* **1999**, 119, 11900–11901.

(43) Look, J. L.; Wick, D. D.; Mayer, J. M.; Goldberg, K. I. *Inorg. Chem.* **2009**, *48*, 1356–1369.

(44) Williams, B. S.; Holland, A. W.; Goldberg, K. I. *J. Am. Chem. Soc.* **1999**, *121*, 252–253.

(45) Williams, B. S.; Goldberg, K. I. *J. Am. Chem. Soc.* **2001**, *123*, 2576–2587.

(46) Blum, O.; Milstein, D. *J. Am. Chem. Soc.* **2002**, *124*, 11456–11467.

(47) Albrecht, M.; Lindner, M. M. *Dalt. Trans.* **2011**, *40*, 8733.

(48) Boisvert, L. U. C.; Goldberg, K. I. *Acc. Chem. Res.* **2012**, *45*, 899–910.

(49) Konnick, M. M.; Stahl, S. S. *J. Am. Chem. Soc.* **2008**, *130*, 5753–5762.

(50) Darwent, B. D. *National Standard Reference Data Series, National Bureau of Standards, vol. 42*; 1970.

(51) Kubas, G. J. *Proc. Natl. Acad. Sci.* **2007**, *104*, 6901–6907.

(52) Heinekey, D. M.; Oldham, W. J. *Chem. Rev.* **1993**, *93*, 913–926.

(53) Chinn, M. S.; Heinekey, D. M.; Payne, N. G.; Sofield, C. D. *Organometallics* **1989**, *8*, 1824–1826.

(54) Lee, D. H.; Patel, B. P.; Clot, E.; Eisenstein, O.; Crabtree, R. H. *Chem. Commun.* **1999**, 3, 297–298.

(55) Almeida Leñero, K. Q.; Guari, Y.; Kamer, P. C. J.; Van Leeuwen, P. W. N. M.; Donnadieu, B.; Sabo-Etienne, S.; Chaudret, B.; Lutz, M.; Spek, A. L. *Dalt. Trans.* **2013**, *42*, 6495–6512.

(56) Bernskoetter, W. H.; Schauer, C. K.; Goldberg, K. I.; Brookhart, M. *Science.* **2015**, *326*, 553–556.

(57) Ligands, N.; Rendina, L. M.; Puddephatt, R. J. *Chem. Rev.* **1997**, *97*, 1735–1754.

(58) Halpern, J. *Acc. Chem. Res.* **1970**, *3*, 386–392.

(59) Bergman, R. G. *Science.* **1984**, *223*, 902–908.

(60) Lei, A.; Shi, W.; Liu, C.; Zhang, H.; He, C. In *Oxidative Cross-Coupling Reactions*; 2016; pp 49–53.

(61) Poverenov, E.; Leitus, G.; Milstein, D. *J. Am. Chem. Soc.* **2006**, *128*, 16450–16451.

(62) Albrecht, M.; Koten, G. *Angew. Chemie, Int. Ed.* **2001**, *40*, 3750–3781.

(63) Cave, G. W. V.; Fanizzi, F. P.; Deeth, R. J.; Errington, W.; Rourke, J. P. *Organometallics* **2000**, *19*, 1355–1364.

(64) Davies, D. L.; Macgregor, S. A.; McMullin, C. L. *Chem. Rev.* **2017**, *117*, 8649–8709.

(65) .Lapointe, D.; Fagnou, K. *Chem. Lett.* **2010**, *39*, 1118

(66) Gorelsky, S. I.; Lapointe, D.; Fagnou, K. *Chem. Lett.* **2010**, *39* (11), 1118.

(67) Ben-Ari, E.; Leitus, G.; Shimon, L. J. W.; Milstein, D. *J. Am. Chem. Soc.* **2006**, *128*, 15390–15391.

(68) Schwartsburd, L.; Iron, M. A.; Konstantinovski, L.; Ben-ari, E.; Milstein, D. *Organometalics* **2011**, *30*, 2721–2729.

(69) Wang, Y.; Zheng, B.; Pan, Y.; Pan, C.; He, L.; Huang, K.-W. *Dalt. Trans.* **2015**, *44*, 15111–15115.

Chapter 2

Synthesis and Reactivity of Bidentate and Hemilabile Pyrazolate Ligated Pt Complexes

2.1 Introduction

Natural gas, a significant feedstock for the chemical industry, is comprised of methane and light alkanes.[1] Viable routes that do not involve high energy steam reforming for the conversion of methane to higher value-added products are not yet available and the development of such systems remains a challenge.[2] Aqueous electrophilic functionalization of methane (CH_4) by a Pt^{II}-Cl complex to generate methanol was first demonstrated by Shilov almost 50 years ago.[1] While remarkable, this system was deemed economically impracticable, as it required stoichiometric amounts of a Pt^{IV} oxidant. Since then, many studies of both stoichiometric and catalytic C-H functionalization using Pt^{II} complexes have been carried out as the community seeks to identify more viable catalyst systems that could potentially be used on commercial scale for alkane functionalization. [2,3]

Activation of C-H bonds by Pt^{II}, the first step in C-H functionalization, often proceeds by oxidative addition, generating a Pt^{IV}-hydrido alkyl complex. The oxidized Pt^{IV} hydrido alkyls are typically less thermodynamically stable relative to their Pt^{II} counterparts and methane. Thus, significant insight into this difficult transformation has been gained through the study of the more

Portions of this chapter have been adapted from: Zahora, B. A.; Gau, M. R.; Goldberg, K. I. *In*

accessible microscopic reverse reaction: reductive elimination of alkane from Pt^{IV} hydrido alkyl complexes. These C-H coupling reactions can be carried out by either using isolated octahedral Pt^{IV} hydrido alkyl complexes or by protonation of square-planar Pt^{II} alkyl compounds. In the latter case, upon addition of a Brønsted acid to a square planar Pt^{II}-alkyl compound, either a Pt^{IV} alkyl hydride species is spectroscopically detected and subsequently undergoes C-H reductive elimination, or the C-H coupled alkane product with a Pt^{II} species is observed directly, without evidence of an intermediate. If no intermediate is observed, it is challenging to conclusively determine whether the reaction takes place by direct protonation of the Pt^{II}-alkyl bond or by protonation of the metal to produce a Pt^{IV}-alkyl hydride intermediate. Most data support that the initial site of protonation in Pt^{II} species is the Pt^{II} center with formation of a Pt^{IV} alkyl hydride species.[4–7] However, computational

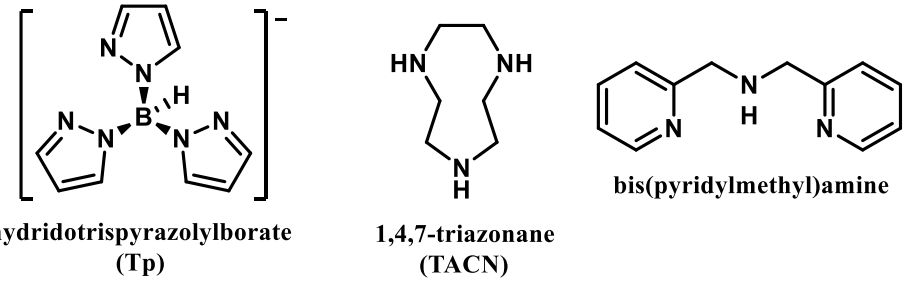

Figure 2.0 1 Ligand examples employed which have allowed isolation of Pt^{IV} methylhydrides

work by Bercaw and Lin has suggested that with electron deficient ancillary ligands, direct protonation of the Pt^{II}-CH_3 bond, bypassing Pt^{IV}, may occur.[8]

It is also significant that most studies of reductive elimination of alkanes from octahedral Pt^{IV} alkyl hydride complexes support that the concerted C-H bond forming step occurs from a five-coordinate intermediate.[9] This mechanistic understanding has made it possible to stabilize octahedral Pt^{IV} alkyl hydride complexes by using strongly bound ligands that resist dissociation. In particular, facially coordinating tridentate nitrogen ligands have been used to stabilize Pt^{IV} dimethyl hydride

complexes (Figure 2.01).[10–12,13] Thus, Pt^{IV} dimethyl hydride complexes of tris(pyrazolyl)borate (Tp), 1,4,7-triazacyclononane (TACN), and bis(pyridylmethyl)amine have all been reported (Figure 2.01). All these ligands coordinate to $Pt^{II}(CH_3)_2$ species in a bidentate fashion and upon protonation, the third arm coordinates, generating a *fac* chelating ligand arrangement in the stable octahedral Pt^{IV} product. Whether the metal is protonated directly or if the ligand is the kinetic site of protonation, followed by proton transfer to the metal is challenging to ascertain. Protonation at the ligand has been observed for pyridinophane (PP)[14] and dimethyl((pyridinylmethylene)amino)(ethyl/propyl)amine (DMEP/DMPP)[15] ligated $Pt^{II}(CH_3)_2$ species (Scheme 2.01).

Scheme 2.01 (a) Protonation of pyridinophane ligated Pt^{II} (b) Protonation of DMEP(n=1) /DMPP(n=2) ligated Pt^{II}

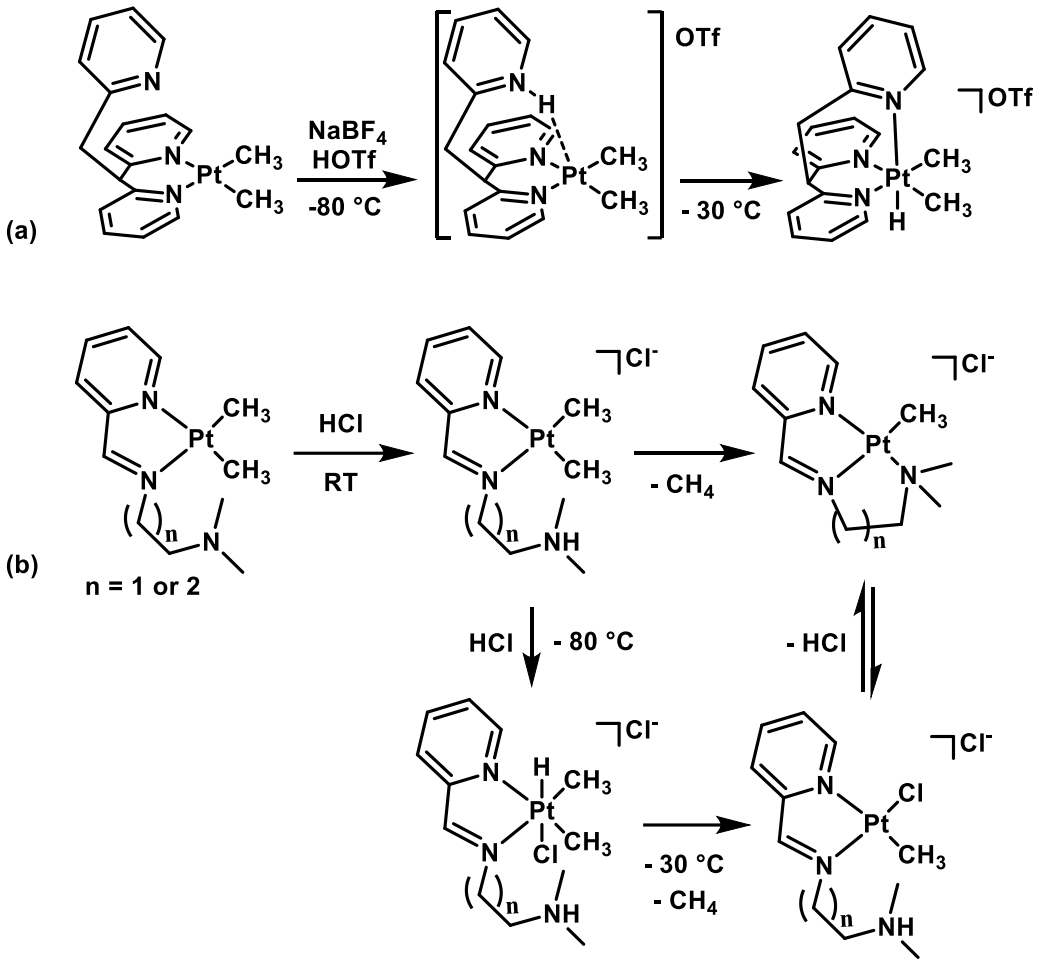

For the PP system, a small amount (8 % yield) of the protonated (^{H}PP)Pt$(CH_3)_2$ intermediate was observed by ^{1}H NMR spectroscopy at -80 °C (Scheme 2.01a). Warming to -30 °C promoted conversion to the oxidized Pt^{IV} hydride product. Here, it was proposed that the pyridyl nitrogen helps shuttle the proton from the ligand to the metal center.[14] In contrast, the ligand protonated (^{H}DMEP/^{H}DMPP) $Pt^{II}(CH_3)_2$ species were reported to be stable for several hours in solution at room temperature before methane elimination (Scheme 2.01b).[15] It is possible that the N-H moiety of the protonated ^{H}DMEP/^{H}DMPP ligand helps to shuttle the proton to the metal

in a similar fashion to the protonated ^{H}PP ligand described above. While in the vast majority of DMEP/DMPP complexes, the ligand adopts a *mer*-orientation, there are several examples where a *fac*-orientation is exhibited.[16,17] The *fac*-orientation would be more suited to aid in direct proton transfer to the open position on a d^8 metal center. While no Pt^{IV} intermediates were observed prior to methane liberation for the DMEP/DMPP complexes, the addition of two equivalents of HCl to (DMEP)$Pt^{II}(CH_3)_2$ did form an observable Pt^{IV} hydride at low temperatures, which quickly liberated methane upon warming to -30 °C. No Pt^{IV} hydride was observed when acid was added to (DMPP)$Pt^{II}(CH_3)_2$.[15]

Our interest lies in exploring ligands that can accept a proton, but do not have the ability to reorient and stabilize Pt^{IV} hydride products. Our studies of the protonation of two Pt^{II}-CH_3 complexes bearing either a bidentate or tridentate ligand and further C-H coupling from these compounds are described below. Previous examples of square planar bidentate ligated $Pt^{II}(CH_3)_2$ complexes with an available basic nitrogen on the ligand have contained either dangling N moieties or N moieties enclosed in aromatic based systems.[14,15,18] Protonation will then either take place at the metal or at the ligand. In bidentate systems with dangling N moieties, such as in L$Pt^{II}(CH_3)_2$, two arms of a potentially tridentate ligand L are coordinated in the Pt^{II} complex. The third arm bears a basic nitrogen that can either be protonated or can bind to the metal when the metal center is protonated to yield an octahedral Pt^{IV} hydride complex. When a Pt^{IV} dimethyl hydride species is formed, the stabilized product adopts a *fac* orientation.

We sought to prepare bidentate and tridentate Pt^{II}-CH_3 complexes wherein the available basic site for protonation is not available to bind to the metal. The basic site is physically constrained to only act as a base and not a ligand. To achieve this arrangement, bidentate and tridentate pyrazolate-supported ligands, 5-(2-pyridyl)-3-*tert*-butylpyrazolate **(^{H}NN^{R})** (R = H or Me) and 2-(5-*tert*-

butylpyrazol-3-yl)-6-(diethylaminomethyl)pyridine **(^{H}NNN)^{Et}**, which have been complexed to several metals (e.g. Ru^{II}, Ir^{III}, Co^{II} and Fe^{II}),[19–21] were used. Notably, these ligands have not yet been found in square planar d^8 complexes. Herein, we describe metalation of **(^{H}NN^{R})** and **(^{H}NNN)^{Et}** to afford d^8 square planar Pt^{II} complexes. These pyrazolate ligated Pt^{II}-CH_3 species will have basic nitrogen sites on the ligands available for protonation.

2.2 Results and Discussion

2.21 Synthesis of Bidentate Ligand Supported Pyrazolate Pt^{II}-Complexes

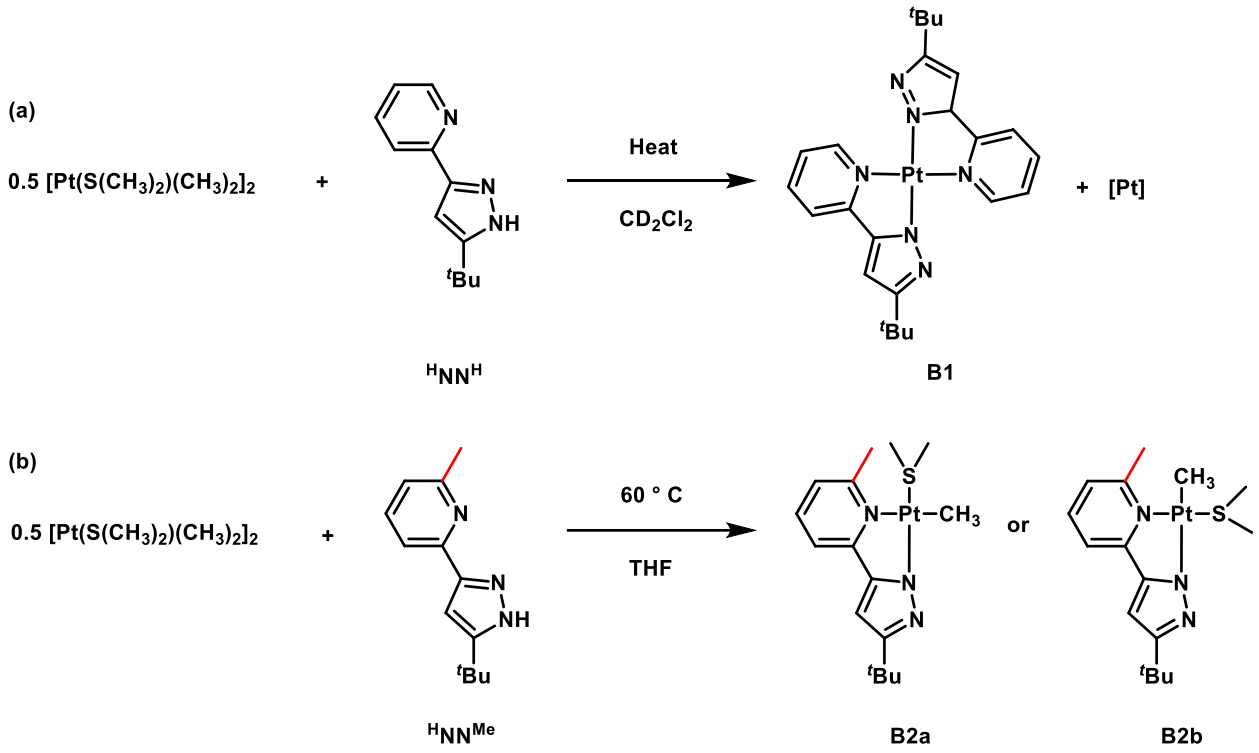

Figure 2.0 2 (a) Metalation of ^{H}**NN**^{H} (b) Metalation of ^{H}**NN**^{Me}

The mono pyrazole ligands, 5-(2-pyridyl)-3-*tert*-butylpyrazolate (^{H}**NN**^{H}) and (5-(6-methyl-2-pyridyl)-3-*tert*-butylpyrazolate (^{H}**NN**^{Me}) were prepared in high yield according to literature procedures.[22] A notable difference in these two ligand types is the methyl substituent in the 6-position, which was initially installed to prevent potential rollover activation of the α-pyridyl C-H bonds. This reactivity has been observed at high temperatures and can result in undesirable Pt cyclometalated complexes from C-H activation of ligand.[23] A 1:1 molar ratios of ligand to metal coordinated differently for ^{H}**NN**^{H} and ^{H}**NN**^{Me} with [Pt(μ-S(CH$_3$)$_2$)(CH$_3$)$_2$]$_2$: two ^{H}**NN**^{H} ligands coordinate to Pt^{II} while only one ^{H}**NN**^{Me} ligand coordinates to Pt^{II} (Figure 2.02). Addition of ^{H}**NN**^{H}

to the Pt-CH_3 starting material at room temperature yielded methane, $S(CH_3)_2$, and a major and multiple minor Pt-containing species by ^{1}H NMR spectroscopy. Further heating of the reaction mixture to 100 °C converged the multiple minor Pt species to the one major complex, which did not display a Pt-CH_3 resonance, or a Pt-$S(CH_3)_2$ resonance by ^{1}H NMR spectroscopy. In addition, a Pt-H resonance was not observed upfield in the ^{1}H NMR spectrum. The same major product was also observed by ^{1}H NMR spectroscopy (without the observance of any free ligand) when 2 equivalents of **^{H}NN^{H}** was added to $[Pt(\mu\text{-}S(CH_3)_2)(CH_3)_2]_2$ and subsequently heated. By ^{1}H NMR spectroscopy, a single species was observed without a Pt-CH_3 or Pt-$S(CH_3)_2$ resonance. The main species is proposed to be the homoleptic $Pt(*NN^H)_2$ complex (**B1**) [Note: * refers to deprotonated pyrazolate N]. Formation of homoleptic ***NN^{H}** ligated Pd^{II} complexes have been previously described in metalation reactions due to the lack of sterics in the 6 position of the ligand pyridyl moiety.[24–26] ^{1}H NMR assignments of reported $Pd(*NN^H)_2$ is in agreement with **B1**.

Metalation of **^{H}NN^{Me}** at 60 °C with $[Pt(\mu\text{-}S(CH_3)_2)(CH_3)_2]_2$ resulted in $Pt(*NN^{Me})(S(CH_3)_2)CH_3$ (Figure 2.02a). The ^{1}H NMR spectrum of $Pt(*NN^{Me})(S(CH_3)_2)CH_3$ exhibits a methyl resonance at 1.39 ppm with $^2J_{Pt\text{-}H}$ coupling of 84 Hz, and a $S(CH_3)_2$ resonance at 2.49 ppm with a $^3J_{Pt\text{-}H}$ of 52 Hz. There are two potential conformers for this product (**B2a**/**B2b**, Figure 2.02). The Chen group have previously reported bidentate 3,5-bis(2,6-dimethylphenyliminoacetyl)-4-methylpyrazole (bdmimp) ligated Pt^{II}-$(CH_3)(S(CH_3)_2)$ complexes. Here, when Pt-CH_3 is *trans* to a pyrazolate moiety, $^2J_{Pt\text{-}H}$ is smaller (69 Hz) than when *trans* to a pyridyl moiety (79 Hz). This suggests **B2a** over **B2b** from examination of the $^2J_{Pt\text{-}H}$ value (80.3 Hz).[27] Complex **B2a/b** was found to be unstable to silica and alumina (neutral and basic) and attempts to purify and fully characterize **B2a/b** were unsuccessful. The formation of **B2a/b** instead of a homoleptic complex can rationalized from the sterics of the methyl substituent in the 6 position of

the bidentate ^{H}**NN**^{Me} ligand. To isolate a more stable complex, the reaction of **B2a/b** with a more strongly bound ligand than $S(CH_3)_2$, namely PPh_3, afforded a single species by ^1H and $^{31}P\{^1H\}$ NMR spectroscopy. Liberation of $S(CH_3)_2$ was observed in the ^1H NMR spectrum and the appearance of a new ^{31}P shift at 18.22 ppm with corresponding Pt satellites ($^1J_{(Pt\text{-}P)}$ = 4186 Hz) allowed for the assignment of Pt(*NN^{Me})(CH_3)(PPh_3) (**B3**). By ^1H NMR spectroscopy, **B3** exhibited a Pt-CH_3 resonance at 0.97 ppm ($^2J_{Pt\text{-}H}$ = 80 Hz, $^3J_{(H\text{-}P)}$ = 5.1 Hz). **B3** was also unstable to isolation; the change from **B2a/b** to **B3** does not appear to have a significant effect on the $^2J_{Pt\text{-}H}$ of the Pt-CH_3 or on ease of isolation.

2.22 Preparation of ***(NNN)^{Et}*** *Ligated Pt^{II} Complexes*

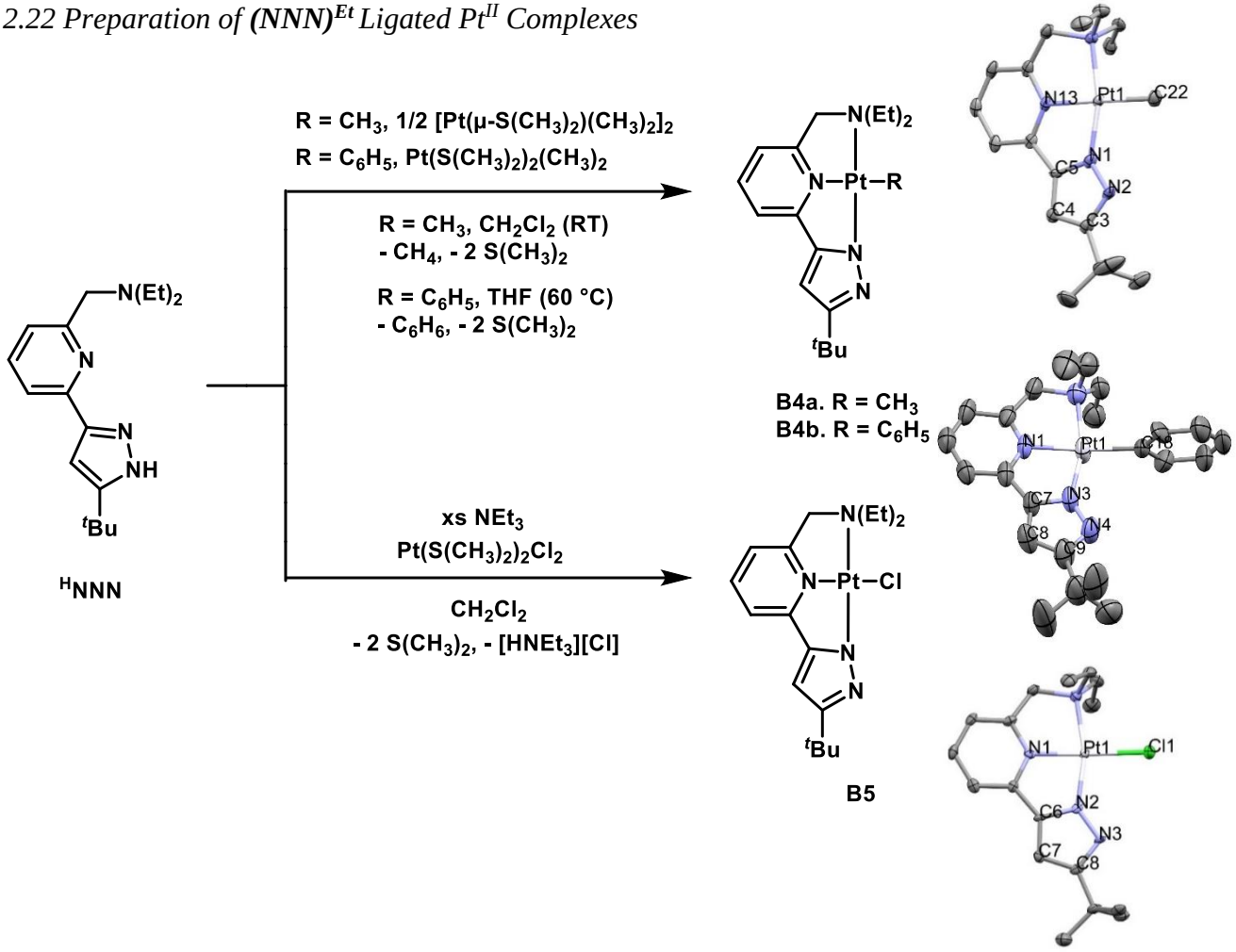

Figure 2.03. Metalation of ^{H}NNN^{Et} to Pt^{II} to form **B4a, B4b** and **B5**. Thermal Ellipsoid plot of Pt(*NNN)^{Et}CH$_3$ (**B4a**) and Pt(*NNN)^{Et}Cl (**B4b**) and Pt(*NNN)^{Et}C$_6$H$_5$ (**B5**) at 50% probability (CH_2Cl_2 in **B4a** omitted for clarity and H-atoms omitted for clarity). Selected bond distances for **B4a** (Å): N(1)-C(6) 1.387(6) Å, N(2)-C(3) 1.355(8) Å, Pt-N(13) 1.948(8) Å, Pt-C(22) 2.062(6) Å. Selected bond distances for **B4b** (Å): N(2)-C(6) 1.377(6) Å, N(3)-C(8) 1.349(8) Å, Pt-N(1) 2.015(4) Å. Selected bond distances for **B5**: N(3)-C(7) 1.38(1) Å, N(4)-C(9) 1.35(1) Å, Pt-C(18) 2.050(7) Å, Pt-N(1) 1.996(7) Å.

Addition of 1 equiv. 2-(5-*tert*-butylpyrazol-3-yl)-6 (diethylaminomethyl)pyridine **(^{H}NNN)^{Et}** to [Pt(μ-S(CH$_3$)$_2$)(CH$_3$)$_2$]$_2$, Pt(S(CH$_3$)$_2$)(C$_6$H$_5$)$_2$ or Pt(S(CH$_3$)$_2$Cl$_2$ affords Pt(*NNN)^{Et}CH$_3$ (**B4a**), Pt(*NNN)^{Et}C$_6$H$_5$, (**B4b**) and Pt(*NNN)^{Et}Cl (**B5**) in 79 %, 81 %, and 67 % isolated yield, respectively (Figure 2.03). An excess of NEt$_3$ is additionally required to form **B5**. The ^{1}H and ^{13}C{^{1}H} NMR spectra are consistent with assignment of **B4a** with a $^{2}J_{Pt\text{-}H}$ = 78 Hz observed for Pt^{II}-CH$_3$ group. The

^{1}H and $^{13}C\{^{1}H\}$ NMR spectrum is consistent with assignment of **B4b** with three additional aryl resonances observed in the ^{1}H NMR spectrum for the Pt-C_6H_5 ligand. Diastereotopic methylene proton signals are observed in the ^{1}H NMR spectra of **B4a**, **B4b**, and **B5**, consistent with chelation of the diethyl amine moiety. **B4a** and **B4b** were additionally characterized by elemental analysis, while complex **B5** was characterized by high resolution mass spectroscopy (*m/z* = 557.2187). The monomeric nature of **B4a**, **B4b**, and **B5** were also crystallographically confirmed (Figure 2.03). C-N bond distances within the pyrazolate group for **B4a**, **B4b**, and **B5** suggest that the C-N bond associated with the non-coordinated N has slightly more double bond character than that of the coordinated one. In **B1**, these values are 1.355(8) Å (N(2)-C(3)) versus 1.387(6) Å (N(1)-C(5)). Similar bond length differences are seen in the crystal structures of other pyrazolate ligands bound to metals.[20,21] Together, the absence of an N-H resonance in the ^{1}H NMR spectrum and the lack of counter anions in the solid-state structure, suggests that the pyrazolate moiety is deprotonated in **B4a**, **B4b**, and **B5.** Additionally, the change in the Pt-pyridine bond distance (1.948(8) Å (**B4a**) vs 1.996(7) Å (**B4b**) vs 2.015(4) Å (**B5**) suggests a *trans*-influence trend where $CH_3 > C_6H_5 > Cl$.

*2.23 The Reactivity of **B2a/B2b and 4a** with Acid*

With bidentate (**B2a/B2b**) and hemilabile tridentate (**B4a**) Pt^{II}-CH_3 complexes in hand, their reactions with acid were examined. Both **B2a/b** and **B4a** contain a single pyrazolate moiety in the ligand, however, **B4a** additionally contains a hemilabile diethyl amine N. Nitrogen sites on the ligand or Pt^{II}/Pt^{II}-CH_3 could act as the site of protonation. If methane is not directly observed, either a $Pt^{IV}(H)(CH_3)$ species or a ligand protonated Pt^{II}-CH_3 is expected. In this case, conditions necessary for methane elimination from either proposed protonated product could then be studied. We set out to investigate reactivity of acid with these complexes.

The protonation of **B2a/b** was first investigated. Upon the addition of 1 equivalent of HBF_4 etherate to a diethyl ether solution of **B2a/b**, a precipitate was observed. When monitored *in situ* in C_6D_6, no methane was observed by ^1H NMR spectroscopy. Upon removal of C_6D_6 or ether and dissolution in THF-d_8, one major product was observed containing an N-H resonance and platinum bound -$S(CH_3)_2$ and -CH_3 ligands with no observable Pt-H resonance (expected upfield of 0 ppm). This species is postulated to be [Pt(^{H}NN^{Me})(S$(CH_3)_2$)CH_3][BF_4] (**B6,** Figure 2.04a); however, additional experiments such as solid state and/or NOSY experiments are required to assign the exact

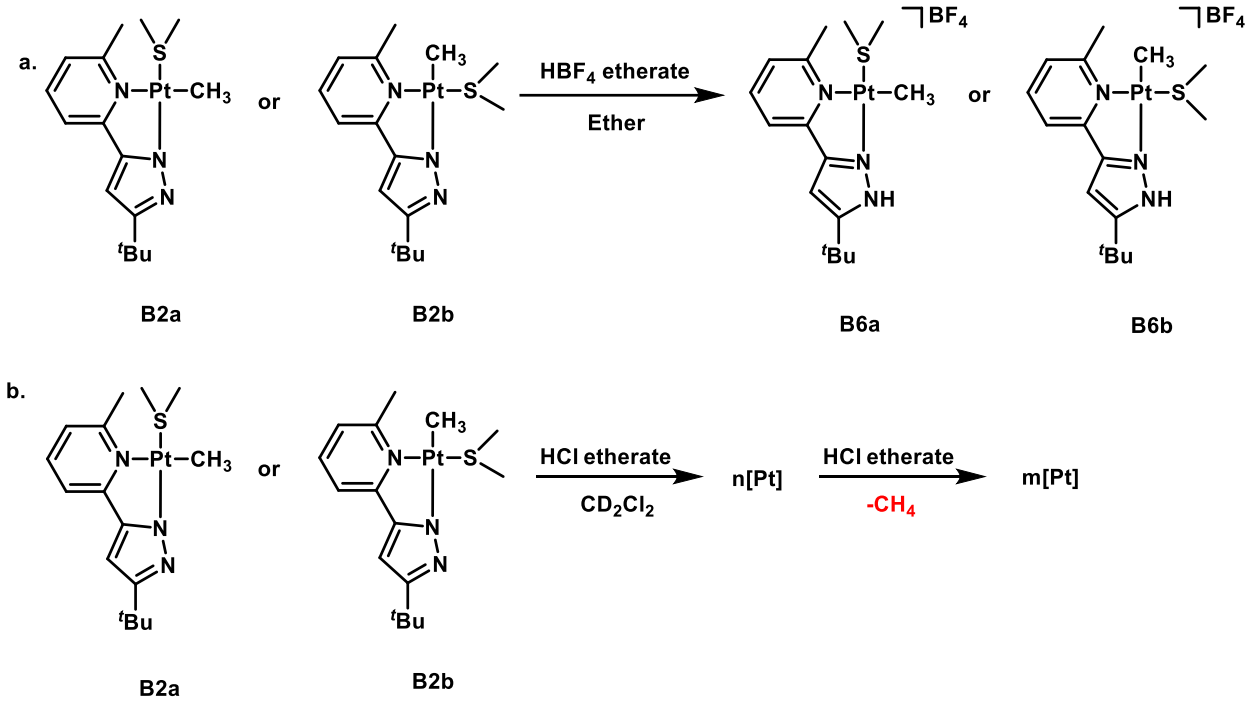

Figure 2.04(a). Protonation of **B2a or B2b** with HBF_4 etherate to form either **B6a** or **B6b** and **(b)**. Protonation with HCl etherate to form methane after 2 added equiv.

structure (i.e. *cis* (**B6a**)*/trans* (**B6b**)). Complex **B6** exhibits a methyl resonance with corresponding $^2J_{Pt\text{-}H}$ coupling of 79 Hz by ^1H NMR spectroscopy. **B6** displayed a smaller $^2J_{Pt\text{-}H}$ coupling than **B2a/B2b** (from 84 to 79 Hz). Additionally, no methane was observed *in situ* when 1 equiv. of HCl etherate was added to a CD_2Cl_2 solution of **B2a/b**; however, at least two Pt products are observed (based on 8 broad aromatic resonances and 2 sharp ^{t}Bu resonances), along with liberation of $S(CH_3)_2$

by ^{1}H NMR spectroscopy. Release of methane was not observed by ^{1}H NMR spectroscopy until 2 total equivalents of HCl etherate was added to a CD_2Cl_2 solution of **B2a/b**. The resulting ^{1}H NMR spectrum after a total of 3 equivalents of HCl etherate reveals at least 2 Pt products (based on 8 aromatic resonances and 2 ^{t}Bu resonances). Additionally, ESI-MS of the reaction mixture in CH_3CN suggests one of the main Pt products is $Pt(^{H}NN^{Me})Cl(CH_3CN)^+$ (*m/z* = 487.5). $Pt(^{H}NN^{Me})Cl(CH_3CN)^+$ could form from solvent ligand exchange with weakly bound $S(CH_3)_2$. The formation of **B6** after 1 equivalent of added HBF_4 etherate to **B2a/b** and additionally, the liberation of methane after the addition of 2 equiv. of HCl etherate to **B2a/b** suggests the basicity of the Pt^{II} center and/or methyl ligand is less than that of the pyrazolate ligand. Only after the pyrazolate ligand is protonated does additional added acid liberate methane. This behavior is in contrast to that of previous examples of bidentate ligated Pt^{II}-CH_3 complexes,[6,7] where addition of 1 equiv. of acid leads to a Pt^{IV}-H or methane release.

To determine if the pyrazolate N-H species (**B6**) is acidic enough to generate methane at elevated temperatures, thermolysis of **B6** was attempted in THF-d_8 in a sealed J. Young NMR tube. At 100 °C, a reaction occurred. After 3 days of heating at 100 °C, no evidence of a Pt^{IV}-H or methane was observed by ^{1}H NMR spectroscopy, although free dimethyl sulfide was present. Additionally, by ^{1}H NMR spectroscopy, 4 Pt species were present at the end of the thermolysis reaction, based on 15 aromatic and 4 ^{t}Bu resonances. It appears that methane elimination is disfavored over dimethyl sulfide release. The weakly binding nature of dimethyl sulfide appears to lead to dissociation which may somehow prevent C-H coupling. To address the lability of dimethyl sulfide, a tridentate ligand with a chelating diethyl amine moiety was targeted.

*2.24 Release of methane from **B4a** under acidic conditions*

Reaction of **B4a** with one equivalent of HBF_4 etherate (Figure 2.05) in diethyl ether or benzene caused the precipitation of an orange solid. Upon isolation, the ^{1}H and $^{13}C\{^{1}H\}$ NMR

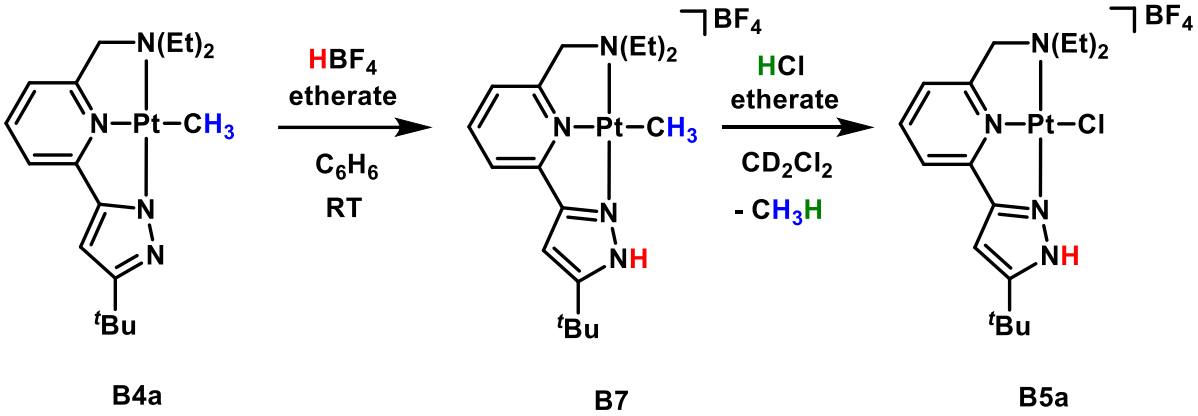

Figure 2.0 3 Protonation of Pt(*NNN)$^{Et}CH_3$ (**B4a**) with HBF_4 etherate to form [Pt(^{H}NNN)$^{Et}CH_3$][BF_4] (**B7**). Further Protonation of **B7** with HCl etherate to form [Pt(^{H}NNN)^{Et}Cl][BF_4] (**B5a**).

spectral data in CD_2Cl_2 were consistent with pyrazolate protonation and the formation of [Pt(^{H}NNN)$^{Et}CH_3$][BF_4] (**B7**). However, unlike earlier observations for the bidentate **B6**, in the ^{1}H NMR spectrum, no N-H resonance was observed when **B7** was formed in C_6D_6 or CD_2Cl_2. When the reaction was monitored *in situ* in C_6D_6, no methane evolution or Pt^{IV}-H was detected by ^{1}H NMR spectroscopy. The $^{19}F\{^{1}H\}$ NMR spectrum of **B7** displayed two broad singlets in a 1:4 ratio, consistent with an outer sphere BF_4^- and in accordance with the natural abundance of ^{10}B: ^{11}B.[28] The $^{2}J_{Pt\text{-}H}$ coupling of the Pt-CH_3 decreased slightly upon protonation from 79 Hz for **B4a** to 77 Hz for **B7** in CD_2Cl_2. **B7** was additionally characterized by high resolution ESI-MS (*m/z* = 495.2043). Under ESI-MS conditions, another species (with a mass consistent with Pt(*NNN^{Et})$^{+}$) is present, presumably from decomposition of **B7**.

We determined that a second equivalent of acid is needed to generate methane. The addition of one equivalent of HBF_4 etherate to a C_6D_6 solution of **B7** generated methane at room temperature with no CDH_3 formation. Thus, when two equivalents of acid are added to the unprotonated complex **B4a**, the first equivalent protonates the ligand. The second equivalent then protonates the Pt or the Pt-CH_3 bond, leading to C-H coupling. The platinum product of this reaction displayed broad resonances in the ^{1}H NMR spectrum and could not be identified. However, when one equivalent HCl etherate, an acid with a coordinating conjugate base, was added to **B4a**, [Pt(^{H}NNN)^{Et}Cl][BF_4] (**B5a**, 69 % spectroscopic yield, Figure 2.05) was confirmed as the product. The formation of **B5a** in this reaction was confirmed by independent synthesis via protonation of the Pt-Cl (**B5)** with either HBF_4 etherate or 2,6-dimethoxypyridinium tetrafluoroborate.

*2.25 Release of methane from **B7** and **B4a** by thermolysis*

To determine if the ligand protonated complex **B7** could release methane directly without an additional proton source, thermolysis studies were undertaken. Thermolysis of **B7** was first attempted in acetonitrile. In contrast to ligand protonated N-H Pt^{II}-CH_3 species which are reported to eliminate methane at low temperatures or upon warming to room temperature,[14,15] no reaction occurred upon heating **B7** in a sealed J. Young NMR tube up to 140 °C by ^{1}H NMR spectroscopy. Upon heating to 120 °C in the presence of H_2O, a potential proton shuttle, **B7** liberated a mixture of CH_4 and CH_3D and at least two new metal complexes formed, neither of which contained an N-

H resonance. Heating for longer times altered the ratios of the two Pt complexes and two broad ^{1}H NMR resonances increased in intensity around 6 ppm. The compound corresponding to these broad resonances was isolated. Upon analyzing by GC-MS, it was revealed that acetamide was being formed from solvent hydrolysis. At 0.1 mol % loading, 10 turnovers were observed. Several Pt complexes have been shown to perform acetonitrile hydrolysis, with much milder conditions

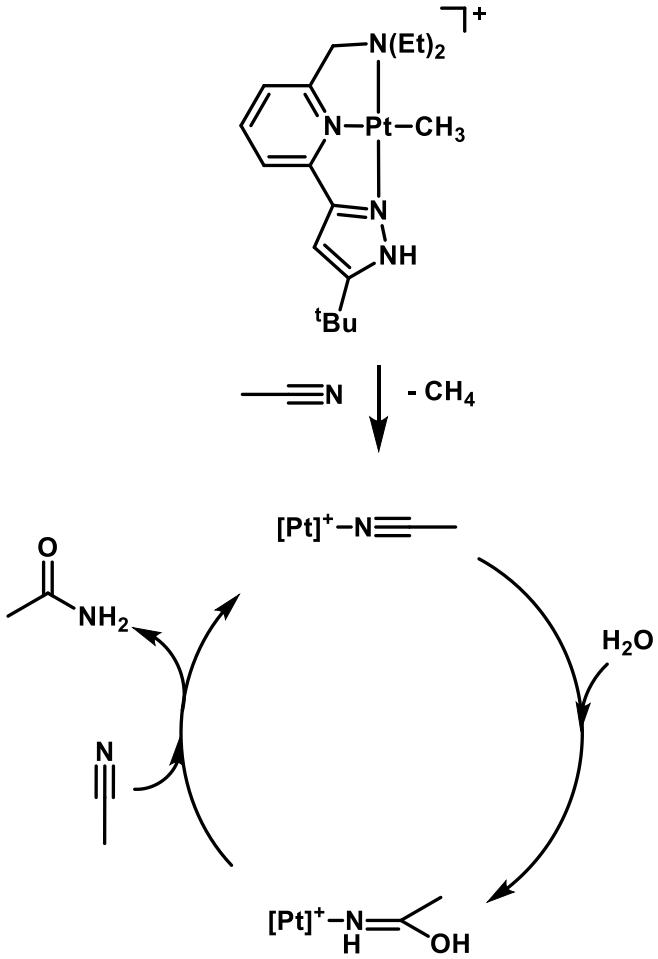

Figure 2.0 4 Potential mechanism of acetonitrile hydrolysis.

and with higher TONs, so this reaction was not further pursued.[29,30] A potential mechanism based on known Pt acetonitrile hydrolysis catalyst is presented in Figure 2.06.[29]

In contrast to experiments in acetonitrile, methane elimination (CH_4 only) was observed when **B7** was subjected to elevated temperatures (100 °C) in C_6D_6 (Figure 2.07).. After three days, the disappearance of starting material was accompanied by the appearance of multiple Pt species (with no N-H resonances) as detected by ^1H NMR spectroscopy, along with deposition of Pt black on the sides of the reaction vessel. Characterization of the reaction mixture by ESI-MS also revealed numerous species. The two major species exhibited an *m/z* of 565 and 481, consistent with the formation of $[Pt(^{D}NNN^{Et})(C_6D_5)]^+$ and $Pt(^{*}NNN^{Et})^+$, respectively.

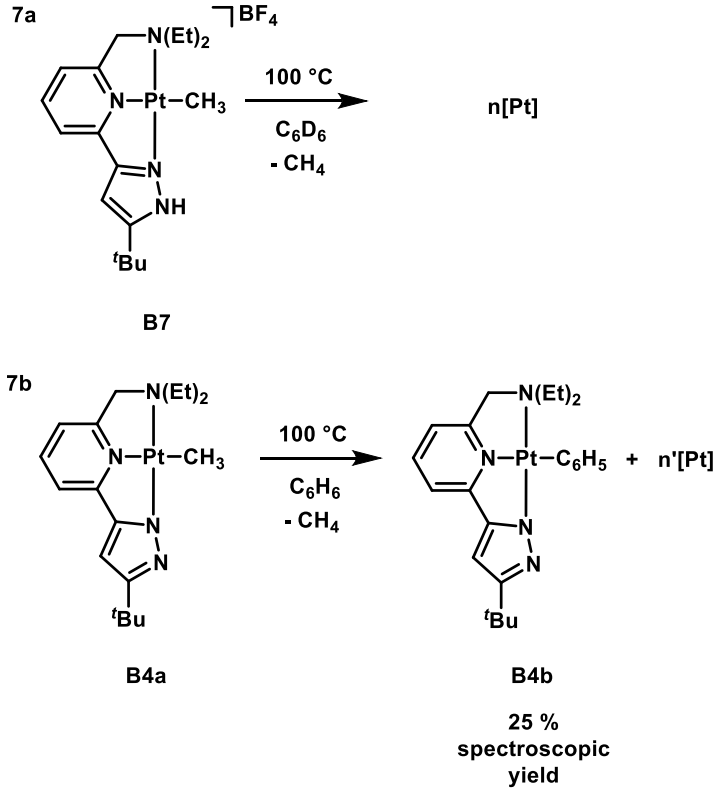

Figure 2.0 5 a) Thermolysis of **B7** in C_6D_6 to form multiple Pt. **b**) Thermolysis of **B4a** in C_6H_6 to form **B4b** and multiple Pt.

Notably, it appears that the proton that combined with the Pt-CH_3 group to form CH_4 did not arise from the ligand-based N-H moiety. Thermolysis of the analogous **B4a**, which lacks a N-H functionality, also eliminated methane under similar conditions. After three days at 100 °C, ^{1}H NMR spectroscopy in C_6D_6 revealed multiple products and redissolution of the reaction mixture in CD_2Cl_2 revealed at least two minor products and one major product. The reaction mixture exhibited an *m/z* of 565 and 481, consistent with the formation of $[Pt(^{D}NNN^{Et})(C_6D_5)]^+$ and $Pt(^{*}NNN^{Et})^+$, respectively, under mass spectroscopy conditions. As the same products were observed by ESI-MS after the thermolysis of **B7**, this suggests the origin of the acidic proton is not from the pyrazolate N-H moiety. Examination of the ^{2}H NMR spectrum (Figure 2.08) of the thermolysis reaction mixture of **B4a** in C_6D_6 revealed two broad singlets at 2.80 ppm and 2.99 ppm, indicating deuteration of the

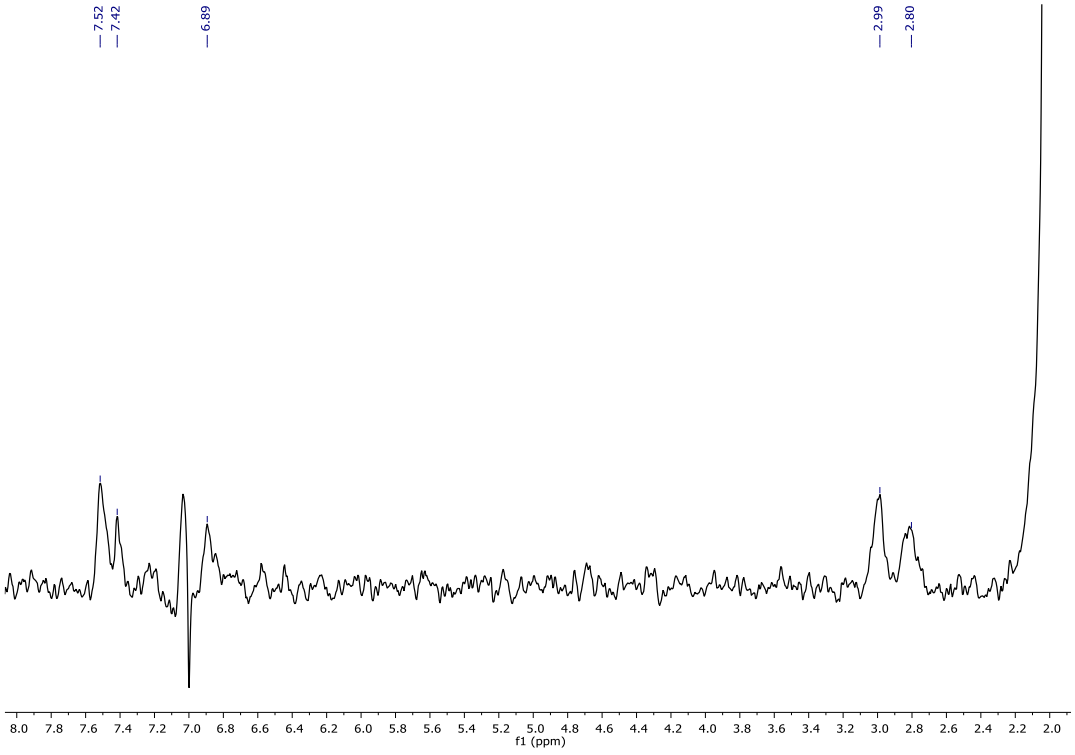

Figure 2.0 6 ^{2}H NMR spectrum (107 MHz) in C_6H_6 of the thermolysis of **B1** in C_6D_6. Referenced to additional CD_3CN at 1.94 ppm. Deuterated methylene deuterons at 2.7 - 3.1 ppm. Aryl Pt-C_6D_5 deuterons at 6.8 – 7.6 ppm.

diethyl amine CH_2 arm. Further confirmation of the major product of the thermolysis reaction was achieved when thermolysis of **B4a** in benzene-H_6 yielded Pt(*NNN)$^{Et}C_6H_5$ (**B4b**, 25 % spectroscopic yield by ^{1}H NMR spectroscopy, Figure 2.07). An authentic sample was added to the reaction mixture to confirm the identity.

These observations are consistent with a mechanism for the deuterium incorporation where, at elevated temperatures, dissociation of the hemilabile amine arm (Figure 2.09A) allows for intramolecular C-H activation of the CH_2 alkyl on the amine to generate a cyclometallated Pt^{IV} species (Figure 2.09B).[31] Reductive elimination of methane (Figure 2.09C), followed by oxidative

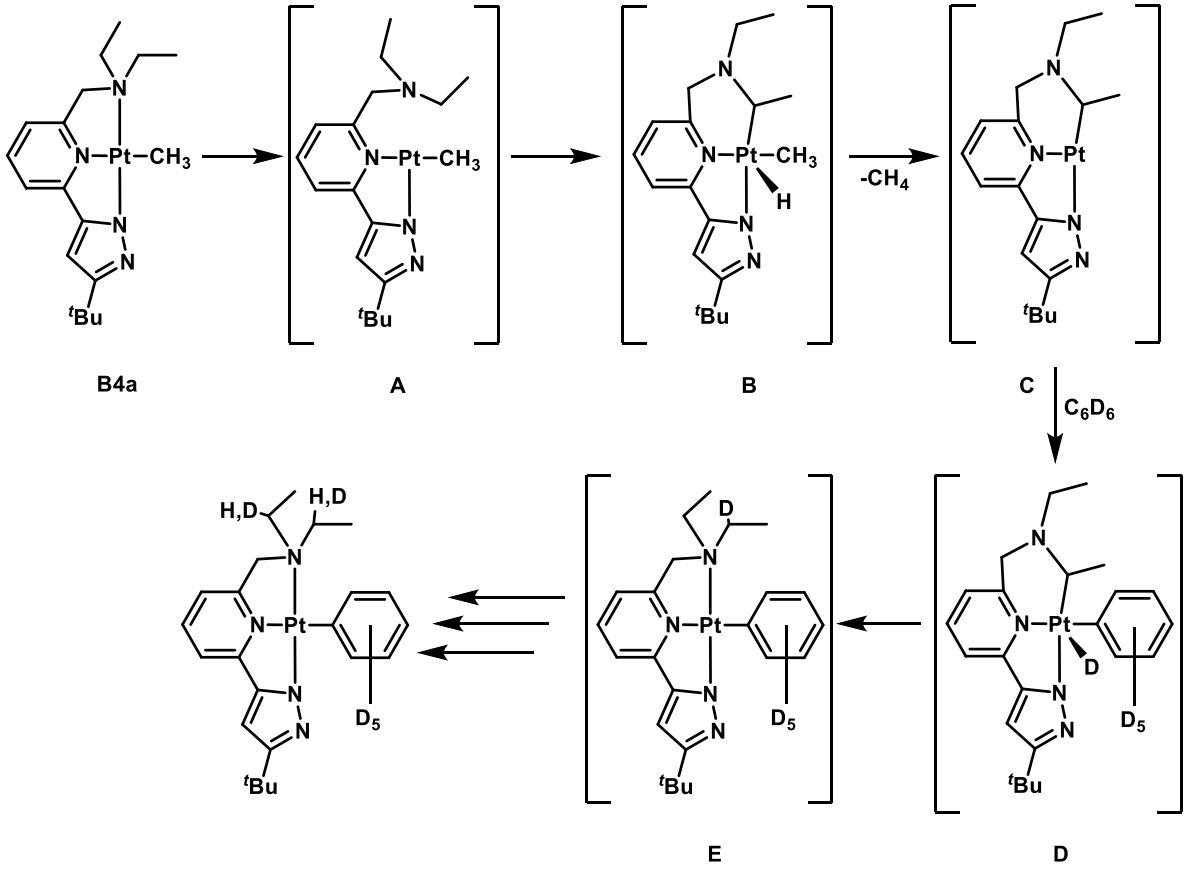

Figure 2.0 7 Potential mechanism for the thermolysis of **B4a** in C_6D_6 to form CH_4 and Pt-C_6D_5.

addition of C_6D_6 solvent (Figure 2.09D) and subsequent reductive elimination of the amine alkyl with the deuteride on the metal (Figure 2.09E), generates the Pt^{II}-C_6D_5 product. Further evidence that the N-H functionality is not involved in the methane elimination was provided by the thermolysis of the deuterated version of **B4a**, Pt(^{D}NNN)^{Et}CH$_3$ (generated by stirring **B4a** in a D_2O/THF (1:4) mixture), which resulted in exclusive elimination of CH_4 (i.e. no CDH_3 was detected by ^{1}H NMR spectroscopy).

*2.26 Reactivity of **Pt(*NNN)^{Et}X** Under Basic Conditions and in the Presence of Exogeneous Ligands*

Reactivity of **B4a** has previously been studied under acidic and neutral conditions (sect. 2.24 and 2.25) and it was determined that the metalated tridentate ligand is not always innocent in the observed reactions. The behavior of the metalated hemilabile ligand on Pt was additionally

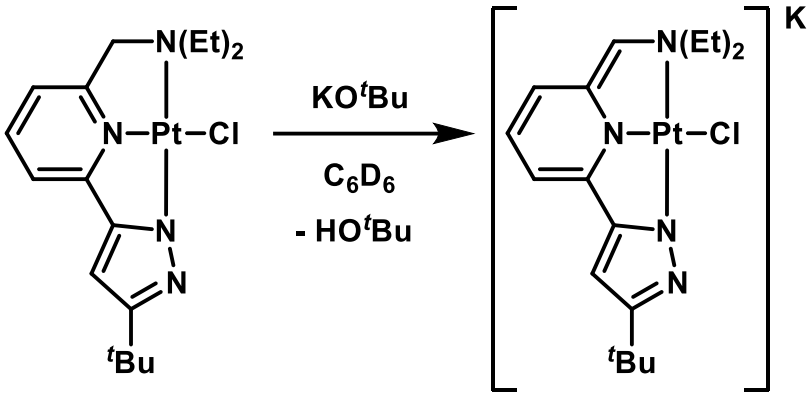

B5 **B5b**

Figure 2. 10 Reaction of **B5** with KO^{t}Bu in C_6D_6 to form **B5b** *in situ*.

investigated under basic conditions. Reaction of **B4a** in C_6D_6 with greater than 4 equivalents of NEt_3 or KO^{t}Bu resulted in no reaction by ^{1}H NMR spectroscopy. Reaction of **B5**, a Pt-Cl analogue of **B4a**, with 1 equiv of KO^{t}Bu in C_6D_6 led to a change from yellow to a bright red solution. A mixture

of new Pt species with broad ^{1}H NMR resonances was observed. Conversion to a single new species, with signals downfield of **B5** by ^{1}H NMR spectroscopy, was achieved after addition of at least 1 more equiv. (total of at least 2 equiv.) of base. Complex **B5b**, presumed to be [K][Pt(*NN$^{\#}$N)^{Et}Cl] (Figure 2.10, $^{\#}$ denotes deprotonation of methylene arm) exhibited broad features by ^{1}H NMR spectroscopy, including a reduction in the relative intensity of the methylene signal from 2H to 1H, as compared to the other ^{1}H resonances for **B5**. Broad ^{1}H NMR signals suggest an exchange process, perhaps with generated *tert*-butanol, whose signals migrated upfield as additional base was added. **B5b** was not isolated. Additionally, reaction of **B4a** (Pt-CH_3) with two or more equivalents of NaO^{t}Bu in CD_3CN caused the resonance of the methylene arm at 4.33 ppm to disappear completely, with no shift in any other resonance, by ^{1}H NMR spectroscopy (Figure 2.11). This suggests either potential deuteration at the methylene arm position from CD_3CN solvent or a rapid exchange process at the methylene C-H position (Figure 2.11(a)), broadening the resonance to the baseline. Attempts to isolate this complex always lead to reappearance of **B4a** (i.e. the methylene proton in the ^{1}H NMR spectrum). However, examination of the reaction mixture by ^{2}H NMR spectroscopy in C_6H_6 exhibits a broad singlet at 2.92 ppm, suggesting deuteration of the methylene arm (methylene CH_2 resonances of **B4a** are exhibited at 3.01 ppm in the ^{1}H NMR spectrum in C_6D_6). Both deprotonation experiments suggest the most acidic proton of **B4a** is not the CH_2 proton of the diethyl amine arm, but instead is that of the methylene linker position. As methane elimination is believed to arise from

the CH_2 of the ethyl groups on the amine arm, this suggests the most acidic proton on **B4a** does not facilitate methane elimination upon thermolysis.

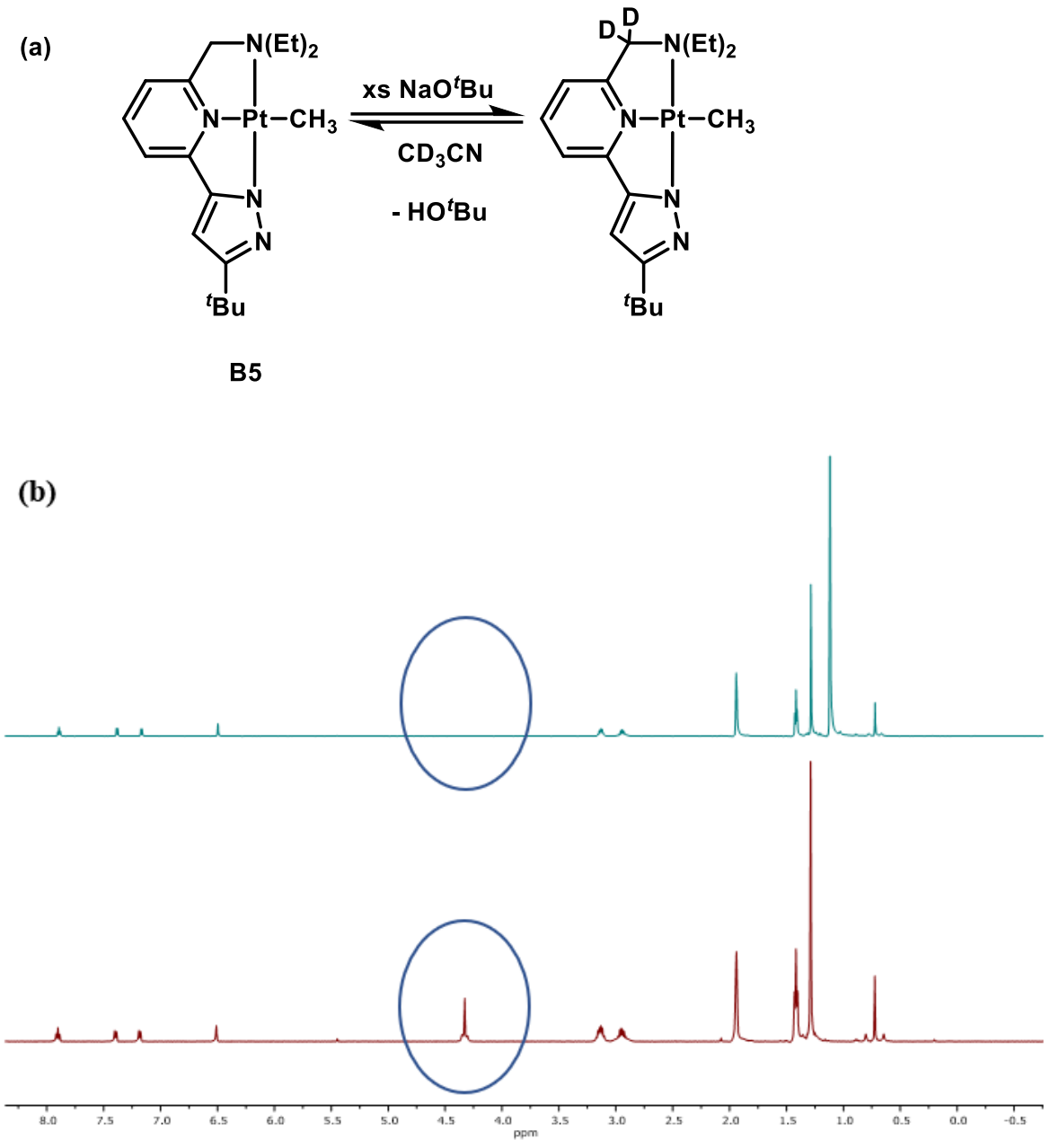

Figure 2.1 1 (a) Proposed reaction resulting in disappearance of methylene proton resonance in the ^{1}H NMR spectrum by deuteration. (b). ^{1}H NMR spectrum of **B4a** in CD_3CN (bottom) and after addition of 2 equiv. of NaO^{t}Bu (top). The methylene proton resonance at 4.33 ppm is no longer present in the top spectrum after the addition of base.

Confirmation of hemilability of the diethyl amine arm to facilitate C-H activation was confirmed by a ligand exchange study. Addition of an excess of pyridine (over 10 equiv.) to **B4a** lead to the disappearance of starting material and appearance of two new Pt species by ^{1}H NMR spectroscopy. One of the new complexes contained an unbound diethyl amine arm by ^{1}H NMR spectroscopy, and numerous new resonances in the aromatic region by ^{1}H NMR spectroscopy. It is noted that de-chelation of the diethyl amine arm is evident by examination of the ^{1}H NMR spectrum where the methylene arm protons are no longer diastereotopic (Figure 2.12). Similar spectral changes

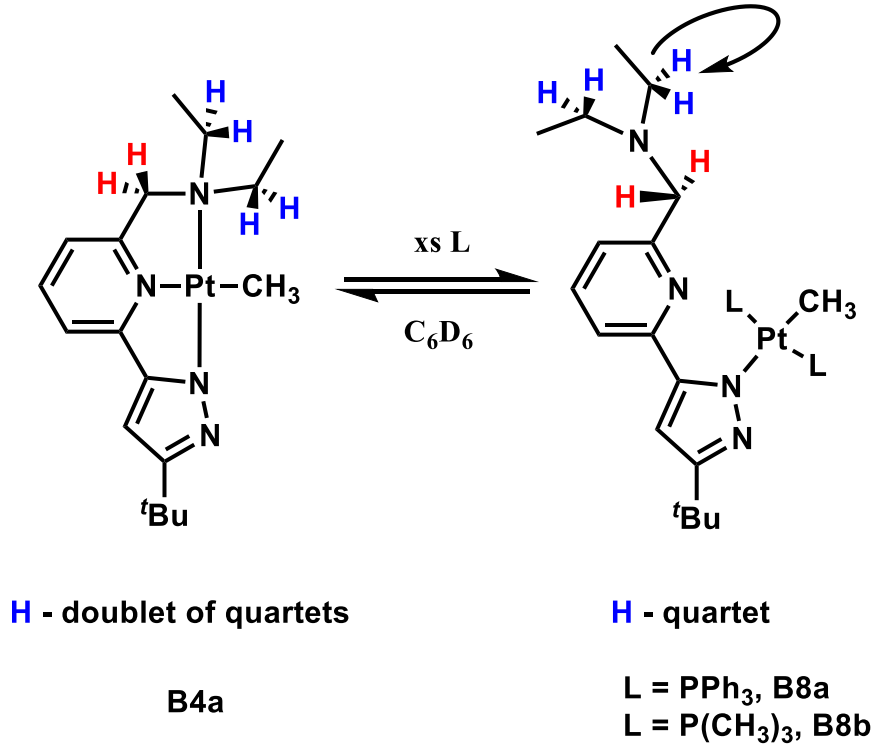

Figure 2.1 2 Reaction of **B4a** with exogeneous L ligands and how methylene protons change in the ^{1}H NMR spectrum

from equivalent to diastereotopic methylene protons are often used to determine chelation of hemilabile ligands.[32] To obtain a single complex, two equivalents of a more strongly coordinating ligand, namely PPh_3, were added to **B4a** in C_6D_6; $Pt(\kappa^1\text{-}*NNN)^{Et}(P(C_5H_6)_3)_2CH_3$ (**B8a**) was cleanly observed *in situ*. The formation of **B8a** was consistent by observations by ^{1}H and ^{31}P NMR

spectroscopy. In the ^{1}H NMR spectrum, the diethyl amine arm is unbound (Figure 2.12) and formation of broad singlet for the Pt-CH_3 resonance with Pt satellites ($^{2}J_{Pt\text{-}H}$ = 58 Hz). The ^{2}J is rather low for a Pt-CH_3 moiety being *trans* to a pyridine ligand and suggests the Pt-CH_3 group is *trans* to stronger pyrazolate donor.[27] In the $^{31}P\{^{1}H\}$ NMR spectrum, appearance of a resonance at 25.19 ppm ($^{1}J_{Pt\text{-}P}$ = 2882 Hz) was observed. Complex **B8a** could not be isolated due to the lability of PPh_3, which was completely removed with reappearance of **B4a** after 5 iterative washes of diethyl ether. Addition of excess $P(CH_3)_3$, a stronger phosphine donor, to a solution of Pt(*NNN)$^{Et}CH_3$ in C_6D_6 generated Pt(κ^1-*NNN)$^{Et}(P(CH_3)_3)_2CH_3$ (**B8b**). **B8b** was isolated and characterized by ^{1}H, $^{31}P\{^{1}H\}$ and $^{13}C\{^{1}H\}$ NMR spectroscopy. Complex **B8b** contains a Pt-CH_3 group with a $^{2}J_{Pt\text{-}H}$ = 72 Hz at 0.60 ppm, which is notably larger than the $^{2}J_{Pt\text{-}H}$ of **B8a** (55 Hz, 0.04 ppm) by ^{1}H NMR spectroscopy, due to reduced sterics on the phosphine ligand.[33] Reaction of **B8b** with excess PPh_3 resulted in no ligand exchange by ^{1}H NMR spectroscopy, confirming the tight binding nature of $P(CH_3)_3$.

2.3 Conclusion

In conclusion, we have reported new Pt^{II} pyrazolate complexes with protic functionality. A series of both Pt^{II} complexes were synthesized, supported by 5-(2-pyridyl)-3-*tert*-butylpyrazolate (**^{H}NN^{H}**), 5-(6-methyl-2-pyridyl)-3-*tert*-butylpyrazolate (**^{H}NN^{Me}**) and 2-(5-*tert*-butylpyrazol-3-yl)-6-(diethylaminomethyl)pyridine **(^{H}NNN)^{Et}** ligands. Metalation of **^{H}NN^{H}** resulted in formation of a homoleptic complex, Pt(*NN^{H})$_2$ (**B1**), however, sterics from the methyl substituent in **^{H}NN^{Me}** prevented homoleptic formation and allowed formation of Pt(*NN^{Me})(S$(CH_3)_2$)CH_3 (**B2a/B2b**). The tridentate nature of **(^{H}NNN)^{Et}** allowed metalation with Pt^{II} to produce Pt(*NNN)$^{Et}CH_3$ (**B4a**), Pt(*NNN)$^{Et}C_6H_5$ (**B4b**), and Pt(*NNN)^{Et}Cl (**B5**). Lability of the diethyl amine moiety of **^{H}NNN^{Et}** when ligated was demonstrated with addition of phosphine ligands to **B4a** to form Pt(κ^1-

*NNN)^{Et}(P(C_5H_6)$_3$)$_2$$CH_3$· (**B8a**) and Pt($\kappa^1$-*NNN)^{Et}(P($CH_3$)$_3$)$_2$$CH_3$· (**B8b**). Conditions necessary for methane elimination were probed for **B2a**/**B2b** and **B4a** at room temperature and a series of acid addition experiments revealed methane elimination does not occur until all pyrazolate sites are protonated. Addition of 1 equivalent of HBF_4 etherate to **B2a**/**B2b** or **B4a** formed [Pt(^{H}NN^{Me})(S(CH_3)$_2$)CH_3][BF_4] (**B6a**/**B6b**) or [Pt(^{H}NNN)^{Et}CH_3][BF_4] (**B7**), respectively. The ligand-based N-H is apparently not acidic enough to form methane from Pt^{II}-CH_3 complexes (**B6a**/**B6b** and **B7**) at room temperatures. Thermolysis of bidentate ligated **B6a**/**B6b** at 100 °C did not generate methane, yet, thermolysis of tridentate **B7** did. It was determined that methane generation from the thermolysis of **B7** was not dependent on the ligand-based N-H. Thermolysis of **B4a** (which does not contain an N-H moiety) also eliminated methane. Activation of the benzene solvent to generate complex **B4b** was observed. Upon further examination of the thermolysis reaction, methane loss and benzene activation likely proceeded through oxidative addition of a C-H bond of the ethyl group on the NEt_2 moiety, followed by reductive elimination, and not through a N-H, methyl coupling. Additionally, reactivity of **B4a** under basic conditions was investigated and the results were consistent with deprotonation of the methylene CH_2 moiety upon addition of base.

2.4 Experimental

2.41 General Experimental

All manipulations were carried out under nitrogen atmosphere using standard Schlenk and glovebox techniques unless otherwise noted. Deuterated solvents were purchased from Cambridge Isotope Laboratories. Dry and O_2 free tetrahydrofuran, benzene, pentane, methylene chloride, acetonitrile, and diethyl ether were obtained by means of a Grubbs-type solvent purification system.[34] THF-d_8 and C_6D_6 were dried over sodium/benzophenone ketyl and were vacuum

transferred prior to use. Acetone-d_6 and CD_3CN were dried over activated 3 Å molecular sieves. CD_2Cl_2 was dried over calcium hydride and vacuum transferred prior to use. $PtCl_2(S(CH_3)_2)_2$, $Pt(C_6H_5)_2(S(CH_3)_2$ and $[Pt(CH_3)_2(\mu\text{-}S(CH_3)_2)]_2$ were synthesized following literature preparations.[35,36] All NMR spectra were obtained on a Bruker Avance 500 or Bruker Avance 400 MHz instrument. NMR spectra were recorded at 300 K. Chemical shifts are reported in units of parts per million (ppm) downfield of TMS and referenced against residual protonated solvent resonances (^1H) and characteristic solvent resonances (^{13}C). $^{31}P\{^1H\}$ NMR spectra were referenced externally to H_3PO_4 (85%, 0 ppm) and ^2H NMR spectra were referenced to the deuterium resonance of extra added CD_3CN (δ 1.94). $^{19}F\{^1H\}$ NMR spectra were referenced externally to C_6H_5F (-113.15 ppm). NMR tubes fitted with a J-Young style Teflon valve were used to obtain inert atmosphere NMR data. The C, N, H elemental analyses were carried out at the CENTC Elemental Analysis Facility at the University of Rochester. Accurate mass measurement analyses were conducted on a LCMS with electrospray ionization (ESI). Samples were taken up in a suitable solvent for analysis. The signals were mass measured against an internal lock mass reference of leucine enkephalin for ESI-LCMS. Waters software calibrates the instruments, and reports measurements, by use of neutral atomic masses. The mass of the electron is not included. Nominal mass accuracy ESI-MS data were obtained by use of a Waters Acquity UPLC system equipped with a Waters TUV detector (254 nm) and a Waters SQD single quadrupole mass analyzer with electrospray ionization.

2.42 Synthesis, Characterization and Spectroscopic Data

Pt(*NN)$_2$ (**B1**)

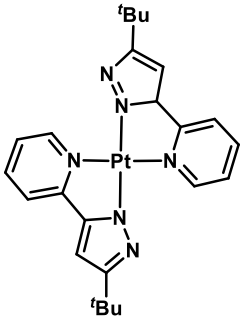

A J. Young NMR tube was charged with $^{\mathbf{H}}$**NN**$^{\mathbf{H}}$ (10.0 mg, 0.0497 mmol) and [Pt(CH$_3$)$_2$(S(CH$_3$)$_2$)]$_2$ (14.3 mg, 0.0248 mmol). CD_2Cl_2 was vacuum transferred to the J. Young tube and the sample was heated for 24 hrs at 60 °C and for 24 hrs at 100 °C. The J. Young NMR tube was cooled to -35 °C overnight and some solid was observed at the bottom of the NMR tube. The liquid was decanted and discarded, and the solid was dissolved in C_6D_6 and an NMR spectrum was recorded.

^{1}H NMR (500 MHz, $CDCl_3$) δ 10.82 (2H, d, pyr, $^3J_{H\text{-}H}$ = 5.9 Hz), 7.84 (1H, t, pyr, $^3J_{H\text{-}H}$ = 7.9 Hz), 7.57 (1H, d, pyr ($^3J_{H\text{-}H}$ = 7.9 Hz)), 7.20 (1H, pyr, m) 6.51 (1H, pyz, s), 1.44 (18H, ^{t}Bu, s).

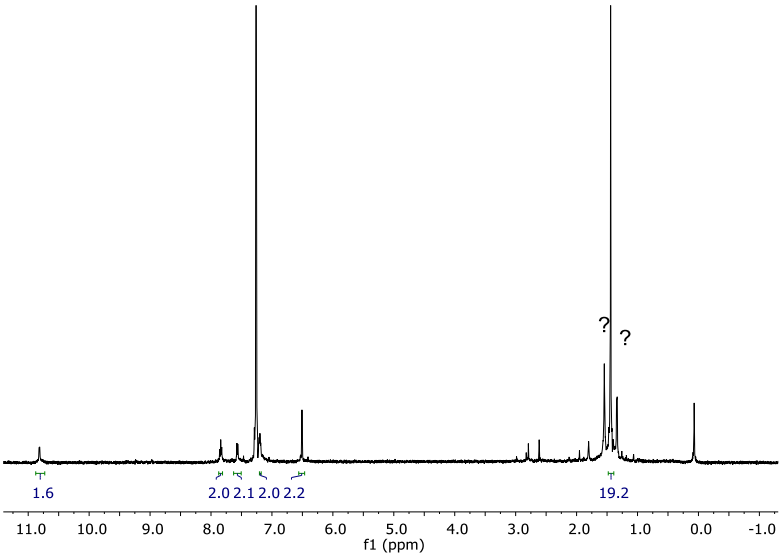

Figure 2.13 ^{1}H NMR spectrum (500 MHz) of **B1** in C_6D_6.

Pt(*NN)($S(CH_3)_2$)(CH_3) **(B2a or B2b**)

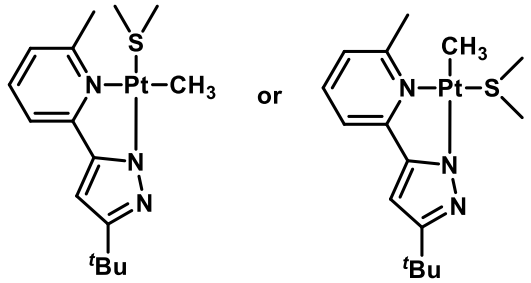

B2a **B2b**

A 50 mL Schlenk flask was charged with the ^{H}**NN**^{Me} (69.5 mg, 0.324 mmol), $Pt(S(CH_3)_2)_2Me_2$ (94.0 mg, 0.162 mmol) and dissolved in THF (5 mL) under inert atmosphere. A reflux condenser was attached under positive nitrogen flow and the solution was heated at reflux for 90 minutes. The solution was then cooled to room temperature and the volatiles were removed in vacuo to yield a yellow solid. **B2** was confirmed as the major product by ^{1}H NMR spectroscopy. The

following observations are noted. **B2** was soluble in pentane (slightly), ether, DCM, benzene, THF, CH_3CN, and MeOH and decomposed when run through silica, neutral and basic alumina plugs. Attempts to precipitate or crystallize out of concentrated pentane solutions did not produce cleaner ^{1}H NMR spectra.

^{1}H NMR (500 MHz, Methanol-d_4) δ 7.74 (1H, t, pyr, $^3J_{H\text{-}H}$ = 7.7 Hz), 7.55 (1H, d, pyr, $^3J_{H\text{-}H}$ = 7.8 Hz), 7.10 (1H , d, pyr, $^3J_{H\text{-}H}$ = 7.6 Hz), 6.54 (1H, pyz, s), 2.78 (3H, s, CH_3), 2.49 (s, 6H, SMe_2, $^3J_{Pt\text{-}H}$ = 52.0 Hz), 1.39 (3H, s, Pt-Me, $^2J_{Pt\text{-}H}$ = 83.5 Hz), 1.33 (9H, s, ^{t}Bu).

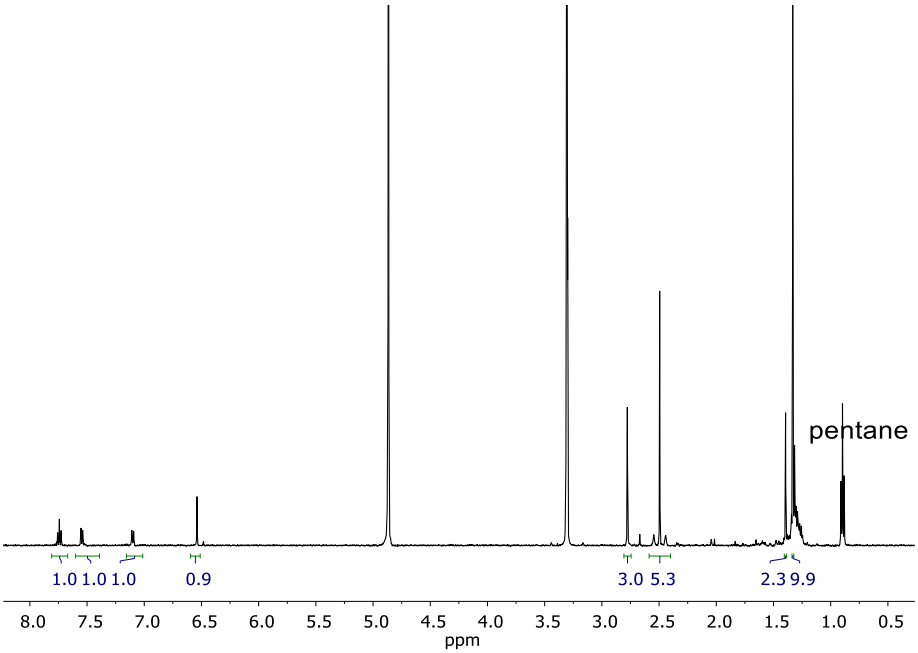

Figure 2.14 ^{1}H NMR spectrum (500 MHz) of **B2** in methanol-d_4.

Pt(*NN)^{Me}(PPh_3)(CH_3) (**B3**)

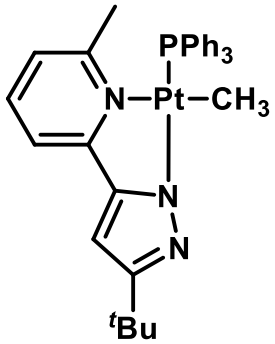

A 20 mL scintillation vial was charged with the **B2a**/**B2b** (2.2 mg, 0.0045 mmol), PPh_3 (1.2 mg, 0.0046 mmol), and a Teflon stir bar and dissolved in diethyl ether (1 mL) under inert atmosphere. After vigorous stirring for 40 minutes, the solvent was removed under reduced pressure to yield a yellow solid. **B3** was confirmed as the major product by ^{1}H NMR spectroscopy. The following observations were noted. **B3** was soluble in methanol, pentane and ether. Decomposition to multiple products was observed by ^{1}H NMR spectroscopy when samples of **B3** run through a diatomaceous earth plug.

^{1}H NMR (500 MHz, Methanol-d_4) δ 7.81-7.65 (7H, m, PPh_3), 7.62 (1H, d, pyr, $^3J_{H\text{-}H}$ = 7.3 Hz), 7.54-7.28 (9H , m, PPh_3), 6.80 (1H, s, pyr, $^3J_{H\text{-}H}$ = 6.9 Hz), 6.63 (1H, s, pyz), 1.80 (3H, s, CH_3), 1.36 (9H, s, Pt-Me, ^{t}Bu), 0.97 (3H, d, $^3J_{H\text{-}P}$ = 5.0 Hz, $^2J_{Pt\text{-}H}$ = 83.5 Hz). ^{31}P{^{1}H} NMR (162 MHz, Methanol-d_4) δ 18.22 ($^1J_{Pt\text{-}P}$ = 4186 Hz). ESI-MS: [Pt(^{H}NN^{Me})(CH_3)(PPh_3)]$^+$ Theoretical Mass, *m/z* = 687.2; Observed Mass, *m/z* = 687.5

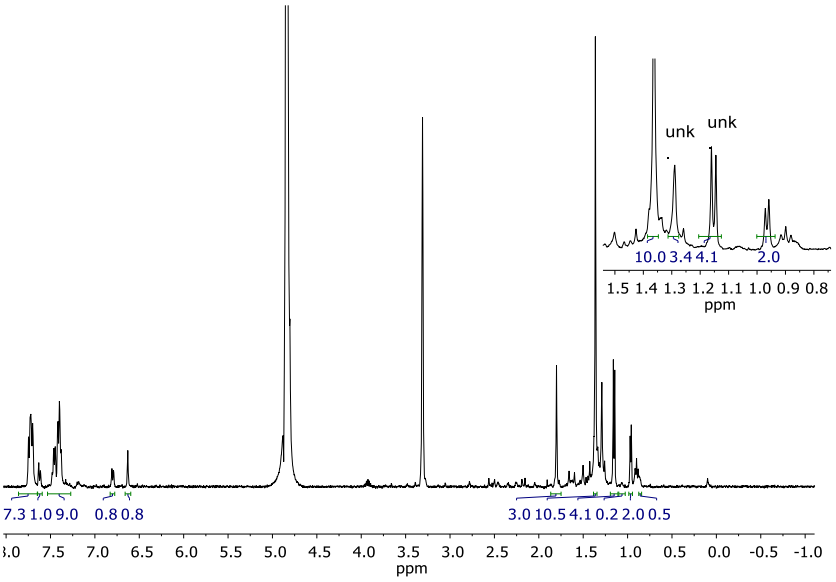

Figure 2.15 ^{1}H NMR spectrum (500 MHz) of **B3** in methanol-d_4.

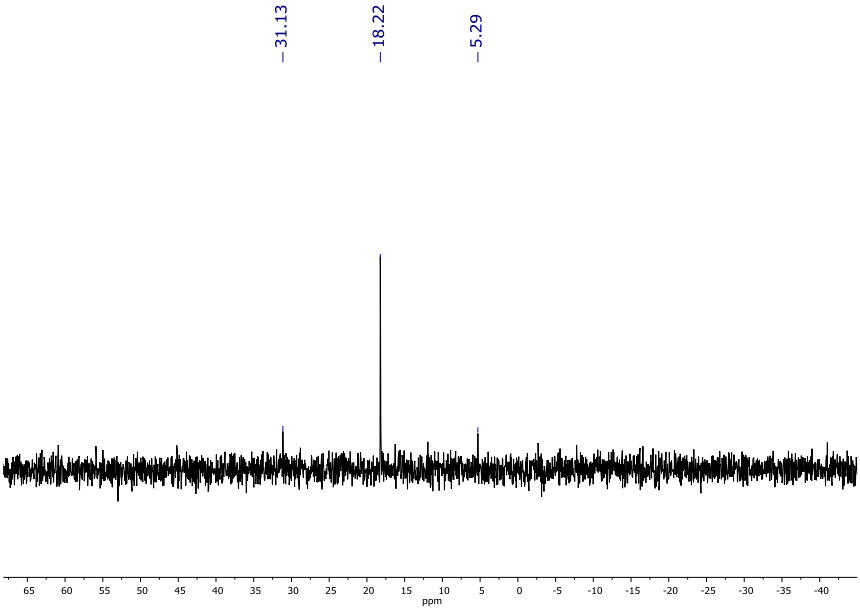

Figure 2.16 ^{31}P{^{1}H} NMR spectrum (500 MHz) of **B3** in methanol-d_4.

Synthesis of Pt(*NNN)^{Et}CH$_3$ **(B4a)**

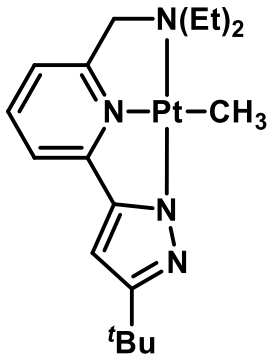

A 20 mL scintillation vial was charged with a Teflon stir bar, 58.4 mg (0.204 mmol) of **^{H}NNN^{Et}**, 58.6 mg (0.102 mmol) [Pt(μ-S(CH$_3$)$_2$)(CH$_3$)$_2$]$_2$ and 4 mL CH$_2$Cl$_2$. The reaction was vigorously stirred for 20 minutes. The solvent was removed *in vacuo* and the remaining solid was then triturated (2 x 2 mL) with pentane and further dried to yield an orange solid (80.1 mg, 79.2 %). ^{1}H NMR (CD$_2$Cl$_2$, 500 MHz): δ 7.83 (1H, t, pyr, $^3J_{H\text{-}H}$ = 7.9 Hz), 7.32 (1H, d, pyr, $^3J_{H\text{-}H}$ = 7.9 Hz), 7.08 (1H, s, pyr), 6.48 (1H, d, pyz, $^3J_{H\text{-}H}$ = 7.9 Hz), 4.23 (2H, t, CH$_2$, $^4J_{Pt\text{-}H}$ = 22 Hz), 3.20 (2H, multiplet, CH$_2$), 2.95 (2H, multiplet, CH$_2$), 1.48 (6H, t, CH$_3$, $^3J_{H\text{-}H}$ = 7.0 Hz), 1.34 (9H, s, CH$_3$), 0.83 (3H, s, Pt-CH$_3$, $^2J_{Pt\text{-}H}$ = 78 Hz). ^{13}C{^{1}H} (CD$_2$Cl$_2$, 126 MHz): δ 161.50(s), 155.98(s), 151.65(s), 137.95(s), 116.43(s), 115.99(s), 100.68(s), 69.63(s), 59.28(s), 32.69(s), 31.20(s), 13.12(s), -15.26(s). Elemental Analysis: Anal. For C$_{18}$H$_{28}$N$_4$Pt: Calc: C, 43.63; H, 5.70; N, 11.31. Found: C, 43.26; H, 5.57; N, 11.35.

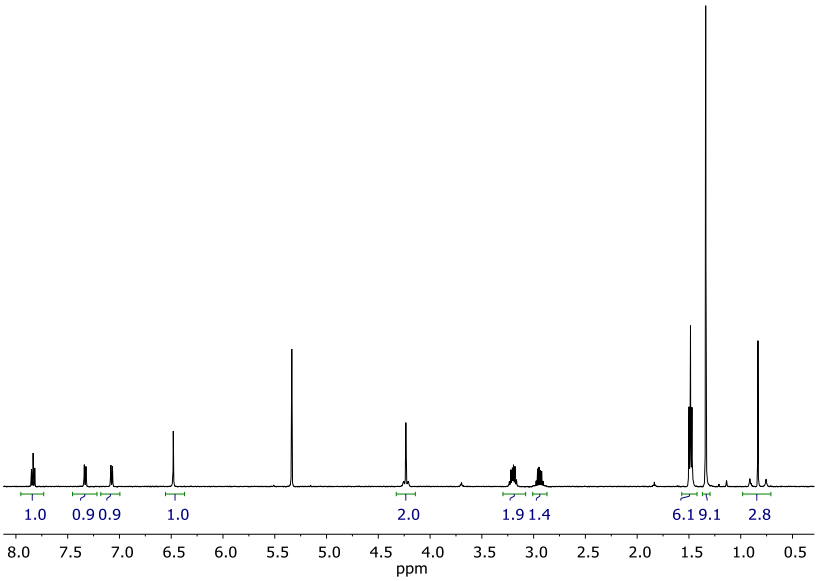

Figure 2.17. ^{1}H NMR spectrum (500 MHz) of **B4a** in CD_2Cl_2

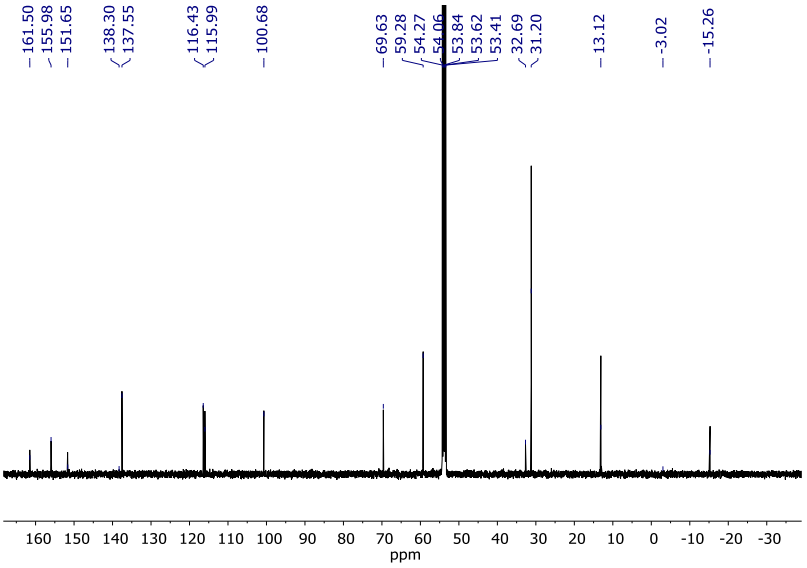

Figure 2.18. $^{13}C\{^{1}H\}$ NMR spectrum (126 MHz) of **B4a** in CD_2Cl_2

Synthesis of $Pt(*NNN)^{Et}C_6H_5$ **(B4b)**

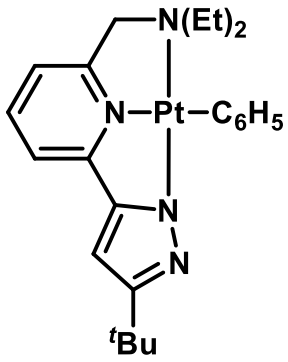

A J. Young NMR tube was charged with $Pt(S(CH_3)_2)_2(C_6H_5)_2$ (7.0 mg, 0.0147 mmol), ^{H}**NNN**^{Et} (4.2 mg, 0.0147 mmol), and 0.5 mL CD_2Cl_2. The reaction was heated to 60 °C for 2.5 hours. After cooling, the yellow solution was concentrated to ~0.1 mL in a 20 mL scintillation vial in air. Diethyl ether (2 mL) was then added until a yellow solid appeared, forming a suspension. The

supernatant was decanted, and the remaining solid washed with pentane (1 x 2 mL), and then dried to obtain a pale yellow solid (6.6 mg, 81 %). ^{1}H (400 MHz, CD_2Cl_2): δ 7.84 (1H, t, pyr-H ($^{3}J_{H\text{-}H}$ = 8.0 Hz)), 7.53 (2H, d, pyr-H ($^{3}J_{H\text{-}H}$ = 7.0 Hz, $^{3}J_{Pt\text{-}H}$ = 39.4 Hz)), 7.37 (1H, d, pyr-H ($^{3}J_{H\text{-}H}$ = 8.0 Hz)), 7.14 – 7.00 (3H, m, Ar-H and pyr-H overlapping), 6.92 (1H, t, Ar-H ($^{3}J_{H\text{-}H}$ = 7.3 Hz)), 6.48 (1H, s, pyz-H), 4.31 (2H, s, CH_2), 3.10 (2H, dq, CH_2 ($^{2}J_{H\text{-}H}$ = 10.4, $^{3}J_{H\text{-}H}$ = 7.1 Hz)), 2.79 (2H, dq, CH_2 ($^{2}J_{H\text{-}H}$ = 13.7, $^{3}J_{H\text{-}H}$ = 7.0 Hz)), 1.53 (6H, CH_3 ($^{3}J_{H\text{-}H}$ = 7.1 Hz)), 1.27 (9H, s, CH_3). ^{13}C{^{1}H} (CD_2Cl_2, 126 MHz): δ 162.08(s), 157.33(s), 152.21(s), 151.61(s), 147.41(s), 138.70(s), 137.92(s), 127.02(s), 122.57(s) 116.38(s), 115.41(s), 101.13(s), 69.21(s), 59.97(s), 32.62(s), 31.15(s), 13.27(s). ESI-MS: $[Pt(^{H}NNN^{Et})C_6H_5]^+$ Theoretical Mass, *m/z* = 557.2176; Observed Mass, *m/z* = 557.2187.

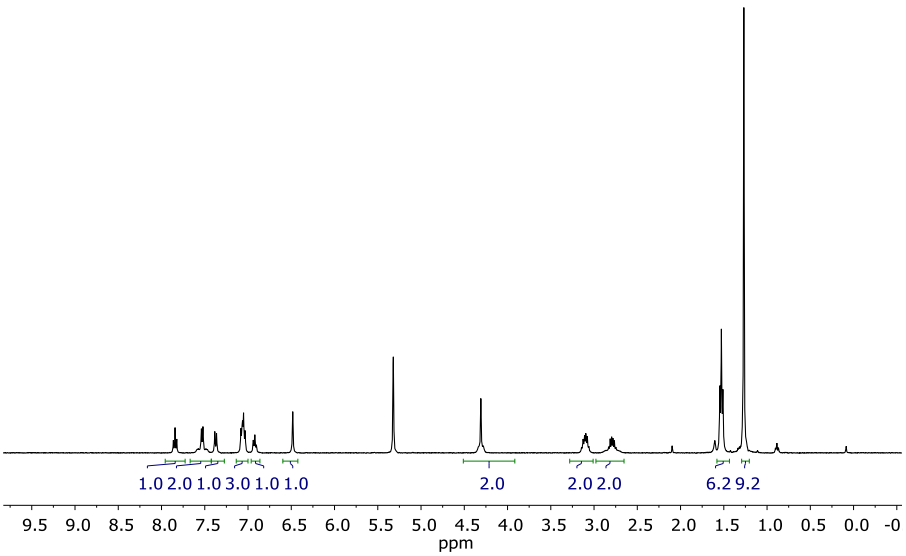

Figure 2.19. ^{1}H NMR spectrum (400 MHz) of **B4b** in CD_2Cl_2.

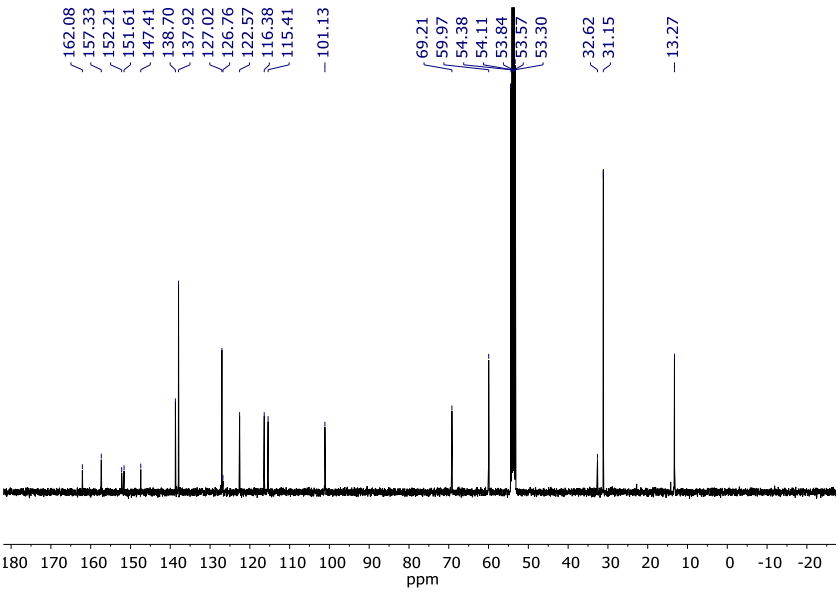

Figure 2.20. $^{13}C\{^{1}H\}$ NMR spectrum (101 MHz) of **B4b** in CD_2Cl_2.

Synthesis of Pt(*NNN)^{Et}Cl **(B5)**

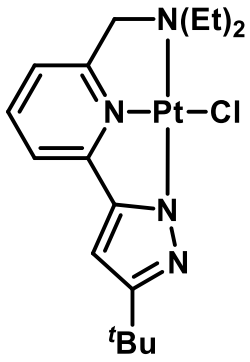

A 20 mL scintillation vial was charged with 35.3 mg (0.123 mmol) of **^{H}NNN^{Et}**, 48.1 mg (0.123 mmol) $Pt(S(CH_3)_2)_2(Cl)_2$, triethyl amine (50 µL, 0.36 mmol) and 4 mL CH_2Cl_2. The reaction was vigorously stirred for 1 hour. The solvent was removed under reduced pressure, and the resulting solid was washed with diethyl ether (3 x 3 mL), and dried in-vacuo (41.9 mg, 66.0 %). ^{1}H NMR (CD_2Cl_2, 500 MHz): δ 7.97 (2H, vt, pyr, $^{3}J_{H\text{-}H}$ = 7.9 Hz, 7.8 Hz), 7.46 (1H, d, pyr, $^{3}J_{H\text{-}H}$ = 7.9 Hz),

7.17 (1H, d, pyr, $^{3}J_{H\text{-}H}$ = 7.8 Hz), 6.57 (1H, s, pyz), 4.39 (2H, s, CH_2), 3.35 (2H, multiplet, CH_2), 2.94 (2H, multiplet, CH_2), 1.53 (6H, t, CH_3, $^{3}J_{H\text{-}H}$ = 7.2 Hz), 1.32 (9H, s, CH_3). $^{13}C\{^{1}H\}$ NMR (CD_2Cl_2, 126 MHz): δ 161.28(s), 158.36(s), 152.82(s), 149.43(s), 138.43(s), 116.28(s), 114.95(s), 100.78(s), 67.53(s), 58.70(s), 30.53(s), 32.27(s), 12.22(s). Elemental Analysis: Anal. For $C_{17}H_{25}ClN_4Pt$: Calc: C, 39.58; H, 4.88; N, 10.86. Found: C, 39.38; H, 4.81; N, 10.63.

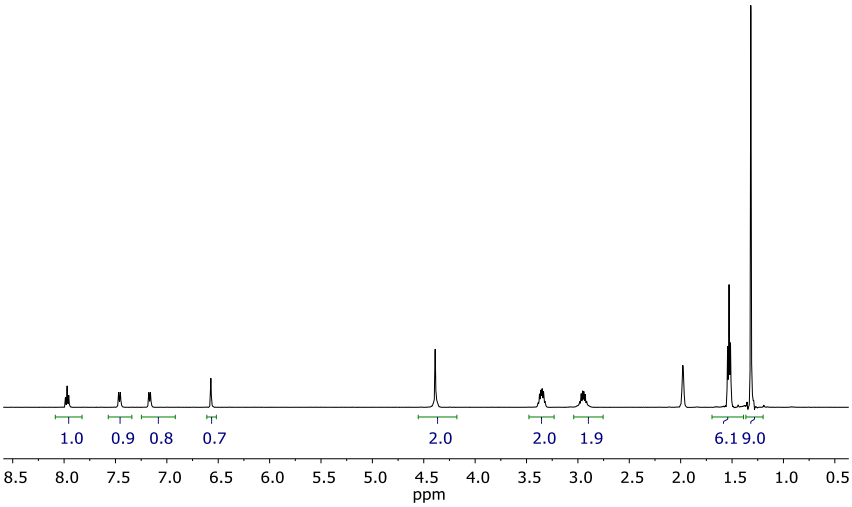

Figure 2.21 ^{1}H NMR spectrum (500 MHz) of **B5** in CD_3CN

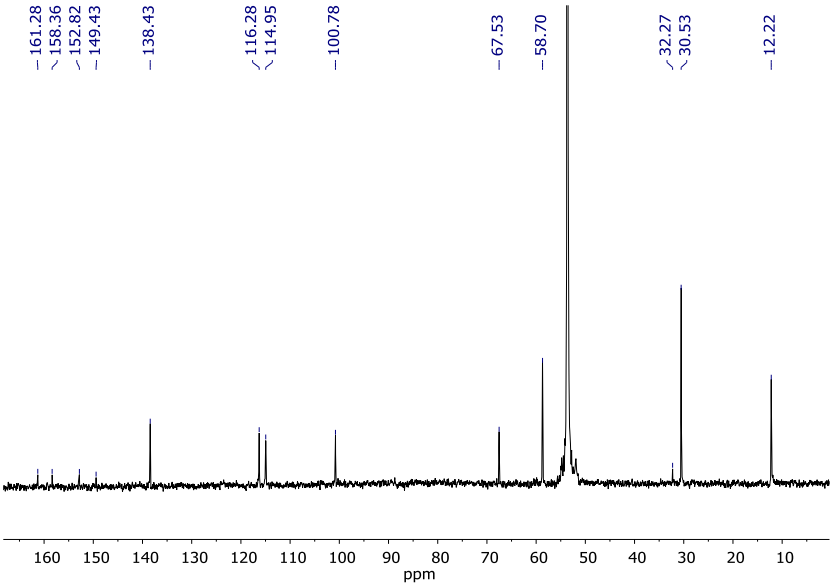

Figure 2.22 $^{13}C\{^{1}H\}$ NMR spectrum (126 MHz) of **B5** in CD_2Cl_2

Synthesis of Pt(^{H}NNN)^{Et}Cl **(B5a)**

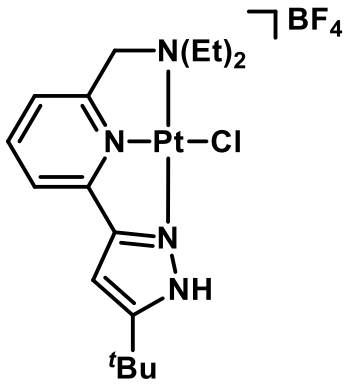

A 20 mL scintillation vial was charged with 7.2 mg (0.014 mmol) **B5**, a Teflon stir bar, 3.2 mg (0.014 mmol) 2,6-dimethoxypyridinium tetrafluoroborate and diethyl ether (3 mL). The suspension was stirred vigorously for 15 minutes. Diethyl ether (5 mL) was added to completely precipitate a very light yellow solid. The mother liquor was decanted, and the resulting solid was triturated with ether (4 mL) and washed with diethyl ether (2 x 3 mL). The solid was collected and dried (8.1 mg, 96 % yield). ^{1}H NMR (CD_2Cl_2, 500 MHz): δ 10.56 (1H, s, N-H), 8.29 (1H, t, pyr, $^{3}J_{H\text{-}H}$ = 8.1 Hz)), 7.86 (1H, d, pyr, $^{3}J_{H\text{-}H}$ = 8.1 Hz), 7.79 (1H, d, pyr, $^{3}J_{H\text{-}H}$ = 8.1 Hz), 6.90 (1H, d, pyz, $^{4}J_{H\text{-}NH}$ = 2.0 Hz), 4.69 (2H, t, CH_2, $^{4}J_{Pt\text{-}H}$ = 16.6 Hz), 3.42 (2H, dq, CH_2, $^{2}J_{H\text{-}H}$ = 12.7, $^{3}J_{H\text{-}H}$ = 7.2 Hz), 3.06 (2H, dq, CH_2, $^{2}J_{H\text{-}H}$ = 12.7, $^{3}J_{H\text{-}H}$ = 6.9 Hz), 1.57 (6H, t, CH_3, $^{3}J_{H\text{-}H}$ = 7.1 Hz), 1.44 (9H, s, CH_3), ^{13}C{^{1}H} (CD_2Cl_2, 126 MHz): δ 161.91 (s), 158.12 (s), 154.51 (s), 148.27 (s), 141.33 (s), 122.60 (s), 121.49 (s), 103.35 (s), 69.81 (s), 60.85 (s), 32.62 (s), 29.87 (s), 13.24 (s). ^{19}F{^{1}H} NMR (CD_2Cl_2, 377 MHz): δ -151.68 (s), -151.73 (s). ESI-MS: [Pt(^{H}NNN)^{Et}Cl]$^{+}$ Theoretical Mass, *m/z* = 515.1473; Observed Mass, *m/z* = 515.1456.

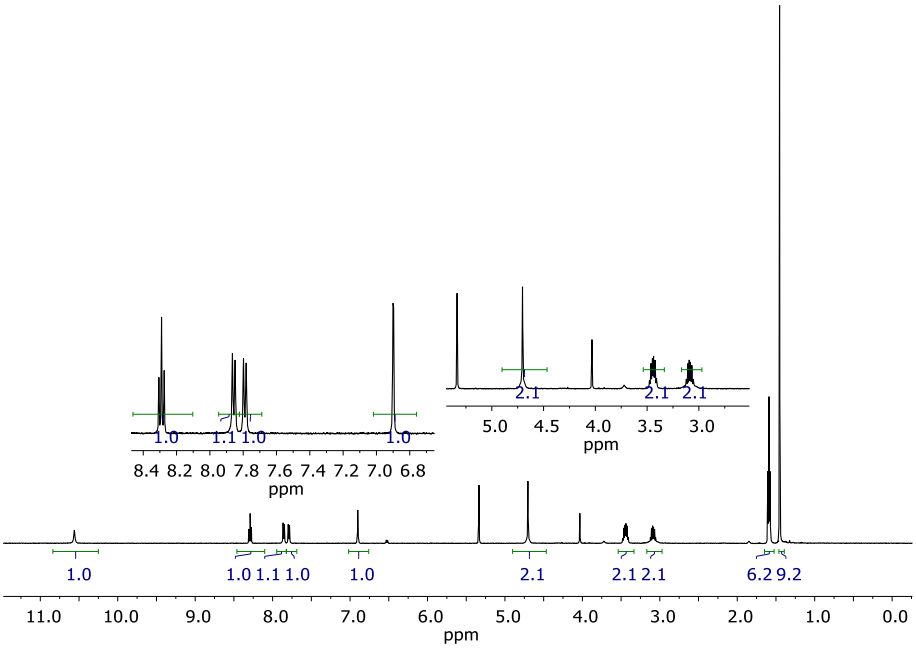

Figure 2.23. ^{1}H NMR spectrum (500 MHz) of **B5a** in CD_2Cl_2. A small amount of 2,6-dimethoxypyridinium tetrafluoroborate could not be removed and is observed at 7.85 (t), 6.49 (d) and 4.00 (s) ppm.

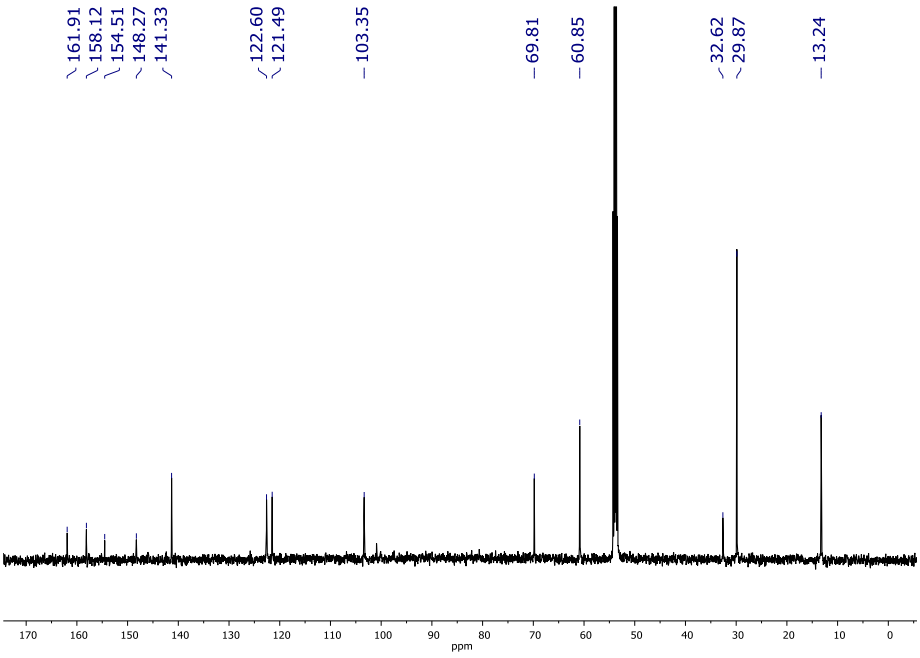

Figure 2.24. ^{13}C{^{1}H} NMR spectrum (126 MHz) of **B5a** in CD_2Cl_2. A small amount of 2,6-dimethoxypyridinium tetrafluoroborate could not be removed and is observed at 100.91 and 125.82 ppm.

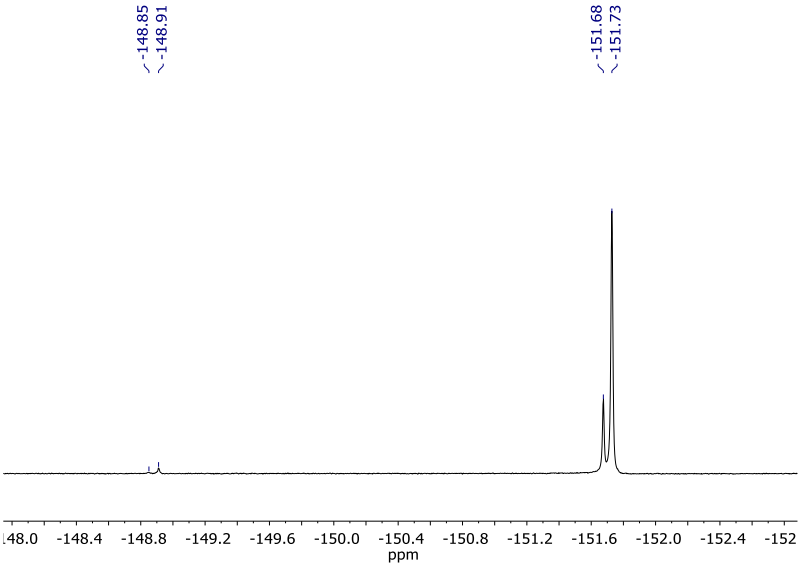

Figure 2.25. $^{19}F\{^{1}H\}$ NMR spectrum (376 MHz) of **B5a** in CD_2Cl_2. A small amount of 2,6-dimethoxypyridinium tetrafluoroborate could not be removed and is observed at -148.85 (s) and -148.91 (s).

In-situ Synthesis of [K][Pt(*NN$^{\#}$N)^{Et}Cl] **(B5b)**

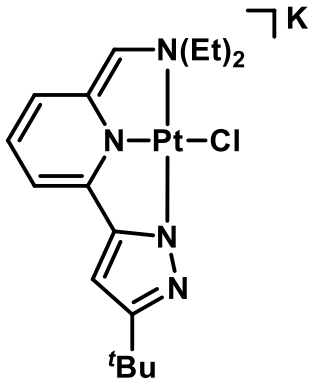

A J. Young NMR tube was charged with 4.1 mg (0.0079 mmol) **B5** and 0.4 mL C_6D_6 to form a yellow suspension. Addition of 2.1 mg (0.019 mmol) KO^{t}Bu resulted in a red solution. The following ^{1}H NMR spectrum was recorded: (C_6D_6, 500 MHz): δ 6.53 (1H, m, pyr), 6.27 (1H, s,

pyz), 5.86 (1H, d, pyr, $^{3}J_{H\text{-}H}$ = 7.5 Hz), 5.58 (1H, d, pyr, $^{3}J_{H\text{-}H}$ = 6.3 Hz), 3.47 (1H, s, C-H), 3.38 (2H, s, CH_2), 2.28 (2H, s, CH_2), 1.67 (6H, s, CH_3), 1.35 (9H, s, CH_3).

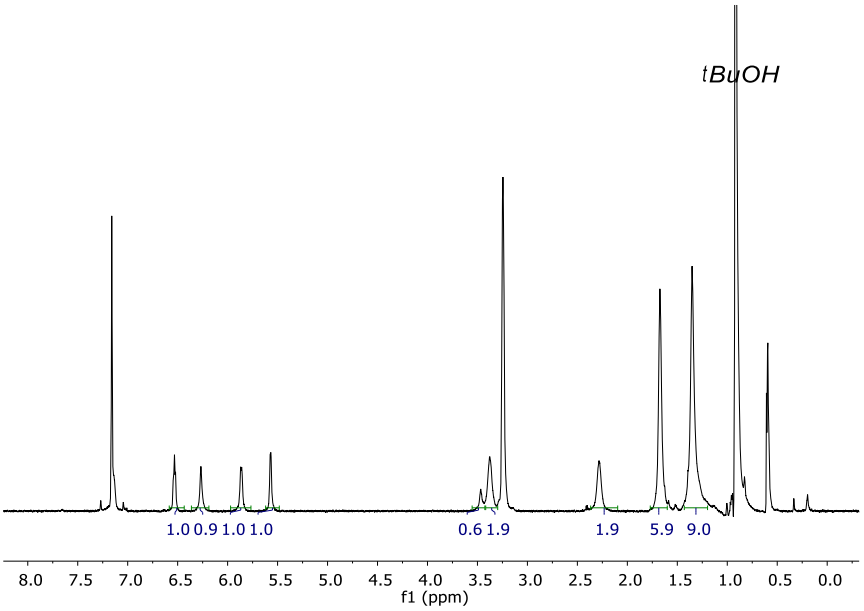

Figure 2.26. ^{1}H NMR spectrum (700 MHz) of **B5b** in C_6D_6

Synthesis of [Pt(^{H}NN)^{Me}(S(CH_3)$_2$)(CH_3)][BF_4] **(B6a or B6b)**

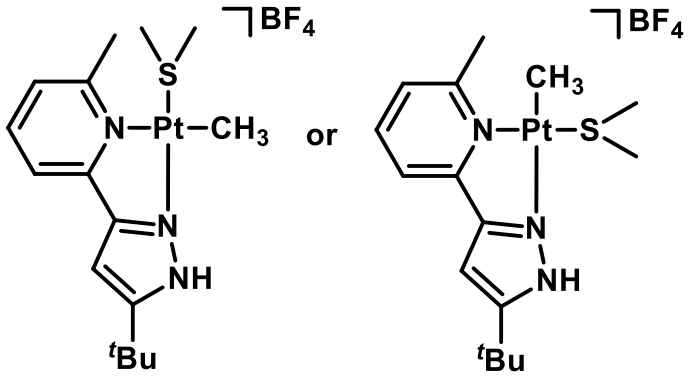

B6a **B6b**

A 20 mL scintillation vial was charged with **B2** (39.0 mg,0.0802 mmol), a stir bar and dissolved in 3 mL of benzene. While stirring, 11 µL HBF_4 etherate (0.080 mmol, 54 % in diethyl ether) was

added to precipitate an orange solid. The solvent was removed in vacuo and the resulting solid was washed with pentane (2 x 3 mL). A representative ^{1}H NMR spectrum was obtained and is consistent with **B6** as the major product.

^{1}H NMR (THF-d_8, 500 MHz): δ 12.53 (1H, br, N-H), 7.96-8.06 (3H, m, pyr and pyz), 7.40 (1H, d, pyr, $^{4}J_{H\text{-}NH}$ = 1.7 Hz), 2.84 (3H, s, CH_3), 2.52 (6H, s, $S(CH_3)_2$, $^{3}J_{Pt\text{-}H}$ = 61 Hz), 1.45 (9H, s, CH_3), 1.29 (3H, s, CH_3, $^{3}J_{Pt\text{-}H}$ = 79 Hz).

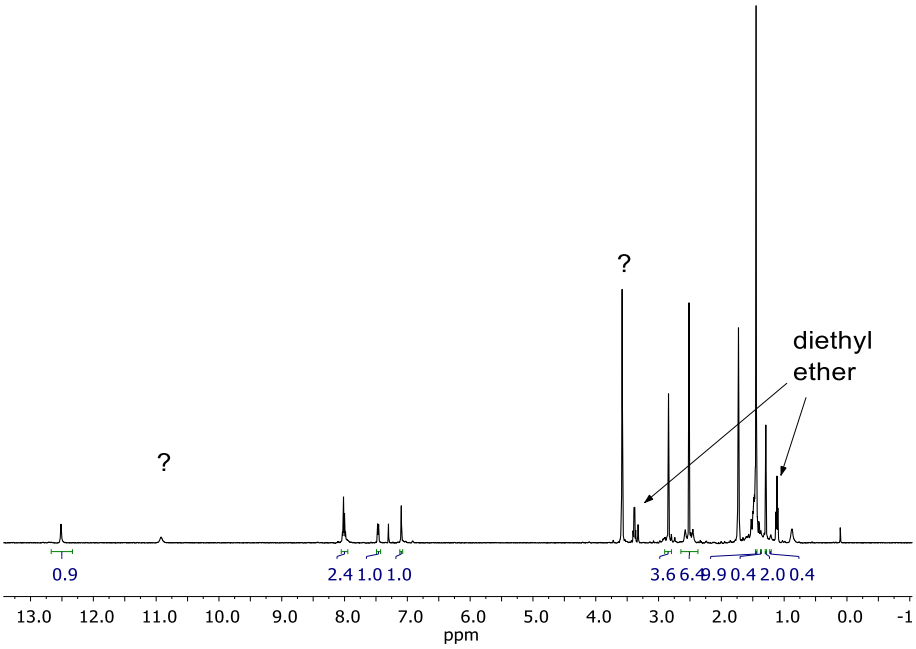

Figure 2.27 ^{1}H NMR spectrum (500 MHz) of **B6** in THF-d_8

Synthesis of [Pt(^{H}NNN)^{Et}CH$_3$][BF$_4$] **(B7)**.

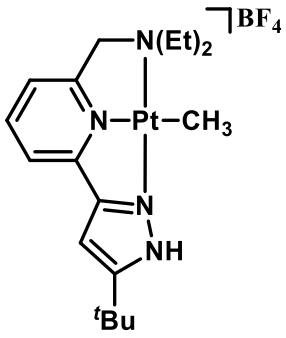

A 20 mL scintillation vial was charged with 19.2 mg (0.0387 mmol) **B4a**, a Teflon stir bar, and benzene (2 mL). The suspension was stirred vigorously while HBF_4 etherate (5.0 µL, 0.0368 mmol, 54 % in diethyl ether) was added by syringe. The mixture was stirred for 5 minutes. Diethyl ether (10 mL) was added to completely precipitate out a yellow solid. The solid was filtered and washed with additional diethyl ether (2 x 5 mL). After the resulting solid was dissolved in minimal acetonitrile, 10 mL diethyl ether was added to form a suspension. The suspension was filtered and the solid collected, and further dried under vacuum (18.8 mg, 83 % yield). ^{1}H NMR (CD_2Cl_2, 400 MHz): δ 7.90 (1H, t, pyr, $^{3}J_{H\text{-}H}$ = 8.0 Hz), 7.41 (1H, d, pyr, $^{3}J_{H\text{-}H}$ = 8.0 Hz), 7.18 (1H, d, pyr, $^{3}J_{H\text{-}H}$ = 7.9 Hz), 6.53 (1H, d, pyz)), 4.28 (2H, t, CH_2, $^{4}J_{Pt\text{-}H}$ = 24 Hz), 3.20 (2H, dq, CH_2, $^{2}J_{H\text{-}H}$ = 12.5, $^{3}J_{H\text{-}H}$ = 7.2 Hz), 2.94 (2H, dq CH_2, $^{2}J_{H\text{-}H}$ = 12.5, $^{3}J_{H\text{-}H}$ = 6.9 Hz), 1.47 (6H, t, CH_3, $^{3}J_{H\text{-}H}$ = 7.0 Hz), 1.34 (9H, s, CH_3), 0.83 (3H, s, Pt-CH_3, $^{2}J_{Pt\text{-}H}$ = 77 Hz). ^{13}C{^{1}H} (CD_2Cl_2, 126 MHz): δ 160.65 (s), 156.31 (s), 152.60 (s), 150.64 (s), 137.98 (s), 117.31 (s), 117.24 (s), 101.18 (s), 69.88 (s), 59.56 (s), 32.64 (s), 30.92 (s), 13.21 (s, $^{3}J_{Pt\text{-}C}$ = 32 Hz), -15.95. ^{19}F{^{1}H} NMR (CD_2Cl_2, 377 MHz): δ -152.2 (s), -152.3 (s). ESI-MS: $[Pt(^{H}NNN)^{Et}CH_3]^{+}$ Theoretical Mass, *m/z* = 495.2019; Observed Mass, *m/z* = 495.2043.

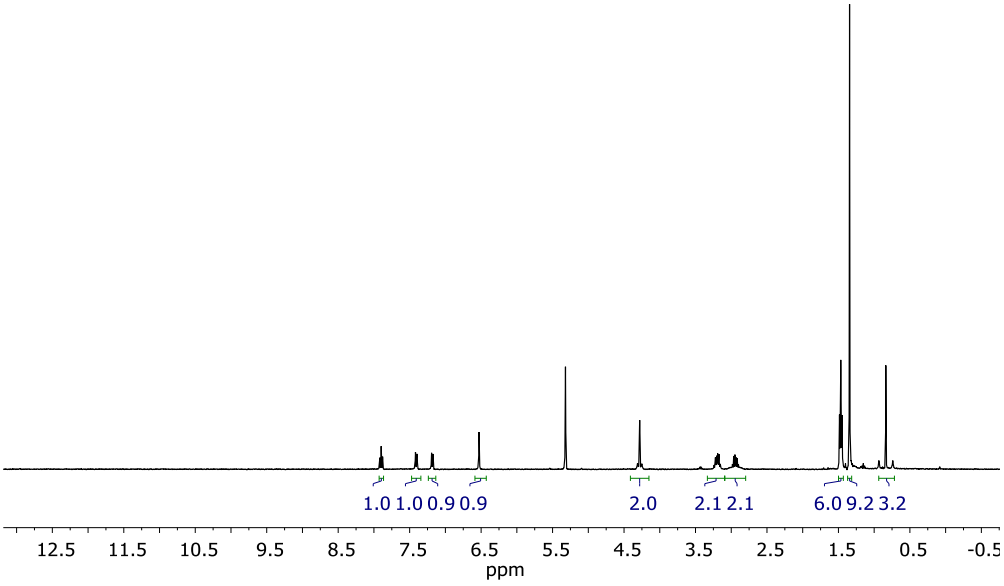

Figure 2.28. ^{1}H NMR spectrum (400 MHz) of **B7** in CD_2Cl_2

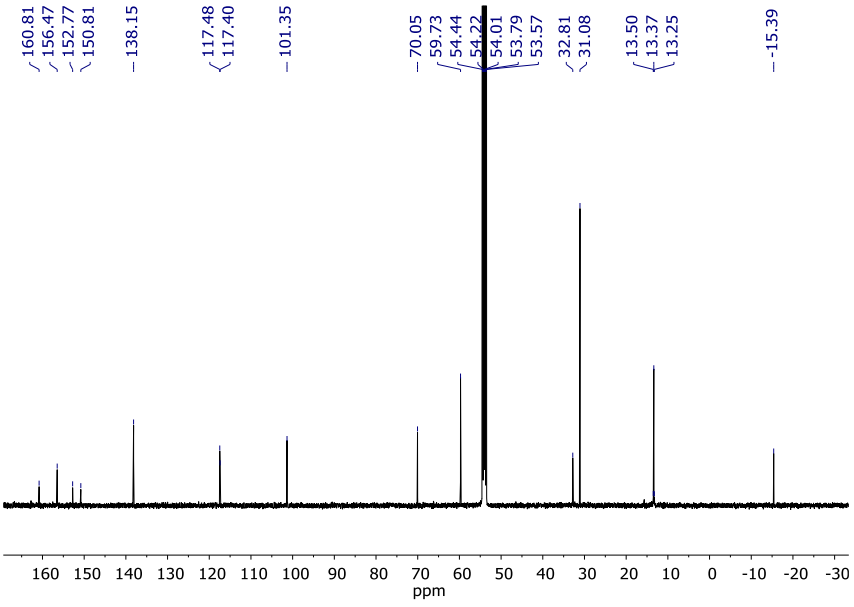

Figure 2.29. $^{13}C\{^{1}H\}$ NMR spectrum (126 MHz) of **B7** in CD_2Cl_2

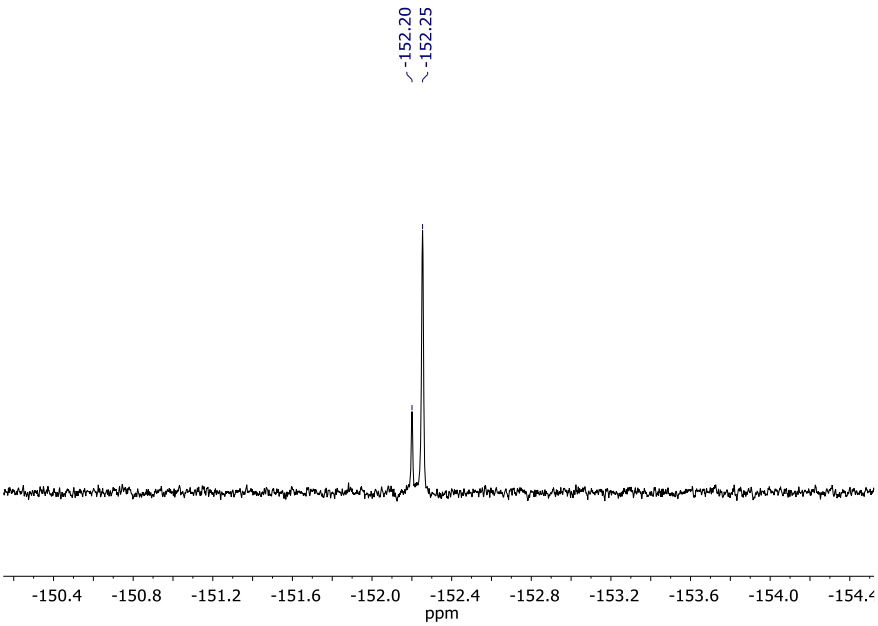

Figure 2.30. $^{19}F\{^{1}H\}$ NMR spectrum (376 MHz) of **B7** in CD_2Cl_2

In-situ Synthesis of $Pt(\kappa^1\text{-*NNN})^{Et}(P(C_5H_6)_3)_2CH_3$**(B8a)**

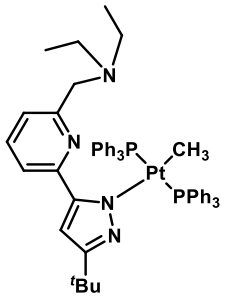

A J. Young NMR tube was charged with 5.0 mg (0.0079 mmol) **B4a**, 5.8 mg (0.022 mmol) PPh_3 and C_6D_6 (0.4 mL) to form a yellow solution. Isolation of **B8a** was attempted by addition of 1 mL diethyl ether to the C_6D_6 solution to precipitate a yellow solid. The suspension was decanted and the resulting solid was washed with diethyl ether (2 x 1 mL) and resulted in reformation of **B4a**. The following ^{1}H NMR spectrum, in the presence of excess PPh_3 was recorded: (C_6D_6, 500 MHz): δ 7.82-7.69 (14H, m, Ar-H), 7.53 (1H, d, pyr, $^{3}J_{H\text{-}H}$ = 7.6 Hz), 7.47 (1H, d, pyr, $^{3}J_{H\text{-}H}$ = 7.6 Hz),

7.44-7.34 (13H, m, Ar-H)), 7.29 (1H, t, pyr, $^{3}J_{H-H}$ = 7.6 Hz), 7.08-6.96 (42H, m, Ar-H), 6.32 (1H, s, pyz), 4.07 (2H, s, CH_2), 2.61 (4H, q, CH_2, ($^{3}J_{H-H}$ = 7.6 Hz)), 1.37 (9H, s, CH_3), 1.05 (6H, t, CH_3, $^{3}J_{H-H}$ = 7.6 Hz), 0.039 (3H, t, Pt-CH_3, $^{3}J_{H-P}$ = 5.9 Hz, $^{2}J_{Pt-H}$ = 55 Hz). $^{31}P\{^{1}H\}$ (C_6D_6, 202 MHz): δ 25.19 (Pt-PPh_3, $^{1}J_{Pt-P}$ = 3310 Hz), -5.30 (free PPh_3).

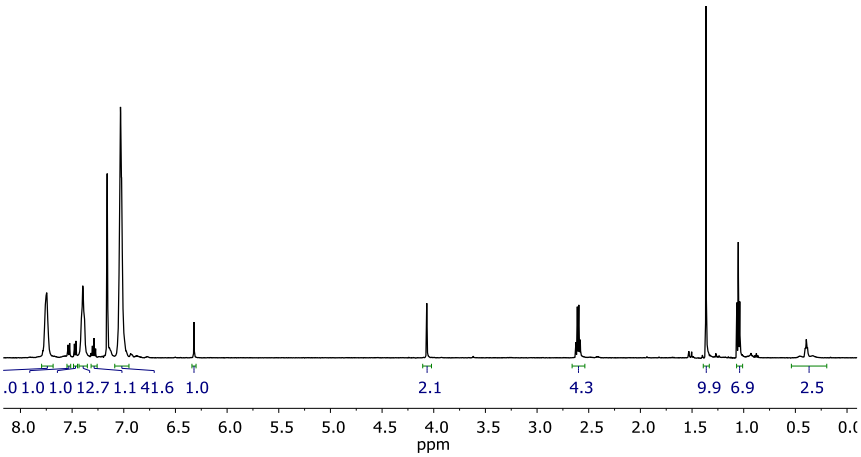

Figure 2.31. ^{1}H NMR spectrum (500 MHz) of **B8a** in C_6D_6

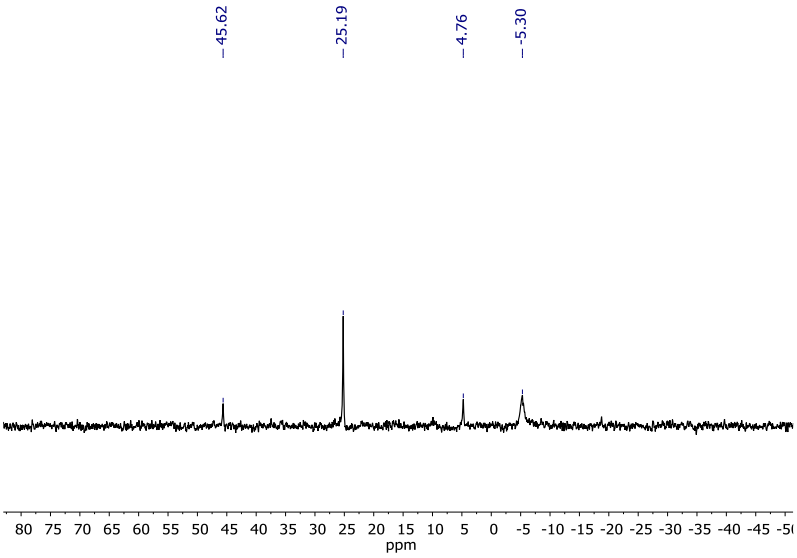

Figure 2.32. $^{31}P\{^{1}H\}$ NMR spectrum (162 Hz) of **B8a**. Resonance at -5.30 is noncoordinated PPh_3.

Synthesis of Pt(κ^1-*NNN)^{Et}(P(CH_3)$_3$)$_2$$CH_3$ **(B8b)**

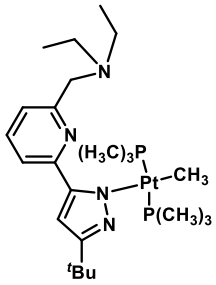

A J. Young NMR tube was charged with 5.0 mg (0.0079 mmol) **B4a** and C_6D_6 (0.4 mL) to form a yellow suspension. An excess of P(CH_3)$_3$ (~0.01 mL) was vacuum transferred to the J. Young NMR tube. The tube was sealed and was allowed to react for 20 mins. The volatiles were removed *in vacuo*, C_6D_6 was added and NMR spectra were recorded.

^{1}H (C_6D_6, 300 MHz): δ 8.75 (1H, d, pyr, $^3J_{H\text{-}H}$ = 7.4 Hz, 1H), 7.39 (1H, d, pyr, $^3J_{H\text{-}H}$ = 15.2 Hz), 7.39 (1H, t, pyr, $^3J_{H\text{-}H}$ = 15.2 Hz), 7.28 (1H, s, pyz), 3.91 (2H, s, CH_2), 2.55 (4H, q, CH_2, $^3J_{H\text{-}H}$ = 7.1 Hz), 1.74 (9H, s), 1.01 (6H, t, CH_3, $^3J_{H\text{-}H}$ = 7.1 Hz), 0.84 (18H, vt, P(CH_3)$_3$, $^2J_{H\text{-}P}$ = 5.7 Hz, $^2J_{H\text{-}P}$ = 5.7 Hz, $^3J_{Pt\text{-}H}$ = 29.9 Hz, 0.60 (3H, t, Pt-CH_3, $^2J_{Pt\text{-}H}$ = 71.7 Hz, $^3J_{H\text{-}P}$ = 6.9 Hz). Virtual triplet simulated on MNova Spin Simulation to obtain coupling constants and are shown below recorded ^{1}H NMR spectrum. ^{13}C NMR (176 MHz, C_6D_6) δ 163.12 (s), 149.70 (s), 135.73 (s), 128.36 (s), 118.61 (s), 117.45 (s), 101.40 (s), 60.69 (s), 47.93 (s), 32.58 (s), 32.01 (s), 12.60 (s), 12.51 (s), 12.40 (s), -27.52 (Pt-CH_3, t, ($^2J_{P\text{-}H}$ = 14.9 Hz)). ^{31}P{^{1}H} (C_6D_6, 202 MHz): δ -18.91 (Pt-P(CH_3)$_3$, $^2J_{P\text{-}P}$ = 7.4 Hz, $^1J_{Pt\text{-}P}$ = 2886 Hz).

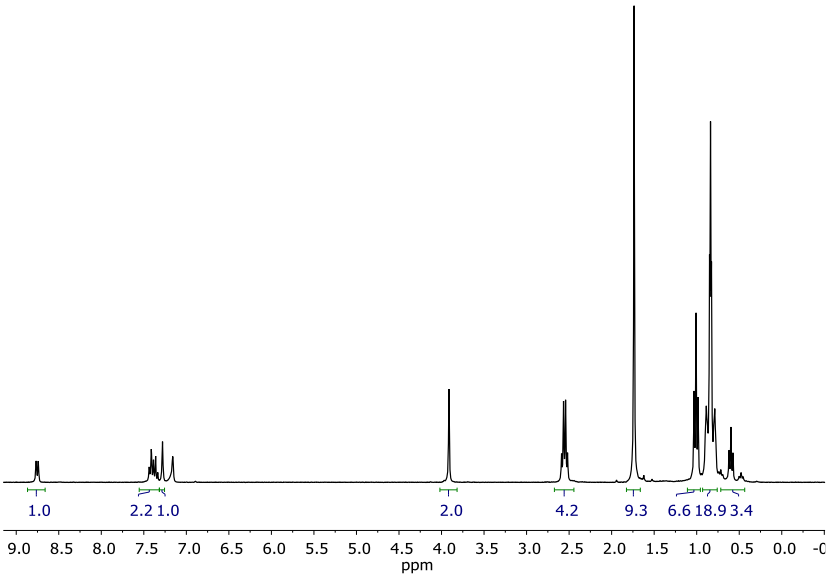

Figure 2.33. ^{1}H NMR spectrum (300 MHz) of **B8b** in C_6D_6

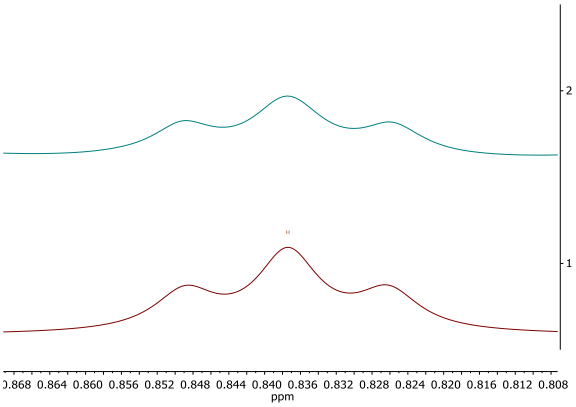

Figure 2.34. Simulated ^{1}H NMR spectrum of Pt-CH_3 resonance of **B8b** in C_6D_6 in top spectrum (1). Figure 2.34-2. Actual ^{1}H NMR spectrum of Pt-CH_3 resonance in C_6D_6.

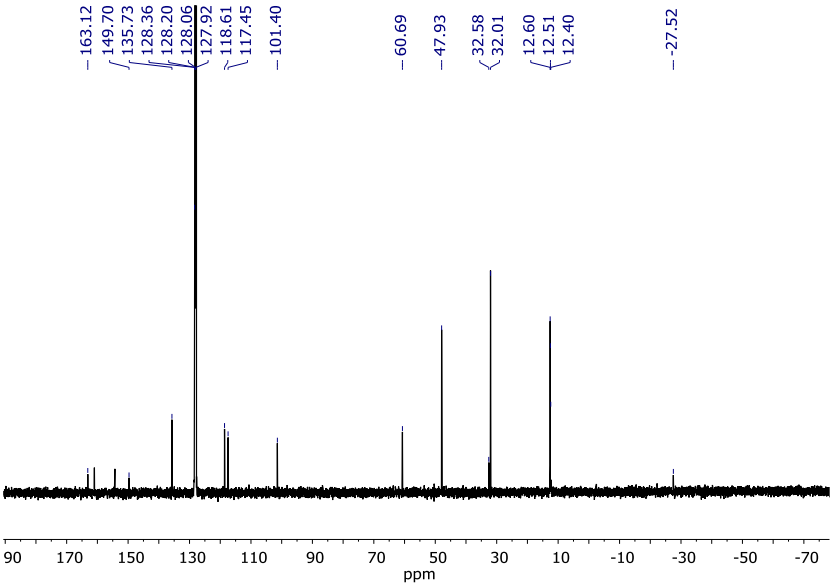

Figure 2.35. $^{13}C\{^{1}H\}$ NMR spectrum (300 MHz) of **B8b** in C_6D_6

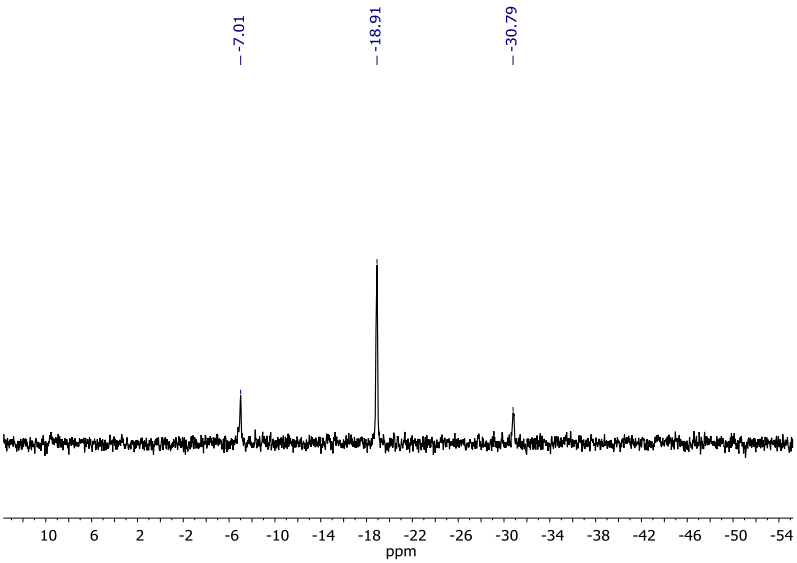

Figure 2.36. $^{31}P\{^{1}H\}$ NMR spectrum (162 MHz) of **B8b** in C_6D_6

2.43 X-ray Crystallography General Information

Complexes **B4a**: X-ray intensity data were collected on a Bruker APEXIII D8QUEST[37] CMOS area detector, both employing graphite monochromated Mo-Kα radiation (λ = 0.71073 Å) at 100(1) K. Preliminary in indexing was performed from a series of twenty-four 0.5° rotation frames with exposures of 10 seconds. Rotation frames were integrated using SAINT[38], producing a listing of unaveraged F^2 and $\sigma(F^2)$ values. The intensity data were corrected for Lorentz and polarization effects and for absorption using SADABS.[39] The structure was solved by direct methods – ShelXT.[40] Refinement was by full-matrix least squares based on F^2 using SHELXL-2018.[41] All reflections were used during refinement. The weighting scheme used was $w=1/[\sigma^2(F_o^2)+(0.0612P)^2 + 1.0285P]$ where $P = (F_o^2 + 2F_c^2)/3$. Non-hydrogen atoms were refined anisotropically and hydrogen atoms were refined using a riding model.

Complexes **B4b** and **B5**: X-ray intensity data were collected at -173 °C on a Bruker APEX II single crystal X-ray diffractometer, Mo-radiation. The data was integrated and scaled using SAINT, SADABS within the APEX2 software package by Bruker.[42] Solution by direct methods (SHELXS, SIR97)[43,44] produced a complete heavy atom phasing model consistent with the proposed structure. The structure was completed by difference Fourier synthesis with SHELXL97.[45,46] Scattering factors are from Waasmair and Kirfel.[47] Hydrogen atoms were placed in geometrically idealised positions and constrained to ride on their parent atoms with C---H distances in the range 0.95-1.00 Angstrom. Isotropic thermal parameters U_{eq} were fixed such that they were $1.2U_{eq}$ of their parent atom U_{eq} for CH's and $1.5U_{eq}$ of their parent atom U_{eq} in case of methyl groups. All non-hydrogen atoms were refined anisotropically by full-matrix least-squares.

Complex	B4b	B5	B4a
Emperical Formula	C_{23} H_{24} D_9 N_4 Pt	C_{17} H_{25} Cl N_4 Pt	$C_{19}H_{30}Cl_2N_4Pt$
Formula weight	566.65	515.95	580.46
Temperature (K)	100(2)	100(2)	100
Wavelength (Å)	0.71073	0.71073	0.71073
Crystal System	Tetragonal	Monoclinic	monoclinic
Space group	I 4_1/a	C 2_1/n	$P2_1/c$
Unit cell axes (Å)	a = 19.9089(8), b = 19.9089(8), c =31.220(3)	a = 14.9564(11), b = 11.0974(7), c = 11.1395(8)	a =23.0153(10), b = 10.8687(5), c = 26.1940(11)
Unit cell angles (°)	a= 90, β=90, γ = 90	a= 90, β= 101.880(4), γ = 90	92.569(2)
Volume ($Å^3$)	12374.6(13)	1809.3(2)	6545.7(5)
Z	16	4	12
Demsity (mg/m^3), calc.	1.217	1.894	1.767
Absorption coeff. (mm^{-1})	4.546	7.907	6.686
F(000)	4384	1000	3408
Crystal size (mm^3)	0.04 x 0.02 x 0.02	0.08 x 0.06 x 0.01	0.32 x 0.09 x 0.05
Theta range for data collection (°)	2.05 to 25.40	2.09 to 26.56	5.942 to 55.112
Index ranges	-23<=h<=23, -23<=k<=23, -37<=l<=37	-18<=h<=18, -13<=k<=13, -13<=l<=13	$-29 \leq h \leq 29$, $-14 \leq k \leq 13$, $-34 \leq l \leq 34$
Reflections collected	92722	69933	156801
Independent reflections, R(int)	5676 [R(int) = 0.0751]	3740 [R(int) = 0.0967]	15082[R(int) = 0.0471]
Completeness to theta (%)	99.8	100	99.8
Max. and min. transmission	0.9349 and 0.8391	0.9251 and 0.5703	0.4984 and 0.7456
Refinement Method	Full-matrix least-squares on F^2	Full-matrix least-squares on F^2	Full-matrix least-squares on F^2
Data/restraints/parameters	5676/15/260	3740/24/226	15082/72/751
Goodness-of-fit on F^2	1.085	1.045	1.087
Final R indices [I>2sigma(I)]	R1 = 0.0567, wR2 = 0.1085	R1 = 0.0301, wR2 = 0.0517	R_1 = 0.0224, wR_2 = 0.0454
R indices (all data)	R1 = 0.1182, wR2 = 0.1471	R1 = 0.0497, wR2 = 0.0574	R_1 = 0.0328, wR_2 = 0.0486
Largest diff. peak and hole ($e.A^{-3}$)	2.452 and -1.097	1.275 and -1.529	0.69 and -1.67

Table 2.1 Parameters for X-Ray Structures in Chapter 2

2.5 Notes to Chapter 2

(1) Shilov, A. E.; Shul, G. B. *Chem. Rev.* **1997**, *2665*, 2879–2932.

(2) Gunsalus, N. J.; Koppaka, A.; Park, S. H.; Bischof, S. M.; Hashiguchi, B. G.; Periana, R. A. *Chem. Rev.* **2017**, *117*, 8521–8573.

(3) Goldberg, K. I.; Goldman, A. S. *Acc. Chem. Res.* **2017**, *50*, 620–626.

(4) Lersch, M.; Tilset, M. *Chem. Rev.* **2005**, *105*, 2471–2526.

(5) Luinstra, G. A.; Wang, L.; Stahl, S. S.; Labinger, J. A.; Bercaw, J. E. *J. Organomet. Chem.* **1995**, *504*, 75–91.

(6) Johansson, L.; Tilset, M.; Labinger, J. A.; Bercaw, J. E. *J. Am. Chem. Soc.* **2000**, *122*, 10846–10855.

(7) Wik, B. J.; Lersch, M.; Tilset, M. *J. Am. Chem. Soc.* **2002**, *124*, 12116–12117.

(8) Bercaw, J. E.; Chen, G. S.; Labinger, J. A.; Lin, B. L. *Organometallics* **2010**, *29*, 4354–4359.

(9) Fekl, U.; Goldberg, K. I. In *Adv. Inorg. Chem*; 2003; pp 259–320.

(10) O'Reilly, S. A.; White, P. S.; Templeton, J. L. *J. Am. Chem. Soc.* **1996**, *118*, 5684–5689.

(11) Prokopchuk, E. M.; Jenkins, H. A.; Puddephatt, R. J. *Organometallics* **1999**, *18*, 2861–2866.

(12) Wick, D. D.; Goldberg, K. I. *J. Am. Chem. Soc.* **1997**, 119, 10235–10236.

(13) Jenkins, H. A.; Yap, G. P. A.; Puddephatt, R. J. *Organometallics* **1997**, *16*, 1946–1955.

(14) Vedernikov, A. N.; Pink, M.; Caulton, K. G. *Inorg. Chem.* **2004**, *43*, 3642–3646.

(15) Hinman, J. G.; Baar, C. R.; Jennings, M. C.; Puddephatt, R. J. *Organometallics* **2000**, *19*, 563–570.

(16) You, Z. L.; Jiao, Q. Z.; Niu, S. Y.; Chi, J. Y. *Z. Anorg. Allg. Chem.* **2006**, *632*, 2486–2490.

(17) Zeng, M.; Li, L.; Herzon, S. B. *J. Am. Chem. Soc.* **2014**, *136*, 7058–7067.

(18) Sutcliffe, V. F.; Young, G. B. *Polyhedron* **1984**, *3*, 87–94.

(19) Toda, T.; Kuwata, S.; Ikariya, T. *Chem. - A Eur. J.* **2014**, *20*, 9539–9542.

(20) Polezhaev, A. V; Chen, C.-H.; Losovyj, Y.; Caulton, K. G. *Chem. - A Eur. J.* **2017**, *23*, 8039–8050.

(21) Toda, T.; Saitoh, K.; Yoshinari, A.; Ikariya, T.; Kuwata, S. *Organometallics* **2017**, *36*, 1188–1195.

(22) Yu, W. S.; Cheng, C. C.; Cheng, Y. M.; Wu, P. C.; Song, Y. H.; Chi, Y.; Chou, P. T. *J. Am. Chem. Soc.* **2003**, *125*, 10800–10801.

(23) Babak, M. V.; Pfaffeneder-Kmen, M.; Meier-Menches, S. M.; Legina, M. S.; Theiner, S.; Licona, C.; Orvain, C.; Hejl, M.; Hanif, M.; Jakupec, M. A.; Keppler, B. K.; Gaiddon, C.; Hartinger, C. G. *Inorg. Chem.* **2018**, *57*, 2851–2864.

(24) Cuerva, C.; Campo, J. A.; Ovejero, P.; Torres, M. R.; Oliveira, E.; Santos, S. M.; Lodeiro, C.; Cano, M. *J. Mater. Chem. C* **2014**, *2*, 9167–9181.

(25) Liao, C. T.; Chen, H. H.; Hsu, H. F.; Poloek, A.; Yeh, H. H.; Chi, Y.; Wang, K. W.; Lai,

C. H.; Lee, G. H.; Shih, C. W.; Chou, P. T. *Chem. - A Eur. J.* **2011**, *17*, 546–556.

(26) Bailey, W. D. Late Transition-Metal Complexes Supported by Pincer Ligands : Applications in Partial Oxidation Catalysis, University of Washington, 2016.

(27) Moret, M.; Chen, P. *Organometallics* **2008**, *27*, 4903–4916.

(28) Veenboer, R. M. P.; Collado, A.; Dupuy, S.; Lebl, T.; Falivene, L.; Cordes, D. B.; Slawin, A. M. Z.; Cazin, C. S. J.; Nolan, S. P. *Organometallics* **2017**, *36*, 2861–2869.

(29) Parkins, B. A. W. *Platin. Met. Rev.* **1996**, *40*, 169–174.

(30) Xing, X.; Xu, C.; Chen, B.; Li, C.; Virgil, S. C.; Grubbs, R. H. *J. Am. Chem. Soc.* **2018**, *140*, 17782–17789.

(31) Luedtke, A. T.; Goldberg, K. I. *Inorg. Chem.* **2007**, *46*, 8496–8498.

(32) Camp, A. M.; Kita, M. R.; Grajeda, J.; White, P. S.; Dickie, D. A.; Miller, A. J. M. *Inorg. Chem.* **2017**, *56*, 11141–11150.

(33) Griffiths, D. C.; MacTavish, D. I.; Male, N. A. H.; Tocher, D. A.; Young, G. B. *J. Chem. Soc. - Dalt. Trans.* **1997**, *2*, 3373–3385.

(34) Pangborn, A. B.; Giardello, M. A.; Grubbs, R. H.; Rosen, R. K.; Timmers, F. J. *Organometallics* **1996**, *15*, 1518–1520.

(35) Anderson, G. K.; Lin, M. *Inorg. Synth.* **1990**, *28*, 60–62.

(36) Hill, G. S.; Irwin, M. J.; Levy, C. J.; Rendina, L. M.; Puddephatt, R. J. *Inorg. Synth.* **1998**, *32*, 149–151.

(37) APEX3, 2016.1-0: Bruker-AXS. Madison, Wisconsin, USA 2016.

(38) Bruker-AXS, S. v8. 38A. Madison, Wisconsin, USA 2014.

(39) Krause, L., Herbst-Irmer, R., Sheldrick, G.M. & Stalke, D. *J. Appl. Cryst.* **2015**, *48*, 3.

(40) Sheldrick, G. . *Acta Cryst.* **2015**, *71*, 3.

(41) Sheldrick, G. . *Acta Cryst.* **2015**, *71*, 3.

(42) Bruker (2007) APEX2 (Version 2.1-4), SAINT (version 7.34A), SADABS (version 2007/4), B. I. Madison, Wisconsin, USA.

(43) Altomare, A.; Burla, M. c. . M. *J. Appl. Cryst.* **1999**, *32*, 115.

(44) Altomare, A.; Cascarano, G. L.; Guagliardi, A. *J. Appl. Cryst.* **1993**, *26*, 343.

(45) Sheldrick, G. M. (1997) SHELXL-97, P. for the refinement of crystal structures. University of Göttingen, Germany.

(46) Sheldrick, G. M. *Acta. Cryst.* **2015**, *A71*, 3.

(47) Waasmaier, D.; Kirfel, A. *Acta Cryst.* **1995**, *51*, 416.

Chapter 3

Synthesis of Pyrazolate Supported Tridentate Pt^{II} Alkyl Complexes and Reactivity with Electrophiles

3.1 Introduction

Oxidative addition is a fundamental reaction in organometallic chemistry. Understanding how d_8 transition metals undergo oxidative addition of E-X (E = CH_3^+, H^+) substrates has led to advances in cross coupling, carbonylation and N-alkylation reactions, to name a few.[1,2] Electron rich precious metals form stronger M-E bonds than their first row counterparts and are often used to study catalytic systems which go through oxidative addition pathways.[3] As Pt can form solution-stable complexes in various oxidation states (0/II/IV), it is often used to explore these 2-electron metal oxidation reactions.

Bidentate ligand-supported $Pt^{II}(CH_3)_2$ complexes are susceptible to oxidative addition of EX substrates.[4] The oxidative addition of E-X to square planar Pt(II) generally proceeds through an associative mechanism involving several steps (Scheme 3.01). In the first step, E-X undergoes nucleophilic attack by Pt(II) to form a five-coordinate $[L_2Pt^{IV}(CH_3)_2E]^+$ cationic intermediate. In the second step, X^- (or solvent) coordinates to form an octahedral $L_2Pt^{IV}(CH_3)_2(E)(X/solv.)$ complex

Portions of this chapter have been adapted from: Zahora, B. A.; Gau, M. R.; Goldberg, K. I. *In Preparation*

Scheme 3.01. Generalized reaction of $L_2Pt^{II}(CH_3)_2$ with HX and CH_3X

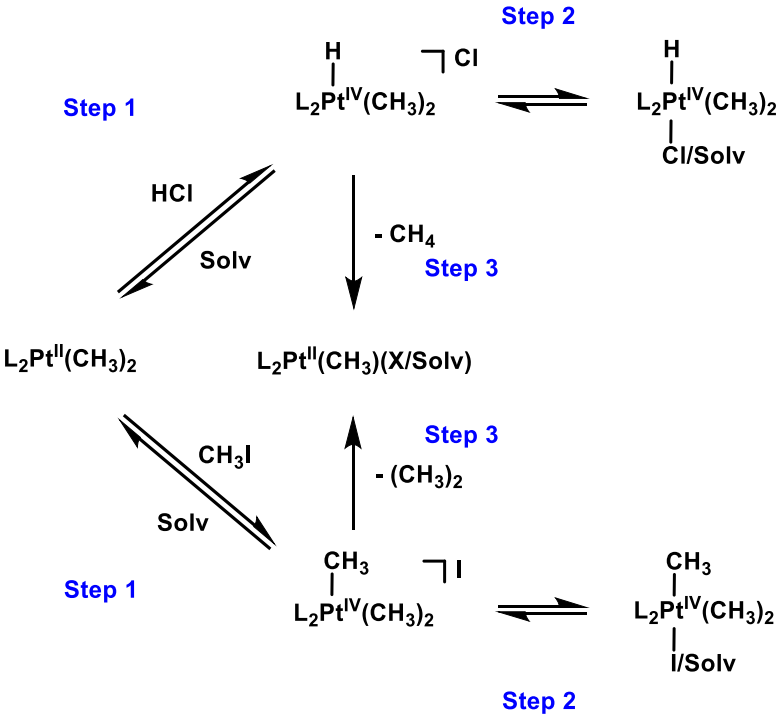

(Scheme 3.01). The oxidized Pt^{IV} product can often be thermodynamically unstable. In this case, the CH_3-E (E = CH_3, H) coupled product and the resulting Pt^{II} product after reductive elimination occurs are often observed (Scheme 3.01, Step 3). This is due, in part, to the thermodynamics of such a system. To start, the entropy of oxidative addition of a C-H moiety requires ca. 10 kcal/mol that needs to be overcome.[5] Additionally, the formation of both CH_3-E bonds [ca. ~100 kcal/mol (C-H bond), ca. ~90 kcal/mol (C-C bond)] and the resulting Pt^{II}-X/solv bond [ca. ~65 kcal/mol (Pt^{II}-Cl bond)] is often greater than the newly formed Pt^{IV}-CH_3 (ca. ~35 kcal/mol) or Pt^{IV}-H (ca. ~75 kcal/mol) bonds once Pt^{II} to Pt^{IV} oxidation occurs.[3,5–7]

For example, HCl addition to a 2,9-dimethyl-l,10-phenanthroline (dmphen) ligated $Pt^{II}(CH_3)_2$ complex formed isolatable 6-coordinate Pt^{IV}(dmphen)$(CH_3)_2$(H)(Cl) (Step 1 and 2 combined, Scheme 3.01), which slowly reductively eliminated methane in solution to form Pt^{II}(dmphen)(CH_3)(Cl) (Step 3, Scheme 3.01).[8] Whether methane liberation occurred from 5-

coordinate $[Pt^{IV}(dmphen)(CH_3)_2(H)]^+$ or 6-coordinate $Pt^{IV}(dmphen)(CH_3)_2(H)(Cl)$ was not studied, however, most studies of reductive elimination of alkanes from Pt^{IV} alkyl hydride complexes support that the concerted C-H bond forming step occurs from a five-coordinate metal species.[9] Similar to HCl, addition of CH_3I to a bipyridine (bpy) ligated $Pt^{II}(CH_3)_2$ complex formed $[Pt^{IV}(bpy)(CH_3)_3(solv)][I]$ in polar solvents (CD_3CN and acetone-d_6) at reduced temperatures (-20 °C).[10] Warming to room temperature resulted in formation of the stable $Pt^{IV}(bpy)(CH_3)_3(I)$ (Scheme 3.01, bottom pathway). While thermolysis of $Pt^{IV}(bpy)(CH_3)_3(I)$ was not studied, thermolysis of a similar 6-coordinate 1,2-bis(diphenylphosphino)ethane (dppe) ligated $Pt^{IV}(dppe)(CH_3)_3(I)$ formed ethane and $Pt^{II}(dppe)(CH_3)(I)$.[11] This C-C reductive elimination was proposed to proceed via a five-coordinate intermediate. For both additions of E-X, E = H^+ and CH_3^+, to Pt^{II}, the Pt^{II} center acts as the initial nucleophile, with subsequent coordination of X^- anion to form the corresponding 6-coordinate Pt^{IV} species (Scheme 3.01, Step 1 and 2). Methane or ethane is then released (CH_3-E reductive elimination; Scheme 3.01, Step 3) from a 5-coordinate Pt^{IV} oxidized product (after X^- dissociation) to form the Pt^{II} product.

Although addition of an E-X (E = H^+, CH_3^+) electrophiles to nitrogen ligated $Pt^{II}(CH_3)_2$ species has generally been thought to be initiated by nucleophilic attack by the metal (Scheme 3.01, Step 1), several examples have been reported for complexes which bear an additional basic/nucleophilic donor site on the ligand.[12–14] In this case, it would be possible for ligand donor sites, such as N, to act as the nucleophile in attacking an electrophilic reagent and oxidation to Pt^{IV} would not occur. For example, HCl addition to a dimethyl((pyridinylmethylene)amino)(ethyl/propyl)amine (DMEP/DMPP) ligated $Pt^{II}(CH_3)_2$ complex formed a protonated $[Pt^{II}(^{H}DMEP/^{H}DMPP)(CH_3)_2][Cl]$ upon the addition of the first equivalent of acid (Figure 3.01a).[12] Once the ligand is protonated, the next equivalent of HCl to

$Pt^{II}(^{H}DMEP/^{H}DMPP)(CH_3)_2$ reacted at the metal to form $[Pt^{IV}(^{H}DMEP/^{H}DMPP)(CH_3)_2(H)(Cl)][Cl]$. Selective protonation at the ligand with the first equivalent of HCl was due to stability of protonated $Pt^{II}(^{H}DMEP/^{H}DMPP)(CH_3)_2$ over $Pt^{IV}(DMEP/DMPP)(CH_3)_2(H)(Cl)$, which was not observed. (A more in-depth analysis of this protonation was investigated in Chapter 2 of this thesis.)

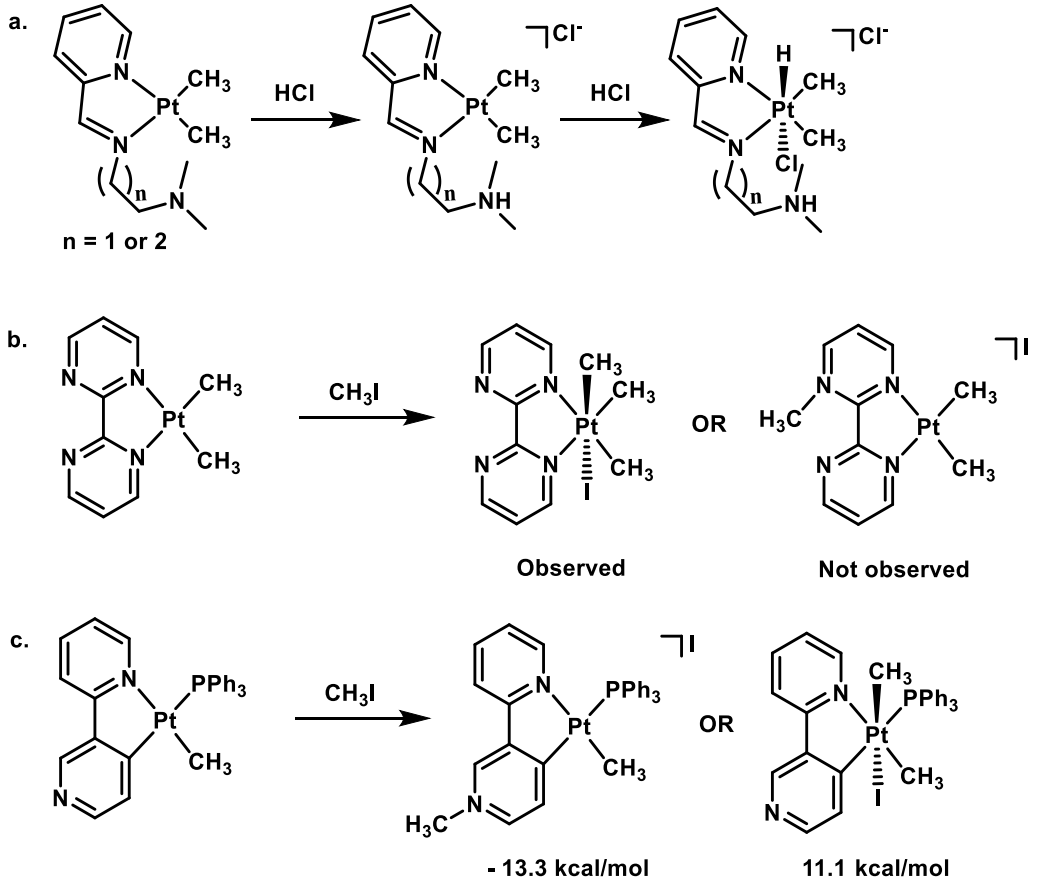

Figure 3.0 1 (a) Reaction of $Pt(DMEP/DMPP)(CH_3)_2$ with HCl. **(b)** Reaction of $Pt(bipym)(CH_3)_2$ with CH_3I. **(c)** Computational predicted products for reaction of $Pt(cbipy)(CH_3)_2$ with CH_3I.

In contrast to H^+ addition, bipyrimidine (bipym) ligated $Pt^{II}(CH_3)_2$ undergoes oxidative addition with methyl iodide at the metal to form $Pt^{IV}(bipym)(CH_3)_3(I)$ (Figure 3.01b).[13] Addition of N-methylation was not observed. Furthermore, cyclometalated bipyridine (cbipy) ligated

$Pt^{II}(CH_3)(PPh_3)$ contains a similar structured complex to $Pt^{II}(bipym)(CH_3)_2$, yet a ligand-based N is unbound and in the *para* position to the cyclometalated aryl ring (Figure 3.01c, initial complex).[14] Computational evidence reveals a 24 kcal preference of N-methylation over Pt^{II} oxidation upon CH_3I addition, although they were unable to independently synthesize the appropriate complexes experimentally in the study. Preference for ligand N-methylation over Pt^{II} oxidation was suggested to be due to the steric accessibility of the ligand-centered N.[14] As seen in Figure 3.01b, the N in $Pt(bipym)(CH_3)_2$ is more sterically crowded than $Pt^{II}(cbipy)(CH_3)_2$ in Figure 3.01c, which would support reactivity at Pt^{II} instead of the ligand N. These two examples are notable, as each ligand contains an additional unbound ligand N atom which can either act as a nucleophile or can be innocent. While in Figure 3.01b, addition of CH_3^+ electrophile occurs first at Pt^{II} to form Pt^{IV} species despite a potential nucleophilic N on the ligand, computational evidence has suggested N-methylation might be possible if a sterically accessible ligand N is present (Figure 3.01c).

While there are many examples of Pt^{II} oxidation with HCl and/or CH_3I to Pt^{IV}, conditions exist which can result in selective protonation or N-methylation, respectively. We set out to explore

Scheme 3.02. Metalation plan to form Pt-CH_3 complexes. Reactivity of Pt-CH_3 with EX (E = CH_3^+ or H^+).

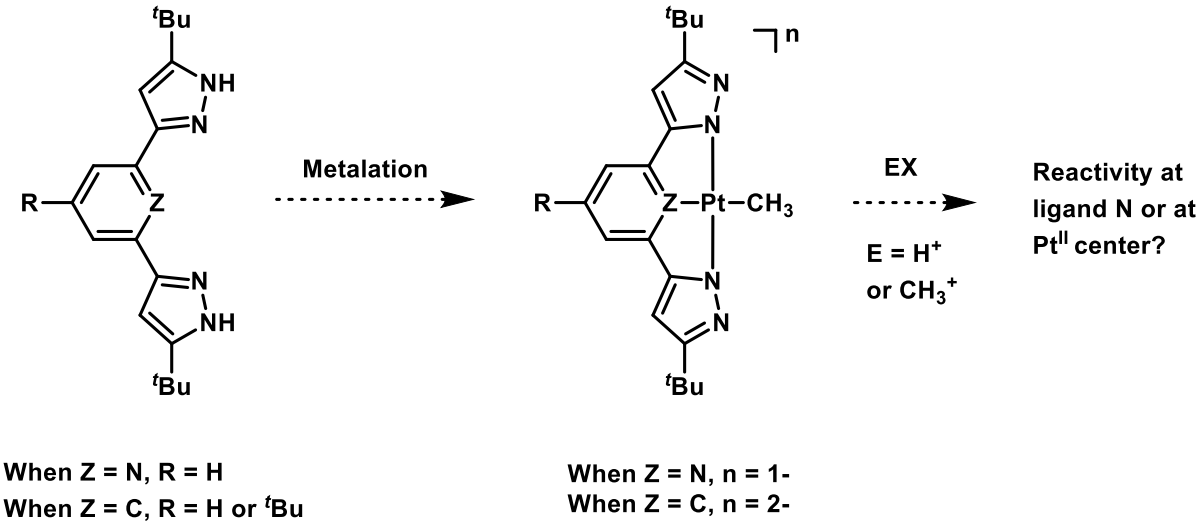

metalation and subsequent reactivity of 5-*tert*-butyl-1,3-bis(pyrazol-3-yl)pyridine (**^{H}NNN^{H}**) and 5-*tert*-butyl-1,3-bis(pyrazol-3-yl)benzene ligand **(^{H}NCN^{H})^{R}** (R = H, ^{t}Bu). Both ligands contain an additional potential reactive ligand-based N (Scheme 3.02). Once metalated, pyrazolate ligated Pt^{II}-CH_3 species were targeted and experiments were conducted to determine whether the ligand can participate in electrophile addition. Electrophile addition (EX) to pyrazolate ligated Pt^{II}-CH_3 will either occur at Pt^{II} to form a Pt^{IV}(E)(X) species or will react with the available ligand-based N atom to form a N-E ligated [Pt^{II}][X] species.

3.2 Results and Discussion

3.21 Preparation of ^{H}NNN^{H} Ligated Complexes

Chelation of multidentate pyrazolate ligands to Pt^{II} has been observed in protic solvents.[15] Similarly, the addition of (**^{H}NNN^{H}**) to $Pt(S(CH_3))_2Cl_2$ in refluxing methanol afforded [Pt(^{H}NNN^{H})Cl][Cl] (**C1**, 78 % isolated yield, Figure 3.02). ^{1}H and ^{13}C{^{1}H} NMR spectroscopy

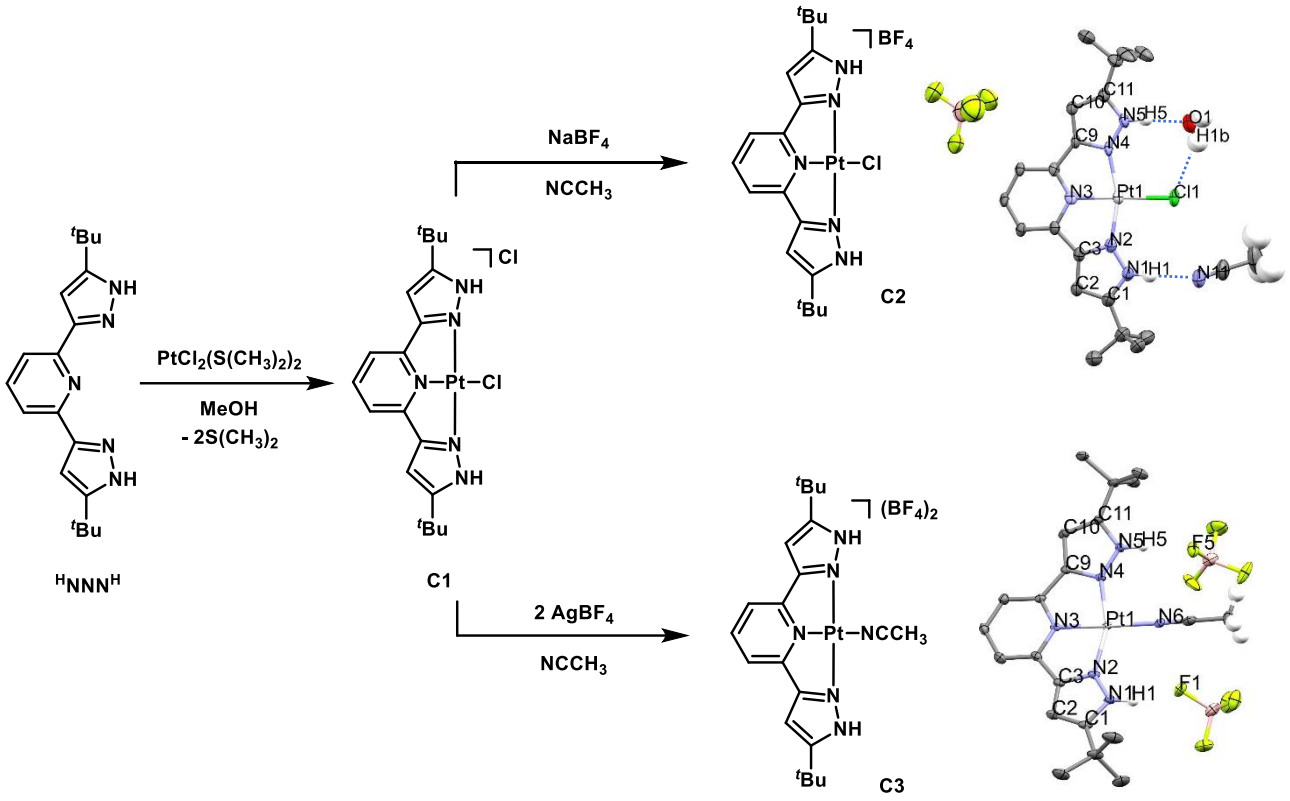

Figure 3.0 2 Metalation of **^{H}NNN^{H}** to Pt^{II} to form [Pt(^{H}NNN^{H})Cl][Cl] (**C1)** and subsequent reactions to form [Pt(^{H}NNN^{H})Cl][BF_4] (**C2)**, and [Pt(^{H}NNN^{H})$NCCH_3$][$(BF_4)_2$] (**C3**). Thermal ellipsoid plots (50% probability) of **C2** and **C3** are shown. Selected H-atoms and 1 molecule of acetylacetone in **C2** omitted for clarity. Selected bond lengths for **C2**: Pt(1)-Cl(1) 2.296(3) Å, H(1)-N(11) 2.01 Å, H(5)-O(1) 1.850 Å, H(1b)-Cl(1) 2.491 Å, **C3**: H(5)-F(5) 1.826 Å.

indicate that **C1** contains a symmetrical ligand environment. Even under rigorously dry deuterated solvents, including C_6D_6, acetone-d_6 or THF-d_8, no N-H signal was observed in the ^{1}H NMR spectra. An anion exchange of **C1** with $NaBF_4$ in CH_3CN gave [Pt(^{H}NNN^{H})Cl][BF_4] (**C2**) in 78 % isolated yield (Figure 3.02). The ^{1}H and ^{13}C{^{1}H} NMR spectral data for **C2** are also consistent with a symmetrical ligand environment. Compared to the ^{1}H NMR spectrum of **C1** in CD_3OD, all resonances were shifted upfield. Additionally, a broad N-H resonance at 12.07 ppm was apparent when dissolved in dry CD_3CN. Two broad singlets at -154.47 and -154.52 ppm, in a 1:4 ratio, were observed by ^{19}F{^{1}H} NMR spectroscopy. These signals are typical for an outer-sphere BF_4^- anion,

in accordance with the natural abundance of ^{10}B : ^{11}B.[16] Complex **C2** was also characterized in the solid state (Figure 3.02) and exhibits several hydrogen bond interactions (indicated by dashed lines in Figure 3.02) between the ligand N-H moieties, acetonitrile solvent, water and the chloride ligand.

Addition of two equiv. of $AgBF_4$ to a CH_3CN solution of **C1** resulted in abstraction of both chlorides to form $[Pt(^{H}NNN^{H})NCCH_3][(BF_4)_2]$ (**C3**) in 88 % isolated yield (Figure 3.02). Similar to **C1** and **C2**, complex **C3** has two protonated ligand-based pyrazolates. The resonance for these N-H protons appears at 12.92 ppm in the ^1H NMR spectrum. The bound acetonitrile is seen in the solid-state structure of **C3** (Figure 3.02) and can additionally be observed by ^1H NMR spectroscopy at 2.94 ppm in CD_2Cl_2 solvent. Notably, in the solid state, both ligand-based N-H's exhibit hydrogen bonding to the BF_4^- anions (1.826 Å). Hydrogen bonding in solution likely contributes to the downfield location of the N-H resonance in the ^1H NMR spectrum.

3.22 Preparation of $^{H}NCN^{H}$ Ligated Complexes

While metalation of tridentate NNN based ligands was performed under mild conditions, metalation of tridentate ligands requiring Ar-H activation to Pt^{II} often requires harsher conditions. It has been performed in refluxing glacial acetic acid (ca. 118 °C) and proceeds by electrophilic aromatic substitution (see chapter 1.3).[17] Addition of 1 equiv. **$(^{H}NCN^{H})^{R}$** (R = H, ^{t}Bu) to 1 equiv. of K_2PtCl_4 in an acetic acid : water (95 : 5) mixture in air affords $Pt(^{H}NCN^{H})^{R}Cl$ (Figure 3.03) after two days at reflux. Formation of $Pt(^{H}NCN^{H})^{R}Cl$ is retarded when no water was added and took an additional 5 days, along with formation of an unidentified side product. However, when significantly

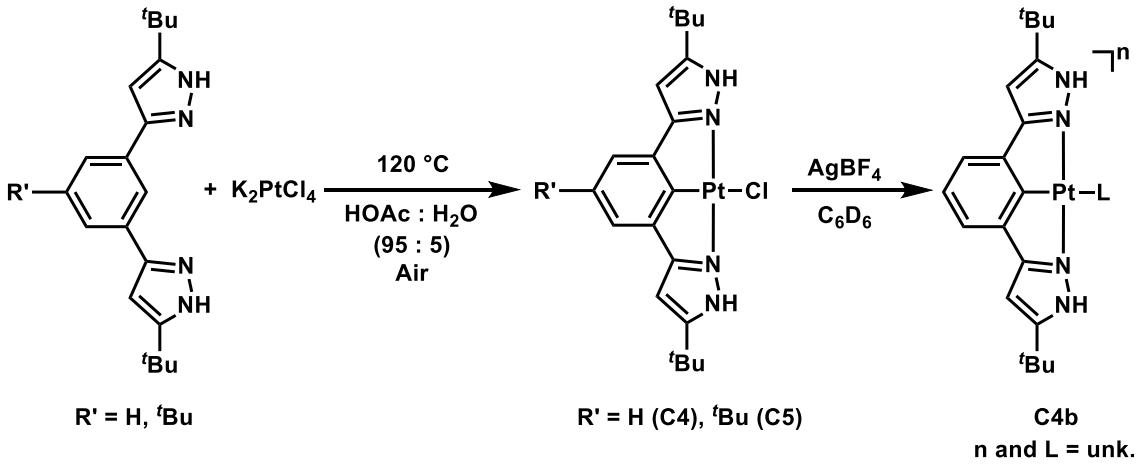

Figure 3.0 3 Metalation of $^{H}NCN^{H}$ to Pt^{II} to form $Pt(^{H}NCN^{H})^{R'}Cl$ (**C4**) and reactivity with $AgBF_4$ to form **C4b**. Thermal ellipsoid plot (50% probability) of **C4** and selected H-atoms omitted for clarity in the solid-state structure. Selected bond lengths for **C4**: O(1)-H(2) 2.144 Å, Pt(1)-Cl(1) 2.421 Å, Cl(1)-H(1) 2.32 Å, C(3)-Pt(1) 1.932 Å.

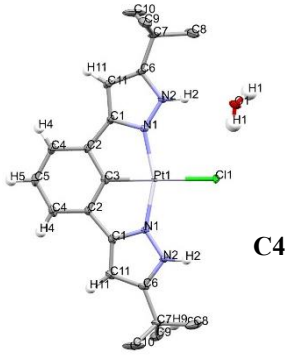

C4

more water was added (50 % water : 50 % acetic acid), significant formation of Pt^0 was observed. When R' = H, $Pt(^{H}NCN^{H})^{H}Cl$ (**C4**, 73 % isolated yield) was formed. However, this reaction was found to be irreproducible and attempts to isolate **C4** resulted in a mixture of products as evidenced by ^{1}H NMR spectroscopy and ESI-MS. Attempts to address the experimental irreproducibility through altering starting material stoichiometry and performing the reaction under inert atmosphere and/or in the absence of ambient light, were targeted, yet ultimately unsuccessful. While the origin of the irreproducibility was not confirmed, one potential explanation is pyridyl ligand Ar-H activation, facilitated by labile protonated pyrazolates.[18–20] Although no Pt-H resonances were observed by ^{1}H NMR spectroscopy, rollover C-H activation of pyrazolate based ligands and pyridyl ligands has been reported for square planar d_8 complexes.[20,21] Characterization of isolated **C4** confirmed a symmetrical ligand environment by both ^{1}H NMR spectroscopy and in the solid state

(Figure 3.03). In the solid state, two hydrogen bond interactions are observed between the ligand N-H and a H_2O molecule, and the water molecule and the Pt-Cl moiety (2.144 Å, and 2.32 Å, respectively). Additionally, the stronger *trans*-influence of the aryl moiety of **C4** compared to the pyridyl moiety of **C1** can be observed in the Pt-Cl bond distance (2.421 Å vs 2.289(4) Å respectively).

When R' = ^{t}Bu, a single product was isolated at the end of the reaction, Pt(^{H}NCN^{H})$^{t Bu}$Cl (**C5**, 88 % isolated yield). By ^{1}H NMR spectroscopy, **C5** is symmetrical in solution and contains 2 aryl resonances, 2 ^{t}Bu resonances and a far downfield N-H resonance. A single side product was sometimes observed by ^{1}H NMR spectroscopy, which could not be separated from **C5**. The side product was additionally symmetric, yet by ESI-MS in CH_3CN, the mixture of products produced only one peak (*m/z* = 557.2, corresponding to Pt(^{H}NCN^{H})NCCH$_3^+$). The side product appears to be similar to **C5** by NMR spectroscopy and ESI-MS and suggests another form of the metalated (**^{H}NCN^{H}**)**^{tBu}** to Pt. At most, two products were observed from the metalation attempts and we hypothesize steric bulk from the central ^{t}Bu moiety of the ligand prevented both the irreproducibility and large number of products observed in metalation of **^{H}NCN^{H}**.

Elimination of the Cl^- ligand through dehydrohalogenation was next attempted. Addition of two equivalents of base (and in some cases excess base) to Pt(NCN)$^{t Bu}$Cl resulted in numerous species by ^{1}H NMR spectroscopy. Bases investigated included NEt_3, NaH, KO^{t}Bu, $C_9H_{16}N_2$ (DBU), $C_{10}H_6(NMe_2)_2$ (proton sponge), and $LiN(C_3H_7)_2$. None of the bases resulted in clean reactivity by ^{1}H NMR spectroscopy. Additionally, when a 3:1 mixture of $NaBH_4$: Pt(^{H}NCN^{H})$^{t Bu}$Cl in MeOH was stirred for 30 minutes, a mixture of products was observed by ^{1}H NMR spectroscopy. Using material from this crude reaction mixture, X-ray quality crystals were grown from slow evaporation of a pentane solution and revealed the complex Pt$_4$(*NCN*)$^{t Bu}$(^{H}NCN^{H})$^{t Bu}_3$

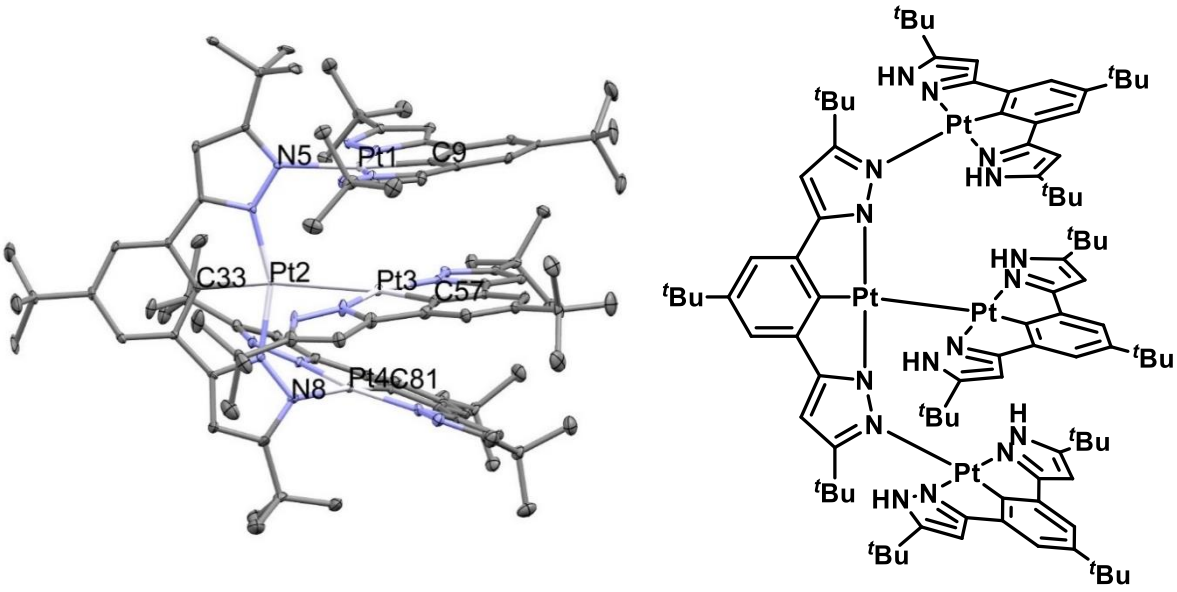

Figure 3.0 4 Thermal ellipsoid plots (50% probability) of $Pt_4(*NCN*)(^{H}NCN^{H})_3$. 2 molecules of pentane, 4 molecules of water and H-atoms omitted for clarity. Selected bond lengths for $Pt_4(*NCN*)(^{H}NCN^{H})_3$: Pt(2)-C(33) 1.959(7) Å, N(5)-Pt(1) 2.129(6) Å, N(8)-Pt(4) 2.182(6) Å, Pt(2)-Pt(3) 2.954 Å

(Figure 3.04). This shows the Cl^- ligand was successfully removed, and a tetranuclear Pt species was formed with a bridging pyrazolate ligand. Multinuclear pyrazolate species have been observed throughout the literature and often occurs when the N-H moiety becomes deprotonated.[18,19,22,23] Additionally, numerous N-H moieties in the solid-state structure were still present. However, dissolution of the crystals in MeOD gave at least one product, which was not representative of the bulk sample by ^{1}H NMR spectroscopy when the deprotonation reaction was performed. As basic solutions of **C5** appeared to form multiple products and/or multinuclear species, a more forcing method of Cl^- removal was next attempted.

Similar to **C1**, the Cl^- ligand can be removed to form a single product by ^{1}H NMR spectroscopy when 1 equivalent of $AgBF_4$ was added to a suspension of **C4** in C_6D_6 (Figure 3.03). Two species initially formed, evidenced by ^{1}H NMR spectroscopy; however, after three days, the species converged to a single species by ^{1}H NMR spectroscopy. This unknown species (**C4b**)

appeared symmetrical in solution and an N-H resonance was observed at 12.02 ppm. No decomposition of **C4b** was observed in a C_6D_6 solution over 24 hours by ^1H NMR spectroscopy. It is unclear what ligand replaced the abstracted Cl^-, however, as neutral **C4** had poor solubility in benzene and **C4b** is fully soluble, it is unlikely the resulting product is cationic. Examination by ESI-MS in CH_3CN revealed a single peak at m/z = 557.2 (corresponding to $[Pt(^{H}NCN^{H})NCCH_3]^+$) and suggests a ligand easily displaced under ESI-MS conditions. When in a C_6H_6 solution, a single deuteride resonance was observed by ^2H NMR spectroscopy at 1.49 ppm with no Pt satellites (referenced to additional C_6D_6). Additionally, no resonance was observed by $^{19}F\{^1H\}$ NMR spectroscopy. A solid-state structure would be required to elucidate the identity of the product. Additionally, performing the chloride abstraction in coordinating solvent (e.g. CH_3CN) would aid in characterization.

*3.23 Synthesis of *NNN* Ligated Pt-Alkyl Species*

The reaction of excess CH_3Li (6 equiv.) with **C1** in THF, followed by quenching with water (3-50 equiv.), afforded $[Li_2Cl][Pt(*NNN*)CH_3](THF)_4$ (**C6**) in 69 % isolated yield (Figure 3.05). ^1H and $^{13}C\{^{13}H\}$ NMR spectroscopy indicated **C6** is symmetrical in solution. A characteristic Pt-

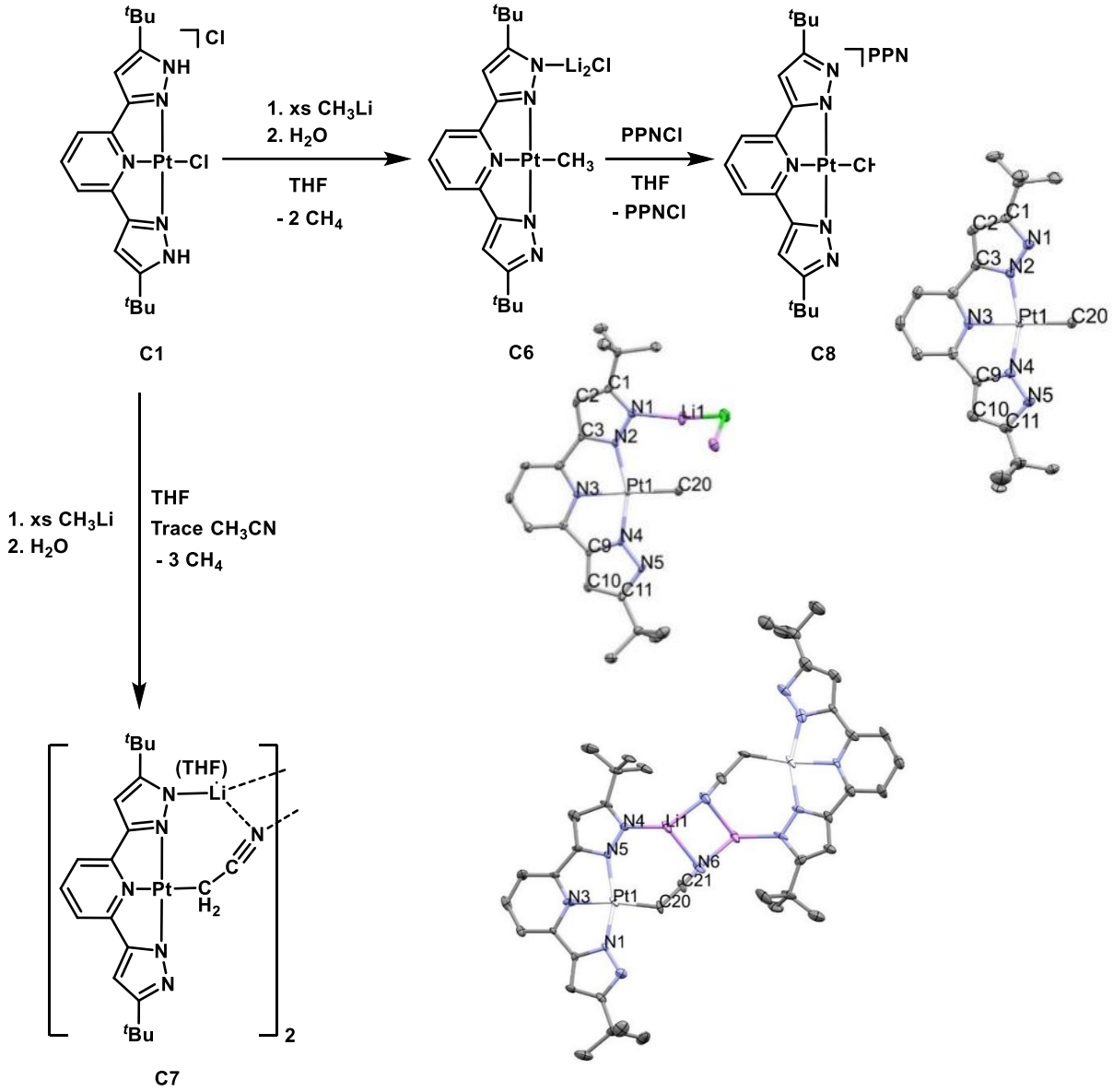

Figure 3.0 5 Reactivity of **C1** with CH_3Li to form $[Li_2Cl][Pt(*NNN*)CH_3]$ (**C6**) and in the presence of CH_3CN to form $[Li(THF)]_2[Pt(*NNN*)CH_2CN]_2$ (**C7**). Cation exchange reaction of **C6** with PPNCl to form $[PPN][Pt(*NNN*)CH_3$ (**C8**). Thermal ellipsoid plots (50 % probability) of **C6**, **C7** and **C8**. Solvents (**C6** – 4 molecules of THF, **C7** – 2 molecules of pentane, **C8** – 2 molecules of THF and 1 molecule of pentane), PPN cation in **C8**, and H-atoms are omitted for clarity. Selected bond lengths for **C6**: C(1)-N(1) 1.358(9) Å, C(3)-N(4) 1.368(9) Å, Li(1)-N(1) 2.01(1) Å, Li(1)-C(20) 2.88(2) Å, C(1)C(2) 1.397(6) Å, C(2)C(3) 1.388(6), Pt(1)-C(20) 2.053(6) Å. **C7**: N(4)-Li(1) 1.94(4) Å, Li(1)-N(6) 2.26(4) Å, C(21)-N(6) 1.15(2) Å, Pt(1)-C(20) 2.05(2) Å, Pt(1)-N(3) 1.96 Å. **C8**: C(1)N(1) 1.357(6), C(3)N(2) 1.376(5), C(1)C(2) 1.39(1) Å, C(2)C(3) 1.39(1) Å, Pt(1)-C(20) 2.061(3) Å.

CH_3 resonance was observed at 1.11 ppm ($^2J_{Pt\text{-}H}$ = 79 Hz) in THF-d_8. Examination of the solid-state

structure of **C6** (Figure 3.05) revealed a pyrazolate Li-Cl-Li interaction with THF solvated Li cations. Further evidence for Li coordination is the broad singlet at -1.20 ppm in the $^{7}Li\{^{1}H\}$ NMR spectrum of **C6** in acetone-d_6. Dissolution of **C6** in CD_3CN or acetone-d_6 results in the liberation of THF by ^{1}H NMR spectroscopy. There have been similar reports of first row transition metals with Li-Cl pyrazolate adducts[24] and these examples help demonstrate the ability of ligand-based pyrazolate N to additionally act as a Lewis base. The Li-N distance of **C6** is 2.01(1) Å and is slightly long compared to other inner-sphere Li ion-pyrazolate pairing distances with other metals (M = Co, Ni, Fe).[24,25] In fact, a much shorter Li-N distance (1.678 Å) was observed in a pyrazolate ligated Co^{I} complex.[24] This was postulated to be due in part from further interaction of Li^{+} with the Co^{I}-Cl ligand.

In the presence of trace amounts of acetonitrile, reaction of **C1** with excess CH_3Li in THF prevents formation of **C6** as the final product and forms $[Li(THF)]_2[Pt(*NNN*)CH_2CN]_2$ (**C7**, Figure 3.05) in 66 % isolated yield. Formation of **C7** is not an intermediate in the formation of **C6** as no reaction was observed by ^{1}H NMR spectroscopy when 3 equiv. CH_3Li were added to a THF-d_8 solution of **C7**. **C7** was characterized by ^{1}H, $^{13}C\{^{1}H\}$, and $^{7}Li\{^{1}H\}$ NMR spectroscopy and X-ray crystallography. ^{1}H, $^{13}C\{^{13}H\}$ and $^{7}Li\{^{1}H\}$ NMR spectroscopy indicated complex **C7** is symmetrical in solution. A characteristic Pt-CH_2CN resonance was observed at 2.50 ppm ($^{2}J_{Pt\text{-}H}$ = 110 Hz) in acetone-d_6. Examination of the solid-state structure revealed dimeric formation through the bridging and bent CH_2CN ligand and Li cation.

Removal of the $LiClLi^{+}$ cation by treatment of **C6** with 1 equiv. bis(triphenylphosphine)iminium chloride (PPNCl) yields $[PPN][Pt(*NNN*)CH_3]$ (**C8**) in (Figure 3.05). The solid-state structure (Figure 3.05), the lack of a resonance in the $^{7}Li\{^{1}H\}$ NMR spectrum, and the presence of a resonance in the $^{31}P\{^{1}H\}$ spectrum, confirms the pyrazolate ligand is no longer

involved in an inner sphere cation interaction with lithium. Complex **C8** appears symmetrical in solution by ^{1}H and $^{13}C\{^{1}H\}$ spectroscopy with a characteristic Pt-CH_3 resonance at 1.11 ppm ($^{2}J_{Pt\text{-}H}$ = 82 Hz) in CD_3CN.

Interestingly, reaction of a THF solution of CH_3MgCl (4.2 equiv.) with 1 equiv. of **C1** in benzene, followed by quenching with water (3 equiv.) did not result in a Pt-CH_3 with an inner sphere Mg, but resulted in the generation of [Pt(^{H}NNN^{H})CH_3][Cl], (**C9**). Isolation of **C9** in the absence of the MgX_2 salts formed (hypothesized as present from THF impurity present in spectral data) has not been possible, yet characterization by ^{1}H NMR spectroscopy indicates that **C9** is symmetrical in solution. A broad N-H resonance was observed downfield at 13.3 ppm and a characteristic Pt-CH_3 resonance was found at 1.24 ppm ($^{2}J_{Pt\text{-}H}$ = 78 Hz) in acetone-d_6 in the ^{1}H NMR spectrum. **C9** was also characterized by X-ray crystallography. In the solid state (Figure 3.07b), a chloride anion is also present at a hydrogen bonding distance (2.270 Å) from the N-H on the ligand. Reaction of **C9** with $NaBAr^{F}_{24}$ (0.9 equiv) yielded [Pt(^{H}NNN^{H})CH_3][BAr^{F}_{24}], (**C10**). Complex **C10** was isolated and characterized by ^{1}H, $^{13}C\{^{1}H\}$, and $^{19}F\{^{1}H\}$ NMR spectroscopy, and the spectra are also indicative of a symmetric species. A similar Pt-CH_3 resonance was also observed at 1.21 ppm ($^{2}J_{Pt\text{-}H}$ = 79 Hz). Even though Pt-CH_3 complexes (**C6**, **C8** and **C9**) all contain unique secondary sphere N interactions, they contain similar spectroscopic features in the solution phase. When solvated in acetone-d_6, a slight change in the ^{1}H NMR resonance of the Pt-CH_3 moiety from **C6** (1.34 ppm, $^{2}J_{Pt\text{-}H}$ = 82 Hz) to **C8** (1.42 ppm, $^{2}J_{Pt\text{-}H}$ = 84 Hz) to **C9** (1.27 ppm, $^{2}J_{Pt\text{-}H}$ = 79 Hz) was noted**.** The bond lengths observed in the solid-state structure are also very similar to one another. Notably, the ligand pyrazolate N interactions do not result in a change in the bond lengths of the C-C and C-N bonds within the pyrazolate moiety (e.g. **C8**: C(1)N(1), 1.357(6) Å and **C6**: C(1)N(1), 1.358(9) and **C9**: C(1)N(1),

1.357(6) Å). Furthermore, no appreciable difference is observed in the Pt-CH_3 bond distance between anionic **C6** (2.053(6) Å) and **C8** (2.061(3) Å) and cationic **C9** (2.064(3) Å).

*3.24 Synthesis of *NCN* Ligated Pt-Alkyl Species*

Addition of 5 equiv. of CH_3Li to Pt(^{H}NCN^{H})^{H}Cl (**C4**) and Pt(^{H}NCN^{H})^{tBu}Cl (**C5**) generated $[Li]_2[Pt(*NCN*)^{R'}CH_3]$ (**C11,** R' = H**; C12**, R' = ^{t}Bu, respectively, Figure 3.06a). **C11** and **C12** were H^+ and O_2 sensitive which made their successful reproducible isolation challenging. Isolation of **C11** was eventually achieved (45.0 % yield) and crystals suitable for X-ray diffraction were obtained (Figure 3.06a). **C11** was not stable in C_6D_6 for extended time and began decomposing after 12 hours to numerous unidentified species with concomitant methane generation. ^{1}H NMR spectroscopy indicated complex **C11** is symmetrical in solution. A characteristic Pt^{II}-CH_3 resonance was observed at 0.09 ppm ($^{2}J_{Pt\text{-}H}$ of 41 Hz) in dry C_6D_6. Similar low ^{2}J has been observed when Pt^{II}-CH_3 is *trans* to aryl moieties.[26,27] Additionally, bound THF can be observed by ^{1}H NMR spectroscopy at l.31 ppm and 3.39 ppm in C_6D_6 (shifted from free THF at 1.47 ppm and 3.47 ppm).[28] Examination of the solid-state structure of **C11** revealed two pyrazolate-Li interactions with THF solvated Li cations at a N-Li distance of 2.00(1) Å, which is similar to the N-Li distance in **C6** (2.01(1) Å). While no difference was observed in the Pt-CH_3 bond distance of **C6** (2.053(6) Å) vs

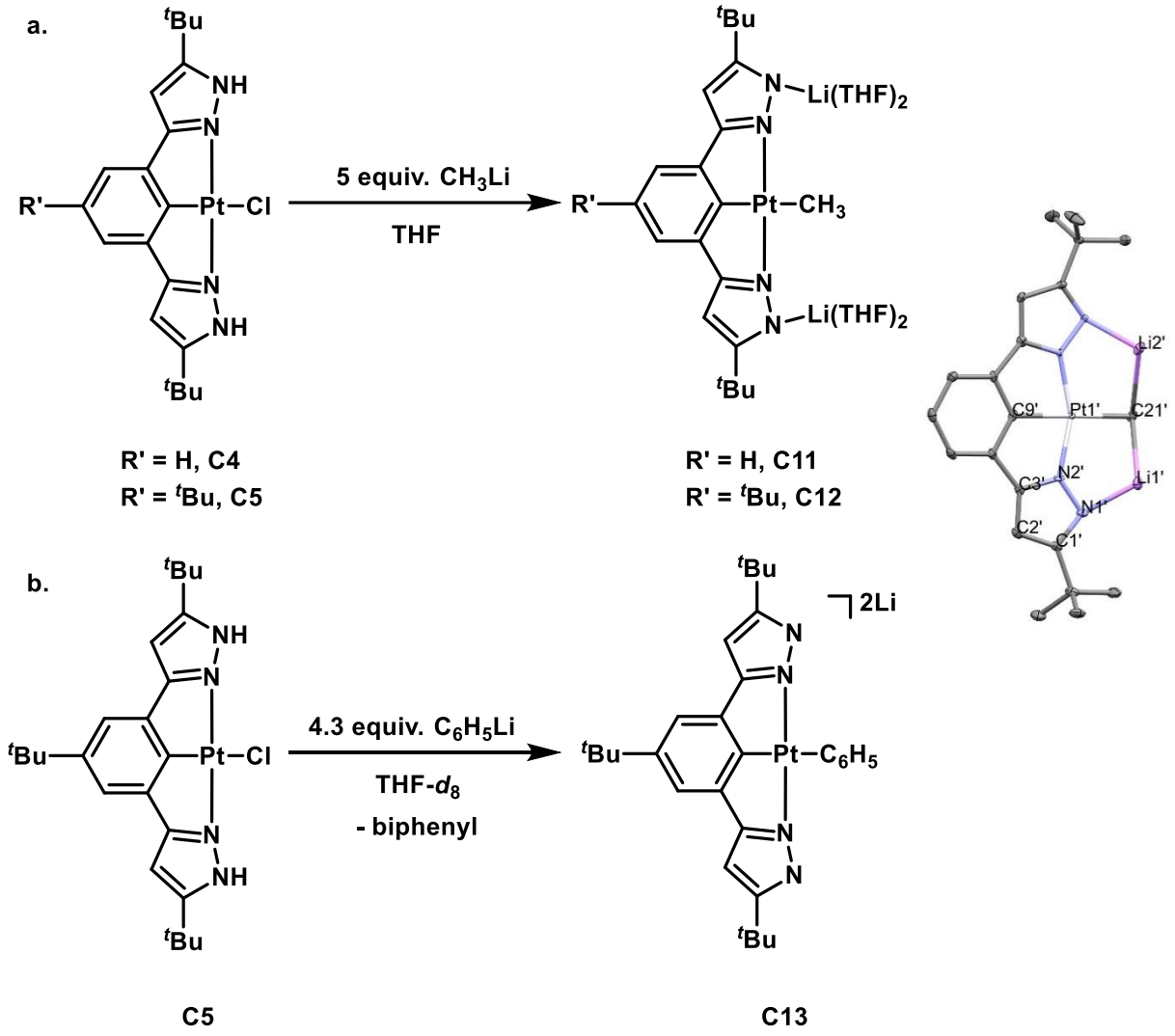

Figure 3.0 6 Reactivity of (a) Pt(^{H}NCN^{H})Cl (R = H, **C4** and R = ^{t}Bu, **C5**) with CH_3Li to form $[Li]_2[Pt(*NCN*)^{R}CH_3]$ (R = H, **C11** and R = ^{t}Bu, **C12**) and (**b**) **C4** with C_6H_5Li to form$[Li]_2[Pt(*NCN*)^{R}C_6H_5]$, **C13.** Thermal ellipsoid plots (50 % probability) of **C11**. 4 molecules of THF and H-atoms are omitted for clarity. Selected bond lengths for **C11**: C(1')-N(1') 1.354(7) Å, C(2')-C(3') 1.382(7) Å, Li(1')-N(1') 2.00(1) Å, Li(1')-C(21') 2.32(1) Å, C(1')C(2') 1.390(7) Å; N(2')C(3'), 1.369(6); Pt(1')C(21') 2.161(5) and Pt(1')C(9') 1.981(5).

C8 (2.061(3) Å), **C11** exhibited a longer Pt-CH_3 bond distance (2.161(5) Å), possibly due to the dianionic nature of the ligand and/or the stronger *trans* aryl moiety. Although it could not be isolated, the formation of **C12** was confirmed by the observation of methane (which resulted from

deprotonation of acidic pyrazole protons with CH_3Li reagent) and the appearance of a new methyl signal in the ^1H NMR spectrum at 0.08 ppm ($^2J_{Pt-H}$ of 43 Hz) in C_6D_6. This Pt^{II}-CH_3 resonance is similar to **C11** in chemical shift and $^2J_{Pt-H}$. A possible explanation for the inability to isolate **C12** in relation to **C11** could be due to the stronger donating ability in the central aryl ring from the additional ^{t}Bu moiety. This would result in a more electron rich Pt^{II} center, promoting protonation reactions at the metal.

The addition of 4.3 equivalents of C_6H_5Li to a suspension of **C5** in THF-d_8 yielded complex $[Li]_2[Pt(*NCN*)^{tBu}C_6H_5]$ (**C13**, Figure 3.06b) along with two equivalents of benzene and half an equivalent of biphenyl (determined by ^1H NMR spectroscopy). **C13** was not isolated and subsequent reactions (*vide infra*) were performed on a crude reaction mixture. The biphenyl appears only after the addition of the second equivalent of phenyl lithium. Biphenyl has been shown to form by C-C cross coupling when aryl lithium and aryl tin reagents are introduced to Pt^{II}/Pd^{II} complexes.[29,30] ^1H NMR spectroscopy indicated **C13** is symmetrical in solution. The Pt-C_6H_5 peaks at 8.2 ppm ($^3J_{Pt-H}$ = 31 Hz), 7.0 ppm ($^4J_{Pt-H}$ = 24 Hz) and 7.25 ppm in the ^1H NMR spectrum confirm Pt-C_6H_5 formation.

3.25 Electrophile (H^+ and CH_3^+) Addition to Pyrazolate Supported Pt^{II}-alkyl Compounds

The reactions of the Pt^{II}-alkyl complexes with pyrazolate N in the ligand with electrophiles (H^+ and/or CH_3^+) was probed to determine if electrophile addition was preferred at the ligand or the Pt^{II} center. We also monitored the reactions to see if direct CH_3-R (R = H, C) bond formation occurred. All species investigated have two pyrazolate functionalities built into the ligand framework. Furthermore, the effect of Li coordination to the deprotonated pyrazolate moiety was investigated using complexes containing N-Li interactions. **C6** and **C7** contain Li coordination to a

single pyrazolate N, while **C11** and **C12** contain Li coordination to both pyrazolate N sites. **C8** does not contain any Li coordination. The presence of a Li pyrazolate interaction might inhibit ligand reactivity at this site. The reactions of electrophilic reagents (HX and CH_3I) with these complexes was also investigated.

*3.25.1 Proton Addition to (*NNN*) ligated Pt^{II}-alkyl (C6, C7, C8) Compounds*

The reactions of **C7** with acids were first investigated. Addition of excess acid (5 equiv. HCl etherate, HBF_4 etherate or 2,6-dimethoxypyridinium tetrafluoroborate) to **C7** generated monomeric [Pt(^{H}NNN^{H})(CH_2CN)][Cl] (**C7a**) or [Pt(^{H}NNN^{H})(CH_2CN)][BF_4] (**C7b**) (68 % and 83 % isolated yield, respectively; Figure 3.07a). Complexes **C7a** and **C7b** were symmetrical in solution, evidenced by ^{1}H and ^{13}C{^{1}H} NMR spectroscopy and exhibited similar Pt-C$\underline{H}_2$CN resonances at 2.87 ppm and 2.88 ppm (both $^{2}J_{Pt\text{-}H}$ = 101 Hz) in MeOD. The $^{2}J_{Pt\text{-}H}$ coupling of the Pt-CH_2CN of **C7** (110 Hz) noticeably decreased when the pyrazolate N's were protonated. Additionally, the Pt-CH_2CN appears to be stable to 0.5 additional equivalents of acid (per Pt^{II} center) as no N bound CH_3CN or release of CH_3CN was observed by ^{1}H NMR spectroscopy. A solid-state structure of **C7b** was obtained (Figure 3.07a) and revealed an H-bonding interaction between pyrazolate N-H and bound CH_2CN based on distance (2.09 Å) and N-H-N bond angle (149.5 °). This study indicates addition of Brønsted acid to **C7** reacted exclusively at the ligand to form **C7a** and **C7b**. Protonation of the Pt-CH_2CN moiety did not occur, even with an additional 0.5 equiv. of acid.

Addition of 2,6-dimethoxypyridinium tetrafluoroborate (pK_a = 7.6 in CH_3CN)[31] to an acetone-d_6 solution of **C6** and to a CD_3CN solution of **C8** were monitored by ^{1}H NMR spectroscopy. Notably, no Pt-H signals were observed during either of the acid addition experiments and methane elimination was not observed until more than two equivalents of acid had been added to either

complex. The results detailed below describe the speciation and overall results of the protonation studies of **C6** and **C8** (summarized in Figure 3.07b and ^{1}H NMR spectra appear in Figure 3.08). After addition of one equivalent of acid (either HCl or HBF_4 etherate) to **C6** or **C8**, a poorly soluble yellow solid precipitated (labeled [Pt] in Figure 3.07b. and 3.07c) and only very broad features were visible in the ^{1}H NMR spectrum (see 0.8 equiv. and 1.4 equiv. in Figure 3.08a; 1.0 equiv in Figure 3.08b). Attempts to characterize these species independently were unsuccessful due to limited solubility in numerous common laboratory solvents (i.e. pentane, diethyl ether, THF, CH_2Cl_2, acetone, CH_3CN and DMF).

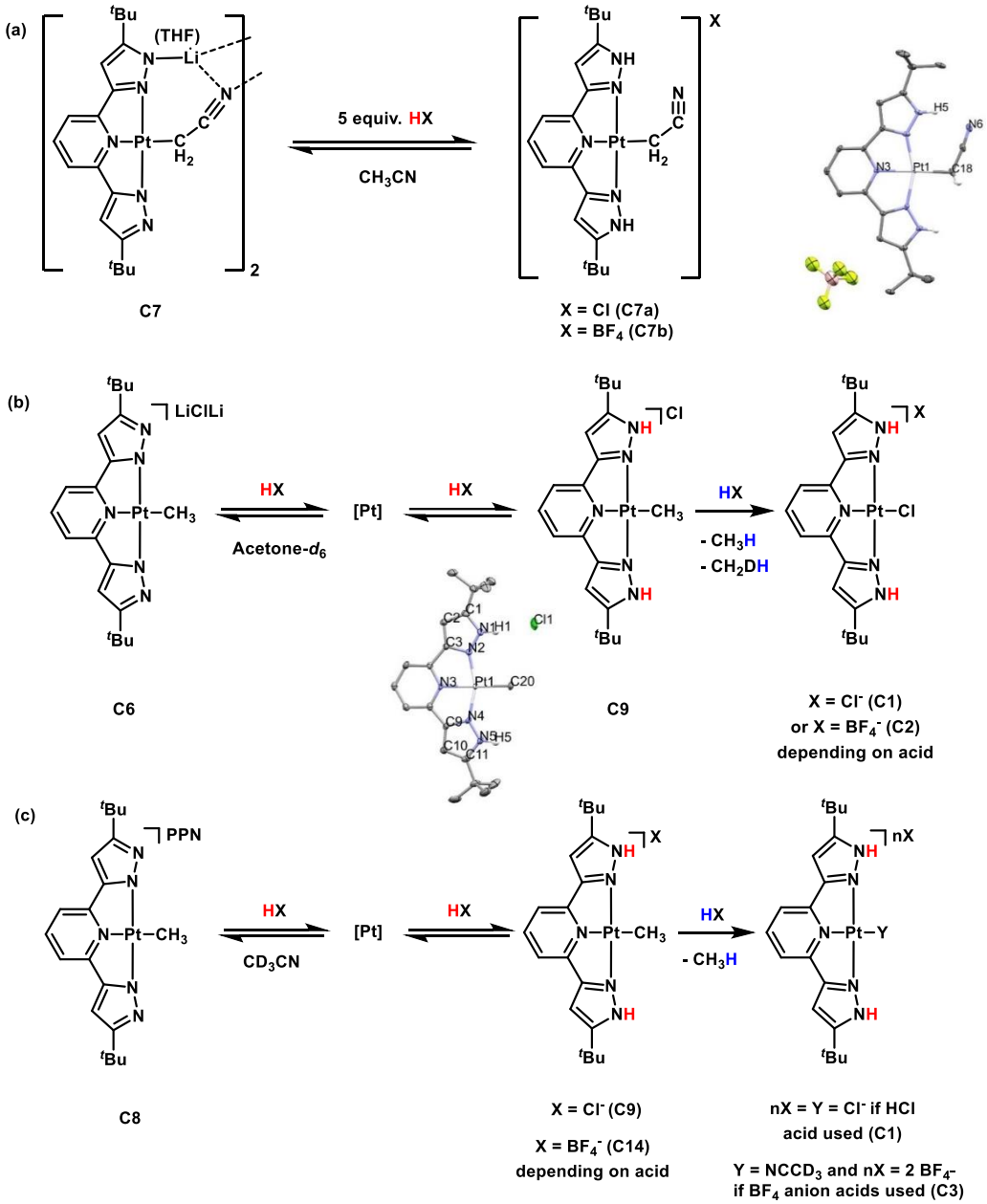

Figure 3.0 7 Protonation of (**a**) **C7** with HCl and HBF_4 etherate/2,6 dimethoxy pyridinium tetrafluoroborate to form [Pt(^{H}NNN^{H})(CH_2CN)][Cl] (**C7a**) and [Pt(^{H}NNN^{H})(CH_2CN)][BF_4] (**C7b**), respectively. (**b**) Speciation during the protonation of [Li_2Cl][Pt(*NNN*)CH_3 (**C6**), and formation of complexes: [Pt(^{H}NNN^{H})CH_3][Cl] (**C9**), [Pt(^{H}NNN^{H})Cl][Cl] (**C1**), and [Pt(^{H}NNN^{H})Cl][BF_4] (**C2**) in acetone-d_6. CDH_3 formation most likely proceeds through N-H/D exchange with solvent. No H/D exchange occurs in CD_3CN. (**c**) Speciation during the protonation of **C8**: [Pt(^{H}NNN^{H})CH_3][Cl] (**C9**), [Pt(^{H}NNN^{H})CH_3][BF_4] (**C14**), [Pt(^{H}NNN^{H})Cl][Cl] (**C1**), and [Pt(^{H}NNN^{H})$NCCD_3$][(BF_4)$_2$] (**C3**). Thermal ellipsoid plots (50% probability) of **C7b** and selected bond lengths: Pt(1)-N(3) 2.002(10) Å, Pt(1)-C(18) 2.076(12) Å, H(5')-N(6) 2.086 Å.

With addition of two equivalents of 2,6-dimethoxypyridinium tetrafluoroborate to **C6**, [Pt(^{H}NNN^{H})CH$_3$][Cl] (**C9**) was observed in the ^{1}H NMR spectrum (Figure 3.07b, Figure 3.08a at 2.2 equiv., 65 % spectroscopic yield). Addition of HBF_4 etherate also resulted in the formation of **C9**. To confirm the assignment of **C9** as the product in these reactions, an authentic sample of **C9** (Section 3.23) was added into the reaction mixtures. Addition of two equivalents of HCl etherate to **C8**, the PPN salt analog of **C6**, was also observed to form **C9** (Figure 3.07c, 90% spectroscopic yield). Formation of **C9** suggests protonation at the ligand is preferred over Pt^{II}/Pt^{II}-CH_3 protonation. Complex **C9** was stable to thermolysis conditions until 150 °C in a C_6D_6 suspension, where slow CH_4 formation was observed by ^{1}H NMR spectroscopy. After heating for 15 hours at 180 °C in C_6D_6, formation of a single new species was observed after removing the solvent *in vacuo* and re-dissolving in CD_3CN. By ^{1}H NMR spectroscopy, a symmetrical complex was observed with all NMR resonances shifted slightly upfield compared to [Pt(^{H}NNN^{H})Cl][Cl] (**C1**, ca. 0.2 ppm change for aryl resonances and 0.05 ppm change for the ^{t}Bu resonance). Examination by ESI-MS revealed a single peak at *m/z* = 553.1 (corresponding to Pt(^{H}NNN^{H})Cl$^+$). The similarity in the ^{1}H NMR spectrum to that of **C1** suggest that the new compound is Pt(^{H}NNN*)Cl. However, numerous attempts to deprotonate **C1** to form Pt(^{H}NNN*)Cl to allow conclusive identification were unsuccessful. A variety of bases (KHMDS, LiOH, NEt_3, DBU, KO^{t}Bu, NaH) were used, but none gave clean reactivity. However, addition of HCl etherate to the thermolysis product reformed **C1**. If

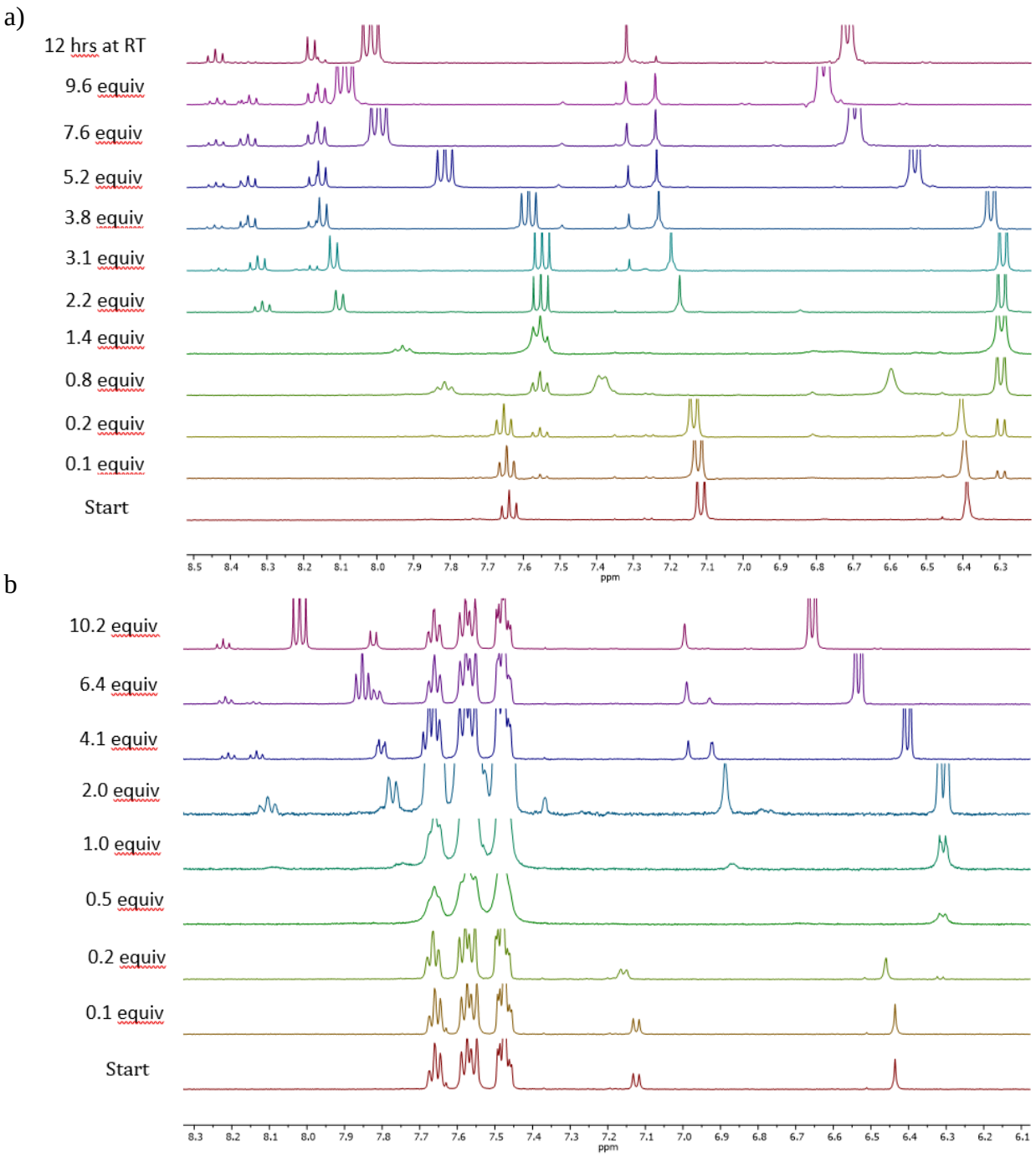

Figure 3.0 8 ^{1}H NMR spectra (500 MHz) showing the addition of 2,6-dimethoxypyridinium tetrafluoroborate to a solution of (**a**) $[Li_2Cl][Pt(*NNN*)CH_3]$ (**C6**) in acetone-d_6 and (**b**) [PPN][Pt(*NNN*)CH_3] (**C8**) in CD_3CN. In the spectra above, the aryl region is highlighted.

Pt(^{H}NNN*)Cl is the product of the thermolysis reaction, it suggests C-H elimination from

cooperation of ligand-based N-H and the Pt-CH_3 from **C9** is possible, although a very high reaction temperature is required.

An analogous species to **C9**, **C14**, was observed *in situ* when two equivalents of 2,6-dimethoxypyridinium tetrafluoroborate were added to **C8** (Figure 3.07c, Figure 3.08b at 2.0 equiv., 77 % spectroscopic yield). Despite multiple attempts, we were unable to isolate **C14** from the addition of acid to **C8** or independently through anion exchange of **C9** with $NaBF_4$. All resonances for **C14** are shifted slightly downfield of **C9** in the ^{1}H NMR spectrum in CD_3CN. The ^{1}H NMR signals for complex **C14** indicate that it is also symmetrical in solution. Additionally, the Pt-CH_3 ligand exhibits the same $^2J_{Pt\text{-}H}$ of 78 Hz as **C9**. The broad N-H resonance of **C14** is observed downfield at 12.3 ppm in CD_3CN, which is similar to that of **C9** (12.1 ppm).

Addition of the acid 2,6-dimethoxypyridinium tetrafluoroborate to complex **C9** in CD_3CN or acetone-d_6 yielded **C2** (Figure 3.07b) with concomitant methane formation over the course of several days. After protonation, the Cl^- counter anion of **C9** preferentially coordinates to the unsaturated Pt center to form **C2**, even in the presence of coordinating solvents, such as acetonitrile. 2,6-lutidinium tetrafluoroborate (pK_a = 14.1 in acetonitrile)[31] will also protonate the methyl ligand to form **C2** (78 % isolated yield).

Protonation of the methyl ligand of **C14** with 2,6- dimethoxypyridinium tetrafluoroborate in CD_3CN formed the dicationic **C3-*d*$_3$** (Figure 3.07c). Confirmation of this species was achieved by comparison with an authentic sample of [Pt(^{H}NNN^H)NCC$\underline{D}_3$][BF_4]$_2$, prepared by stirring non-deuterated **C3** in CD_3CN and removing the solvent. Here, the acetonitrile solvent traps the unsaturated metal center to form a Pt-solvento complex. Additionally, both **C9** and **C14** contain protonated ligands with a methyl ligand still intact after two equivalents of added acid. Generation

of **C9** and **C14** in our acid addition studies indicates that the ligand pyrazolate sites are protonated in preference to the metal or metal-methyl bond.

*3.25.2 Proton Addition to Pt(*NCN*)CH_3 (**C11, C12**) and Pt(*NCN*)C_6H_5 (**C13**)*

Addition of H_2O (2 equiv) and HCl (1 equiv) at room temperature to **C11** and **C12**, respectively, yielded **C4a** and **C5a** (Figure 3.09). **C4a** and **C5a** are both symmetrical in solution by

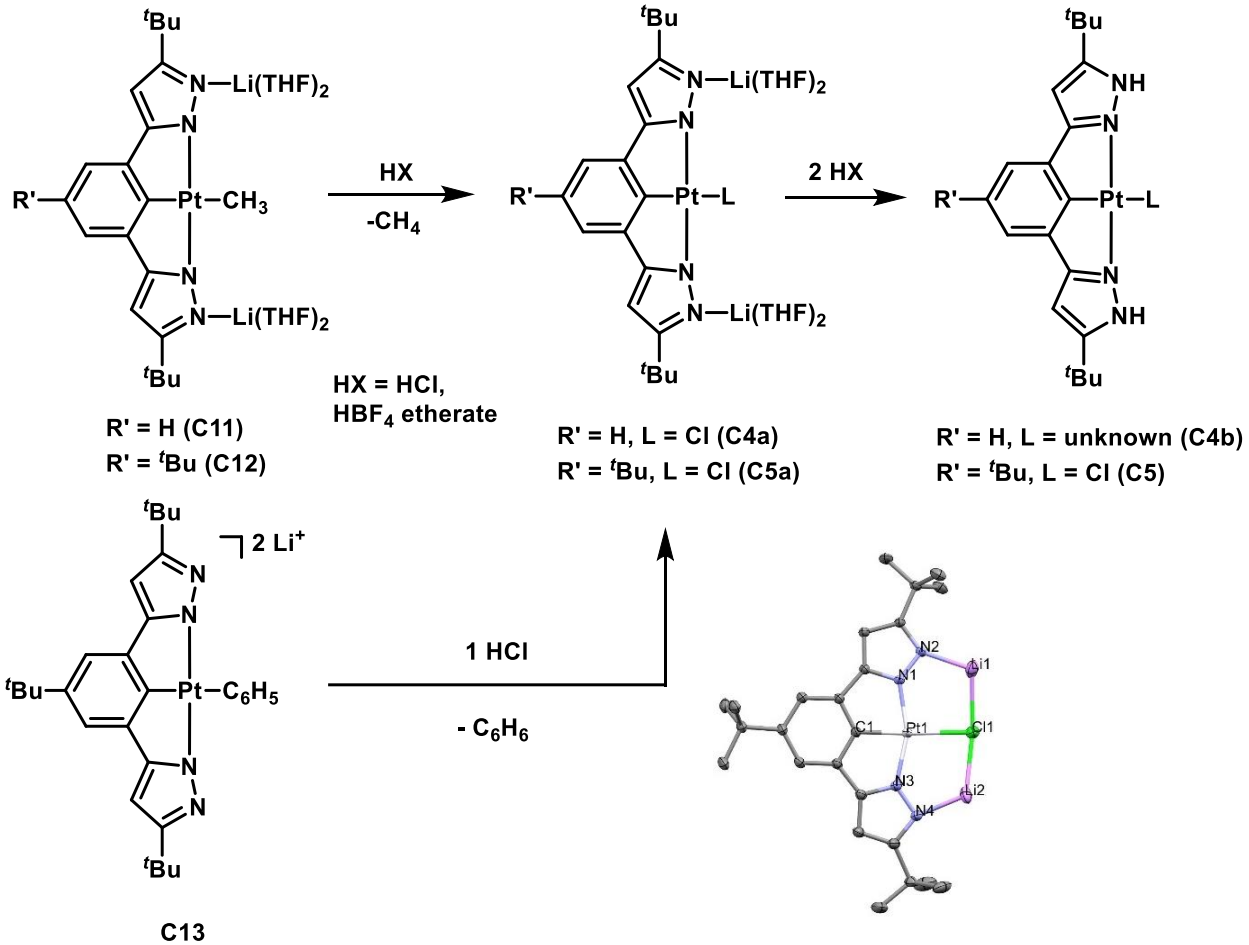

Figure 3.0 9 Speciation during the protonation of $[Li_2][Pt(*NCN*)R]$ (R = CH_3: [R' = H (**C11**), R' = ^{t}Bu (**C12**)]; R = C_6H_5 [R' = ^{t}Bu (**C13**)]) and formation of complexes: $[Li_2][Pt(*NCN*)^RL]$ (L = Cl^-: R' = ^{t}Bu (**C5a**), H (**C4a**)), $Pt(^HNCN^H)^{R'}L$ (L = Cl^- [R' = ^{t}Bu (**C5**)]); L = unknown [R' = H]) in THF-d_8. Thermal ellipsoid plots (50 % probability) of **C5a.** 4 THF molecules and H-atoms omitted for clarity. Selected bond lengths for **C5a**: Pt(1)-C(1) 1.929(4) Å, Pt(1)-Cl(1) 2.452(2) Å, Li(1)-Cl(1) 2.38(1) Å, Li(1)-N(2) 2.034(9).

^{1}H NMR spectroscopy and release of CH_4 was observed when the reaction was monitored *in-situ*. The symmetrical nature is further evidenced by a solid-state structure of **C5a**, which compared to **C11**, also contains two N-Li interactions. Similar reactivity to protonation of **C4a** and **C5a** was observed when 1 equiv. of HCl was added to *in situ* generated **C13** and formed **C5a** by ^{1}H NMR spectroscopy. The protonation of **C12** with HCl was additionally studied at -73 °C in THF-d_8 by ^{1}H NMR spectroscopy, where a mixture of products was observed (Figure 3.10). In the ^{1}H NMR spectrum at -73 °C, **C12** and **C5a** are observed, along with an unsymmetrical unknown species and concomitant methane loss. This unknown species contains a resonance centered at 12.02 ppm, likely

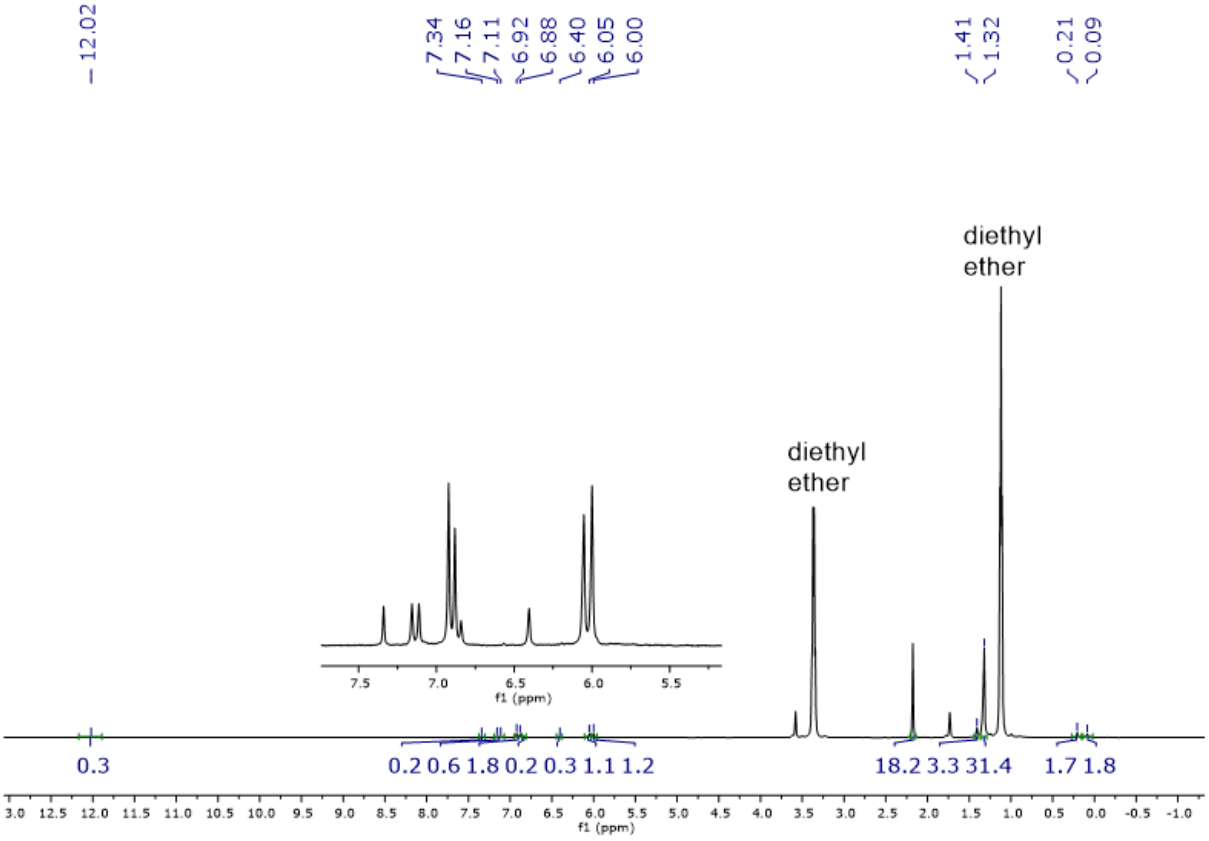

Figure 3. 10 VT ^{1}H NMR spectrum (500 MHz) of addition of HCl etherate (1M, 0.016 mmol) to a solution of **C12** at -73 °C.

corresponding to an N-H of the pyrazole arm. However, there was no observable methyl resonance associated with this intermediate. Upon warming the reaction vessel with 1 equiv. of HCl and **C12**

to room temperature, **C5a** was the only product observed by ^{1}H NMR spectroscopy. Further protonation of **C5a** with 2 or 10 equivalents of HCl formed **C5**. To investigate an acid with a weakly coordinating anion that doesn't have a driving force for formation of a Pt-X species, 1 equiv. HBF_4 etherate was added to a C_6D_6 solution of **C12**. Methane was observed, along with a number of unidentifiable resonances in the ^{1}H NMR spectrum. The ^{1}H NMR spectrum converged to a single species when 3 or more equiv. of HBF_4 etherate were added, matching those for **C4b**. These experiments suggest that the Pt^{II}/Pt^{II}-R of **C11**, **C12 and C13** are too basic compared to the ligand N, given the propensity to loss of R-H (CH_4 or C_6H_6) upon acid addition. Ligand protonation of **C11**, **C12** or **C13** was not observed and could be due to the strong aryl *trans* moiety, compared to *NNN* ligated Pt-alkyl species.

*3.25.3 Reactivity of *NCN* ligated (C11) and *NNN* ligated (C8) Pt^{II}-CH_3 complexes with CH_3I*

Reaction of a C_6D_6 solution of **C11** $(Pt(*NCN*)^{H}CH_3)^{2-}$ with 2 equiv. methyl iodide initially revealed a broad symmetrical major and minor Pt complex with Pt-CH_3 resonances at 0.72 ppm ($^{2}J_{Pt\text{-}H}$ = 43 Hz, 80 % spectroscopic yield) and 0.10 ppm ($^{2}J_{Pt\text{-}H}$ = 44 Hz, 20 % spectroscopic yield), respectively. No ethane or methane were observed by ^{1}H NMR spectroscopy. The Pt-CH_3 resonances of both complexes integrated to 6H when compared to their respective aryl ligand resonances. Additionally, bound THF can be observed by ^{1}H NMR spectroscopy at l.40 ppm and 3.65 ppm in C_6D_6 (shifted from uncoordinated THF). As the ligand and two $Pt(CH_3)_2$ resonances are broad, there could be possible exchange occurring between different $Pt^{IV}(CH_3)_2$ conformers of $[Li(THF)_2]_2[Pt(*NCN*)^{tBu}(CH_3)_2I]$ (Figure 3.11). Over 16 hours, the major and minor Pt product

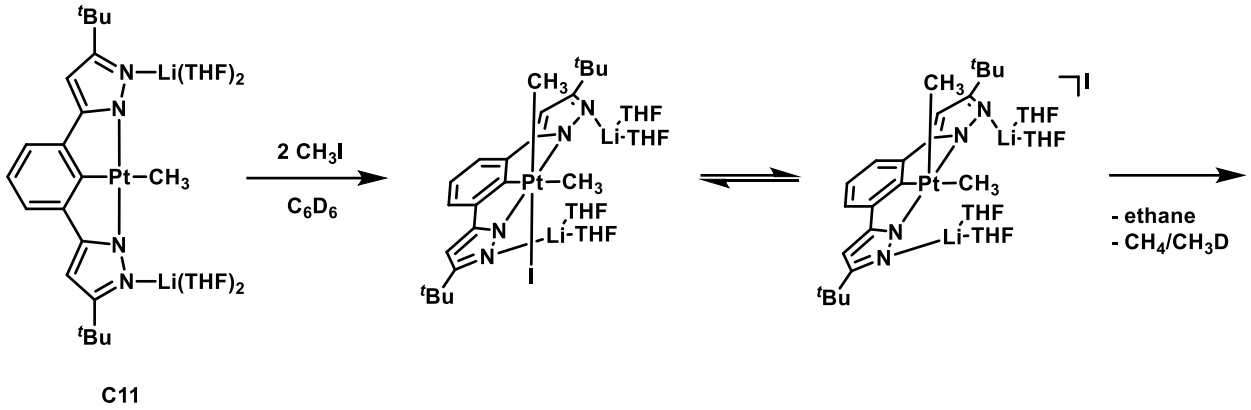

C11

Figure 3.1 1 Reaction of **C11** ([Li(THF)$_2$][Pt(*NCN*)CH$_3$]) with 2 equiv. CH$_3$I to form a mixture of two Pt^{IV}-(CH$_3$)$_2$ complexes, proposed to be [Li(THF)$_2$]$_2$[Pt(*NCN*)^{tBu}(CH$_3$)$_2$I] and a potential 5 coordinate [Li$_2$(THF)$_4$I][Pt(*NCN*)^{tBu}(CH$_3$)$_2$]. These two Pt compounds decompose to form ethane, CH$_4$, CH$_3$D, and unknown Pt complexes.

began to diminish with the growth of several new Pt-CH$_3$ resonances at 2.14 ppm ($^2J_{Pt\text{-}H}$ = 69 Hz) and 1.74 ppm ($^2J_{Pt\text{-}H}$ = 77 Hz) and concomitant methane (CH$_4$/CH$_3$D) and ethane formation. Even in the presence of 2 equiv. CH$_3$I, N-methylation was not observed by ^{1}H NMR spectroscopy, suggesting that reactivity occurs exclusively at Pt^{II}. While the exact reason has not yet been determined, it could be due to the inability of ligand N in **C11** to act as a nucleophile, having the ligand N-site blocked by Li coordination. However, a more likely explanation is due to the strong *trans* influence of the aryl moiety, putting more electron density on the Pt^{II} center.

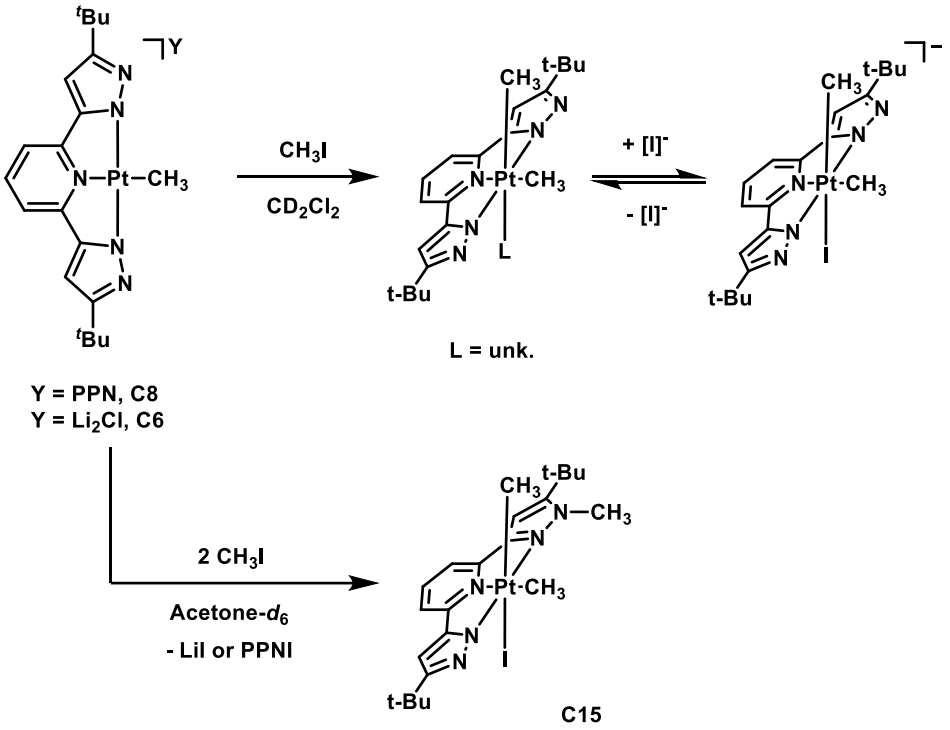

Figure 3.1 2 Reaction of **C6** ([Li_2Cl][Pt(*NNN*)CH_3]) and **C8** ([PPN][Pt(*NNN*)CH_3]) with 1 equiv. CH_3I to form a mixture of two Pt^{IV}-(CH_3) complexes. Addition of KI to the [Pt] mixture to form proposed [Pt(*NNN*)$^{H}(CH_3)_2I]^-$. Reaction of **C8** with 2 equiv. CH_3I to form [Pt(^{CH3}NNN*)$^{H}(CH_3)_2I$][I] (**C15**).

Reaction of a CD_2Cl_2 solution of **C8** with one equiv. of CH_3I formed two different symmetrical Pt-$(CH_3)_2$ complexes in a 1:4 ratio. By ^{1}H NMR spectroscopy, the first complex contained Pt-$(CH_3)_2$ resonances at 1.93 and 1.03 ppm ($^2J_{Pt\text{-}H}$ = 68, 76 Hz, respectively) and the second contained Pt-$(CH_3)_2$ resonances at 1.72 and 0.85 ppm ($^2J_{Pt\text{-}H}$ = 70, 74 Hz, respectively). To attempt to drive the mixture of complexes to a single complex, 1 equiv. KI was added to the CD_2Cl_2 reaction mixture. The added KI perturbed the product distribution in CD_2Cl_2 to a 60:40 ratio ($^2J_{Pt\text{-}H}$ = 68; 76 Hz and $^2J_{Pt\text{-}H}$ = 70; 74 Hz, respectively). Removal of CD_2Cl_2 solvent and redissolution of the reaction mixture into CD_3CN resulted in observation of a single Pt-$(CH_3)_2$ species with Pt-CH_3 resonances at 1.86 and 0.93 ppm ($^2J_{Pt\text{-}H}$ = 69, 75 Hz, respectively) by ^{1}H NMR spectroscopy. The change in product distribution might be due to the limited solubility of KI in CD_2Cl_2. The

single Pt-$(CH_3)_2$ species is additionally observed when 1 equiv. of CH_3I and 1 equiv. of KI is added to a CD_3CN solution of **C8**. Examination of the reaction mixture by ESI-MS in CH_3CN revealed a single peak at *m/z* = 673.2 (corresponding to $[Pt(*NNN*)(CH_3)_2I]^-$). No evidence of N-methylation was observed by ^1H NMR spectroscopy. Additionally, whether the counter cation to the likely product ($[Pt(*NNN*)(CH_3)_2I]^-$) is PPN^+ or K^+ is unknown. This could be probed by addition of crown ether, which would shift the resonance of unbound crown ether if K^+ was present. The proposed reactivity and speciation is summarized in Figure 3.12. Addition of excess CH_3I (> 2 equiv.) to a solution of **C6** or **C8** in THF-d_8 or acetone-d_6, respectively, formed $Pt(^{CH3}NNN*)(CH_3)_2I$ (**C15**) as the main product by ^1H NMR spectroscopy (Figure 3.12) and this product was isolated. Examination of the ^1H NMR spectrum revealed an unsymmetrical ligand environment, two Pt-(CH_3) resonances at 2.37 ppm ($^2J_{Pt\text{-}H}$ = 69 Hz) and 1.19 ppm ($^2J_{Pt\text{-}H}$ = 70 Hz) and a ligand N-CH_3 resonance at 4.23 ppm. Additionally, ESI-MS revealed the main Pt product contained a *m/z* = 688.2 (corresponding to $[Pt(^{CH3}NNN^H)(CH_3)_2I]^+$). It appears methyl iodide reacts first with the Pt^{II} center to form a mixture of two different Pt-$(CH_3)_2$ complexes, which can further be pushed to one Pt-$(CH_3)_2$ species, likely $[Pt(*NNN*)(CH_3)_2I]^-$ by KI addition. Addition of 2 total equiv. of CH_3I to **C8** not only oxidizes Pt^{II} and forms a new Pt^{IV}-(CH_3) bond, but methylates the ligand N to form **C15** as the main Pt product.

3.3 Conclusion

A series of Pt^{II}-Cl and Pt^{II}-alkyl complexes supported by 2,6-bis(5-*tert*-butyl-1H-pyrazol-3-yl)pyridine (**^{H}NNN^H**) and 5-*tert*-butyl-1,3-bis(pyrazol-3-yl)benzene (**^{H}NCN^H**)^R (R = H, ^{t}Bu) ligands were synthesized and characterized. Once formed, the reactivity of Pt^{II}-alkyl complexes with electrophilic reagents (HX and CH_3I) was explored and is summarized below.

Addition of 1 equiv. of acid to $[Li(THF)_2]_2[Pt(*NCN*)^{R}CH_3]$ (R = H, **C11**; R = ^{t}Bu, **C12**) and $[Li(THF)_2]_2[Pt(*NCN*)^{R}C_6H_5]$ (**C13**) generated R-H (R = CH_3 or C_6H_5) and the corresponding Pt^{II} complex, $[Li(THF)_2]_2[Pt(*NCN*)^{R}Cl]$ (R = H, **C4a**; R = ^{t}Bu, **C5a**), even at reduced temperatures. However, acid addition experiments to $[Li_2Cl][Pt(*NNN*)CH_3]$ (**C6**), $[Li(THF)]_2[Pt(*NNN*)CH_2CN]_2$ (**C7**), and $[PPN][Pt(*NNN*)CH_3]$ (**C8**) revealed ligand protonation in preference to Pt/Pt-CH_3 protonation. NMR spectroscopy and solid-state studies revealed **C6** and **C8** can both uptake two equivalents of acid without methane liberation. Addition of >2 equivalents of acid to **C6** and **C8** liberates methane. In all, tridentate pyrazolate ligated Pt^{II}-R systems can store protons before R-H elimination if there is a weak *trans* donor to the Pt^{II}-R bond (pyridine vs phenyl) and/or if the Pt complex is not dianionic (**C11**, **C12** and **C13** vs **C6** and **C8**).

Reaction of 2 equiv. of CH_3I with **C11** ($[Li(THF)_2]_2[Pt(*NCN*)^{H}(CH_3)]$) formed two Pt^{IV}-CH_3 species, whose identity is likely $[Li(THF)_2]_2[Pt(*NCN*)^{tBu}(CH_3)_2I]$ or a 5-coordinate analog, with no evidence of N-methylation products formed, as evidenced by ^{1}H NMR spectroscopy. Addition of 1 equivalent of CH_3I with $[PPN][Pt(*NNN*)CH_3]$ (**C8**) also reacted to form two Pt^{IV}-$(CH_3)_2$ products. Addition of KI to this mixture resulted in a single Pt^{IV} product, likely $[Pt(*NNN*)(CH_3)_2(I)]^{-}$. Addition of two equiv. of CH_3I to $[Li_2Cl][Pt(*NNN*)CH_3]$ (**C6**) or **C8** generates the oxidized N-methylation product $Pt(^{CH3}NNN*)(CH_3)_2I$ (**C15**). While reactivity of 2 equiv. CH_3I to **C11** did not appear to form any N-CH_3 product, N-alkylation was observed when CH_3I added to **C6** or **C8**. Similar to the H^{+} addition experiments, ligand reactivity with CH_3^{+} was observed for NNN ligated Pt^{II}-CH_3 species as opposed to an NCN ligated Pt^{II}-CH_3 complex, where no ligand N-alkylation was observed by ^{1}H NMR spectroscopy.

3.4 Experimental and NMR Data

3.41 General Experimental

All manipulations were carried out under nitrogen atmosphere using standard Schlenk and glovebox techniques unless otherwise noted. Deuterated solvents were purchased from Cambridge Isotope Laboratories. Dry tetrahydrofuran, benzene, pentane, methylene chloride, acetone, acetonitrile, and diethyl ether were obtained by means of a Grubbs-type solvent purification system.[32] THF-d_8 and C_6D_6 were dried over sodium/benzophenone ketyl and were vacuum transferred prior to use. Acetone-d_6 and CD_3CN were dried over activated 3 Å molecular sieves. CD_2Cl_2 was dried over calcium hydride and vacuum transferred prior to use. $PtCl_2(S(CH_3)_2)_2$, $Pt(C_6H_5)_2(S(CH_3)_2$ and $[Pt(CH_3)_2(\mu\text{-}S(CH_3)_2)]_2$ were synthesized following literature preparations.[33,34] K_2PtCl_4 was purchased from Pressure Chemicals. All NMR spectra were obtained on a Bruker Avance 500, Bruker Avance 400 or Bruker Avance 300 MHz instrument. The spectra were recorded at 300 K. Chemical shifts are reported in units of parts per million (ppm) downfield of TMS and referenced against residual protonated solvent resonances (^{1}H) and characteristic solvent resonances (^{13}C). $^{31}P\{^1H\}$ NMR spectra were referenced externally to H_3PO_4 (85%, 0 ppm) and ^{2}H NMR spectra were referenced to the deuterium resonance of extra added CD_3CN (δ 1.94). $^{19}F\{^1H\}$ NMR spectra were referenced externally to C_6H_5F (-113.15 ppm).$^7Li\{^1H\}$ NMR spectra were referenced externally to LiCl in D_2O (0.0 ppm). NMR tubes fitted with a J-Young style Teflon valve were used to obtain inert atmosphere NMR data. The C, N, H elemental analyses were carried out at the CENTC Elemental Analysis Facility at the University of Rochester. Accurate mass measurement analyses were conducted on either a Waters GCT Premier, time-of-flight, GCMS with electron ionization (EI), or an LCT Premier XE, time-of-flight, LCMS with electrospray ionization (ESI). Samples were taken up in a suitable solvent

for analysis. The signals were mass measured against an internal lock mass reference of perfluorotributylamine (PFTBA) for EI-GCMS, and leucine enkephalin for ESI-LCMS. Waters software calibrates the instruments, and reports measurements, by use of neutral atomic masses. The mass of the electron is not included. Nominal mass accuracy ESI-MS data were obtained by use of a Waters Acquity UPLC system equipped with a Waters TUV detector (254 nm) and a Waters SQD single quadrupole mass analyzer with electrospray ionization.

3.42 Synthesis, Characterization and Spectroscopic Data

[Pt(^{H}NNN^{H})Cl][Cl] **(C1)**

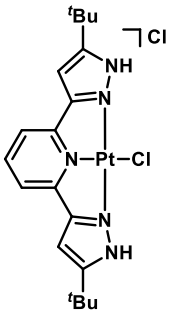

A 100 mL Schlenk flask was charged with 282.5 mg (0.873 mmol) of ^{H}NNN^{H}, 339.1 mg (0.869 mmol) Pt(S(CH_3)$_2$)Cl_2 and 15 mL methanol in air. The solution was sparged with N_2 and heated at reflux for 2 hours to yield a yellow solution. The solution was cooled to room temperature and then concentrated under reduced pressure. Diethyl ether (20 mL) was added, precipitating a yellow solid. The solid was collected, re-dissolved in methanol and concentrated under reduced pressure. Diethyl ether was again added, and the suspension was filtered via a fritted funnel. The yellow solid was collected and dried under reduced pressure (437.1 mg, 84.9 %). ^{1}H NMR (CH_3OD, 500 MHz): δ 8.27 (1H, t, pyr, $^{3}J_{H\text{-}H}$ = 8.0 Hz), 7.96 (2H, s, pyr, $^{3}J_{H\text{-}H}$ = 8.0 Hz), 7.09 (2H, s, pyz), 1.46 (18H, s, ^{t}Bu). ^{13}C{^{1}H} (CH_3OD, 126 MHz): δ 162.83 (s), 158.16 (s), 154.78

(s), 146.30 (s), 123.62 (s), 107.59 (s), 35.96 (s), 32.65 (s). Elemental Analysis: Anal. For $C_{17}H_{25}ClN_4Pt•2H_2O$: Calc: C, 36.49; H, 4.67; N, 11.20. Found: C, 36.68; H, 4.55; N, 11.23.

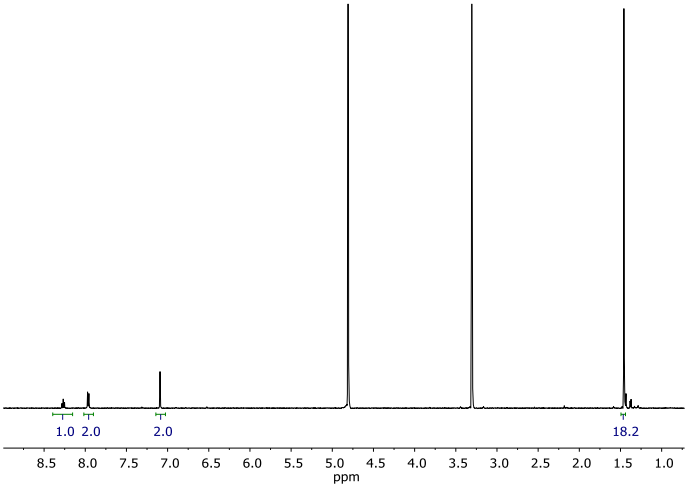

Figure 3.13. ^{1}H NMR spectrum (500 MHz) of **C1** in MeOD

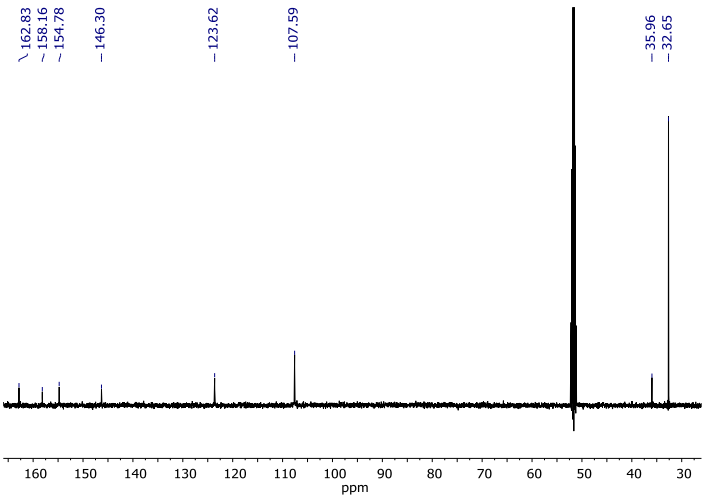

Figure 3.14. $^{13}C\{^{1}H\}$ NMR spectrum (126 MHz) of **C1** in MeOD

[Pt(^{H}NNN^{H})Cl][BF_4] **(C2)**

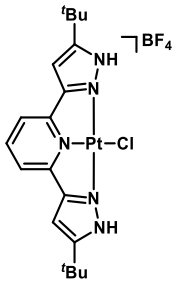

A 20 mL scintillation vial was charged with 23.5 mg (0.0399 mmol) **C1**, a Teflon stir bar, 4.4 mg (0.399 mmol) sodium tetrafluoroborate, and acetonitrile (2 mL) in air. The suspension was stirred vigorously for 1 hour. The resulting suspension was filtered by fritted funnel and extracted with CH_2Cl_2 (2 x 2 mL). The volatiles were removed from the resulting filtrate by rotary evaporation to yield a yellow solid. The solid was re-dissolved in methanol (10 mL) and concentrated to (~3 mL). Pentane (20 mL) was added and the resulting suspension was filtered via fritted funnel. The solid was collected and dried (21.0 mg, 82.1 %). ^{1}H NMR (CD_3CN, 500 MHz): δ 12.07 (2H, br, N-H), 8.21 (1H, t, pyr, $^{3}J_{H\text{-}H}$ = 8.0 Hz), 7.81 (2H, d, pyr, $^{3}J_{H\text{-}H}$ = 8.0 Hz), 6.99 (2H, s, pyz), 1.43 (18H, s, ^{t}Bu), ^{1}H NMR (CD_3OD, 400 MHz): 8.22 (1H, t, pyr, $^{3}J_{H\text{-}H}$ = 7.8 Hz), 7.89 (2H, d, pyr, $^{3}J_{H\text{-}H}$ = 7.8 Hz), 7.03 (2H, s, pyz), 1.45 (18H, s, ^{t}Bu) ^{13}C{^{1}H} (CD_3CN, 126 MHz): δ 159.98 (s), 155.33 (s), 151.67 (s), 143.63 (s), 121.06 (s), 105.04 (s), 33.09 (s), 29.86 (s). ^{19}F NMR (CD_3CN, 377 MHz): δ -154.47 (s), -154.52 (s). Elemental Analysis: Anal. For $C_{19}H_{25}BClF_4N_5Pt•2H_2O$: Calc: C, 33.72; H, 4.32; N, 10.35. Found: C, 33.00; H, 3.82; N, 10.46.

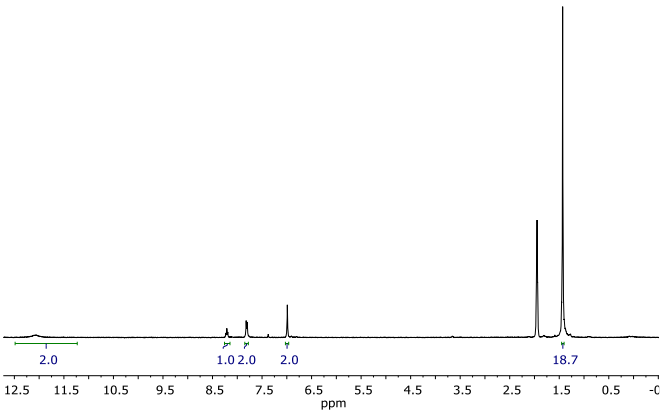

Figure 3.15. ^{1}H NMR spectrum (400 MHz) of **C2** in CD_3CN

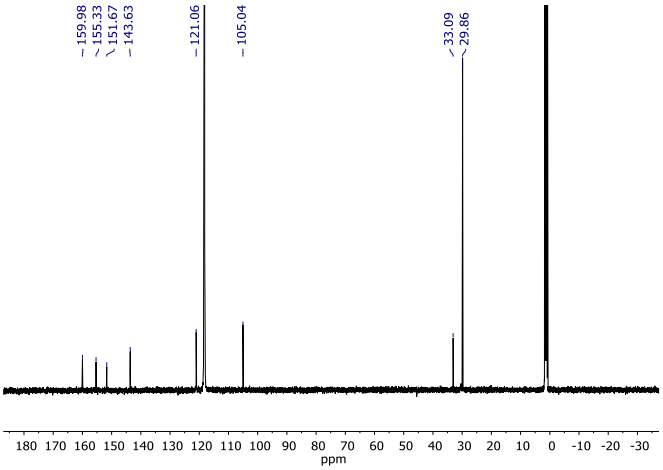

Figure 3.16. $^{13}C\{^{1}H\}$ NMR spectrum (126 MHz) of **C2** in CD_3CN

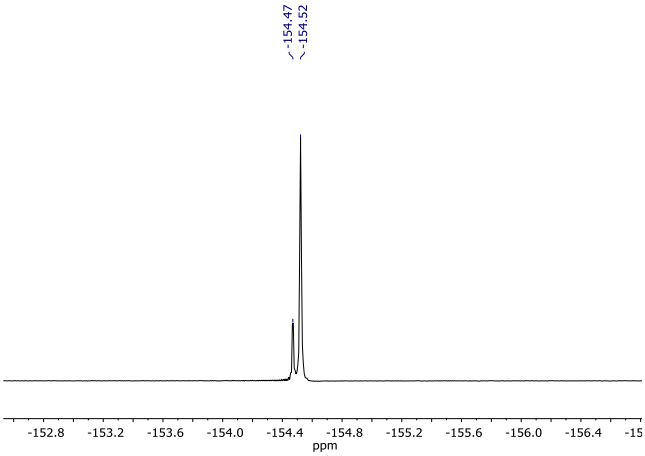

Figure 3.17. $^{19}F\{^{1}H\}$ NMR spectrum (376 MHz) of **C2** in CD_3CN

$[Pt(^{H}NNN^{H})NCCH_3][(BF_4)_2]$ **(C3)**

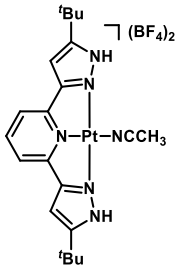

A 20 mL scintillation vial was charged with 31.3 mg (0.0533 mmol) **C1**, a Teflon stir bar, 20.7 mg (0.107 mmol) silver tetrafluoroborate, and acetonitrile (3 mL). The suspension was stirred vigorously for 1 hour in the absence of light. The resulting suspension was filtered through a PTFE syringe filter. The filtrate was concentrated under reduced pressure (~ 1 mL) and diethyl ether (5 mL) was added to precipitate a light yellow solid. The mother liquor was decanted and the solid was washed with ether (2 x 5 mL) and dried under reduced pressure (27.2 mg, 66.5 %). ^{1}H NMR (CD_2Cl_2, 500 MHz): δ 12.92 (2H, s, N-H), 8.23 (1H, t, pyr, $^{3}J_{H\text{-}H}$ = 8.0 Hz), 7.72 (2H, d, pyr, $^{3}J_{H\text{-}H}$ = 8.0 Hz), 6.75 (2H, s, pyz), 2.94 (3H, s, $NCCH_3$) 1.43 (18H, s, ^{t}Bu), ^{1}H NMR (CD_3CN, 500 MHz): 12.13 (2H, s, N-H), 8.29 (1H, t, pyr, $^{3}J_{H\text{-}H}$ = 8.0 Hz), 7.88 (2H, d, pyr, $^{3}J_{H\text{-}H}$ = 8.0 Hz), 7.05 (2H, s, pyz), 1.45 (18H, s, ^{t}Bu), $^{13}C\{^{1}H\}$ (CD_3CN, 126 MHz): δ 160.91 (s), 155.09

(s), 152.25 (s), 146.05 (s), 121.66 (s), 105.65 (s), 33.13 (s), 29.81 (s) ^{19}F NMR (CD_3CN, 377 MHz): δ -150.89 (s), -150.94 (s). Elemental Analysis: Anal. For $C_{21}H_{28}B_2F_8N_6Pt$: Calc: C, 34.40; H, 3.85; N, 11.46. Found: C, 34.21; H, 3.52; N, 11.22.

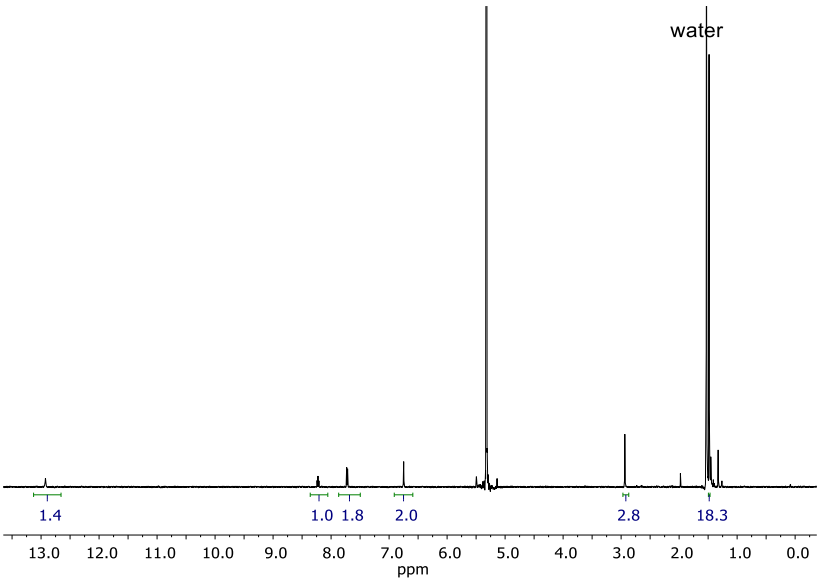

Figure 3.18. ^{1}H NMR spectrum (500 MHz) of **C3** in benchtop CD_2Cl_2

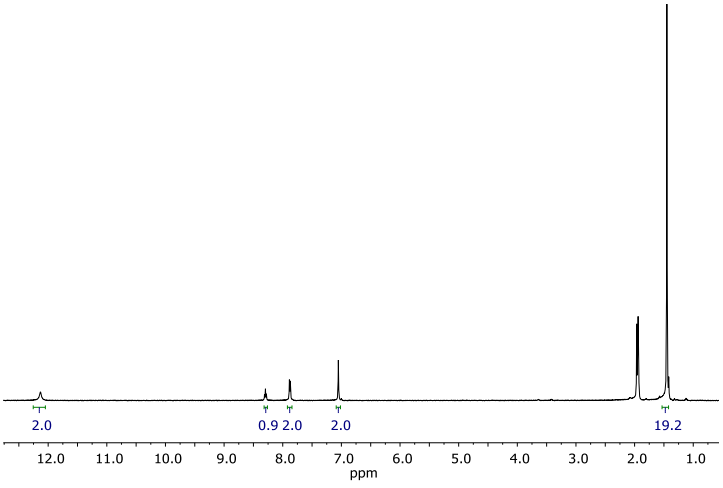

Figure 3.19. ^{1}H NMR spectrum (500 MHz) of **C3** in CD_3CN

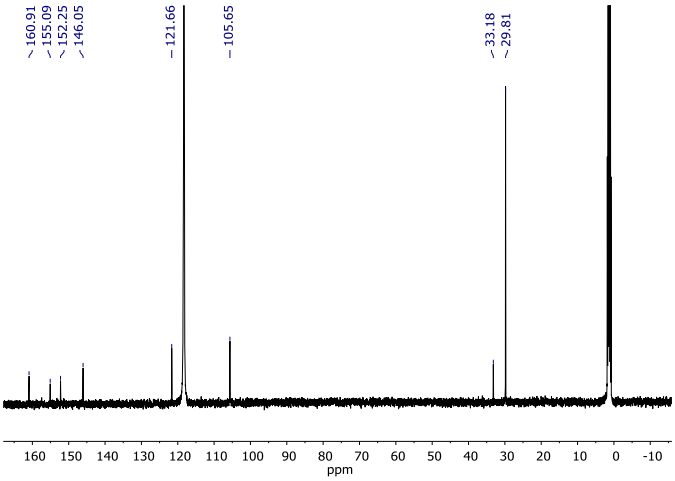

Figure 3.20. $^{13}C\{^{1}H\}$ NMR spectrum (126 MHz) of **C3** in CD_3CN

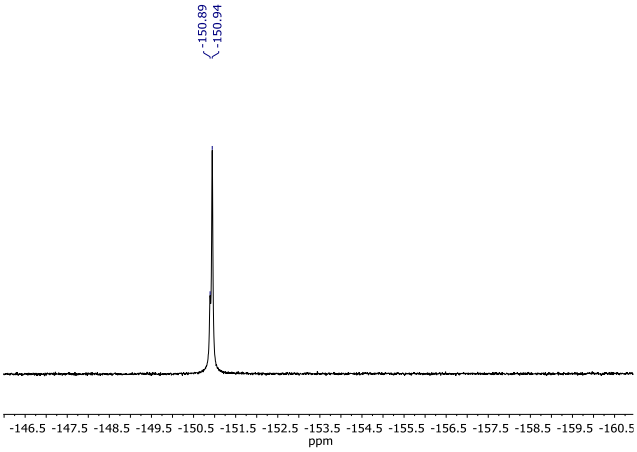

Figure 3.21. $^{19}F\{^{1}H\}$ NMR spectrum (376 MHz) of **C3** in MeOD

$Pt(^{H}NCN^{H})^{H}Cl$ **(C4)**

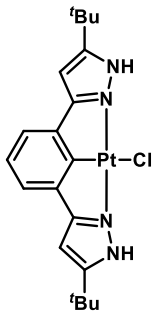

In a 50 mL round bottomed flask, 47.2 mg (0.202 mmol) of **(^{H}NCN^{H})^{H}** and 51.8 mg (0.125 mmol) of potassium tetrachloroplatinate were added. Glacial acetic acid (25 mL) was added

and the resulting suspension was heated to reflux (ca. 118 °C). Water (1.5 mL) was slowly added through the condenser to yield a yellow solution. After 48 hours, the solution became a yellow suspension and the reaction was cooled. To the suspension was added, H_2O (50 mL). The solid was collected via filtration using a fritted glass funnel to yield an oily solid. The oily solid was washed with H_2O (2 x 20 mL). The solid was collected by extraction with MeOH and filtration through the frit. The solvent of the resulting filtrate was removed *in vacuo* to yield a yellow solid (48.2 mg, 87 %). Irreproducibility plagued this reaction; repeating this reaction for further characterization to obtain the same main product could not be achieved. Attempts were made to vary the reagent stoichiometry, reagent conditions (solvent, O_2 vs N_2 and without ambient light) and Pt^{II} starting materials. ^{1}H NMR ($CDCl_3$, 500MHz): δ 10.72 (2H, s, NH), 7.20 (2H, d, pyr, $^3J_{Ar\text{-}H}$ = 7.1 Hz), 7.12 (1H, d, pyr, $^3J_{Ar\text{-}H}$ = 7.1 Hz), 6.36 (2H, s, pyz), 1.40 (18H, s, ^{t}Bu).

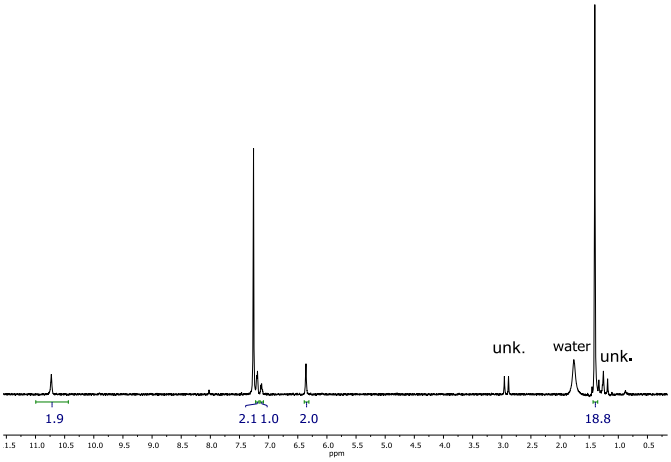

Figure 3.22 ^{1}H NMR spectrum (500 MHz) of **C4** in C_6D_6.

$[Li(THF)_2]_2[Pt(*NCN*)^{tBu}Cl]$ (**C4A)**

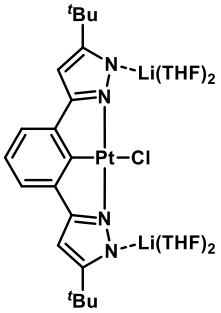

A 500 mL Schlenk tube was charged with **C5** (68.2 mg, 0.124 mmol), THF (70 mL) and a stir bar. The resulting suspension was put in a freezer (-35 °C) for 45 mins. A 1.6 M diethyl ether solution of CH_3Li (386 µL, 0.618 mmol) was added and the resulting mixture was allowed to warm to room temperature and stir for 2 hours. To the mixture, H_2O (4.5 µL, 0.25 mmol) was added, allowed to stir for 30 mins. The reaction mixture was filtered through a fritted funnel. The solvent was removed from the filtrate under reduced pressure and an NMR was taken of the resulting solid. ^1H NMR (CD_3CN, 500MHz): δ 6.86-6.91 (1H, m, pyr), 6.83 (2H, d, pyr, $^3J_{Ar-H}$ = 7.1 Hz), 6.12 (2H, s, pyz), 1.34 (18H, s, ^{t}Bu).

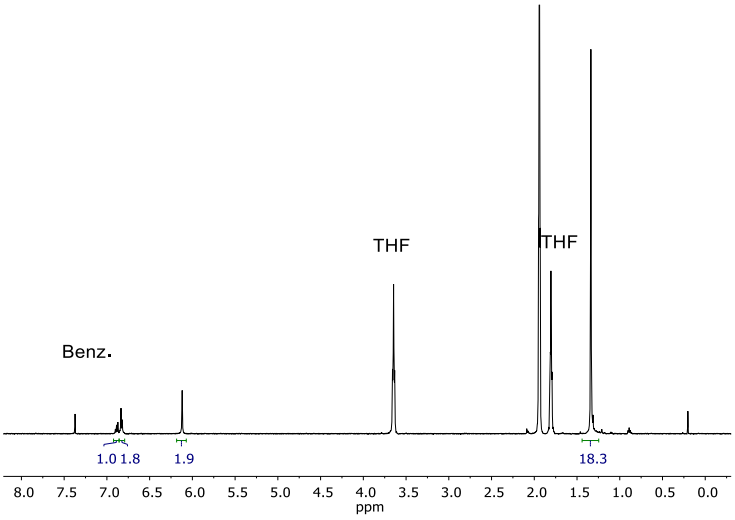

Figure 3.23 ^1H NMR spectrum (500 MHz) of **C4A** in CD_3CN.

Pt(^{H}NCN^{H})^{tBu}Cl **(C5)**

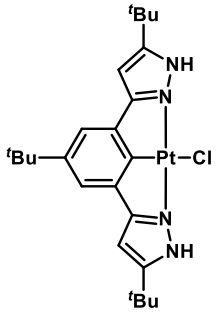

In a 250 mL round bottom flask, 395 mg (1.06 mmol) of (**^{H}NCN^{H})^{tBu}** and 439 mg (1.06 mmol) of potassium tetrachloroplatinate were added. Glacial acetic acid (100 mL) was added and the resulting suspension was heated to reflux (ca. 118 °C). Water (27 mL) was slowly added through the condenser to yield a yellow solution. After 48 hours, the solution became a yellow suspension and the reaction was cooled. To the suspension was added, H_2O (40 mL). The solid was collected via filtration using a fritted glass funnel to yield a green oily solid. THF (50 mL) was added to the oily solid to form a yellow green suspension. After an hour, solid black particles were observed, and the suspension was filtered via fritted glass funnel. The solvent was removed *in vacuo* overnight to yield a yellow solid. (561 mg, 88 %). ^{1}H NMR ($CDCl_3$, 300MHz): δ 10.60 (2H, s, NH), 7.29 (2H, d, pyr, $^{4}J_{Ar-H}$ = 4.5 Hz), 6.40 (2H, m, pyz), 1.42 (18H, s, ^{t}Bu), 1.39 (9H, s, ^{t}Bu).

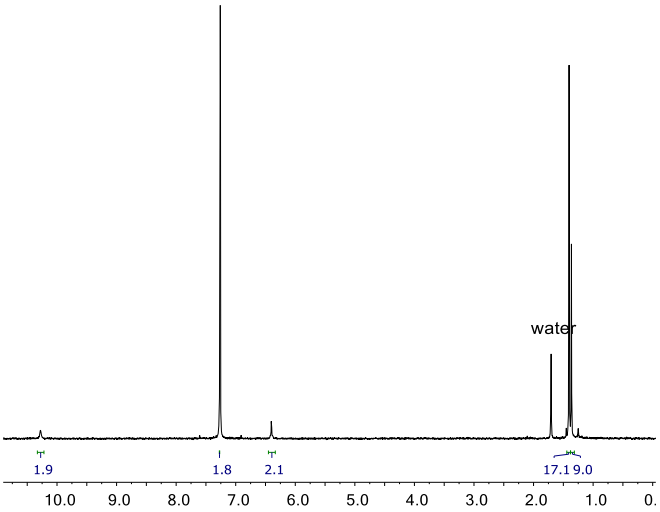

Figure 3.24. ^{1}H NMR spectrum (300 MHz) of **C5** in $CDCl_3$

$[Li(THF)_2]_2[Pt(*NCN*)^{tBu}Cl]$ **(C5A)**

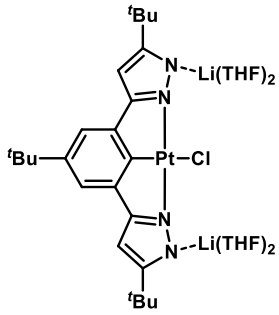

A 20 mL scintillation vial was charged with 2 mL of THF, a stir bar, and **C5** (33.3 mg, 0.0548 mmol). The resulting suspension was cooled to -30 °C, and 69 µL of a 1.6 M (0.11 mmol) diethyl ether solution of CH_3Li was added. The THF/diethyl ether solution was put in a -35 °C freezer and crystals formed. A small amount of the crystals was collected and an ^{1}H NMR spectrum in THF-d_8 was recorded below. ^{1}H NMR (THF-d_8, 500MHz): δ 6.87 (2H, s, pyr), 6.04 (2H, s, pyz), 6.12 (2H, s, Ar-H), 1.33 (9H, s, ^{t}Bu), 1.32 (18H, s, ^{t}Bu).

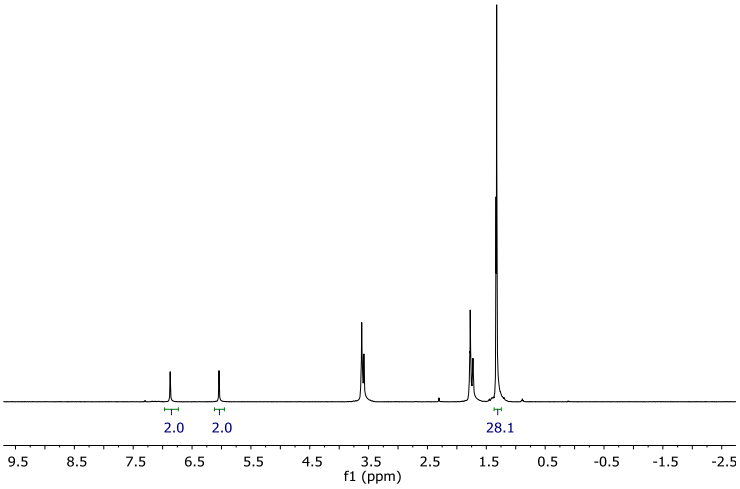

Figure 3.25. ^{1}H NMR spectrum (300 MHz) of **C5A** in THF-d_8

$[Li_2Cl(THF)_4][Pt(*NNN*)CH_3]$ **(C6)**

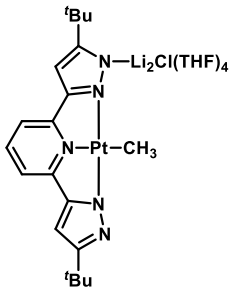

A 500 mL Schlenk tube was charged with 179 mg (0.325 mmol) of **C1** and 200 mL THF. While vigorously stirring, 1.5 mL (1.95 mmol) of CH_3Li (1.3 M in diethyl ether) was added via syringe under a nitrogen atmosphere and stirred for 2 hours. Water (15.6 µL, 0.98 mmol) was added via microliter syringe and stirred for 5 minutes. The solution was concentrated to 5 mL, and pentane was added (50 mL) to yield a dark solid, which was filtered and discarded. The filtrate was dried *in vacuo* to yield a yellow solid. (173.7 mg, 57.2 %). ^{1}H NMR (THF-d_8, 500 MHz): δ 7.61 (1H, t, pyr, $^{3}J_{H\text{-}H}$ = 7.8 Hz), 7.10 (2H, d, pyr, $^{3}J_{H\text{-}H}$ = 7.8 Hz), 6.38 (2H, d, pyz), 1.32 (1H, s, ^{t}Bu), 1.11 (3H, s, Pt-CH_3, $^{2}J_{Pt\text{-}H}$ = 78 Hz). ^{13}C{^{1}H} NMR (THF-d_8, 126 MHz): δ 160.65 (s), 153.52 (s), 153.21 (s), 138.56 (s), 112.06 (s), 100.39 (s), 32.79 (s), 31.39 (s), -24.03 (s). ^{7}Li{^{1}H} NMR

(acetone-d_6, 155.5 MHz): δ -1.40 (s). ESI-MS: $[Pt(^{H}NNN^{H})CH_3]^+$ Theoretical Mass, *m/z* = 532.1972; Observed Mass, *m/z* = 532.1952.

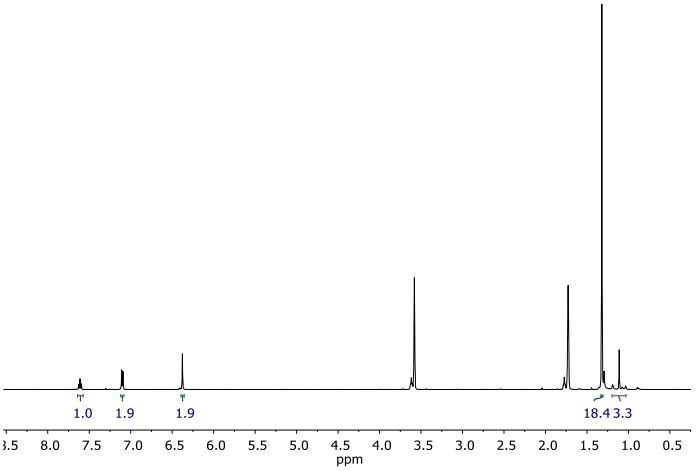

Figure 3.26. ^{1}H NMR spectrum (500 MHz) of **C6** in THF-d_8.

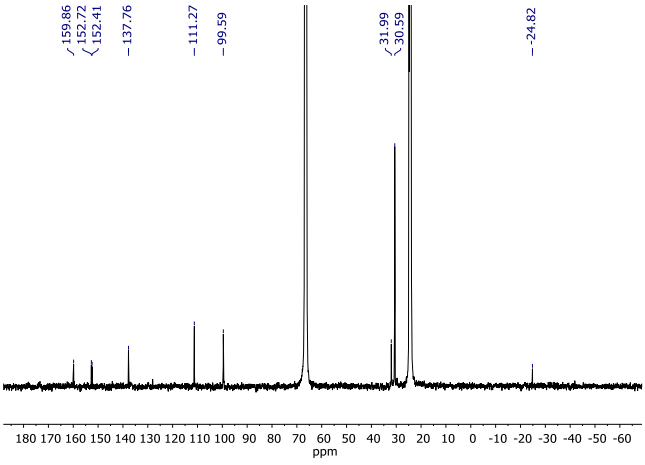

Figure 3.27. $^{13}C\{^{1}H\}$ NMR spectrum (126 MHz) of **C6** in THF-d_8

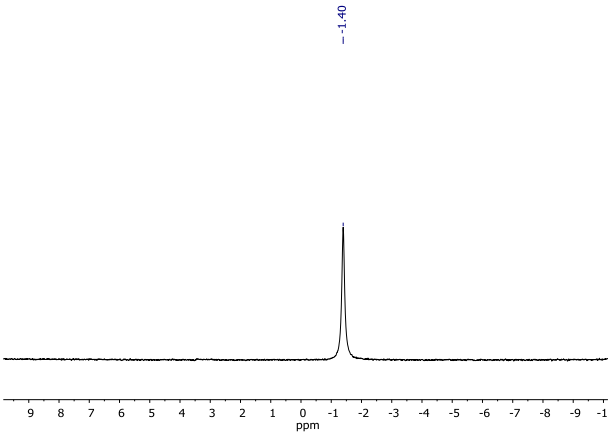

Figure 3.28. $^{7}Li\{^{1}H\}$ NMR spectrum (376 MHz) of **C6** in Acetone-d_6

$[Li(THF)]_2[Pt(*NNN)CH_2CN]_2$ **(C7)**

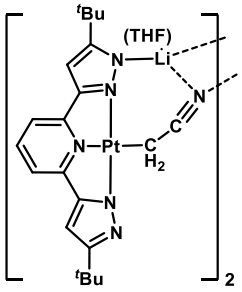

A 200 mL round bottom was charged with 123.5 mg (0.210 mmol) **C1**, 100 mL of THF, and a stir bar to yield a yellow suspension. While vigorously stirring, 786 µL of a 1.6 M diethyl ether solution of CH_3Li (0.904 mmol) was added and the resulting blue solution was stirred for 2.2 hours. Water (11 µL) was added and effervescence was observed. The solution was concentrated to 10 mL and 100 mL of pentane was added to yield a yellow suspension. The suspension was filtered through a fritted funnel and the solid discarded. The solvent was removed from the filtrate under reduced pressure. The yellow solid was collected and further dried under reduced pressure (97.4 mg, 66 % yield). Note - the source of the CH_2CN moiety in the product is unknown. ^{1}H NMR (Acetone-d_6, 500 MHz): δ 7.70 (2H, t, pyr, $^{3}J_{H\text{-}H}$ = 7.8 Hz), 7.18 (4H, d, pyr, $^{3}J_{H\text{-}H}$ = 7.8 Hz), 6.43 (4H, d, pyz), 2.50 (2H, s, Pt-CH_3, $^{2}J_{Pt\text{-}H}$ = 110 Hz) 1.31 (1H, s, ^{t}Bu). $^{13}C\{^{1}H\}$ NMR (THF-d_8, 126

MHz): δ 160.94 (s), 154.04 (s), 152.75 (s), 140.09 (s), 132.54 (s), 111.97 (s), 100.91 (s), 68.11 (s), 32.98 (s), 31.60 (s), 26.21 (s), -23.06 (s, $^{2}J_{Pt\text{-}H}$ = 723 Hz). ^{7}Li{^{1}H} NMR (acetone-d_6, 155.5 MHz): δ 0.96 (s).

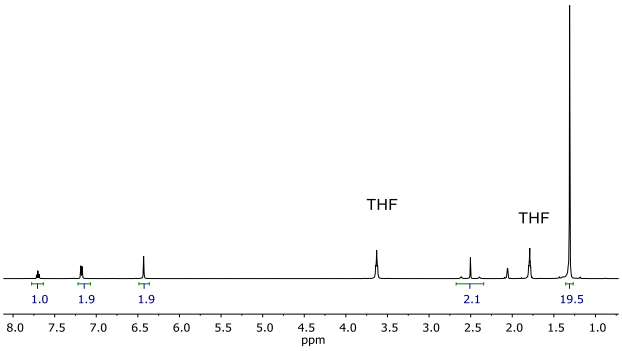

Figure 3.29. ^{1}H NMR spectrum (500 MHz) of **C7** in Acetone-d_6

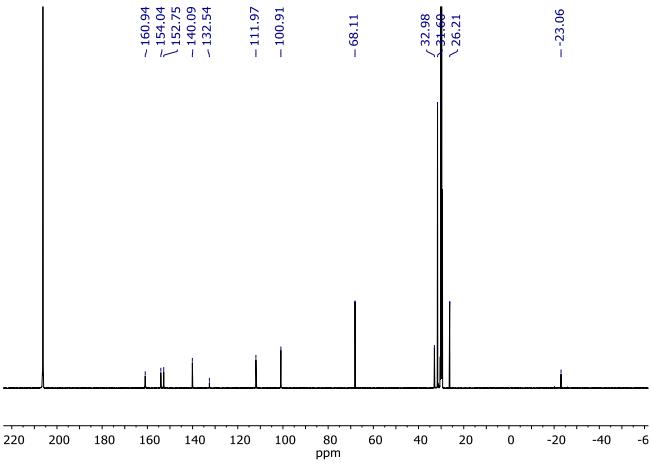

Figure 3.30. ^{13}C{^{1}H} NMR spectrum (126 MHz) of **C7** in Acetone-d_6

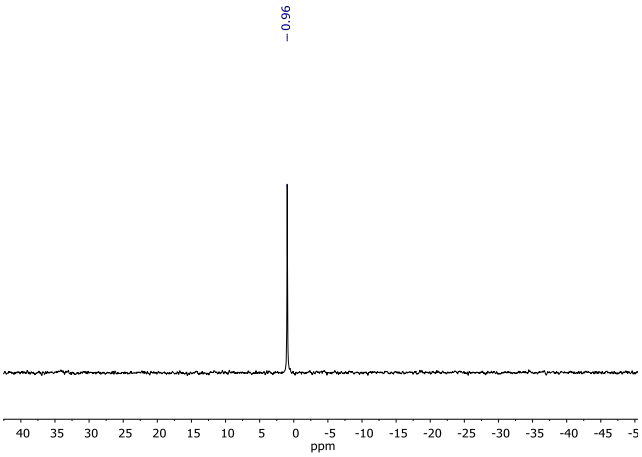

Figure 3.31 $^{7}Li\{^{1}H\}$ NMR spectrum (156 MHz) of **C7** in CD_3CN

[PPN][Pt(*NNN*)CH_3] **(C8)**

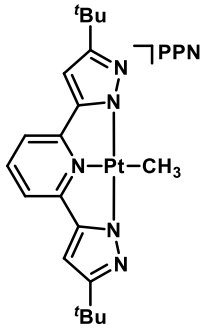

A 25 mL Schlenk flask was charged with a Teflon stir bar, **6** (42.6 mg, 0.0792 mmol), [PPN][Cl] (43.0 mg, 0.0752 mmol) and 10 mL of THF. The suspension was vigorously stirred for 1 hour to precipitate a white solid. The solid was separated by transferring the solvent using a cannula with a filter tip. The solvent was then removed under reduced pressure from the filtrate to yield a solid, which was extracted with 3 mL of CH_2Cl_2. The resulting solution was dried *in vacuo* to yield an orange solid (63.0 mg, 74.3 %). ^{1}H NMR (CD_3CN, 400 MHz): δ 7.63 (1H, t, pyr, $^{3}J_{H\text{-}H}$ = 7.9 Hz), 7.58 (36H, multiplet, PPN), 7.10 (2H, d, pyr, $^{3}J_{H\text{-}H}$ = 7.9 Hz), 6.42 (2H, s, pyz), 1.31 (18H, s, ^{t}Bu), 1.11 (3H, s, Pt-CH_3, $^{2}J_{Pt\text{-}H}$ = 82 Hz). $^{31}P\{^{1}H\}$ (CD_3CN, 162 Hz): δ 22.00. $^{13}C\{^{1}H\}$ NMR (CD_3CN, 126 MHz): δ 161.32 (s), 153.53 (s), 153.03 (s), 139.01 (s), 133.17 (m, PPN), 130.30 (m, PPN), 128.95 (dd, $^{1}J_{C\text{-}P}$ = 107.8 Hz, $^{3}J_{C\text{-}P}$ = 1.8 Hz, PPN), 112.15 (s), 100.52 (s), 32.87 (s), 31.50 (s), -18.28 (s) Attempts to characterize the material by Elemental Analysis were not successful. ESI-MS: Theoretical Mass $[Pt(^{H}NNN^{H})CH_3]^{+}$ *m/z* = 532.1972; Observed Mass, *m/z* = 532.1967.

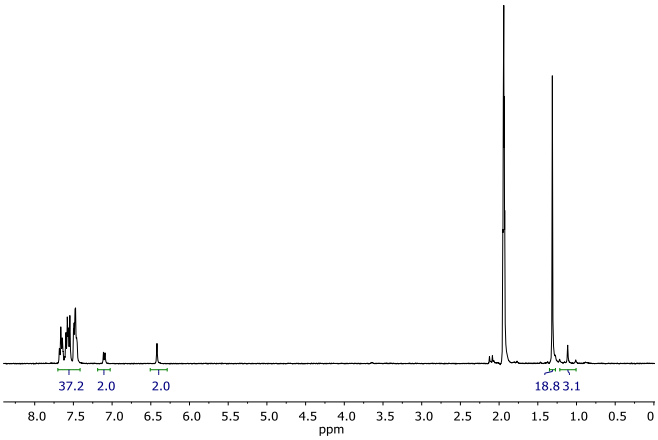

Figure 3.32. ^{1}H NMR spectrum (400 MHz) of **C8** in CD_3CN

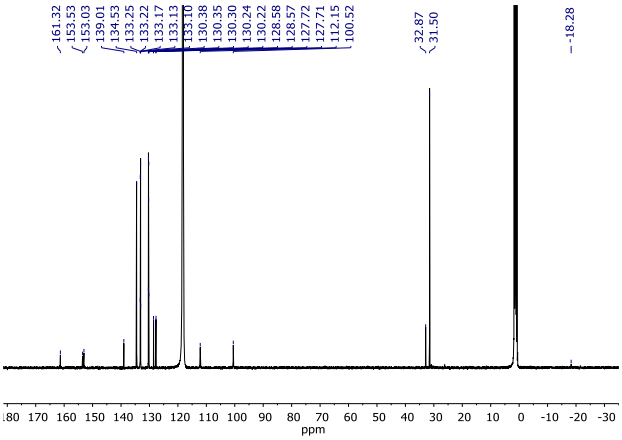

Figure 3.33. $^{13}C\{^{1}H\}$ NMR spectrum (125 MHz) of **C8** in CD_3CN. Low S/N sensitivity of the Pt-**C**H_3 resonance at -18.28 ppm. Confirmed ^{13}C signal in HSQC of **C8**.

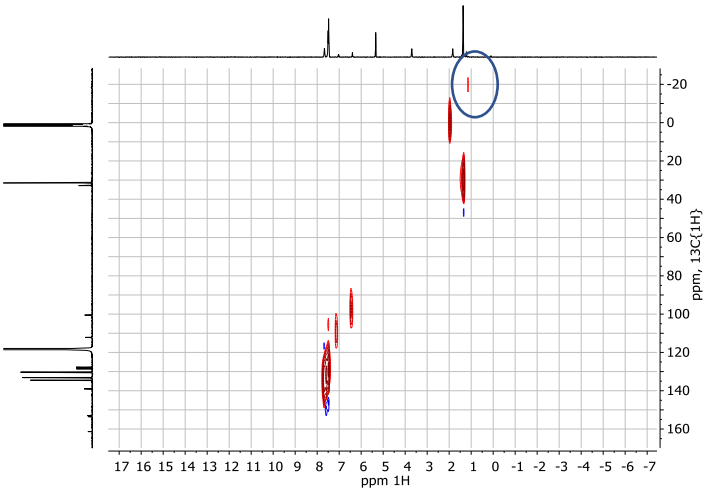

Figure 3.34. HSQC NMR spectrum (500, 126 MHz) of **C8** in CD_3CN. Pt-CH_3 resonance circled for clarity.

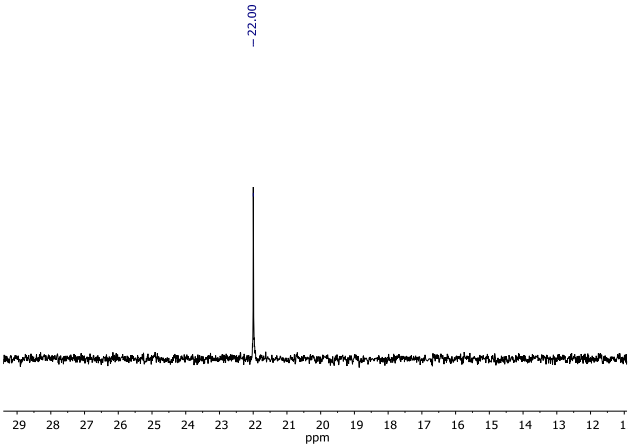

Figure 3.35. $^{31}P\{^1H\}$ NMR spectrum (162 MHz) of **C8** in CD_3CN

$[Pt(^{H}NNN^{H})CH_3][Cl]$ **(C9)**

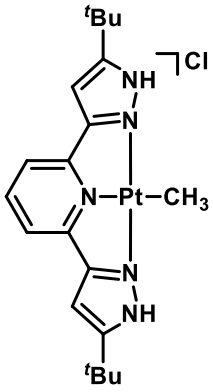

A 20 mL scintillation vial was charged with 137 mg (0.233 mmol) **C1**, a Teflon stir bar, and benzene (10 mL). While vigorously stirring, a 2.9 M CH_3MgCl (0.337 mL, 0.977 mmol) was added via syringe and stirred for 20 mins. A water (17 µL) and THF (2 mL) solution was added and the reaction mixture was let stir for 20 minutes. The resulting suspension was filtered by fritted funnel and the orange and white solid was dried (155.2 mg). Note: THF resonances in the ^{1}H NMR spectrum likely due to MgX_2 impurities, as a less than 100 % yield was not attainable, even after rigorous drying. ^{1}H NMR (Acetone-d_6, 400 MHz): δ 13.28 (2H, br, N-H), 8.34 (1H, t, pyr, $^3J_{H\text{-}H}$ = 8.0 Hz), 8.11 (2H, d, pyr, $^3J_{H\text{-}H}$ = 8.0 Hz), 7.20 (2H, s, pyz), 1.47 (18H, s, ^{t}Bu), 1.24 (3H, s, Pt-CH_3, $^2J_{Pt\text{-}H}$ = 79 Hz).

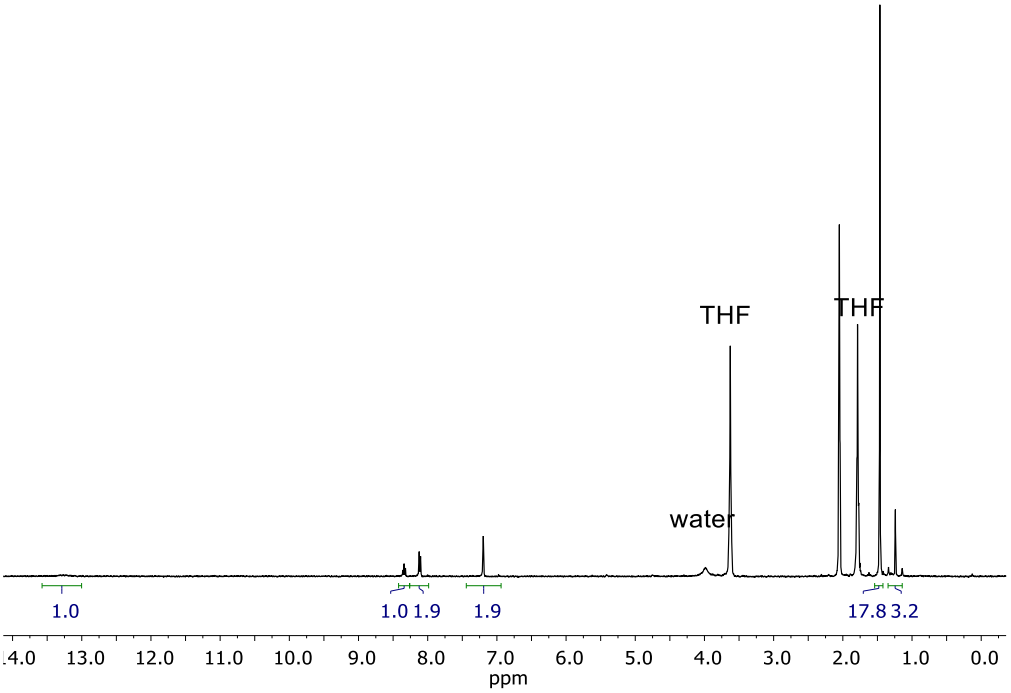

Figure 3.36. ^{1}H NMR spectrum (400 MHz) of **C9** in Acetone-d_6.

[Pt(^{H}NNN^{H})CH$_3$][BAr$_F^{24}$] **(C10)**

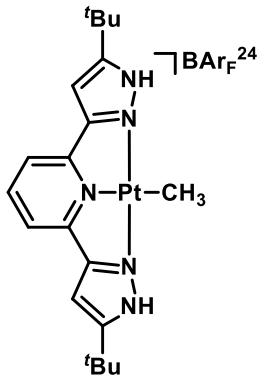

A 20 mL scintillation vial was charged with 46.0 mg (0.078 mmol) **C1**, a Teflon stir bar, and benzene (3 mL). While vigorously stirring, 0.117 mL (0.328 mmol) of CH_3MgCl (2.9 M in THF) was added via syringe and stirred for 20 mins. A solution of water (5 µL, 0.224 mmol) and THF (1 mL) was added and the reaction mixture was let stir for 20 minutes. The resulting suspension was filtered by a fritted funnel and the mixture of orange and white solid was collected into a 20 mL scintillation vial (35.5 mg). The vial was additionally charged with NaBAr$^F_{24}$ (49.8 mg, 0.0562 mmol), acetone (3 mL) and a Teflon stir bar and stirred for 1.5 hours to form a suspension. The mixture was reduced by half under vacuum and 10 mL of diethyl ether was added. The resulting suspension was filtered by PTFE syringe filter. The filtrate was concentrated under reduced pressure to 1 mL, and 10 mL of pentane was added to form a suspension. The mother liquor was decanted, and the resulting orange oil was pumped to dryness to form an orange solid (62.7 mg, 56.7 % yield). ^{1}H NMR (Acetone-d$_6$, 500 MHz): δ 13.14 (2H, s, N-H), 8.38 (1H, t, pyr, $^3J_{H\text{-}H}$ = 8.0 Hz), 8.17 (2H, d, pyr, $^3J_{H\text{-}H}$ = 8.0 Hz), 7.78 (8H, s, BAr$^F_{24}$), 7.78 (4H, s, BAr$^F_{24}$), 7.24 (2H, s, pyz), 1.46 (18H, s, ^{t}Bu), 1.21 (3H, s, Pt-CH$_3$, $^2J_{Pt\text{-}H}$ = 79 Hz). ^{13}C{^{1}H} (Acetone-d$_6$, 126 MHz): δ 162.76 (q, $^1J_{BC}$ = 50.0 Hz), 159.07 (s), 157.2 (s), 149.94 (s), 142.47 (s), 135.70 (s), 130.18 (q, $^3J_{CF}$ = 32.6 Hz), 125.51 (q, $^1J_{CF}$ = 271.9 Hz), 120.75, 118.6 (s), 104.87 (s), 32.99 (s), 30.75 (s), -22.69 (s). ^{19}F{^{1}H} NMR (CD_2Cl_2, 377 MHz): δ -62.85 (s). ESI-MS: [Pt(^{H}NNN^H)CH$_3$]$^+$ Theoretical Mass, *m/z* = 532.1972; Observed Mass, *m/z* = 532.2000.

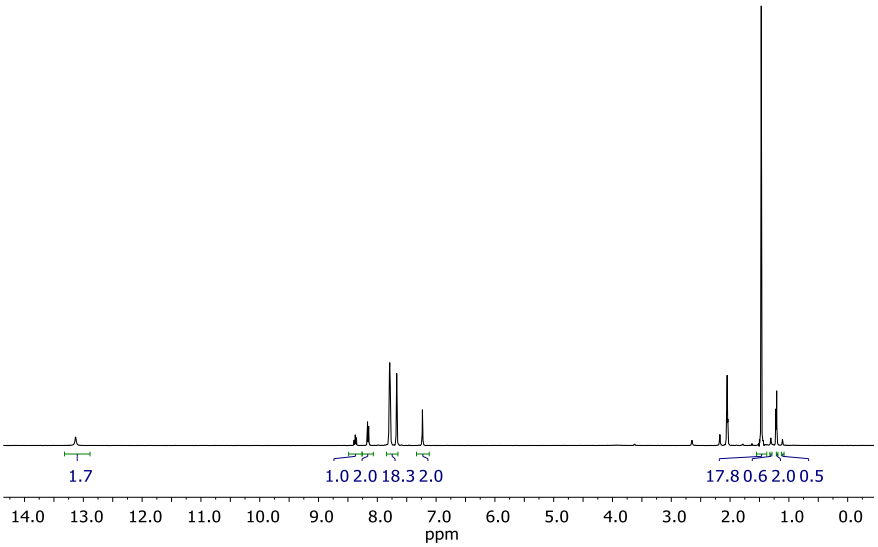

Figure 3.37. ^{1}H NMR spectrum (400 MHz) of **C10** in Acetone-d_6.

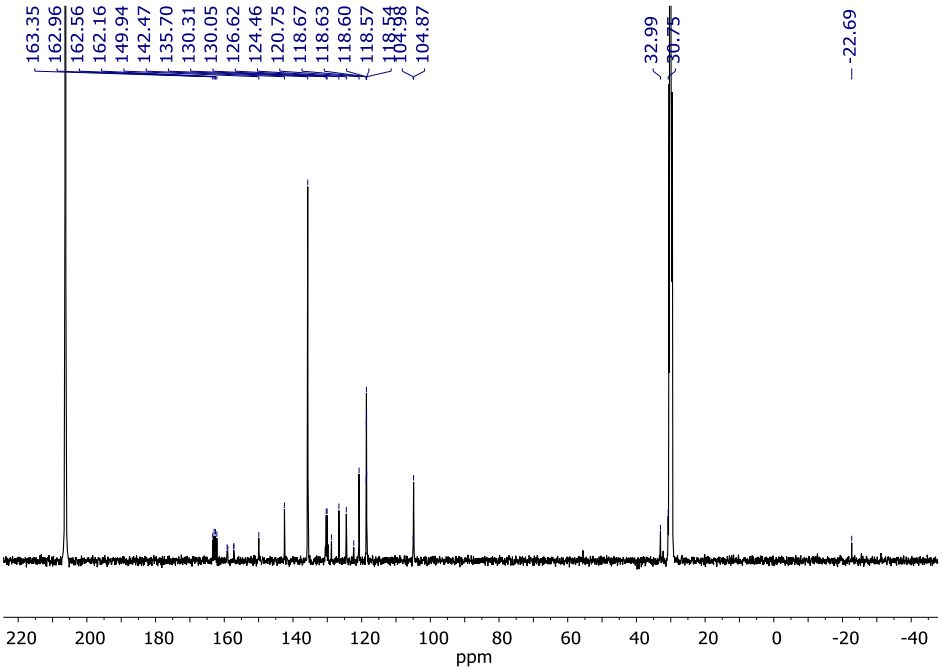

Figure 3.38. ^{13}C{^{1}H} NMR spectrum (126 MHz) of **C10** in Acetone-d_6.

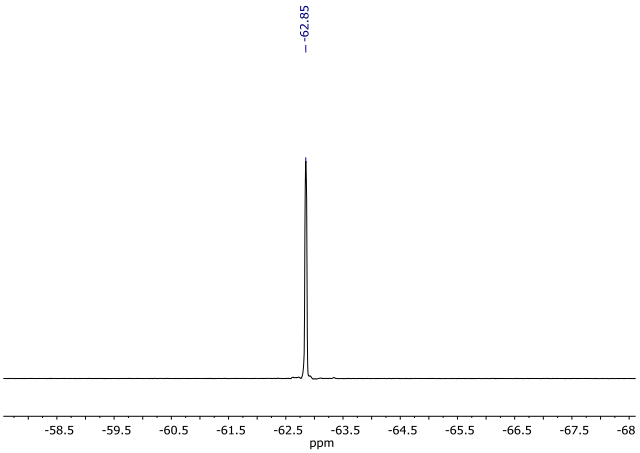

Figure 3.39. $^{19}F\{^{1}H\}$ NMR spectrum (400 MHz) of **C10** in Acetone-d_6.

$[Li(THF)_2]_2[Pt(*NCN*)^{H}(CH_3)]$ **(C11)**

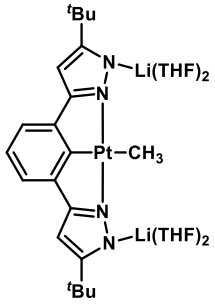

A 50 mL Schlenk flask was charged with **C4** (37.7 mg, 0.0683 mmol), 20 mL THF, and a stir bar. The solution was cooled to -35 °C and 5 equiv. of 1.5 M CH_3Li (228 µL) in diethyl ether was added while vigorously stirring. After 45 mins, the volume was reduced to 5 mL *in-vacuo*. 20 mL of pentane was added, causing yellow solid to fall out of solution. After 45 mins, the suspension was carefully decanted and then redissolved in THF. The solution was concentrated *in-vacuo* and 10 mL pentane was added, precipitating out a yellow solid. The suspension was again decanted, and the yellow solid was extracted with benzene and further dried (25.5 mg, 0.031 mmol). ^{1}H NMR (THF-d_8, 500 MHz): δ 7.25 (2H, d, pyr, $^{3}J_{H\text{-}H}$ = 7.2 Hz), 7.16-7.22 (1H, m, pyr), 6.32 (2H, d, pyz), 3.36 (16H, m, THF), 1.48 (18H, s, ^{t}Bu), 1.28 (16H, m, THF), 0.06 (3H, s, Pt-CH_3, $^{2}J_{Pt\text{-}H}$ = 41 Hz).

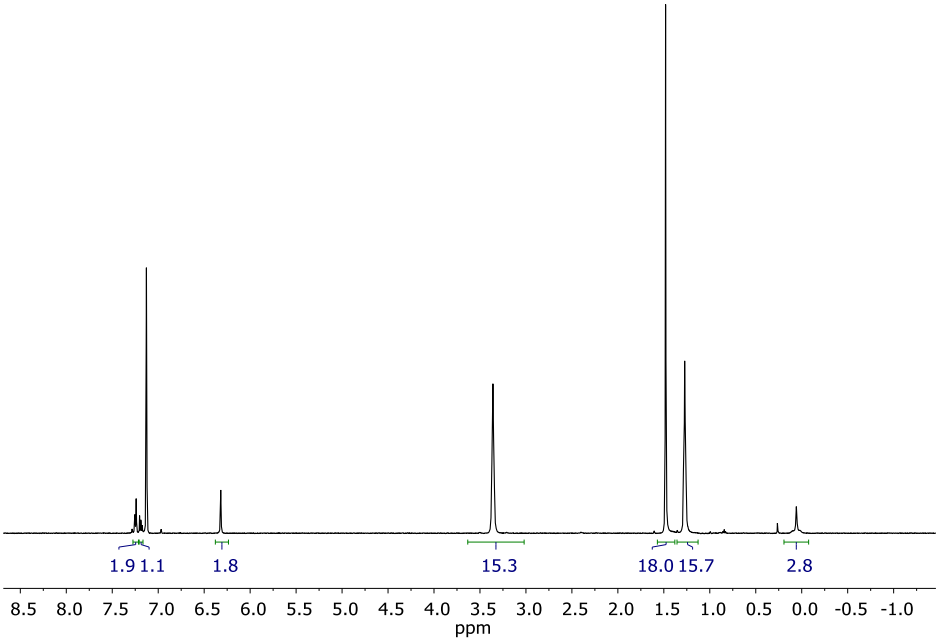

Figure 3.40 ^{1}H NMR spectrum (500 MHz) of **C11** in C_6D_6

$[Li(THF)_2]_2[Pt(*NCN*)^{tBu}(CH_3)]$ **(C12)**

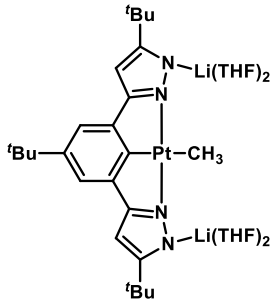

A J. Young tube was charged with 10 mg (0.016 mmol) of **C5** under nitrogen. THF-d_8 (0.4 mL) was added via vacuum transfer to afford a yellow solution. The solution was cooled to -35 °C and then 34 µL (0.057 mmol) of methyllithium (1.6 M) in diethyl ether was added. The solution became a lighter yellow shade and **C12** was formed cleanly. ^{1}H NMR (THF-d_8, 500MHz: δ 6.94 (2H, s, pyr), 6.01 (2H, s, pyz), 1.33 (9H, s, ^{t}Bu), 1.32 (18H, s, ^{t}Bu), 0.07 (3H, s, Pt-CH_3, $^{2}J_{Pt\text{-}H}$ = 44 Hz).

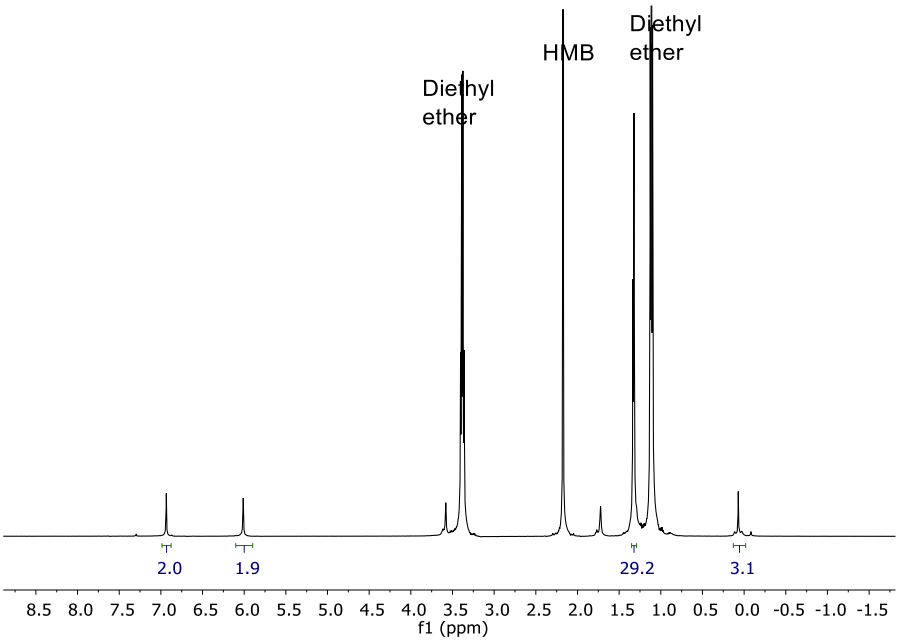

Figure 3.41 ^{1}H NMR spectrum (500 MHz) of **C12** *in-situ* in THF-d_8. Diethyl ether was present from HCl etherate addition. Hexamethylbenzene (HMB) is present for internal reference.

$[Li]_2[Pt(*NCN*)^{t\text{Bu}}(C_6H_5)]$ **(C13)**

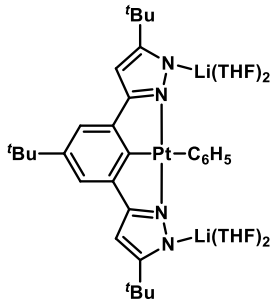

A J. Young tube was charged with 5.3 mg (0.0090 mmol) of **5** under nitrogen. THF-d_8 was added via vacuum transfer to yield a yellow solution. The solution was cooled to -35 °C and then 19.2 µL (0.035 mmol) of phenyllithium (1.6 M) in n-butyl ether was added. The solution became a lighter yellow shade. ^{1}H NMR (THF-d_8, 500MHz): δ 8.15 (2H, m, Ar-H, $^{3}J_{Pt\text{-}H}$ = 31 Hz), 7.23 (1H, m, pyr $^{4}J_{Pt\text{-}H}$ = 24 Hz), 7.00 (2H, m, Ar-H), 6.98 (2H, s, pyr), 6.04 (2H, s, pyz), 1.36 (9H, s, ^{t}Bu), 1.26 (18H, s, ^{t}Bu).

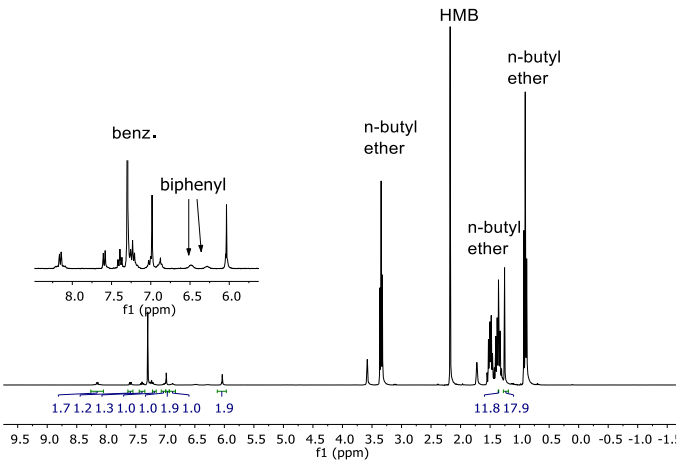

Figure 3.42. ^{1}H NMR spectrum (300 MHz) of **C13** *in-situ* in THF-d_8. Formation of biphenyl and benzene shown in the magnified aryl region. Hexamethylbenzene (HMB) used as an internal standard.

Pt(^{CH3}NNN*)$(CH_3)_2$(I) (**C15**)

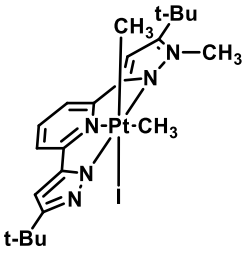

A J. Young tube was charged with 4.4 mg (0.0041 mmol) of **C8** under nitrogen. Acetone-d_6 (0.4 mL) was added under N_2 to yield a yellow solution. To the solution, 2.5 equivalent of CH_3I (1.0 µL, 0.016 mmol) was added. The reaction was vigorously shaken and allowed to react for 6 hours. A ^{1}H NMR spectrum was obtained and is shown below. The volatiles were then removed under reduced pressure. The resulting yellow solid was washed with pentane (1 x 1 mL) and collected with diethyl ether (1 x 1 mL). The ethereal solvent was removed by bubbling air through the solution over 30 mins to yield a yellow solid. The following ^{1}H NMR spectrum of the

yellow solid was recorded in CD_3CN. ^1H NMR (acetone-d_6, 500MHz): δ 8.14 (1H, t, pyr, $^3J_{H-H}$ = 7.9 Hz), 7.95 (1H, d, pyr, $^3J_{H-H}$ = 7.9 Hz), 7.83 (1H, d, pyr, $^3J_{H-H}$ = 7.9 Hz), 7.19 (1H, s, pyz), 6.74 (1H, s, pyz), 4.22 (3H, s, N-CH_3), 2.37 (3H, s, $^2J_{Pt-H}$ = 69 Hz), 1.52 (9H, s, ^{t}Bu), 1.32 (9H, s, ^{t}Bu), (3H, s, $^2J_{Pt-H}$ = 70 Hz). ^1H NMR (CD_3CN, 500MHz): δ 8.07 (1H, t, pyr $^3J_{H-H}$ = 8.0 Hz), 7.76 (1H, dd, pyr $^3J_{H-H}$ = 8.0 Hz, $^4J_{H-H}$ = 0.6 Hz), 7.73 (1H, dd, pyr, $^3J_{H-H}$ = 8.0 Hz, $^4J_{H-H}$ = 0.6 Hz), 7.01 (1H, s, pyz), 6.77 (1H, s, pyz), 4.08 (3H, s, N-CH_3), 2.28 (3H, s, $^2J_{Pt-H}$ = 68 Hz), 1.47 (9H, s, ^{t}Bu), 1.33 (9H, s, ^{t}Bu), 1.24 (3H, s, $^2J_{Pt-H}$ = 70 Hz).

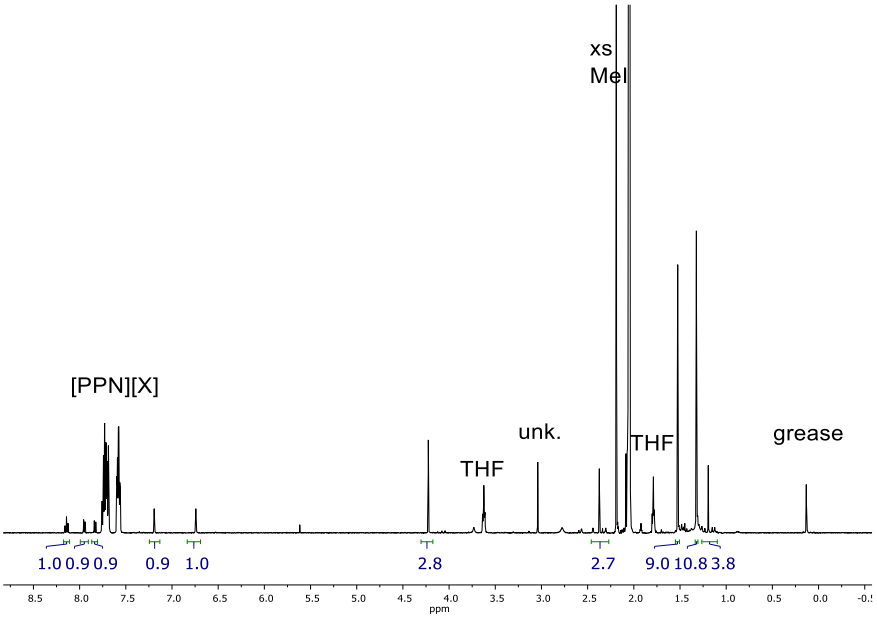

Figure 3.43. ^1H NMR spectrum (500 MHz) of **C15** *in-situ* in acetone-d_6.

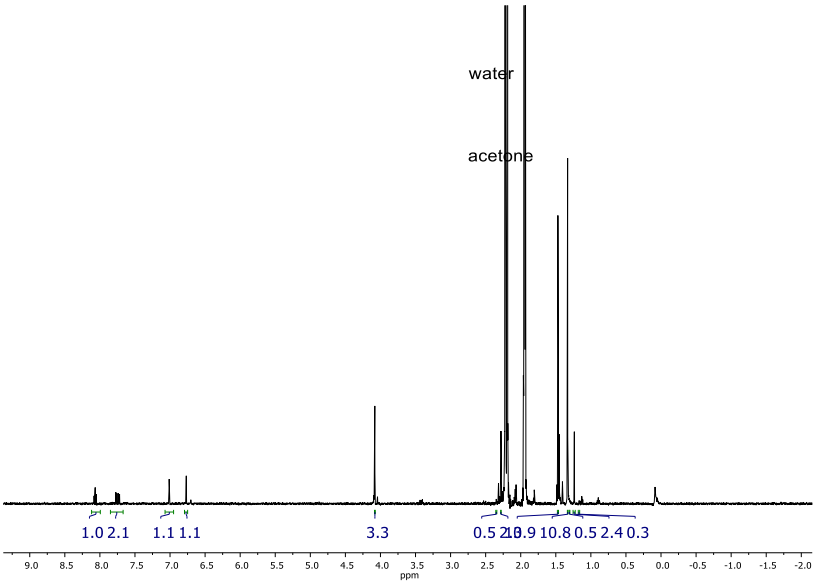

Figure 3.44. ^{1}H NMR spectrum (500 MHz) of **C15** in benchtop CD_3CN

NMR Data for the portion-wise addition of acid

Acid addition to **C6** and **C8**

A J. Young NMR tube was charged with **C6** or **C8** and an internal standard (hexamethyl benzene) under nitrogen. Acetone-d_6 or CD_3CN (0.4 mL for both) were vacuum transferred to the NMR tube. An initial NMR spectrum was recorded, and then 2,6-dimethoxypyridinium tetrfluoroborate acid was added (amounts shown in Figure 3.08a and 3.08b) in a nitrogen filled glovebox. After each acid addition, the NMR tube was sealed, agitated and an NMR spectrum was recorded (Figure 3.08a and 3.08b).

3.43 X-ray Crystallography General Information

Complexes **C2**, **C3**, **C4**, (**Pt_4(*NCN*)(^{H}NCN^{H})$_3$)**, **C6**, **C8**, **C9**, and **C11** : X-ray intensity data were collected on a Bruker APEXIII D8QUEST[35] CMOS area detector, both employing graphite monochromated Mo-Kα radiation (λ = 0.71073 Å) at 100(1) K. Preliminary in indexing was performed from a series of twenty-four 0.5° rotation frames with exposures of 10 seconds. Rotation frames were integrated using SAINT[36], producing a listing of unaveraged F^2 and $\sigma(F^2)$ values. The intensity data were corrected for Lorentz and polarization effects and for absorption using SADABS.[37] The structure was solved by direct methods – ShelXT.[38] Refinement was by full-matrix least squares based on F^2 using SHELXL-2018.[39] All reflections were used during refinement. The weighting scheme used was $w=1/[\sigma^2(F_o^2)+ (0.0612P)^2 + 1.0285P]$ where $P = (F_o^2 + 2F_c^2)/3$. Non-hydrogen atoms were refined anisotropically and hydrogen atoms were refined using a riding model.

Complexes **C5a**: X-ray intensity data were collected at -173 °C on a Bruker APEX II single crystal X-ray diffractometer, Mo-radiation. The data was integrated and scaled using SAINT, SADABS within the APEX2 software package by Bruker.[40] Solution by direct methods (SHELXS, SIR97)[41,42] produced a complete heavy atom phasing model consistent with the proposed structure. The structure was completed by difference Fourier synthesis with SHELXL97.[43,44] Scattering factors are from Waasmair and Kirfel.[45] Hydrogen atoms were placed in geometrically idealised positions and constrained to ride on their parent atoms with C---H distances in the range 0.95-1.00 Angstrom. Isotropic thermal parameters U_{eq} were fixed such that they were $1.2U_{eq}$ of their parent atom U_{eq} for CH's and $1.5U_{eq}$ of their parent atom U_{eq} in case of methyl groups. All non-hydrogen atoms were refined anisotropically by full-matrix least-squares.

Complex	**C2**	**C3**	**C4**
Emperical Formula	$C_{21.5}H_{30.625}BClF_4N_{5.625}O_{1.375}Pt$	$C_{21}H_{28}B_2F_8N_6Pt$	$C_{20}H_{27}ClN_4OPt$
Formula weight	707.24	733.2	569.99
Temperature (K)	100	100	100
Wavelength (Å)	0.71073	0.71073	0.71073
Crystal System	orthorhombic	triclinic	trigonal
Space group	$Pca2_1$	PT	$P3_121$
Unit cell axes (Å)	a =29.3015(12), b = 13.7435(6), c =26.6867(12)	a = 10.8637(4), b =11.2865(4), c =11.9333(4)	a = 11.0452(4), c = 14.8251(7)
Unit cell angles (°)	orthorhombic	α = 65.3770(10), β = 83.4580(10), γ = 76.1960(10)	trigonal
Volume ($Å^3$)	10746.9(8)	1291.54(8)	1566.30(14)
Z	16	2	3
Demsity (mg/m^3), calc.	1.748	1.885	1.813
Absorption coeff. (mm^{-1})	5.376	5.513	6.864
F(000)	5536	712	834
Crystal size (mm^3)	0.54 x 0.07 x 0.03	0.25 x 0.18 x 0.15	0.35 x 0.16 x 0.16
Theta range for data collection (°)	5.768 to 55.108	6.17 to 55.07	6.954 to 55.052
Index ranges	-38 ≤ h ≤ 38, -17 ≤ k ≤ 17, -34 ≤ l ≤ 34	-14 ≤ h ≤ 14, -14 ≤ k ≤ 14, -15 ≤ l ≤ 14	-14 ≤ h ≤ 14, -14 ≤ k ≤ 14, -18 ≤ l ≤ 19
Reflections collected	234573	30499	18874
Independent reflections, R(int)	24738[R(int) = 0.0624]	5960[R(int) = 0.0475]	2422 [R(int) = 0.0237]
Completeness to theta (%)	99.8	99.8	99.7
Max. and min. transmission	0.5087 and 0.7456	0.5996 and 0.7456	0.4798 and 0.7456
Refinement Method	Full-matrix least-squares on F^2	Full-matrix least-squares on F^2	Full-matrix least-squares on F^2
Data/restraints/parameters	24738/2819/1680	5960/6/377	2422/0/132
Goodness-of-fit on F^2	1.101	1.168	1.211
Final R indices [I>2sigma(I)]	R_1 = 0.0472, wR_2 = 0.1009	R_1 = 0.0297, wR_2 = 0.0517	R1 = 0.0129, wR2 = 0.0323
R indices (all data)	R_1 = 0.0588, wR_2 = 0.1070	R_1 = 0.0372, wR_2 = 0.0543	R1 = 0.0130, wR2 = 0.0323
Largest diff. peak and hole ($e.A^{-3}$)	2.38 and -1.85	1.28 and -1.37	0.40 and -1.44

Table 3.1 Parameters for X-Ray Structures in Chapter 3

Complex	**Pt(NCN) tetramer**	**C5a**	**C6**
Emperical Formula	$C_{113.5}H_{179}N_{16}O_{3.5}Pt_4$	$C_{40}\ H_{63}\ Cl\ Li_2\ N_4\ O_4\ Pt$	$C_{36}H_{58}ClLi_2N_5O_4Pt$
Formula weight	2604.08	908.36	869.29
Temperature (K)	100	100(2)	100
Wavelength (Å)	0.71073	0.71073	0.71073
Crystal System	monoclinic	Monoclinic	orthorhombic
Space group	$P2_1/c$	C 2/c	$Pna2_1$
Unit cell axes (Å)	a = 14.1078(12), b = 17.8284(15), c = 46.663(4)	a = 36.847(4), b = 12.1393(13), c = 23.040(3)	a = 9.5565(5), b = 26.8313(14), c = 15.1803(8)
Unit cell angles (°)	β = 94.074(2)°	α= 90, β= 124.349(11), γ = 90	orthorhombic
Volume ($Å^3$)	11707.1(17)	8508.4(16)	3892.4(4)
Z	4	8	4
Demsity (mg/m^3), calc.	1.477	1.418	1.483
Absorption coeff. (mm^{-1})	4.819	3.403	3.716
F(000)	5248	3712	1768
Crystal size (mm^3)	0.16 x 0.12 x 0.05	0.21 x 0.12 x 0.07	0.35 x 0.06 x 0.04
Theta range for data collection (°)	5.79 to 55.142	1.34 to 28.40	5.882 to 55.134
Index ranges	$-18 \le h \le 18, -23 \le k \le 23, -60 \le l \le 60$	-49<=h<=49, -16<=k<=16, -30<=l<=30	$-12 \le h \le 12, -34 \le k \le 34, -19 \le l \le 19$
Reflections collected	292634	145652	92641
Independent reflections, R(int)	26958[R(int) = 0.0972]	10254 [R(int) = 0.0499]	8963[R(int) = 0.0605]
Completeness to theta (%)	99.8	98.5	99.8
Max. and min. transmission	0.6049 and 0.7456	0.7966 and 0.5351	0.5391 and 0.7456
Refinement Method	Full-matrix least-squares on F^2	Full-matrix least-squares on F^2	Full-matrix least-squares on F^2
Data/restraints/parameters	26958/342/1412	10254/166/526	8963/25/449
Goodness-of-fit on F^2	1.21	1.043	1.265
Final R indices [I>2sigma(I)]	$R_1 = 0.0569, wR_2 = 0.0969$	R1 = 0.0346, wR2 = 0.0648	$R_1 = 0.0380, wR_2 = 0.0602$
R indices (all data)	$R_1 = 0.0790, wR_2 = 0.1027$	R1 = 0.0480, wR2 = 0.0708	$R_1 = 0.0457, wR_2 = 0.0617$
Largest diff. peak and hole ($e.A^{-3}$)	283 and -3.96	2.572 and -1.952	2.00 and -2.96

Table 3.2 Parameters for X-Ray Structures in Chapter 3

Complex	**C8**	**C9**	**C11**
Emperical Formula	$C_{64.75}H_{75}N_6O_{1.25}P_2Pt$	$C_{23}H_{34}ClN_5OPt$	$C_{37}H_{58}Li_2N_4O_4Pt$
Formula weight	1214.33	627.09	831.84
Temperature (K)	100	100	100
Wavelength (Å)	0.71073	0.71073	0.71073
Crystal System	Monoclinic	monoclinic	Monoclinic
Space group	$P2_1/C$	$P2_1/c$	$P2_1/C$
Unit cell axes (Å)	a = 15.1308(6), b = 26.3162(11), c = 15.2971(6)	a = 16.4244(6), b = 7.8124(3), c =20.8885(8)	a = 10.2030(6), b = 24.8268(14), c = 30.4664(17)
Unit cell angles (°)	β= 106.2490	β =112.4040(10)	
Volume ($Å^3$)	5847.8(4)	2477.98(16)	7717.3(8)
Z	4	4	8
Demsity (mg/m^3), calc.	1.379	1.681	1.432
Absorption coeff. (mm^{-1})	2.501	5.794	3.677
F(000)	2494	1240	3392
Crystal size (mm^3)	0.2 x 0.14 x 0.01	0.15 x 0.09 x 0.09	0.15 x 0.09 x 0.05
Theta range for data collection (°)	5.818 to 55.134	5.858 to 55.068	5.812 to 55.214
Index ranges	$-19 \le h \le 19, -34 \le k \le 34, -19 \le l \le 19$	$-21 \le h \le 21, -10 \le k \le 10, -27 \le l \le 27$	$-13 \le h \le 13, -32 \le k \le 32, -39 \le l \le 39$
Reflections collected	134940	55644	146793
Independent reflections, R(int)	13493[R(int) = 0.0660]	5696[R(int) = 0.0467]	17802[R(int) = 0.0525]
Completeness to theta (%)	99.8	99.9	99.8
Max. and min. transmission	0.6058 and 0.7456	0.6114 and 0.7456	0.6490 to 0.7456
Refinement Method	Full-matrix least-squares on F^2	Full-matrix least-squares on F^2	Full-matrix least-squares on F^2
Data/restraints/parameters	13493/577/814	5696/6/327	17802/36/898
Goodness-of-fit on F^2	1.106	1.236	1.249
Final R indices [I>2sigma(I)]	$R_1 = 0.0383, wR_2 = 0.0672$	$R_1 = 0.0300, wR_2 = 0.0518$	$R_1 = 0.0363, wR_2 = 0.0625$
R indices (all data)	$R_1 = 0.0558, wR_2 = 0.0732$	$R_1 = 0.0379, wR_2 = 0.0546$	$R_1 = 0.0434, wR_2 = 0.0645$
Largest diff. peak and hole ($e.A^{-3}$)	0.82 and -1.19	1.60 and -1.38	2.11 and -2.69

Table 3.3 Parameters for X-Ray Structures in Chapter 3

3.5 References to Chapter 3

(1) Labinger, J. A. *Organometallics* **2015**, *34*, 4784–4795.

(2) Ruiz-Castillo, P.; Buchwald, S. L. *Chem. Rev.* **2016**, *116*, 12564–12649.

(3) Simoes, J. A. M.; Beauchamp, J. L. *Chem. Rev.* **1990**, *90*, 629–688.

(4) Ligands, N.; Rendina, L. M.; Puddephatt, R. J. *Chem. Rev.* **1997**, *97*, 1735–1754.

(5) Lersch, M.; Tilset, M. *Chem. Rev.* **2005**, *105*, 2471–2526.

(6) Souillart, L.; Cramer, N. *Chem. Rev.* **2015**, *115*, 9410–9464.

(7) Juhasz, M.; Takahashi, S.; Arulmozhiraja, S.; Fujii, T. *J. Struct. Chem.* **2012**, *53*, 443–448.

(8) Felice, V. De; Renzi, A. De; Panunzi, A.; Tesauro, D. *J. Organomet. Chem.* **1995**, *488*, C13–C14.

(9) Fekl, U.; Goldberg, K. I. In *Adv. Inorg. Chem*; 2003; pp 259–320.

(10) Crespo, M.; Puddephatt, R. J. *Organometallics* **1987**, *6*, 2548–2550.

(11) Goldberg, K. I.; Yan, J.; Breitung, E. M. *J. Am. Chem. Soc.* **1995**, *117*, 6889–6896.

(12) Hinman, J. G.; Baar, C. R.; Jennings, M. C.; Puddephatt, R. J. *Organometallics* **2000**, *19*, 563–570.

(13) Scott, J. D.; Puddephatt, R. J. *Organometallics* **1986**, *5*, 2522–2529.

(14) Niroomand Hosseini, F.; Nabavizadeh, S. M.; Abu-Omar, M. M. *Inorg. Chem.* **2017**, *56*, 14706–14713.

(15) Moret, M.; Chen, P. *Organometallics* **2008**, *27*, 4903–4916.

(16) Veenboer, R. M. P.; Collado, A.; Dupuy, S.; Lebl, T.; Falivene, L.; Cordes, D. B.; Slawin, A. M. Z.; Cazin, C. S. J.; Nolan, S. P. *Organometallics* **2017**, *36*, 2861–2869.

(17) Cave, G. W. V.; Fanizzi, F. P.; Deeth, R. J.; Errington, W.; Rourke, J. P. *Organometallics* **2000**, *19*, 1355–1364.

(18) Cook, B. J.; Chen, C.-H.; Pink, M.; Caulton, K. G. *Dalt. Trans.* **2018**, *47*, 2052–2060.

(19) Bailey, W. D. Late Transition-Metal Complexes Supported by Pincer Ligands : Applications in Partial Oxidation Catalysis, University of Washington, 2016.

(20) Minghetti, G.; Stoccoro, S.; Cinellu, M. A.; Soro, B.; Zucca, A. *Organometallics* **2003**, *22*, 4770–4777.

(21) Bailey, W. D.; Luconi, L.; Rossin, A.; Yakhvarov, D.; Flowers, S. E.; Kaminsky, W.; Kemp, R. A.; Giambastiani, G.; Goldberg, K. I. *Organometallics* **2015**, *34*, 3998–4010.

(22) Dias, H. V. R.; Diyabalanage, H. V. K.; Eldabaja, M. G.; Elbjeirami, O.; Rawashdeh-Omary, M. A.; Omary, M. A. *J. Am. Chem. Soc.* **2005**, *127*, 7489–7501.

(23) Singh, K.; Long, J. R.; Stavropoulos, P. *Inorg. Chem.* **1998**, *37*, 1073.

(24) Polezhaev, A. V; Chen, C.-H.; Losovyj, Y.; Caulton, K. G. *Chem. - A Eur. J.* **2017**, *23* , 8039–8050.

(25) Vela, J.; Vaddadi, S.; Kingsley, S.; Flaschenriem, C. J.; Lachicotte, R. J.; Cundari, T. R.; Holland, P. L. *Angew. Chem. Int. Ed.* **2006**, *45*, 1607–1611.

(26) Madison, B. L.; Thyme, S. B.; Keene, S.; Williams, B. S. *J. Am. Chem. Soc.* **2007**, *129*,

9538–9539.

(27) Nilsson, P.; Plamper, F.; Wendt, O. F. *Organometallics* **2003**, *22*, 5235–5242.

(28) Fulmer, G. R.; Miller, A. J. M.; Sherden, N. H.; Gottlieb, H. E.; Nudelman, A.; Stoltz, B. M.; Bercaw, J. E.; Goldberg, K. I. *Organometallics* **2010**, *29*, 2176–2179.

(29) Brune, H. A.; Stapp, B.; Schmidtberg, G. *J. Organomet. Chem.* **1986**, *301*, 129–137.

(30) Negishi, E.; Takahashi, T.; Akiyoshi, K. *J. Organomet. Chem.* **1987**, *334*, 181–194.

(31) Kaljurand, I.; Kütt, A.; Sooväli, L.; Rodima, T.; Mäemets, V.; Leito, I.; Koppel, I. A. *J. Org. Chem.* **2005**, *70*, 1019–1028.

(32) Pangborn, A. B.; Giardello, M. A.; Grubbs, R. H.; Rosen, R. K.; Timmers, F. J. *Organometallics* **1996**, *15*, 1518–1520.

(33) Anderson, G. K.; Lin, M. *Inorg. Synth.* **1990**, *28*, 60–62.

(34) Hill, G. S.; Irwin, M. J.; Levy, C. J.; Rendina, L. M.; Puddephatt, R. J. *Inorg. Synth.* **1998**, *32*, 149–151.

(35) APEX3, 2016.1-0: Bruker-AXS. Madison, Wisconsin, USA 2016.

(36) Bruker-AXS, S. v8. 38A. Madison, Wisconsin, USA 2014.

(37) Krause, L., Herbst-Irmer, R., Sheldrick, G.M. & Stalke, D. *J. Appl. Cryst.* **2015**, *48*, 3.

(38) Sheldrick, G. . *Acta Cryst.* **2015**, *71*, 3.

(39) Sheldrick, G. . *Acta Cryst.* **2015**, *71*, 3.

(40) Bruker (2007) APEX2 (Version 2.1-4), SAINT (version 7.34A), SADABS (version

2007/4), B. I. Madison, Wisconsin, USA.

(41) Altomare, A.; Burla, M. c. . M. *J. Appl. Cryst.* **1999**, *32*, 115.

(42) Altomare, A.; Cascarano, G. L.; Guagliardi, A. *J. Appl. Cryst.* **1993**, *26*, 343.

(43) Sheldrick, G. M. (1997) SHELXL-97, P. for the refinement of crystal structures. University of Göttingen, Germany.

(44) Sheldrick, G. M. *Acta. Cryst.* **2015**, *A71*, 3.

(45) Waasmaier, D.; Kirfel, A. *Acta Cryst.* **1995**, *51*, 416.

Chapter 4

Synthesis of Bis(phosphino)amine Ligated Pt^{II} Species and Investigations Towards C-H coupling

4.1 Introduction

Many recently reported metal precatalysts for hydrogenation leverage the ability of the ligand to assist in the manipulation of dihydrogen to reduce small molecules.[1] Such metal-ligand cooperation (MLC) contrasts with traditional reaction mechanisms which usually invoke oxidation and reduction at the metal center, with the ligand(s) acting as a spectator. An example of MLC is Noyori's asymmetric hydrogenation system (first published in 1987)[2] where a multifunctional amine ligand promotes hydrogenation.[3] Noyori originally proposed a 2 + 2 addition mechanism for hydrogenating ketones (Figure 4.01a). Here, a Ru-H intermediate with a ligand NH_2 moiety promoted a hydride transfer and an N-H transfer to a carbonyl by a concerted addition pathway. The starting Ru species could then be regenerated by heterolytic H_2 cleavage across a Ru-NH bond. However, computational work by Gordon revealed a different mechanism (Figure 4.01b). In this case, a hydride is first transferred to the ketone substrate, which is then stabilized through H-bonding. After, a substrate bridge promotes protonation from a Ru-(H_2) moiety, regenerating the starting Ru species. Since then, the concept of small molecule activation by MLC has expanded to include a greater range of substrates and a broader class of ligands.[1]

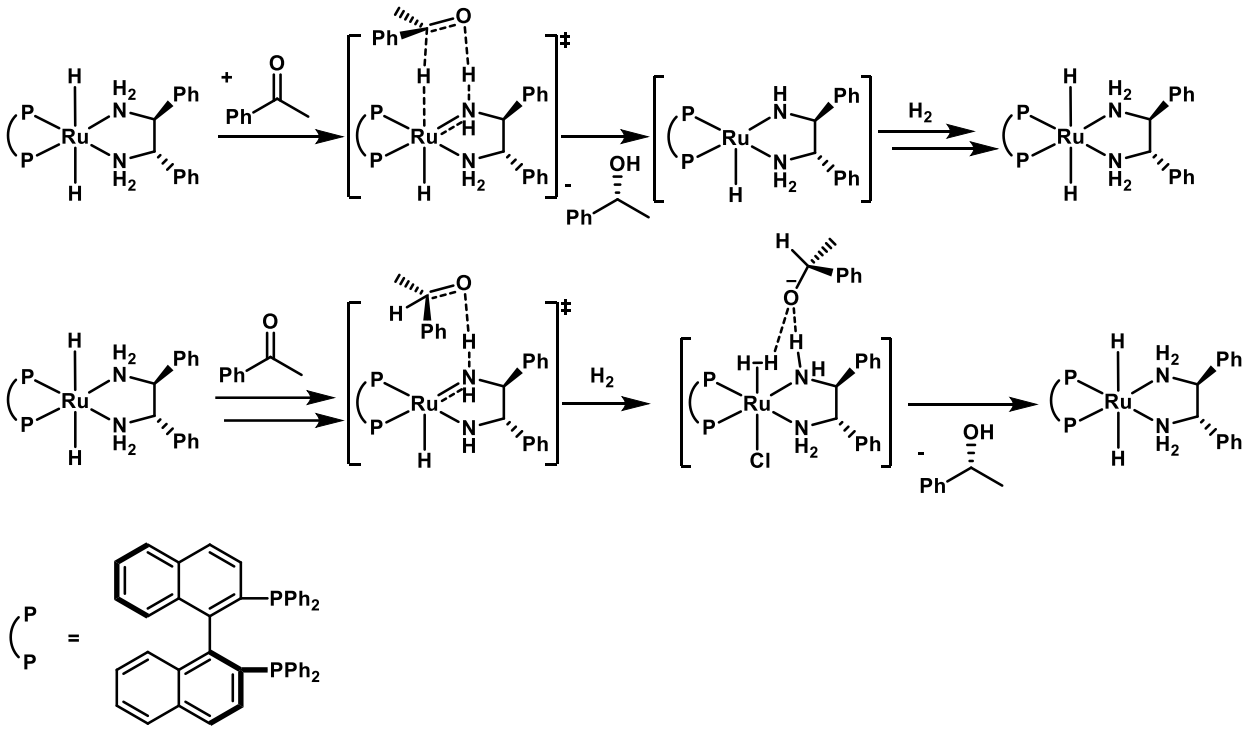

Figure 4.0 1 Proposed acetophenone hydrogenation by (a) Noyori and (b) Gordon.

One new class of ligands used in MLC reactions are chelating aminophosphine ligands, containing P and N donor atoms. Numerous catalytic reactions including hydroformylation, alkene isomerization, hydration and transfer hydrogenation reactions, among others, have employed these ligands.[4] In fact, bidentate aminophosphine (PN) ligated systems can often accomplish more efficient catalysis than their analogous bidentate diphosphine (PP) and diamine (NN) counterparts due in part to their ability to participate in MLC.[4] PN ligated aminophosphine complexes are known to exhibit hemilability at the bound N moiety, providing a potential low valent metal with an additional reactive site. This is due to strained chelate rings and a preference for ligation of soft P donors over hard N donors when bound to soft metals (Ru^{II}, Pt^{II}, Pd^{II}, Rh^{III} and others).[5–8] For example, a PN ligated Ru complex was shown to facilitate isomerization of 1-pentene by a mechanism invoking MLC (Figure 4.02a).[9] By density functional theory (DFT), calculations suggest that the aminophosphine ligand

helps deprotonate the 1-pentene α-CH_2 moiety (a formal C-H oxidative addition).[9] Additionally, a deprotonated bis(diphenylphosphino)amine (dppa) ligand, when bound to Fe, has been reported to heterolytically cleave dihydrogen (an analog to a C-H bond) to form an Fe-H complex with a protonated ligand backbone, bound in a κ^1 fashion (Figure 4.02b).[10] Further addition of H_2 leads to formation of a $Fe(H)_2$ complex, with loss of ligand. Along with formation of Fe-H and N-H bonds, an additional driving force for this activation was postulated to be relief of strained 4 membered deprotonated chelates. Once protonated, the P-Fe-P bite angle increased by 4-5 degrees, leading to a more stable complex.[10] These examples illustrate the ability of coordinated aminophosphines to help cleave strong X-H bonds.

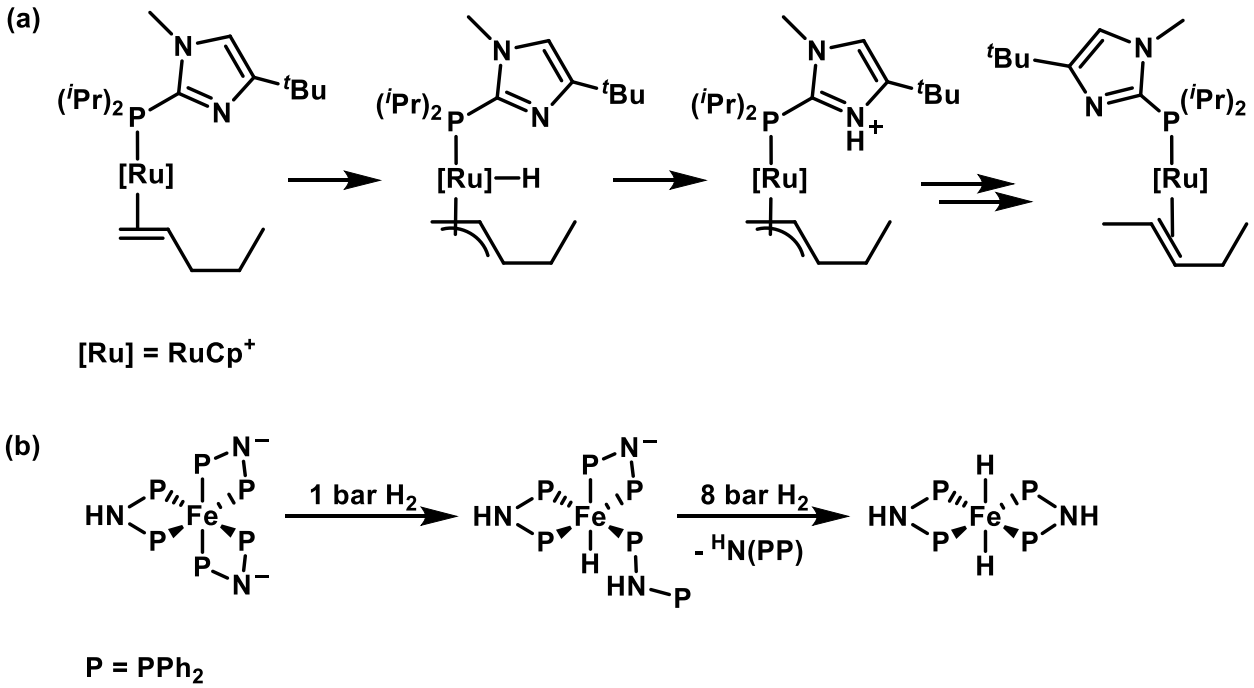

Figure 4.0 2 (**a**) Proposed mechanism of isomerization of 1-pentene to *trans* 2-pentene by MLC. (**b**) Heterolytic hydrogen cleavage by $Fe(*N(P(C_6H_5)_2)_2)_2(^HN(P(C_6H_5)_2)_2)$ to form $Fe(^HN(P(C_6H_5)_2)_2)_2(H)_2$ by MLC.

While the main goal of this project is geared towards heterolytic cleavage of C-H bonds by Pt^{II} complexes, it is often helpful to look at the microscopic reverse of this process, i.e. elimination of the alkane from a Pt^{II}-CH_3 complex, facilitated by a protic ligand. Indirect evidence for elimination of methane through an MLC type mechanism was observed by the Goldberg group while studying a platinum dimethyl di-*tert*-butylphosphino-2-aminopyridine [Pt(^{tBu}PN^{H}N)$(CH_3)_2$] complex (Scheme 4.01).[11] Upon thermolysis, methane was formed in the presence of trapping pyridine ligand

Scheme 4.01. Elimination of methane upon thermolysis in the (a) presence of pyridine (b) absence of pyridine

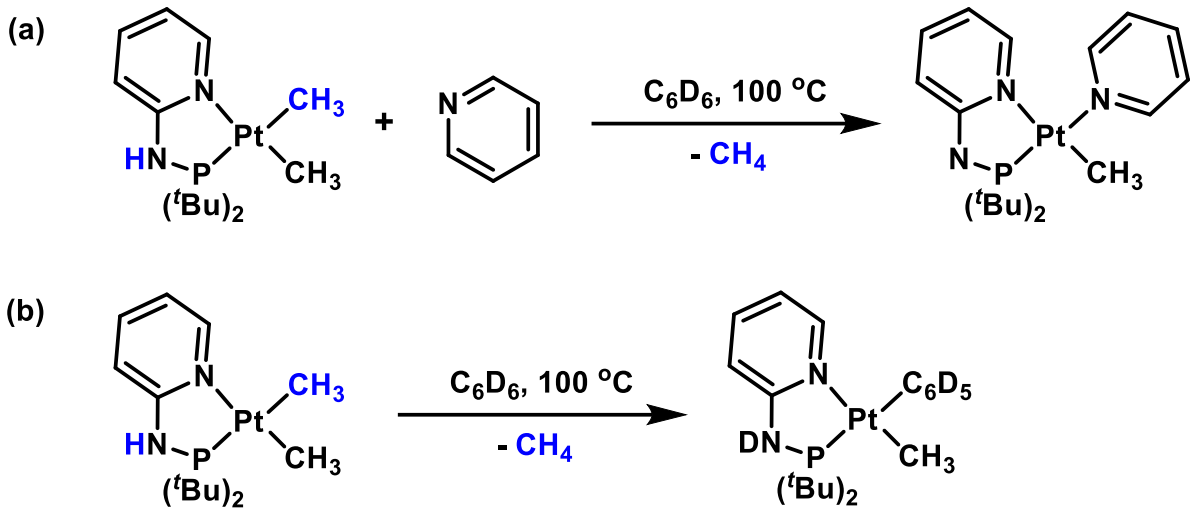

to yield a new deprotonated platinum complex. The formation of Pt(^{tBu}PN*N)(CH_3)(pyr-d_5) suggested coupling of the acidic N-H proton on the ligand and the methyl group bound to the metal center. Interestingly, thermolysis of Pt(^{tBu}PN^{H}N)$(CH_3)_2$ in C_6D_6, in the absence of exogeneous ligands, led to a significant amount of Pt(^{tBu}PN^{D}N)$(CH_3)(C_6D_5)$ being formed, along with methane (Scheme 4.01b). This suggests that in the absence of a coordinating ligand, C-H bond formation occurred (forming methane), followed by C-H heterolytic cleavage of solvent. However, in the presence of pyridine, an intermediate can be trapped after C-H bond formation occurs, demonstrating a platform for studying the microscopic reverse of C-H activation.

Leveraging the ability of the ligand to assist in the activation of strong bonds has led us to investigate similar aminophosphine based ligands. Described below are preliminary investigations of new and previously reported dppa ligated Pt species and their reactivity towards the cleavage or formation of X-H (X = C, H) bonds. The dppa ligand contains a N-H moiety which has been shown to exhibit MLC in dihydrogen cleavage when ligated to Fe, as discussed above.[10] The Pt dppa complexes $Pt^{II}(dppa)(X)_2$ (X = CH_3, Cl) have been previously reported.[12–14] The reactivity of this and other aminophosphine ligated Pt^{II} complexes were investigated and compared to the reactivity of the similar bidentate phosphinopyridine ligated Pt^{II} complex previously studied by the Goldberg group. The complexes all contain a secondary sphere N-H moiety.

4.2 Results and Discussion

4.21 Ligation of Protic Amino(bisphosphines) to Pt^{II}

Synthesis of aminophosphine and bis(phosphino)amine ligands generally proceed by condensation reaction mechanisms.[15] While, $^{H}N(P(C_6H_5)_2)_2$ is formed from condensation of $(C_6H_5)_2PCl$ with $^{H}N(Si(CH_3)_3)$, this does not work for the analogous $^{H}N(P(^{t}Bu)_2)_2$ ligand. Instead, $^{H}N(P(^{t}Bu)_2)_2$ can be synthesized by a self-condensation route of $^{t}Bu_2PCl$ with $NaNH_2$.[16] Subsequently, $^{H}N(P(C_6H_5)_2)_2$ and $^{H}N(P(^{t}Bu)_2)_2$ were both prepared. In 1970, Tolman quantified that $^{H}N(P(^{t}Bu)_2)_2$ contains a more electronically donating and sterically congested phosphine groups than $^{H}N(P(C_6H_5)_2)_2$, as evidenced by ν_{CO} data and cone angle analysis of their PR_3 analogs, respectively.[17] However, both bis(phosphino)amine ligands are quite sterically crowded and might allow us to exploit disfavored geometries.

To probe how the size of the PR_2 groups affects coordination, bis(phosphino)amine ligands were ligated to $Pt^{II}X_2$ to form several complexes (Figure 4.03 and 4.04). More specifically, $^{H}N(P(C_6H_5)_2)_2$ was ligated to Pt^{II} to form the previously reported $Pt(^{H}N(P(C_6H_5)_2)_2)(CH_3)_2$ (**D1a**)[14], $[Pt(^{H}N(P(C_6H_5)_2)_2)_2][BF_4]_2$ (**D2**)[13], and $Pt((*N(P(C_6H_5)_2)_2)_2$ (**D3**)[13], (Note: * indicates deprotonated amine) with $^{31}P\{^{1}H\}$ NMR resonances at 29.7 ppm ($^{1}J_{Pt\text{-}P}$ = 1489 Hz), 22.0 ppm ($^{1}J_{Pt\text{-}P}$ = 2100 Hz),

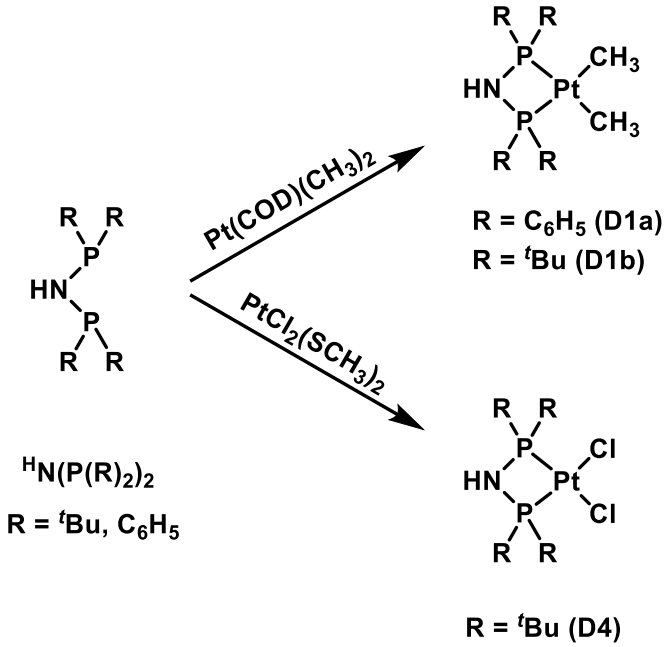

Figure 4.0 3 Metalation of $^{H}N(PR_2)_2$ (R = C_6H_5, ^{t}Bu) with Pt^{II} to form $Pt(^{H}N(P(R)_2)(CH_3)_2$ [R = C_6H_5 (**D1a**), ^{t}Bu (**D1b**)] and $Pt(^{H}N(P(^{t}Bu)_2)_2)(Cl)_2$ (**D4**).

and -17.4 ppm ($^{1}J_{Pt\text{-}P}$ = 1660 Hz), respectively. Additionally, **D1a** also contains a diagnostic Pt-CH_3 resonance at 0.69 ppm ($^{2}J_{Pt\text{-}H}$ = 75 Hz, $^{3}J_{P\text{-}H}$ = 12 Hz) and a N-H resonance at 5.65 ppm ($^{2}J_{P\text{-}H}$ = 9 Hz, $^{3}J_{Pt\text{-}H}$ = 63 Hz) in the ^{1}H NMR spectrum.

The analogous $^{H}N(P(^{t}Bu)_2)_2$ complex was synthesized at elevated temperatures (100 °C) to form $Pt(^{H}N(P(^{t}Bu)_2)_2)(CH_3)_2$ (**D1b**) and is one of only a handful of examples of transition metal ligation by $^{H}N(P(^{t}Bu)_2)_2$ (Figure 4.03).[18,19] This species exhibited a characteristic Pt-CH_3 resonance at 0.44 ppm ($^{3}J_{P\text{-}H}$ = 8 Hz, $^{2}J_{Pt\text{-}H}$ = 74 Hz) and a N-H resonance at 4.43 ppm ($^{3}J_{Pt\text{-}H}$ = 56 Hz) in the

^{1}H NMR spectrum. The ^{31}P{^{1}H} NMR spectrum also contained a singlet at 73.3 ppm ($^{1}J_{Pt\text{-}P}$ = 1501 Hz). Although the spectroscopic resonances and *J* values are similar to those exhibited by **D1a** (e.g. $^{1}J_{Pt\text{-}P}$ = 1475 Hz),[14] the $^{1}J_{Pt\text{-}P}$ of **D1b** was found to be slightly larger. It has previously been shown using similar bidentate diphosphine ligands (with varying PR_2 groups) that larger $^{1}J_{Pt\text{-}P}$ values correlate with wider P-M-P bite angles.[17,20] This suggests the P-Pt-P bite angle of **D1b** would be larger than **D1a**. While Tolman cone angles do not directly correlate with P-M-P bite angles, a cone analysis is an estimation to compare sterics on different phosphine ligands.[21] A similar correlation was made describing the relationship between the small cone angle of PMe_3 and the small bite angle of a bidentate P_2Pt complex.[22] Obtaining solid state structures of **D1a** and **D1b** would confirm this trend, and this is demonstrated for homoleptic complexes later in this chapter.

Similarly, addition of $^{H}N(P(^{t}Bu)_2)_2$ to a CD_2Cl_2 solution of $Pt(S(CH_3)_2)_2Cl_2$ gave one major product by ^{1}H and ^{31}P{^{1}H} NMR spectroscopy. The same product was observed spectroscopically in CD_2Cl_2 (along with free ligand) when 2 equiv. of $^{H}N(P(^{t}Bu)_2)_2$ and 9 equiv. NEt_3 were added to a toluene suspension of $Pt(S(CH_3)_2)_2Cl_2$. The major product contains a larger $^{1}J_{Pt\text{-}P}$ = 3260 Hz to $Pt(^{H}N(P(C_6H_5)_2)_2)Cl_2$ ($^{1}J_{Pt\text{-}P}$ = 3130 Hz)[13] by ^{31}P{^{1}H} NMR spectroscopy, suggesting $Pt(^{H}N(P(^{t}Bu)_2)_2)Cl_2$ (**D4**, Figure 4.03), which is also in accordance with the comparison of **D1a** and **D1b**, previously discussed. Additionally, by ^{1}H NMR spectroscopy, the ^{t}Bu moieties exhibited a broad doublet ($^{3}J_{P\text{-}H}$ = 16 Hz), which is similar to the $Pt(CH_3)_2$ variant ($^{3}J_{P\text{-}H}$ = 13 Hz). However, the N-H moiety contains a large $J_{Pt\text{-}H}$ coupling (210 Hz), which is in stark contrast to **D1b** ($^{3}J_{Pt\text{-}H}$ = 56 Hz) and could suggest it is more represented as a $^{1}J_{Pt\text{-}H}$ interaction, where $^{1}J_{Pt\text{-}H}$ values as high as 180 Hz were observed in zwitterionic Pt^{II} complexes with a direct N-H—Pt interaction.[23] A similar

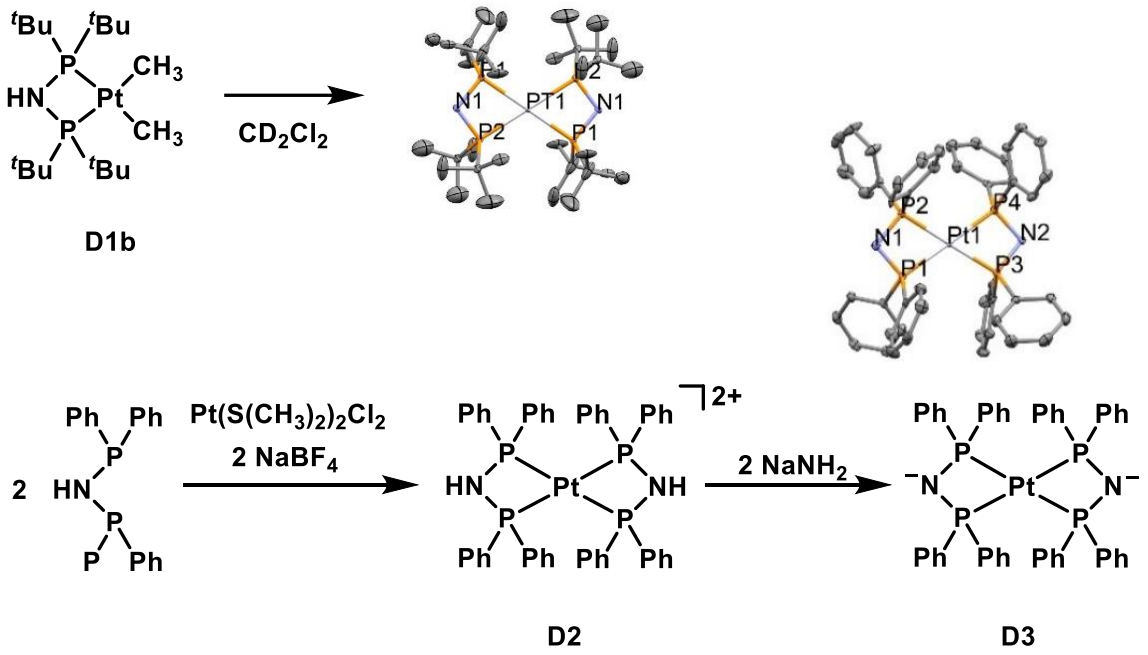

Figure 4.0 4 Synthetic pathway resulting in formation of Pt(*N(PR$_2$)$_2$)$_2$ [R = C_6H_5 (**D3**), ^{t}Bu]. Homoleptic [Pt(^{H}N(P(C_6H_5)$_2$)$_2$)$_2$][BF_4] (**D2**) is an intermediate in the formation of **D3**. Thermal Ellipsoid plot of **D3** and Pt(*N(P(^{t}Bu)$_2$)$_2$)$_2$ at 50 % probability and H-atoms omitted for clarity. Selected bond lengths and angles for **D3**: Pt(1)-P(1) 2.331(1) Å, Pt(1)-P(3) 2.325(2) Å, P(1)-N(1) 1.654(7) Å, P(3)-N(2) 1.650(4) Å, P(1)-Pt(1)-P(2) 65.00(7) ° P(3)-Pt(1)-P(4) 64.51(7) ° and Pt(*N(P(^{t}Bu)$_2$)$_2$)$_2$: Pt(1)-P(1) 2.383(2) Å, P(1)-N(1) 1.656(6) Å, P(1)-Pt(1)-P(2) 65.52(5) °.

interaction could be present in **D4**, where the N-H moiety would be pointed towards the metal. When metalation with 2 equiv. of ^{H}N(P(^{t}Bu)$_2$)$_2$ to Pt($S(CH_3)_2$)$_2Cl_2$ was performed in the presence of 2 equiv. of $NaNH_2$ at 60 °C in toluene-d_8, a mixture of species was observed by both ^{1}H and ^{31}P{^{1}H} NMR spectroscopy. Removal of the solvent and redissolution of the reaction mixture in CD_2Cl_2 revealed a single complex, presumably deprotonated Pt(*N(P(^{t}Bu)$_2$)Cl_2, evidenced by ^{1}H and ^{31}P{^{1}H} spectroscopy. The deprotonated Pt(*N(P(^{t}Bu)$_2$)Cl_2 contained similar ^{31}P{^{1}H} and ^{1}H NMR resonances compared protonated **D4** however no N-H resonance was observed. Upon exposure of a CD_2Cl_2 solution of Pt(*N(P(^{t}Bu)$_2$)Cl_2 to air, reformation of protonated **D4** was observed (determined by reappearance of the N-H resonance at 5.22 ppm). It is possible that the homoleptic Pt(^{H}N(P(^{t}Bu)$_2$)$_2$)$_2^{2+}$ cannot be formed, as it was not observed spectroscopically when 2 equiv. of

$^{H}N(P(^{t}Bu)_2)_2$ was added to a neutral or basic $Pt(S(CH_3)_2)_2Cl_2$ solution. Only the monoligated **D4** was formed. However, an X-ray quality crystal was obtained of $Pt(*N(P(^{t}Bu)_2)_2)_2$ after a CD_2Cl_2 solution of $Pt(*N(P(^{t}Bu)_2)_2)(CH_3)_2$ (**D1b**) decomposed over the course of several weeks (Figure 4.04). Further characterization of $Pt(*N(P(^{t}Bu)_2)_2)_2$ was not performed, although it is noted that this is the first X-ray structure obtained of transition metal bound $^{H}N(P(^{t}Bu)_2)_2$. It is unclear how homoleptic $Pt(*N(P(^{t}Bu)_2)_2)_2$ was formed and further investigations are required.

The known $Pt(*N(P(C_6H_5)_2)_2)_2$ (**D3**) was synthesized according to literature procedures and previously unobtained solid-state data was collected (Figure 4.04).[13] As with protonated $Pt(^{H}N(P(C_6H_5)_2)_2)_2$ (**D2**), deprotonated **D3** appeared symmetric in solution by ^{1}H and $^{31}P\{^{1}H\}$ NMR spectroscopy. $Pt(*N(P(^{t}Bu)_2)_2)_2$ is similarly symmetric in the solid-state, noted by the similar Pt-P bonds (2.325(2) Å and 2.331(1) Å) and P-Pt-P bite angles (65.00(7) ° and 64.51(7) °, Figure 4.04). Complex **D3** contains an additional strain which is manifested by a smaller P-Pt-P bite angle (by 5 °) and a slightly longer Pt-P bond (by 0.04 Å), compared to the previously reported X-ray structure of the protonated $Pt(^{H}N(P(C_6H_5)_2)_2)_2^{2+}$ (**D2**, 69.90(7) °, 2.293(2) Å).[13] Clearly, deprotonation of the metalated ligand, which already contains a strained 4 member ring, causes an additional distortion to promote potential increased intramolecular steric contact of the $P(C_6H_5)_2$ groups. It should be noted that the P-Pt-P bite angles observed in the solid state are unusually small. Out of the large number of bidentate P-Pt-P complexes in the literature (> 1000), only a few are known to have smaller bite angles (< 10).[24–26] The P-Pt-P bite angle of deprotonated $Pt(*N(P(^{t}Bu)_2)_2)_2$ (65.52(5) °, Figure 4.04), which contains a larger $P(^{t}Bu)_2$ moiety, is greater than analogous $Pt(*N(P(C_6H_5)_2)_2)_2$ **(D3**, 64.51(7) °, Figure 4.04) in the solid state.

*4.22 Reactivity of Pt(*N(P(C_6H_5)$_2$)$_2$)$_2$ (**D3**) towards X-H Activation*

As Fe(^{H}N(P(C_6H_5)$_2$)(*N(P(C_6H_5)$_2$)$_2$ was able to heterolytically cleave H_2 to form Fe(^{H}N(P(C_6H_5)$_2$)$_2$(*N(P(C_6H_5)$_2$)H due to the strained nature of the deprotonated metal-ligand chelate,[10] Pt(*N(P(C_6H_5)$_2$)$_2$)$_2$ (**D3**) was investigated for its ability to cleave X-H (X = C and H) bonds. Heating of **D3** in C_6D_6 resulted in no reaction up to 140 °C. Higher temperatures were not investigated. To investigate activation of a kinetically more accessible X-H substrate, dihydrogen was used. Compound **D3** was pressurized with 3 atm. of dihydrogen in C_6D_6 at room temperature

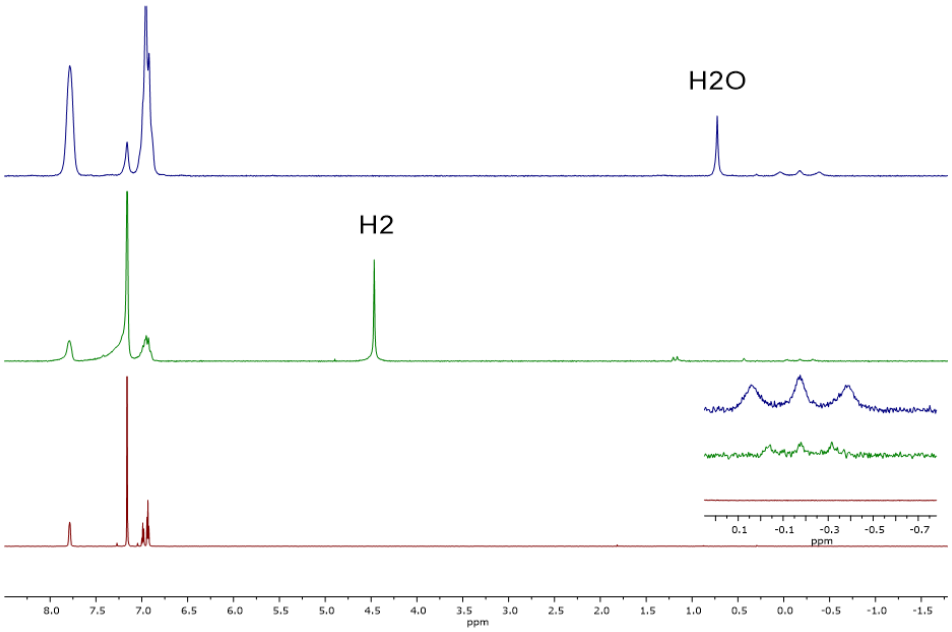

Figure 4.0 5 ^{1}H NMR spectra of **D3** (bottom) and subsequent pressurization with H_2 (middle) or addition of H_2O (top) and generation of triplet at -0.18 ppm (in middle and top spectra).

and a 3-line pattern (with the middle line being slightly larger than the two outside) was recorded at -0.18 ppm in the ^{1}H NMR spectrum (Figure 4.05). Complex **D3** was observed as the only metallic product by ^{1}H and ^{31}P{^{1}H} NMR spectroscopy and ESI-MS. The integration of the 3-line pattern increased over time (compared to ligand signals of **D3**) which suggests it may not be associated with **D3**. Additionally, the same 3-line resonance was observed with the addition of 2 equiv. H_2O (no H_2

present, Figure 4.05) and disappeared upon addition of D_2O by ^1H NMR spectroscopy. A potential explanation is H being split by another spin active (I = 1) nucleus, possibly ^{14}N or ^2H.[27,28] Performing a $^1H\{^{14}N\}$ and/or a ^2H NMR experiment will elucidate if this triplet is the result of N-H or H-D splitting. However, another explanation is the 3-line resonance is a singlet with a doublet additionally centered at -0.18 ppm. Performing decoupling experiments with other spin active (I = ½) nuclei, (e.g. $^1H\{^{31}P\}$ or $^1H\{^{195}Pt\}$) could elucidate if this is the source of the 3-line resonance.

After pressurizing a **D3** suspension with 3 atm. dihydrogen in C_6D_6, the reaction was heated by gradually raising the temperature and reactivity was not observed until 100 °C. The reaction mixture was subsequently heated at 100 °C for 21 hours and the disappearance of starting material was accompanied by the appearance of multiple broad aromatic resonances with no associated hydride resonances in the ^1H NMR spectrum. A single resonance was observed in the $^{31}P\{^1H\}$ NMR spectrum at 13.28 ppm, which did not correspond to free protonated ligand $^{H}N(P(C_6H_5)_2)_2$ (although $^*N(P(C_6H_5)_2)_2$ ligand was never synthesized to compare). No ^{195}Pt splitting was observed; however, this could be due to poor signal to noise resulting from low solubility in benzene. Aryl activation of $P\text{-}C_6H_5$ and/or ligand degradation is possible, yet undetermined. Reactivity in more solubilizing solvents will allow for more facile spectroscopic monitoring. Additionally, further characterization of this reaction mixture by GC-MS and ESI-MS could elucidate if ligand degradation is occurring or if another Pt complex is forming.

*4.23 Towards C-H coupling from $Pt(^{H}N(P(C_6H_5)_2)_2(CH_3)_2$ (**D1a**) and $Pt(^{H}N(P(^tBu)_2)_2(CH_3)_2$ (**D1b**)*

With two similar $Pt(CH_3)_2$ complexes in hand (**D1a** and **D1b**), thermolysis was explored. The goal was to observe if C-H coupling between the $Pt\text{-}CH_3$ ligand and the N-H moiety is possible.

Complex **D1b** was heated in C_6D_6 for 15 hrs. at 140 °C; no reaction was noted by ^{1}H or $^{31}P\{^{1}H\}$ NMR spectroscopy and higher temperatures were not explored. Proton shuttles have been used in a variety of systems and have even been shown computationally to significantly lower the activation barrier for reactions that involve proton transfer.[1] Upon thermolysis of **D1b** in the presence of a potential proton shuttle, namely water (150 equiv.), a reaction occurred at 120 °C in C_6D_6. After two hours, a new, symmetric complex had cleanly formed. This complex exhibited a singlet in the $^{31}P\{^{1}H\}$ NMR spectrum with a large $^{1}J_{Pt\text{-}P}$ splitting of 3860 Hz (Figure 4.15b). Coupling of this magnitude is highly unusual for Pt^{II} species and could indicate a reduction to Pt^{0}.[29] Another explanation would be formation of a dinuclear species with each ligand bridging between the two metals and relieving the strain from the small bite angle of the ligand. Similar $^{1}J_{Pt\text{-}P}$ to that of this unidentified product have been observed for such dinuclear species.[13,30] In the ^{1}H NMR spectrum, a highly deshielded singlet at 17 ppm and a singlet at -0.5 ppm (neither with observable ^{195}Pt coupling) were also observed with a relative 1:2 integration (Figure 4.15a). The former is perhaps indicative of a proton involved in hydrogen-bonding and the latter perhaps belonging to a hydroxide ligand. Strangely, no Pt-CH_3 resonances were observed in C_6D_6 or CD_2Cl_2, although it could be hidden under the broad ^{t}Bu resonances around 1.28 ppm. Dissolution of the thermolysis product in C_6H_6 revealed no ^{2}H resonances. Examination by ESI-MS in a MeOH/*i*PrOH mixture generated peaks with an *m/z* of 1122.2 (potentially $[Pt(\mu\text{-}*N(P(^{t}Bu)_2)_2)(CH_3)(OH)]_2(^{i}PrOH)^{+}$) and 565.2 (potentially $[Pt(\kappa^{1}\text{-}^{H}N(P(^{t}Bu)_2)_2)(CH_3)(OH)(MeOH)]^{+}$), additionally suggesting a dinuclear complex. Platinum complexes with sterically encumbered phosphine and bis(phosphino)amine ligand architectures often exhibit an "A frame" architecture,[14,31] so this dinuclear Pt complex with bulky ^{t}Bu ligands could show this geometry. The exact identity of this complex is still currently unknown; however, no observance of methane (or ethane) elimination suggests that water is promoting a different

reaction other than C-H coupling (reverse of C-H activation). Additional proton shuttles, such as alcohols, could be investigated to see if water is unique in its reactivity with **D1b**. Other proton shuttles might not exhibit this reactivity and the desired C-H coupling might be observed. Additionally, a solid-state structure would help identity the thermolysis product.

As thermolysis of **D1b** did not form a C-H coupled product, Pt(^{H}N(P(C_6H_5)$_2$)$_2$)(CH_3)$_2$ (**D1a)** was next investigated. Thermolysis of **D1a** in C_6D_6 for 48 hrs. at 100 °C was monitored by ^{1}H and ^{31}P{^{1}H} NMR spectroscopy until complete disappearance of starting material was observed. Although no Pt product was observed by ^{1}H or ^{31}P{^{1}H} NMR spectroscopy, gratifyingly, CH_4 (C-H coupled product) was observed (Figure 4.06a). When the N-D variant of **D1a** (Pt(^{D}N(P(C_6H_5)$_2$)$_2$)(CH_3)$_2$, generated by stirring **D1a** in a D_2O/THF mixture and confirmed by comparison to similar complexes)[32] was thermolyzed in C_6D_6, a mixture of CH_4 and CH_3D was observed. Formation of CH_3D likely occurs through N-D/Pt-CH_3 coupling[11] and CH_4 either forms through an H-D exchange pathway (through a transient Pt^{IV}-(D)(CH_3)) or through some other unknown pathway. Examination of the product mixture by ESI-MS in CH_3CN (in air) revealed a main peak at *m*/*z* = 1191 (potentially corresponding to [Pt(^{H}N(P(C_6H_5)$_2$)$_2$)(CH_3)]$_2^+$). As the thermolysis product is not diamagnetic, the Evans Method test was used to gain additional data.[33] The Evans Method revealed a shift in an internal standard (hexamethylbenzene) by 3.26 Hz

(corresponding to μ_{eff} = 0.97, assuming a M.W. of 1191) under N_2, and 13.70 Hz (corresponding to μ_{eff} = 2.0, assuming a M.W. of 1191) in air. Evans' method experiments suggest different paramagnetic solutions under inert atmosphere and in the presence of oxygen. Performing an EPR

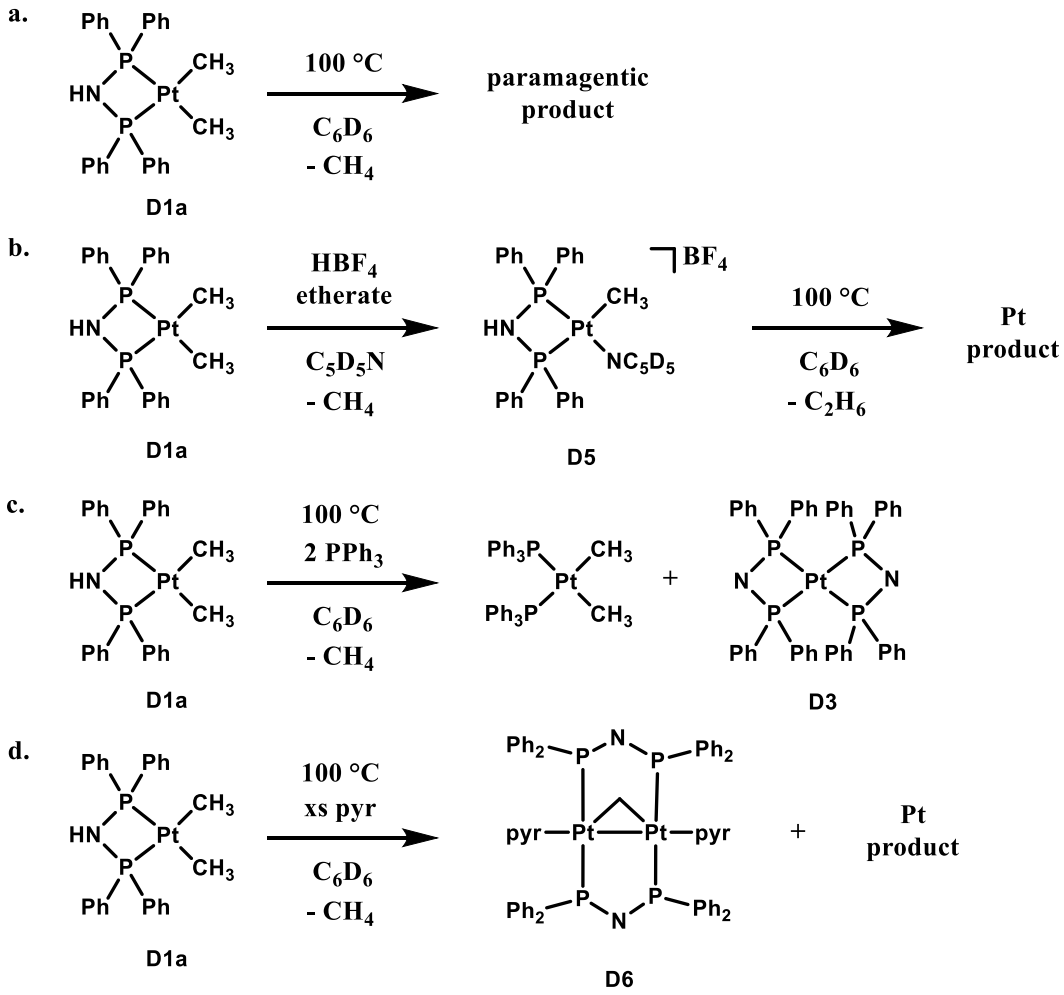

Figure 4.0 6 (**a**) Thermolysis of **D1a** in C_6D_6 to form a paramagnetic species. (**b**) Addition of HBF_4 etherate to **D1a** in pyridine-d_5 to form [Pt(^{H}N(P(C_6H_5)$_2$)$_2$)(CH_3)(pyr-d_5)][BF_4] (**D5**) and subsequent thermolysis to generate ethane. (**c**) Thermolysis of **D1a** in C_6D_6 with 2 equiv. P(C_6H_5)$_3$ to form Pt(P(C_6H_5)$_3$)$_2$(CH_3)$_2$ and **D3**. (d) Thermolysis of **D1a** to form Pt_2(μ-*N(P(C_6H_5)$_2$)$_2$)(μ-CH_2)(pyr)$_2$ (**D6**) and a paramagnetic product.

study could help elucidate whether these radical species are metal based or ligand based. Obtaining a solid-state structure would additionally reveal the structure of the thermolysis product.

To further elucidate how methane could be forming, reaction of **D1a** with 1 equiv. of HBF_4 etherate in pyridine-d_5 generated a new species, proposed to be [Pt(^{H}N(P(C_6H_5)$_2$)$_2$)(CH_3)(pyr-d_5)][BF_4] (**D5**, Figure 4.06b 88 % spectroscopic yield), along with methane. Examination of the ^{1}H NMR spectrum of **D5** revealed a downfield N-H resonance at 10.59 ppm ($^3J_{H\text{-}Pt}$ = 126 Hz) and a methyl ligand at 0.97 ppm (dd, $^2J_{Pt\text{-}H}$ = 57 Hz, $^3J_{H(trans)\text{-}P}$ = 7.3 Hz, $^3J_{H(cis)\text{-}P}$ = ~2 Hz*). (*Note – the broad doublet of doublets prevents accurate assignment of $^3J_{H(cis)\text{-}P}$ and additional NMR experiments are required). Examination of the ^{31}P{^{1}H} NMR spectrum revealed two doublets at 11.9 ppm ($^2J_{P\text{-}P}$ = 39 Hz, $^1J_{Pt\text{-}P}$ = 3476 Hz) and 36.5 ppm ($^2J_{P\text{-}P}$ = 39 Hz, $^1J_{Pt\text{-}P}$ = 1340 Hz). The NMR shifts and *J* values are similar to a previously reported cationic diphosphine ligated Pt-(pyr)(CH_3)$^+$ complex.[34]

Interestingly, thermolysis of the proposed monomethyl species **D5** at 100 °C did not eliminate methane and instead generated ethane, along with no resonances in either the ^{1}H NMR or ^{31}P{^{1}H} NMR spectra. A small amount of yellow solid was observed at the bottom of the J. Young NMR tube. Redissolution of the solid in CD_3CN revealed a single main resonance by ^{31}P{^{1}H} with no ^{195}Pt coupling (which could be due to poor signal to noise resulting from the very small amount of solid). Additionally, the solid contained many aromatic resonances in the ^{1}H NMR spectrum and a Pt-CH_3 resonance at 0.65 ppm ($^2J_{Pt\text{-}H}$ = 61 Hz, $^3J_{trans,P\text{-}H}$ = 7.9 Hz, $^3J_{cis,P\text{-}H}$ = 2.5 Hz). It is unclear what this Pt-CH_3 species is (which contains a ligated phosphine) and could be unreacted starting material due to similar coupling constants of **D5** in pyr-d_5. It is possible that an additional paramagnetic species was formed, however, additional experiments are required to assign the product species (i.e. an Evan's Method test, EPR experiments, ESI-MS and/or a solid-state structure). Liberation of ethane over methane in C_6D_6 is contrary to previous examples of cationic bidentate diphosphine Pt-(CH_3)(L)$^+$ reactivity in the literature (which typically generate methane

after C-H activation of solvent).[35] There is precedent for C-C bond forming reactions from Pd^{II}-Ar complexes.[36]

To try and trap an intermediate in the formation of the unknown paramagnetic compound when Pt(^{H}N(P(C_6H_5)$_2$)$_2$)(CH_3)$_2$ (**D1a**) was thermolyzed in C_6D_6, **D1a** was again was thermolyzed at

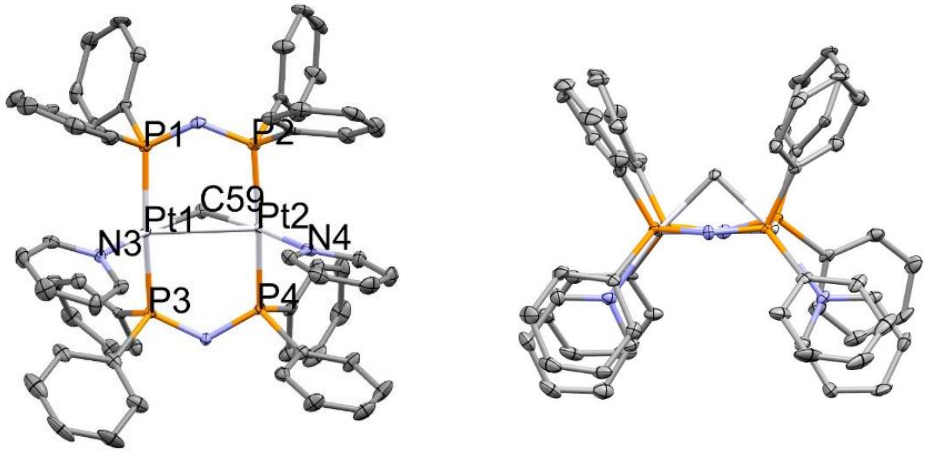

Figure 4.0 7 Thermal ellipsoid plot of **D6** at 50 % probability and H-atoms omitted for clarity. Right orientation highlights "A-Frame". Selected bond lengths and angles for **D6**: Pt(1)-P(1) 2.299(1) Å, Pt(1)-C(59) 2.070(4) Å, Pt(1)-N(3) 2.153(4) Å, Pt(1)-Pt(2) 2.9701(6) Å.

100 °C in the presence of 2 equiv. of P(C_6H_5)$_3$ in C_6D_6. This cleanly formed the known Pt(P(C_6H_5)$_3$)$_2$(CH_3)$_2$[37] and Pt(*N(P(C_6H_5)$_2$)$_2$)$_2$ (**D3**), with concomitant release of CH_4 (Figure 4.06c). Presence of a strongly donating ligand, P(C_6H_5)$_3$, does not appear to trap an intermediate and instead forms the homoleptic **D3** as the only *N(P(C_6H_5)$_2$)$_2$ containing product. Pyridine, a weaker binding ligand than P(C_6H_5)$_3$, which could additionally act as a base, was next used. It should be noted that pyridine does not deprotonate the N-H moiety; **D1a** is stable for at least 1 hour in pyridine-d_5 by ^{1}H NMR spectroscopy, although longer times were not explored. Thermolysis of **D1a** with an excess of pyridine (50 equiv.) in C_6D_6 liberated CH_4 and a single diamagnetic product by ^{1}H and ^{31}P{^{1}H} NMR spectroscopy (15 % spectroscopic yield). Up to 20 % spectroscopic yield of the diamagnetic

product can be obtained in neat pyridine-d_5. A solid state structure of the diamagnetic product was additionally obtained and indeed revealed an "A-Frame" type structure, $Pt_2(\mu\text{-}*N(P(C_6H_5)_2)_2)(\mu\text{-}CH_2)(pyr\text{-}d_5)_2$ (**D6,** Figure 4.06 and 4.07). Pt-P bonds lengths (2.299(1) Å) in deprotonated **D6** are slightly shorter than the deprotonated homoleptic **D1a** and **D1b** analogous bonds (2.331(1) Å and 2.383(2) Å, respectively) and demonstrate the relief in ring strain obtained in "A-Frame" type structures from 4 membered ring small bite angle complexes. Formation of Pt methylene dimers are known, yet only a handful of solid-state structures have been obtained.[30,38] Reported Pt methylene dimers are often synthesized with reagents such as diazomethane and formation from thermolysis reactions of $Pt\text{-}(CH_3)_2$ complexes have not been reported. Interestingly, formation of a methylene bridged Pt complex was obtained from deprotonation of a cyclometalated 1,2-Bis(diphenylphosphino)ethane (dppe) ligated $[Pt\text{-}CH_3][I]$ complex with NaOMe,[39] and basic pyridine could be acting in a similar manner to NaOMe under thermolysis conditions. Evaluating thermolysis of **D6** with NaOMe addition could test this hypothesis and could form a diamagnetic analog to **D6**, or potentially $Pt_2(\mu\text{-}*N(P(C_6H_5)_2)_2)(\mu\text{-}CH_2)(\underline{OMe})_2$. Formation of this Pt-OMe complex could then indicate a similar mechanism is at play to the previously reported dppe ligated Pt methylene dimer. Complex **D6** exhibited a singlet by $^{31}P\{^1H\}$ NMR spectroscopy with a complex P-Pt AA'A''A'''XX' spin system (Figure 4.14b). While the exact $J_{Pt\text{-}P}$ and $J_{P\text{-}P}$ values were not obtained and require additional 2D NMR experiments, similar $^{31}P\{^1H\}$ NMR spectra have been observed in similar "A-Frame" type structures.[40] As **D6** was formed in only 15 % yield in a C_6D_6/pyridine mixture, the remaining 85% could be accounted for by ligand decomposition, and/or a paramagnetic Pt complex. An Evan's Method test was not performed to determine if paramagnetic species were present. Examination of the product mixture by ESI-MS in CH_3CN in air revealed two peaks at m/z = 636.2 and 679.2 (potentially corresponding to $[Pt(^{H}N(P(C_6H_5)_2)_2)(CH_3)(NCCH_3)]^+$

and [Pt(^{H}N(P(C_6H_5)$_2$)$_2$)(CH_3)(pyr-d_5)]$^+$, respectively). **D6** does not appear to be stable to ESI-MS conditions.

4.3 Conclusion

In conclusion, bidentate $^{H}N(P(C_6H_5)_2)_2$ and $^{H}N(P(^tBu)_2)_2$ were ligated to Pt^{II} to form complexes that were investigated for their ability to undergo X-H activation (X = C, H) and C-H elimination reactions through an MLC-type mechanism. Synthesis of $Pt(^{H}N(P(^tBu)_2)_2)(X)_2$ [X = Cl, **D4**, X = CH_3, **D1b**] and known $Pt(*N(P(C_6H_5)_2)_2)_2$ (**D3**) and $Pt(^{H}N(P(C_6H_5)_2)_2)(CH_3)_2$ (**D1a)** was achieved. Although a viable synthesis of homoleptic $Pt(*N(P(^tBu)_2)_2)_2$ was not accomplished in solution, a small amount was observed to form in the solid state. While **D3**, a complex prepared to be studied for C-H activation, did not react with C_6D_6 solvent up to 140 °C, **D1b** appeared to react with dihydrogen. An unknown species was formed, evidenced by a single resonance by $^{31}P\{^1H\}$ NMR spectroscopy and by the appearance of multiple new ^1H aromatic resonances, with no observable Pt-H resonance. Aiming to study the microscopic reverse of C-H activation using Pt-CH_3 species with protonated backbones, **D1a** and **D1b** were investigated. Surprisingly, a thermolysis reaction did not occur for **D1b** in C_6D_6 upon heating to 140 °C, yet upon the addition of water, a new Pt-OH species was generated at 120 °C with no methane loss or Pt-CH_3 resonance by ^1H NMR spectroscopy. Additionally, examination of the reaction mixture by ESI-MS suggests a dimeric species could have been formed. Absence of methane in the ^1H NMR spectrum indicates that water might not be acting as a proton shuttle and is instead reacting with **D1b**. Conversely, thermolysis of **D1a** in C_6D_6 occurred at 100 °C (with or without water present) to generate methane and a paramagnetic compound (determined by Evan's Method analysis), potentially a binuclear complex by ESI-MS. Additionally, thermolysis of the N-D variant of **D1a** formed a mixture of CH_4/CH_3D, indicating cooperation of the N-D moiety with Pt-CH_3. Thermolysis of **D1a** in a C_6D_6/pyridine mixture additionally led to methane liberation and a new diamagnetic "A-Frame" complex (**D6**) in low yield. While the origin of the trapped diamagnetic **D6** species is not known at this point, it could

be due to presence of a base and additional bases should be explored. In all, generation of methane (C-H coupling) was achieved. Deuteration experiments suggest some of the formed methane is due to cooperation of the N-H moiety and Pt-CH_3 moiety, although additional experiments are necessary to determine how all the generated methane was formed.

4.4 Experimental

4.41 General Experimental

All manipulations were carried out under nitrogen atmosphere using standard Schlenk and glovebox techniques unless otherwise noted. Deuterated solvents were purchased from Cambridge Isotope Laboratories. Dry tetrahydrofuran, benzene, toluene, pentane, methylene chloride and diethyl ether were obtained by means of a Grubbs-type solvent purification system.[41] C_6D_6 was dried over sodium/benzophenone ketyl and were vacuum transferred prior to use. CD_3CN and pyridine-d_5 were dried over activated 3 Å and 4 Å, respectively, molecular sieves. MeOD was dried over dematiaceous earth and vacuum transferred prior to use. CD_2Cl_2 was dried over calcium hydride and vacuum transferred prior to use. $PtCl_2(S(CH_3)_2)_2$ and $Pt(COD)(CH_3)_2$ were synthesized following literature preparations.[42] All NMR spectra were obtained on a Bruker Avance 200 MHz, Bruker Avance 300 MHz or Bruker Avance 500 MHz instrument. The spectra were recorded at 300 K. Chemical shifts are reported in units of parts per million (ppm) downfield of TMS and referenced against proteo-solvent residual resonances (^1H) and characteristic solvent resonances (^{13}C). $^{31}P\{^1H\}$ NMR spectra were referenced externally to H_3PO_4 (85%, 0 ppm). NMR tubes fitted with a J-Young style Teflon valve were used to obtain inert atmosphere NMR data. Nominal mass accuracy ESI-MS data were obtained by use of a Waters Acquity UPLC system

equipped with a Waters TUV detector (254 nm) and a Waters SQD single quadrupole mass analyzer with electrospray ionization.

4.42 Synthesis, Characterization and Spectroscopic Data

Pt(^{H}N(P(C_6H_5)$_2$)$_2$)(CH_3)$_2$ (**D1a**)

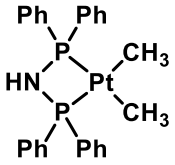

A 50 mL Schlenk tube was charged with 148.2 mg (0.385 mmol) ^{H}N(P(C_6H_5)$_2$)$_2$, 128.2 mg (0.385 mmol) Pt(COD)(CH_3)$_2$ and 10 mL THF. The vessel was sealed with a Teflon pin and heated to 60 °C for 6.5 hours. The yellow solution was cooled to room temperature and concentrated to 5 mL. The solution was layered with pentane and placed into a -30 °C freezer for 12 hours. Colorless crystals formed from the solution, which were collected by filtration, washed with pentane (3 x 1 mL) and dried under reduced pressure (211.6 mg, 90.0 % yield). **D1a** is a known compound and ^{1}H and ^{31}P{^{1}H} NMR spectroscopy agrees with the previously reported compound.[14] ^{1}H NMR (CD_2Cl_2, 200 MHz): δ 7.72-7.27 (20H, m, Ar-H), 5.64 (1H, s, N-H, $^{3}J_{Pt-H}$ = 65 Hz), 0.68 (6H, t, Ar-H, $^{3}J_{H-P}$ = 12 Hz, $^{3}J_{Pt-H}$ = 75 Hz). ^{31}P{^{1}H} (CD_3CN, 162 Hz): δ 29.73 ($^{3}J_{Pt-H}$ = 1475 Hz).

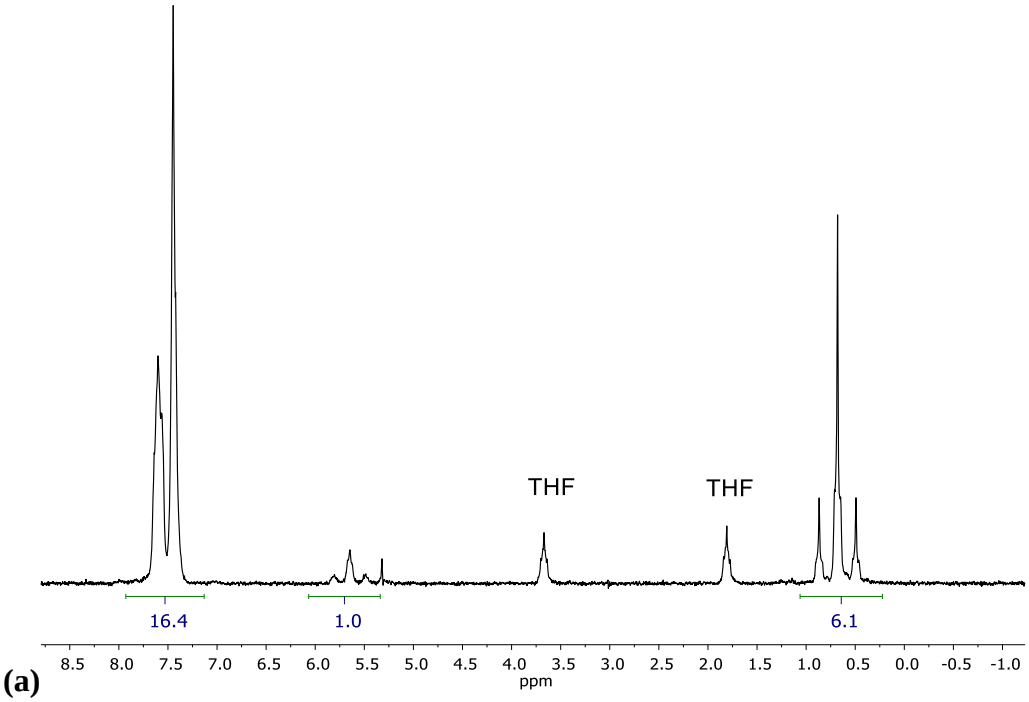

(a)

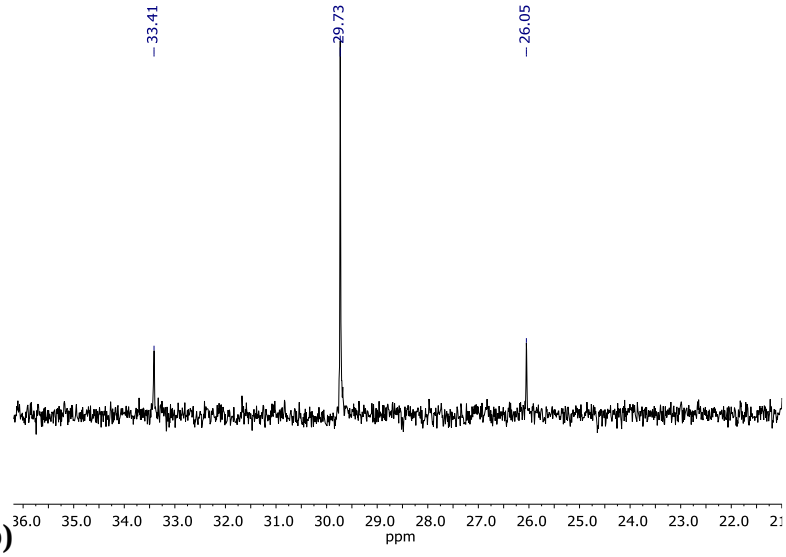

(b)

Figure 4.08a. ^{1}H NMR spectrum (200 MHz) of **D1a** in CD_2Cl_2. (b) $^{31}P\{^{1}H\}$ NMR spectrum (81 MHz) of **D1a** in C_6D_6.

Pt(^{H}N(P(^{t}Bu)$_2$)$_2$)(CH$_3$)$_2$ (**D1b**)

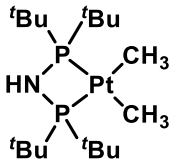

A 50 mL Schlenk tube was charged with 65.0 mg (0.206 mmol) ^{H}N(P(^{t}Bu)$_2$)$_2$, 68.7 mg (0.206 mmol) Pt(COD)(CH$_3$)$_2$ and 10 mL toluene. The vessel was sealed with a Teflon pin and heated to 100 °C for 20 hours. The yellow solution was cooled to room temperature and the volatiles were removed. The yellow mixture was washed with pentane (3 x 3 mL) and the resulting solid collected and dried under reduced pressure (32.2 mg, 29.3 % yield). ^{1}H NMR (CD$_2$Cl$_2$, 300 MHz): δ 4.43 (1H, s, N-H, $^{3}J_{Pt-H}$ = 56 Hz), 1.35 (36H, d, ^{t}Bu, $^{3}J_{H-P}$ = 13 Hz), 0.44 (6H, t, Ar-H, $^{3}J_{H-P}$ = 8 Hz, $^{3}J_{Pt-H}$ = 74 Hz). ^{31}P{^{1}H} (CD$_3$CN, 162 Hz): δ 73.25 ($^{3}J_{Pt-H}$ = 1501 Hz).

(a)

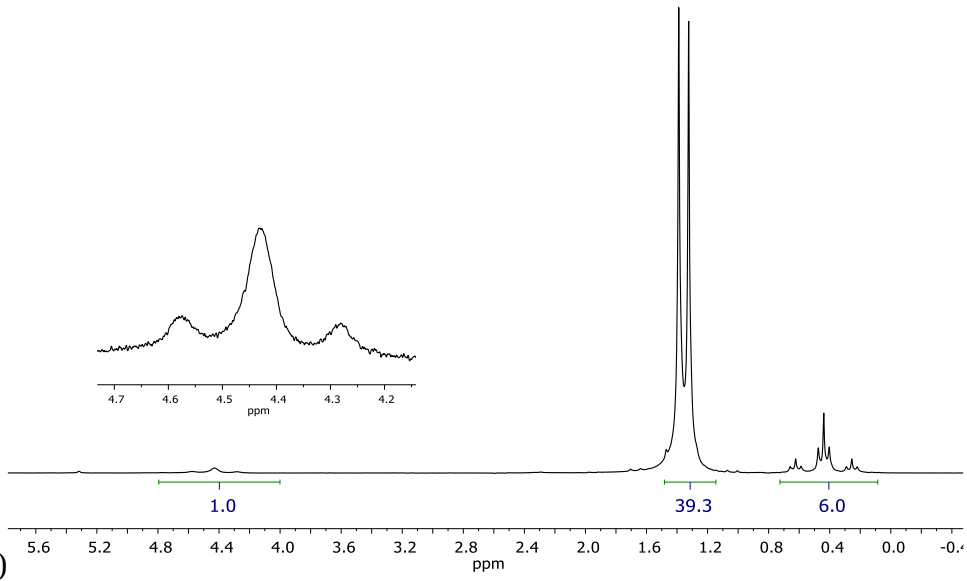

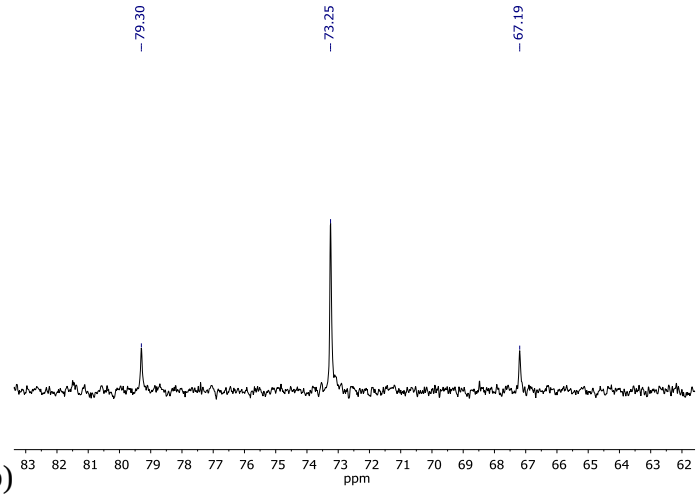

(b)

Figure 4.09a. ^{1}H NMR spectrum (300 MHz) of **D1b** in CD_2Cl_2. (b) $^{31}P\{^{1}H\}$ NMR spectrum (81 MHz) of **D1b** in C_6D_6.

$[Pt(^{H}N(P(C_6H_5)_2)_2)_2][BF_4]_2$ (**D2)**

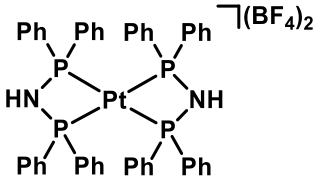

A 50 mL round bottom was charged with 155 mg (0.402 mmol) $^{H}N(P(C_6H_5)_2)_2$, 78.6 mg (0.201 mmol) $Pt(S(CH_3)_2)(Cl)_2$, 44.1 mg (0.402 mmol) $NaBF_4$, 10 mL CH_2Cl_2 and 5 mL MeOH. The solution was stirred for 15 mins and the volatiles were subsequently removed to yield a white solid. The product was extracted with CH_2Cl_2 (15 mL) and run through a fritted funnel. The filtrate's volatiles were subsequently removed under reduced pressure and the solid was washed with diethyl ether (2 x 10 mL) to yield a white solid (75.8 mg, 33.1 %).^{1}H NMR (MeOD, 300 MHz): δ 7.67-7.19 (40H, m, Ar-H). $^{31}P\{^{1}H\}$ (CD_3CN, 162 Hz): δ 5.20 (br s, no $^{1}J_{Pt\text{-}H}$ observed). Broadness is believed to be due to exchange of the N-H moiety, possibly with H_2O..

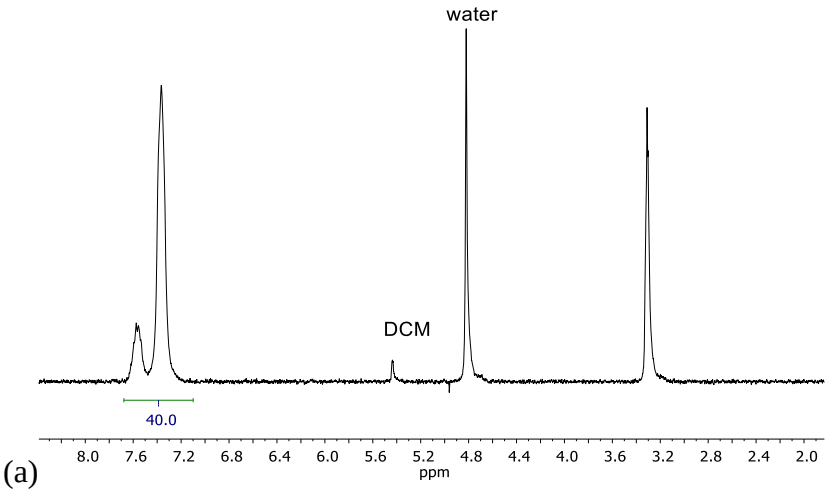

(a)

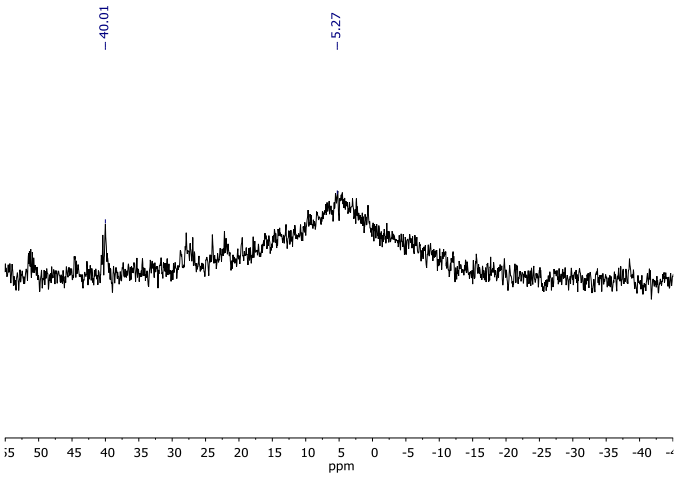

(b)

Figure 4.10a. ^{1}H NMR spectrum (200 MHz) of **D2** in MeOD. (b) $^{31}P\{^{1}H\}$ NMR spectrum (81 MHz) of **D2** in DMF-h_6. Unknown compound observed in $^{31}P\{^{1}H\}$ NMR spectrum at 40.01 ppm.

$Pt(*N(P(C_6H_5)_2)_2)_2$ (**D3**)

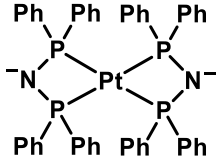

A 20 mL scintillation vial was charged with 64.5 mg (0.0566 mmol) **D2** and 5 mL THF to yield a suspension. While vigorously stirring, 4.5 mg (0.0113 mmol) $NaNH_2$ was added and allowed to stir for 2 hours. The solution was cooled and filtered via a fritted funnel and washed with cold THF (1 x 3 mL). The solid was collected and dried under reduced pressure (49 mg, 88 %).^{1}H NMR (CD_2Cl_2, 300 MHz): δ 7.60-7.11 (40H, m, Ar-H) $^{31}P\{^{1}H\}$ (CD_3CN, 162 Hz): δ -17.67 ($^{1}J_{Pt-H}$ = 1660 Hz).

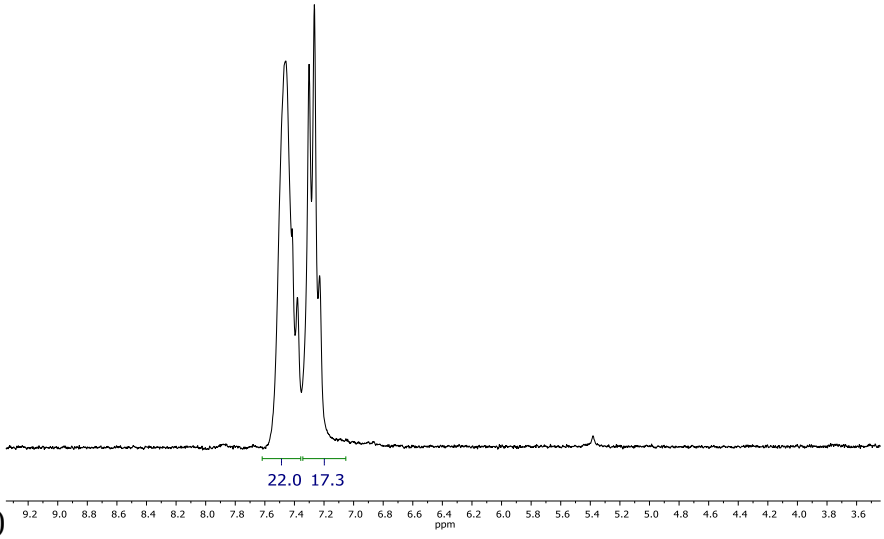

(a)

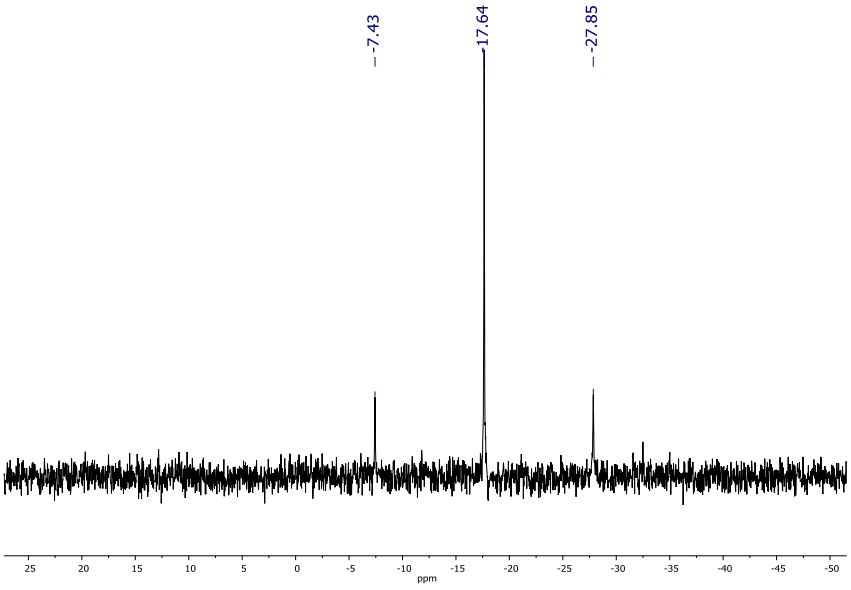

(b)

Figure 4.11a. ^{1}H NMR spectrum (200 MHz) of **D3** in CD_2Cl_2. (b) $^{31}P\{^{1}H\}$ NMR spectrum (81 MHz) of **D3** in CD_2Cl_2

$Pt(^{H}N(P(^{t}Bu)_2)_2)(Cl)_2$ (**D4**)

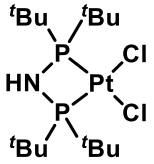

A 50 mL Schlenk flask was charged with 47.2 mg (0.155 mmol) $^{H}N(P(^{t}Bu)_2)_2$, 30.2 mg (0.0773 mmol) $Pt(S(CH_3)_2)_2(Cl)_2$ and toluene (10 mL). A reflux condenser was attached under a positive N_2 flow and the vessel was heated to reflux for 15 hours to form a yellow solid. The mixture was filtered via a fritted funnel and the solid was extracted from the fritted funnel with CH_2Cl_2 (5 mL). The volatiles were removed under reduced pressure and a sample of the solid was added to a J. Young NMR tube and the following NMR spectra were recorded. ^{1}H NMR (CD_2Cl_2, 200 MHz):

δ 5.97 (1H, s, N-H, $^{1}J_{Pt\text{-}H}$ = 210 Hz), 1.51 (36H, d, ^{t}Bu, $^{3}J_{H\text{-}P}$ = 16 Hz). $^{31}P\{^{1}H\}$ (CD_3CN, 162 Hz): δ 73.25 ($^{3}J_{Pt\text{-}H}$ = 3260 Hz).

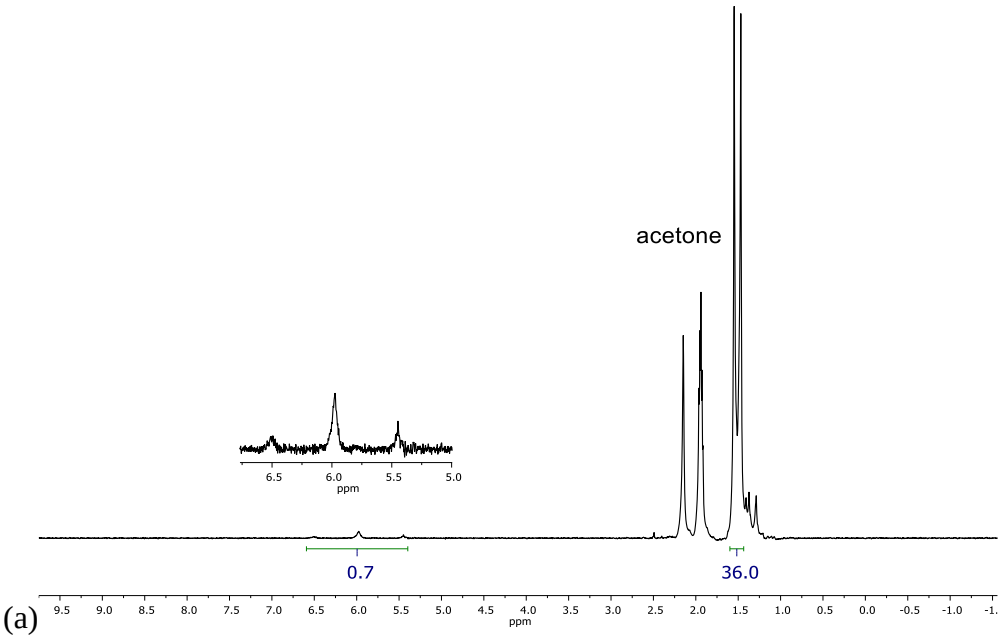

(a)

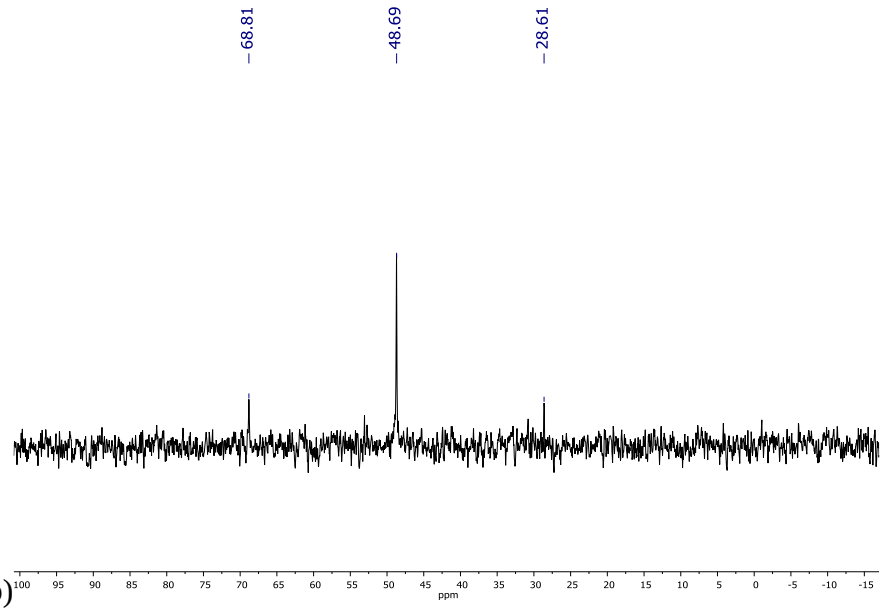

(b)

Figure 4.12a. ^{1}H NMR spectrum (200 MHz) of **D4** in CD_3CN. (b) $^{31}P\{^{1}H\}$ NMR spectrum (81 MHz) of **D4** in CD_3CN.

[Pt(^{H}N(P(C_6H_5)$_2$)$_2$)(CH_3)(pyr-d_5)][BF_4] (**D5**)

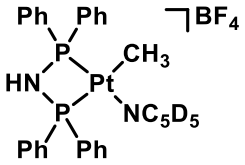

A J. Young NMR tube was charged with 6.7 mg (0.011 mmol) **D1a** and pyridine-d_5. 1.5 µL of HBF_4 etherate (0.011 mmol, 54 % in diethyl ether) was added and the following NMR spectra were recorded. ^{1}H NMR (pyridine-d_5, 400 MHz): δ 9.55 (1H, s, N-H, $^{3}J_{Pt\text{-}H}$ = 126 Hz), 7.99-7.87 (8H, m, Ar-H), 7.38-7.28 (12H, m, Ar-H), 1.45 ppm (6H, t, Pt-CH_3, $^{2}J_{Pt\text{-}H}$ = 57 Hz, $^{3}J_{H(trans)\text{-}P}$ = 7.3 Hz, $^{3}J_{H(cis)\text{-}P}$ = ~2 Hz). $^{31}P\{^{1}H\}$ (CD_3CN, 162 Hz): δ 36.54 (d, $^{2}J_{P\text{-}P}$ = 39 Hz, $^{1}J_{Pt\text{-}H}$ = 1340 Hz), 11.88 (d, $^{2}J_{P\text{-}P}$ = 39 Hz, $^{1}J_{Pt\text{-}H}$ = 3476 Hz).

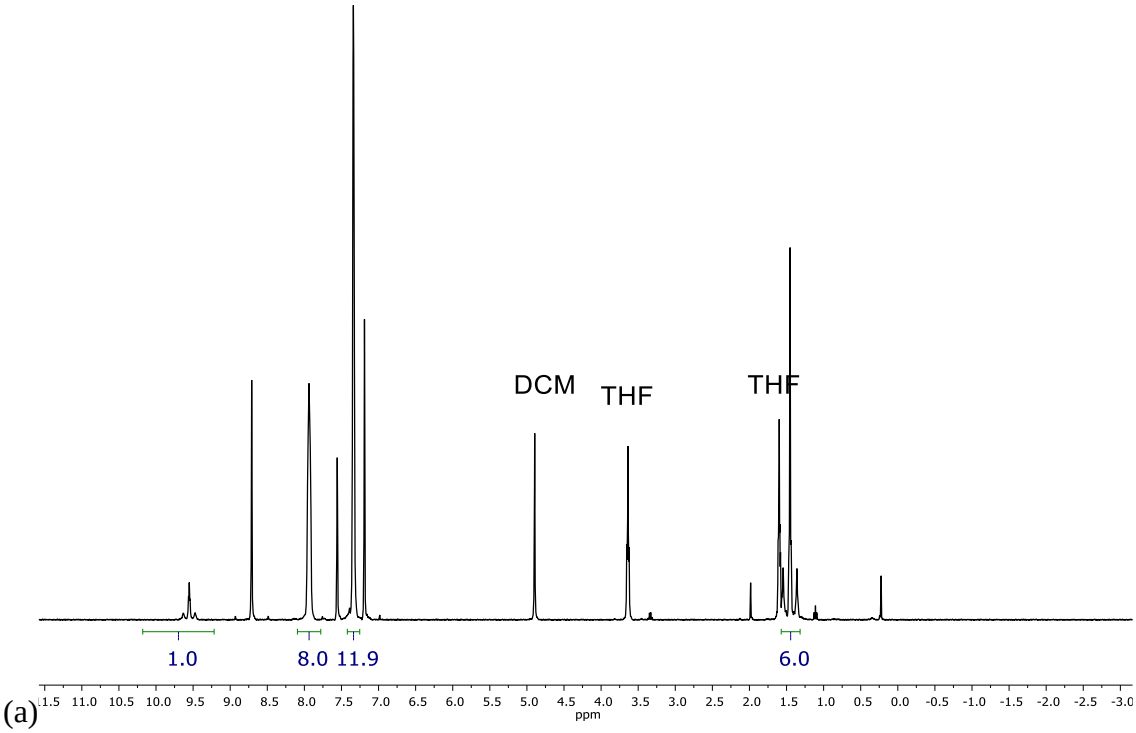

(a)

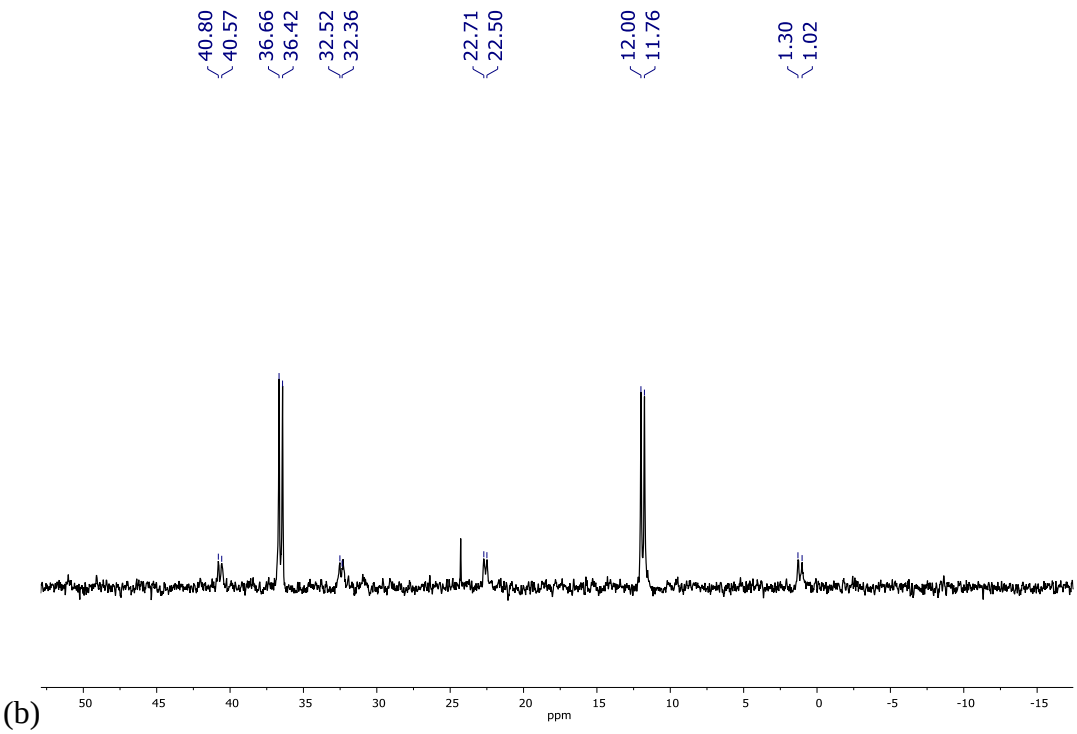

(b)

Figure 4.13. ^{1}H NMR spectrum (200 MHz) of **D5** in pyridine-d_5. (b) ^{31}P{^{1}H} NMR spectrum (81 MHz) of **D5** in pyridine-d_5.

$Pt_2(\mu\text{-}*N(P(C_6H_5)_2)_2)(\mu\text{-}CH_2)(pyr)_2$ (**D6**)

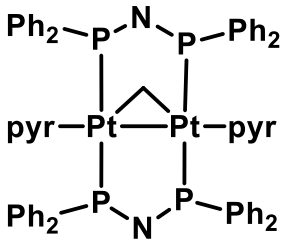

A J. Young NMR tube was charged with 6.7 mg (0.011 mmol) **D1a,** C_6D_6 (500 µL) and pyridine-d_5 (50 µL). The NMR tube was sealed, heated to 100 °C for 2 days, and cooled to room temperature. The following NMR spectra were recorded. ^{1}H NMR (C_6D_6, 400 MHz): δ 8.65-8.54 (8H, m, Ar-H), 8.10-8.06 (1H, m, Ar-H), 7.81-7.71 (1H, m, Ar-H), 7.59-7.49 (9H, m, Ar-H), 7.32-6.68 (21H, m, Ar-H), 3.11 (2H, m, Pt-CH_2). ^{31}P{^{1}H} (CD_3CN, 162 Hz): δ 42.83 (s, $^2J_{P\text{-}P}$, $^3J_{P\text{-}P}$, $^1J_{P\text{-}Pt}$, and $^2J_{P\text{-}Pt}$ could not be determined and require additional 2D experiments).

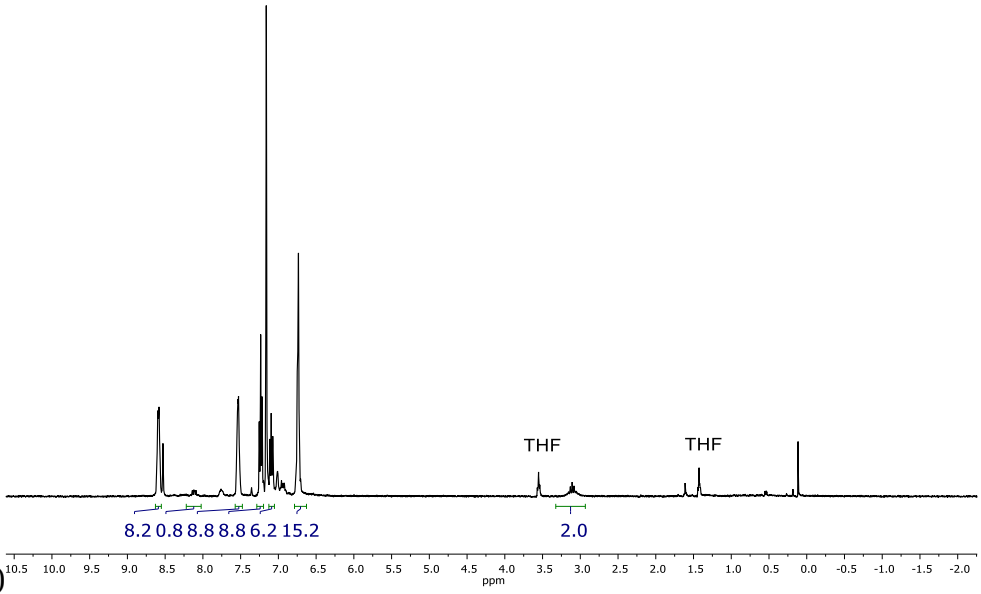

(a)

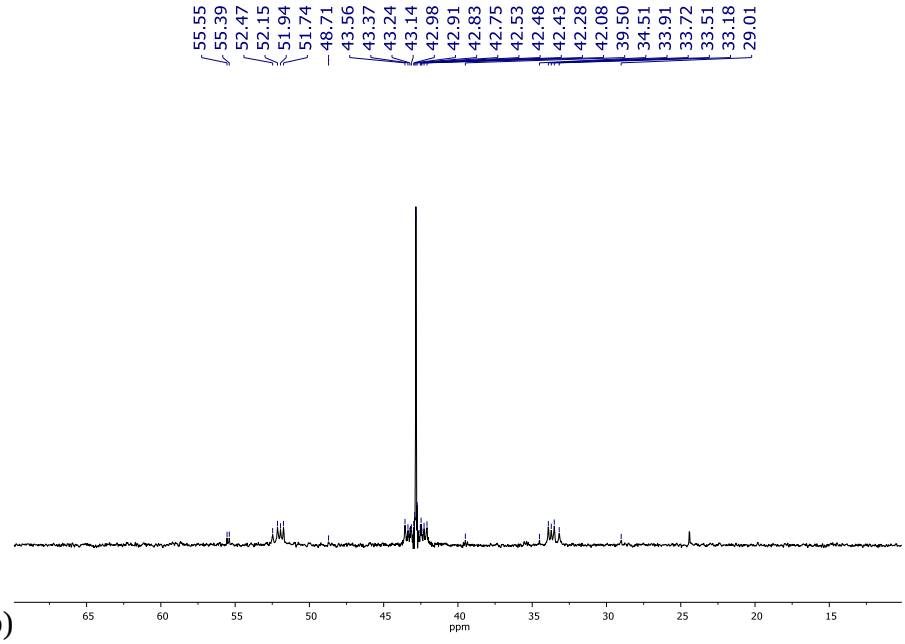

(b)

Figure 4.14. ^{1}H NMR spectrum (400 MHz) of impure **D6**. NMR spectrum obtained from reaction mixture of the thermolysis of **1a** in C_6D_6 with pyridine-d_5 addition. (b) $^{31}P\{^{1}H\}$ NMR spectrum (162 MHz) of **D6** in C_6D_6.

Thermolysis product of **D1b** in C_6D_6/H_2O mixture (Section 4.23)

A J. Young tube was charged with 2 mg (0.004 mmol) **D1b**, 10 µL (0.56 mmol) H_2O and 0.4 mL C_6D_6. The NMR tube was heated in an oil bath at 120 °C for 2 hours. The NMR tube was cooled and spectroscopic data was obtained and is shown below. ^{1}H NMR (CD_2Cl_2, 200 MHz): δ 15.43 (1H, s, N-H), 1.27 (72H, br d, $^{3}J_{P\text{-}H}$ = 13.1 Hz), -0.83 (2H, s, OH), 7.59-7.49 (9H, m, Ar-H), 7.32-6.68 (21H, m, Ar-H), 3.11 (2H, m, Pt-CH_2). $^{31}P\{^{1}H\}$ (CD_2Cl_2, 162 Hz): δ 42.83 ppm

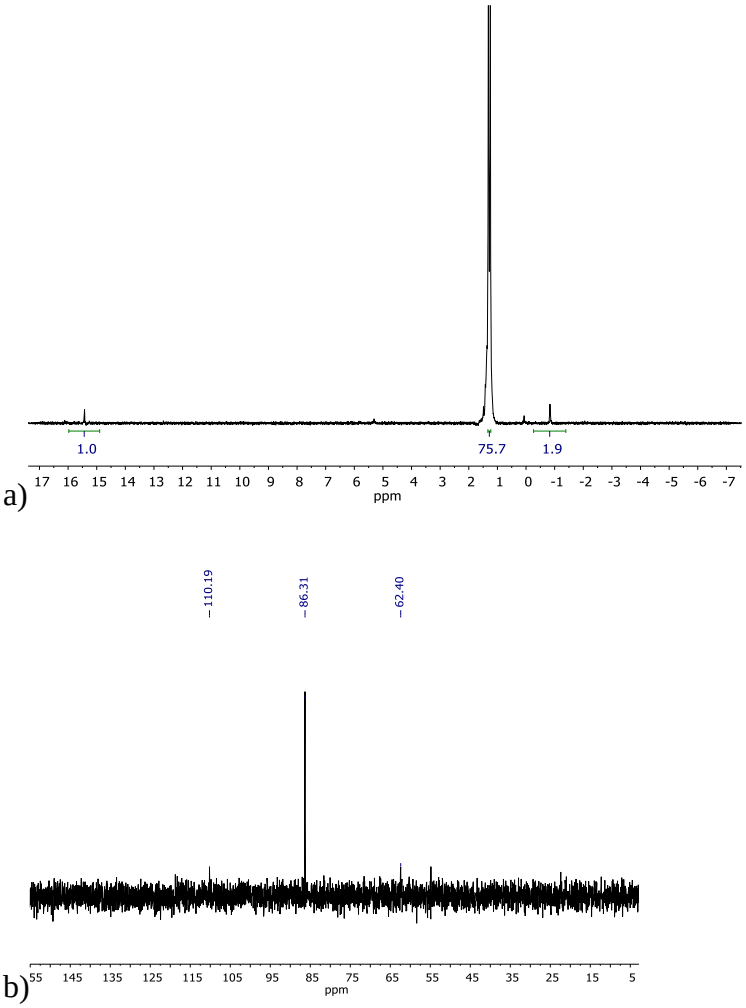

Figure 4.15. ^{1}H NMR spectrum (200 MHz) in CD_2Cl_2 of thermolysis product of **D1b** in C_6D_6/H_2O mixture. (b) $^{31}P\{^{1}H\}$ NMR spectrum (162 MHz) in CD_2Cl_2 of thermolysis product of **D1b** in C_6D_6/H_2O mixture.

4.43 X-ray Crystallography General Information

Pt(*N(P(^{t}Bu)$_2$)$_2$)$_2$ complex: X-ray intensity data were collected at -173 °C on a Bruker APEX II single crystal X-ray diffractometer, Mo-radiation. The data was integrated and scaled using SAINT, SADABS within the APEX2 software package by Bruker.[43] Solution by direct methods

(SHELXS, SIR97)[44,45] produced a complete heavy atom phasing model consistent with the proposed structure. The structure was completed by difference Fourier synthesis with SHELXL97.[46,47] Scattering factors are from Waasmair and Kirfel.[48] Hydrogen atoms were placed in geometrically idealised positions and constrained to ride on their parent atoms with C---H distances in the range 0.95-1.00 Angstrom. Isotropic thermal parameters U_{eq} were fixed such that they were $1.2U_{eq}$ of their parent atom U_{eq} for CH's and $1.5U_{eq}$ of their parent atom U_{eq} in case of methyl groups. All non-hydrogen atoms were refined anisotropically by full-matrix least-squares. Even though twinning was resolved, the molecule appeared disordered via lattice symmetry operation –x, y, -z in junction with inversion symmetry. Because of the massive disorder, many restraints were required to stabilize displacement parameters and ensure meaningful t-butyl geometry.

D3 and **D6**: X-ray intensity data were collected on a Bruker APEXIII D8QUEST[49] CMOS area detector, both employing graphite monochromated Mo-Kα radiation (λ = 0.71073 Å) at 100(1) K. Preliminary in indexing was performed from a series of twenty-four 0.5° rotation frames with exposures of 10 seconds. Rotation frames were integrated using SAINT[50], producing a listing of unaveraged F^2 and $\sigma(F^2)$ values. The intensity data were corrected for Lorentz and polarization effects and for absorption using SADABS.[51] The structure was solved by direct methods – ShelXT.[52] Refinement was by full-matrix least squares based on F^2 using SHELXL-2018.[53] All reflections were used during refinement. Non-hydrogen atoms were refined anisotropically and hydrogen atoms were refined using a riding model.

Table 4.01 Parameters for X-ray Structures in Chapter 4

Complex	**Pt(*N(P(tBu)2)2)2**	**3**	**6**
Emperical Formula	$C_{32}H_{72}N_2P_4Pt$	$C_{48}H_{40}N_2P_4Pt$	$C_{59}H_{52}N_4P_4Pt_2$
Formula weight	803.88	963.79	1331.1
Temperature (K)	100(2)	100	100
Wavelength (Å)	0.71073	0.71073	0.71073
Crystal System	Monoclinic	monoclinic	monoclinic
Space group	C 2/m	Cc	$P2_1/c$
Unit cell axes (Å)	a = 18.231(3), b = 12.484(2), c = 8.8708(15)	a = 23.8432(11), b = 12.4021(6), c = 17.6773(8)	a =10.1832(4), b = 23.6934(6), c = 21.4033(8)
Unit cell angles (°)	α = 90, β = 115.713(6), γ = 90	β = 130.2320(10)	β = 93.7200(10)
Volume ($Å^3$)	1819.1(5)	3990.7(3)	5153.2(3)
Z	2	4	4
Demsity (mg/m^3), calc.	1.468	1.604	1.716
Absorption coeff. (mm^{-1})	4.056	3.714	5.591
F(000)	832	1920	2600
Crystal size (mm^3)	0.130 x 0.070 x 0.070	0.15 x 0.14 x 0.08	0.21 x 0.08 x 0.06
Theta range for data collection (°)	2.049 to 28.404	5.8 to 55.1	5.964 to 55.21
Index ranges	-24<=h<=24, -16<=k<=0, -11<=l<=11	$-30 \le h \le 30$, $-16 \le k \le 16$, $-22 \le l \le 22$	$-13 \le h \le 13$, $-30 \le k \le 30$, $-27 \le l \le 27$
Reflections collected	4501	47747	146293
Independent reflections, R(int)	2350 [R(int) = 0.0580]	9150[R(int) = 0.0296]	11915[R(int) = 0.0936]
Completeness to theta (%)	99	99.9	99.8
Max. and min. transmission	0.745688 and 0.590347	0.6463 and 0.7456	0.5720 and 0.7456
Refinement Method	Full-matrix least-squares on F^2	Full-matrix least-squares on F^2	Full-matrix least-squares on F^2
Data/restraints/parameters	2350/165/158	9150/2/497	11915/0/622

Goodness-of-fit on F^2	1.006	1.231	1.105
Final R indices [I>2sigma(I)]	R1 = 0.0374, wR2 = 0.0899	R_1 = 0.0231, wR_2 = 0.0435	R_1 = 0.0394, wR_2 = 0.0586
R indices (all data)	R1 = 0.0375, wR2 = 0.0899	R_1 = 0.0248, wR_2 = 0.0439	R_1 = 0.0627, wR_2 = 0.0636
Largest diff. peak and hole ($e.A^{-3}$)	2.305 and -1.338	0.54 and -1.17	1.49 and -2.17

.

.

4.5 Notes to Chapter 4

(1) Khusnutdinova, J. R.; Milstein, D. *Angew. Chem. Int. Ed.* **2015**, *54*, 12236.

(2) Noyori, R.; Ohkuma, T.; Kitamura, M.; Takaya, H.; Sayo, N.; Kumobayashi, H.; Akutagawa, S. *J. Am. Chem. Soc.* **1987**, *109*, 5856–5858.

(3) Noyori, R. *Angew. Chem. Int. Ed.* **2002**, *41*, 2008.

(4) Rong, M. K.; Holtrop, F.; Slootweg, J. C.; Lammertsma, K. *Coord. Chem. Rev.* **2019**, *382*, 57–68.

(5) Bowes, E. G.; Dawson Beattie, D.; Love, J. A. *Inorg. Chem.* **2019**, *58*, 2925–2929.

(6) Poverenov, E.; Gandelman, M.; Shimon, L. J. W.; Rozenberg, H.; Ben-David, Y.; Milstein, D. *Organometallics* **2005**, *24*, 1082–1090.

(7) Lee, W. C.; Sears, J. M.; Enow, R. A.; Eads, K.; Krogstad, D. A.; Frost, B. J. *Inorg. Chem.* **2013**, *52*, 1737–1746.

(8) Bálint, E.; Tajti, Á.; Tripolszky, A.; Keglevich, G. *Dalt. Trans.* **2018**, *47*, 4755–4778.

(9) Tao, J.; Sun, F.; Fang, T. *J. Organomet. Chem.* **2012**, *698*, 1–6.

(10) Frank, N.; Hanau, K.; Langer, R. *Inorg. Chem.* **2014**, *53*, 11335.

(11) Scheuermann, M.; Grice, K.; Ruppel, M.; Roselló-merino, M.; Kaminsky, W.; Goldberg, K. I. *Dalton Trans.* **2014**, No. 31, 12018–12025.

(12) Bhattacharyya, P.; Sheppard, R. N.; Slawin, A. M.; Williams, D. J.; Woollins, J. D. *J. Chem. Soc. Dalt. Trans.* **1993**, No. 1, 2393–2400.

(13) Browning, C. S.; Farrar, D. H. *J. Chem. Soc. Dalt. Trans* **1995**, No. 4, 521.

(14) Jamali, S.; Rashidi, M.; Jennings, M. C.; Puddephatt, R. J. *J. Chem. Soc. Dalt. Trans.* **2003**, *3*, 2313–2317.

(15) Gopalakrishnan, J. *Appl. Organomet. Chem.* **2009**, *23*, 291–318.

(16) Ritch, J. S.; Chivers, T.; Eisler, D. J.; Tuononen, H. M. *Chem. Eur. J.* **2007**, *13*, 4643–4653.

(17) Tolman, C. A. *Chem. Rev.* **1977**, *77*, 313–348.

(18) Eisler, D. J.; Robertson, S. D.; Chivers, T. *Can. J. Chem.* **2009**, *87*, 39–46.

(19) Stoessel, P.; Joosten, D.; Breuning, E.; Yersin, H.; Monkowius, U. Organic electroluminescent devices employing multinuclear metal complexes and their production using organic vapor deposition and selected platinum-containing complexes and their preparation, 2010.

(20) Kégl, T. R.; Pálinkás, N.; Kollár, L.; Kégl, T. *Molecules* **2018**, *23*, 1–11.

(21) Van Leeuwen, P. W. N. M.; Kamer, P. C. J.; Reek, J. N. H.; Dierkes, P. *Chem. Rev.* **2000**, *100*, 2741–2769.

(22) Dierkes, P.; van Leeuwen, P. N. M. *J. Chem. Soc., Dalt. Trans.* **1999**, 1519–1529.

(23) Wehman-Ooyevaar, I. C. M.; Grove, D. M.; Kooijman, H.; van der Sluis, P.; Spek, A. L.; van Koten, G. *J. Am. Chem. Soc.* **1992**, *114*, 9916–9924.

(24) Ellermann, J.; Gabold, P.; Schelle, C.; Knoch, F. A.; Moll, M.; Bauer, W. *Z. Anorg. Allg. Chem.* **1995**, *621*, 1832–1843.

(25) Domańska-Babul, W.; Chojnacki, J.; Matern, E.; Pikies, J. *J. Organomet. Chem.* **2007**,

692, 3640–3648.

(26) Di Vaira, M.; Sacconi, L.; Stoppioni, P. *J. Organomet. Chem.* **1983**, *250*, 183–195.

(27) Askevold, B.; Nieto, J. T.; Tussupbayev, S.; Diefenbach, M.; Herdtweck, E.; Holthausen, M. C.; Schneider, S. *Nat. Chem.* **2011**, *3*, 532–537.

(28) Oddershede, J.; Geertsen, J.; Scuseria, G. E. *J. Phys. Chem.* **1988**, *92*, 3056–3059.

(29) Hackett, M.; Ibers, J.; Whitesides, G. *J. Am. Chem. Soc.* **1988**, *110*, 1436.

(30) Azam, K. A.; Frew, A. A.; Lloyd, B. R.; Manojlovic-Muir, L.; Muir, K. W.; Puddephatt, R. J. *Organometallics* **1985**, *4*, 1400–1406.

(31) Janka, M.; Anderson, G. K.; P., R. N. *Organometallics* **2000**, *19*, 5071–5076.

(32) Denney, M. C.; Smythe, N. A.; Cetto, K. L.; Kemp, R. A.; Goldberg, K. I. *J. Am. Chem. Soc.* **2006**, *128*, 2508–2509.

(33) Evans, D. F. *J. Chem. Soc.* **1959**, *0*, 2003–2005.

(34) Procelewska, J.; Zahl, A.; Liehr, G.; Van Eldik, R.; Smythe, N. A.; Williams, B. S.; Goldberg, K. I. *Inorg. Chem.* **2005**, *44*, 7732–7742.

(35) Thomas, J. C.; Peters, J. C. *J. Am. Chem. Soc.* **2003**, *125*, 8870–8888.

(36) Lotz, M. D.; Remy, M. S.; Lao, D. B.; Ariafard, A.; Yates, B. F.; Canty, A. J.; Mayer, J. M.; Sanford, M. S. *J. Am. Chem. Soc.* **2014**, *136*, 8237–8242.

(37) Laporte, C.; Frison, G.; Grützmacher, H.; Hillier, A. C.; Sommer, W.; Nolan, S. P. *Organometallics* **2003**, *22*, 2202–2208.

(38) Schulz, A. J.; Williams, J. M.; Koetzle, T. F.; Dawoodi, Z.; Green, M. L. H.; Prout, K.

Acta Cryst. **1984**, *A* (40), C292.

(39) Arnold, D. P.; Bennett, M. A.; McLaughlin, G. M.; Robertson, G. B. *J. Chem. Soc. Chem. Commun.* **1983**, *1983*, 34–36.

(40) Krevor, J. V. Z.; Simonis, U.; Karson, A.; Castro, C.; Aliakbar, M. *Inorg. Chem.* **1992**, *31* , 312–317.

(41) Pangborn, A. B.; Giardello, M. A.; Grubbs, R. H.; Rosen, R. K.; Timmers, F. J. *Organometallics* **1996**, *1*5, 1518–1520.

(42) Anderson, G. K.; Lin, M. *Inorg. Synth.* **1990**, *28*, 60–62.

(43) Bruker (2007) APEX2 (Version 2.1-4), SAINT (version 7.34A), SADABS (version 2007/4), B. I. Madison, Wisconsin, USA.

(44) Altomare, A.; Burla, M. c. . M. *J. Appl. Cryst.* **1999**, *32*, 115.

(45) Altomare, A.; Cascarano, G. L.; Guagliardi, A. *J. Appl. Cryst.* **1993**, *26*, 343.

(46) Sheldrick, G. M. (1997) SHELXL-97, P. for the refinement of crystal structures. University of Göttingen, Germany.

(47) Sheldrick, G. M. *Acta. Cryst.* **2015**, *A71*, 3.

(48) Waasmaier, D.; Kirfel, A. *Acta Cryst.* **1995**, *51*, 416.

(49) APEX3, 2016.1-0: Bruker-AXS. Madison, Wisconsin, USA 2016.

(50) Bruker-AXS, S. v8. 38A. Madison, Wisconsin, USA 2014.

(51) Krause, L., Herbst-Irmer, R., Sheldrick, G.M. & Stalke, D. *J. Appl. Cryst.* **2015**, *48*, 3.

(52) Sheldrick, G. . *Acta Cryst.* **2015**, *71*, 3.

Bibliography

Albrecht, M.; Koten, G. *Angew. Chemie, Int. Ed.* **2001**, *40*, 3750–3781.

Albrecht, M.; Lindner, M. M. *Dalt. Trans.* **2011**, *40*, 8733.

Almeida Leñero, K. Q.; Guari, Y.; Kamer, P. C. J.; Van Leeuwen, P. W. N. M.; Donnadieu, B.; Sabo-Etienne, S.; Chaudret, B.; Lutz, M.; Spek, A. L. *Dalt. Trans.* **2013**, *42*, 6495–6512.

Altomare, A.; Burla, M. c. . M. *J. Appl. Cryst.* **1999**, *32*, 115.

Altomare, A.; Cascarano, G. L.; Guagliardi, A. *J. Appl. Cryst.* **1993**, *26*, 343.

Anderson, G. K.; Lin, M. *Inorg. Synth.* **1990**, *28*, 60–62.

APEX3, 2016.1-0: Bruker-AXS. Madison, Wisconsin, USA 2016.

Arnold, D. P.; Bennett, M. A.; McLaughlin, G. M.; Robertson, G. B. *J. Chem. Soc. Chem. Commun.* **1983**, *1983*, 34–36.

Askevold, B.; Nieto, J. T.; Tussupbayev, S.; Diefenbach, M.; Herdtweck, E.; Holthausen, M. C.; Schneider, S. *Nat. Chem.* **2011**, *3*, 532–537.

Azam, K. A.; Frew, A. A.; Lloyd, B. R.; Manojlovic-Muir, L.; Muir, K. W.; Puddephatt, R. J. *Organometallics* **1985**, *4*, 1400–1406.

Babak, M. V.; Pfaffeneder-Kmen, M.; Meier-Menches, S. M.; Legina, M. S.; Theiner, S.; Licona, C.; Orvain, C.; Hejl, M.; Hanif, M.; Jakupec, M. A.; Keppler, B. K.; Gaiddon, C.; Hartinger, C. G. *Inorg. Chem.* **2018**, *57*, 2851–2864.

Bailey, W. D. Late Transition-Metal Complexes Supported by Pincer Ligands : Applications in Partial Oxidation Catalysis, University of Washington, 2016.

Bailey, W. D.; Luconi, L.; Rossin, A.; Yakhvarov, D.; Flowers, S. E.; Kaminsky, W.; Kemp, R. A.; Giambastiani, G.; Goldberg, K. I. *Organometallics* **2015**, *34*, 3998–4010.

Bálint, E.; Tajti, Á.; Tripolszky, A.; Keglevich, G. *Dalt. Trans.* **2018**, *47*, 4755–4778.

Basickes, N.; Hogan, T. E.; Sen, A. *J. Am. Chem. Soc.* **1996**, *118*, 13111–13112.

Ben-Ari, E.; Leitus, G.; Shimon, L. J. W.; Milstein, D. *J. Am. Chem. Soc.* **2006**, *128*, 15390–15391.

Bercaw, J. E.; Chen, G. S.; Labinger, J. A.; Lin, B. L. *Organometallics* **2010**, *29*, 4354–4359.

Bergman, R. G. *Nature* **2007**, *446*, 391–393.

Bergman, R. G. *Science* **1984**, *223*, 902–908.

Bernskoetter, W. H.; Schauer, C. K.; Goldberg, K. I.; Brookhart, M. *Science.* **2015**, *326*, 553–

556.

Bhattacharyya, P.; Sheppard, R. N.; Slawin, A. M.; Williams, D. J.; Woollins, J. D. *J. Chem. Soc. Dalt. Trans.* **1993**, No. 1, 2393–2400.

Blum, O.; Milstein, D. *J. Am. Chem. Soc.* **2002**, *124*, 11456–11467.

Boisvert, L. U. C.; Goldberg, K. I. *Acc. Chem. Res.* **2012**, *45*, 899–910.

Bowes, E. G.; Dawson Beattie, D.; Love, J. A. *Inorg. Chem.* **2019**, *58*, 2925–2929.

Boyd, G.; Burden, S.; Joffe, A. T.; Marker, D.; Sharkey, S.; Souders, S.; Tinsley, C.; Wiser, N. *Review of Well Operator Files for Hydraulically Fractured Oil and Gas Production Wells.*. Report for U.S. Envirnmental Protection Agency: Washinton, D.C., 2016.

Browning, C. S.; Farrar, D. H. *J. Chem. Soc. Dalt. Trans* **1995**, No. 4, 521.

Bruker (2007) APEX2 (Version 2.1-4), SAINT (version 7.34A), SADABS (version 2007/4), B. I. Madison, Wisconsin, USA.

Bruker-AXS, S. v8. 38A. Madison, Wisconsin, USA 2014.

Brune, H. A.; Stapp, B.; Schmidtberg, G. *J. Organomet. Chem.* **1986**, *301*, 129–137.

Camp, A. M.; Kita, M. R.; Grajeda, J.; White, P. S.; Dickie, D. A.; Miller, A. J. M. *Inorg. Chem.* **2017**, *56*, 11141–11150.

Cave, G. W. V.; Fanizzi, F. P.; Deeth, R. J.; Errington, W.; Rourke, J. P. *Organometallics* **2000**, *19*, 1355–1364.

Chinn, M. S.; Heinekey, D. M.; Payne, N. G.; Sofield, C. D. *Organometallics* **1989**, *8*, 1824–1826.

Cook, B. J.; Chen, C.-H.; Pink, M.; Caulton, K. G. *Dalt. Trans.* **2018**, *47*, 2052–2060.

Crespo, M.; Puddephatt, R. J. *Organometallics* **1987**, *6*, 2548–2550.G

Cuerva, C.; Campo, J. A.; Ovejero, P.; Torres, M. R.; Oliveira, E.; Santos, S. M.; Lodeiro, C.; Cano, M. *J. Mater. Chem. C* **2014**, *2*, 9167–9181.

Dalrymple, A. New Natural Gas Processing Plant Announced for Bakken *Bismarck Tribune*. (Online) **2018**, https://bismarcktribune.com/bakken/new-natural-gas-processing-plant-announced-for-bakken/article_d4004e1b-7b82-5d9b-9d7c-50310aa51056.html (accessed Nov 2, 2019)

Darwent, B. D. *National Standard Reference Data Series, National Bureau of Standards, vol. 42*; 1970.

Davies, D. L.; Macgregor, S. A.; McMullin, C. L. *Chem. Rev.* **2017**, *117*, 8649–8709.

Denney, M. C.; Smythe, N. A.; Cetto, K. L.; Kemp, R. A.; Goldberg, K. I. *J. Am. Chem. Soc.* **2006**, *128*, 2508–2509.

Di Vaira, M.; Sacconi, L.; Stoppioni, P. *J. Organomet. Chem.* **1983**, *250*, 183–195.

Dias, H. V. R.; Diyabalanage, H. V. K.; Eldabaja, M. G.; Elbjeirami, O.; Rawashdeh-Omary, M. A.; Omary, M. A. *J. Am. Chem. Soc.* **2005**, *127*, 7489–7501.

Dierkes, P.; van Leeuwen, P. N. M. *J. Chem. Soc., Dalt. Trans.* **1999**, 1519–1529.

Domańska-Babul, W.; Chojnacki, J.; Matern, E.; Pikies, J. *J. Organomet. Chem.* **2007**, *692*, 3640–3648.

Drilling Productivity Report. U.S. Energy Information Administration; U.S. Governement Printing Office: Washington, D.C. 2019

Eisler, D. J.; Robertson, S. D.; Chivers, T. *Can. J. Chem.* **2009**, *87*, 39–46.

Ellermann, J.; Gabold, P.; Schelle, C.; Knoch, F. A.; Moll, M.; Bauer, W. *Z. Anorg. Allg. Chem.* **1995**, *621*, 1832–1843.

Evans, D. F. *J. Chem. Soc.* **1959**, *0*, 2003–2005.

Fekl, U.; Goldberg, K. I. In *Adv. Inorg. Chem*; 2003; pp 259–320.

Felice, V. De; Renzi, A. De; Panunzi, A.; Tesauro, D. *J. Organomet. Chem.* **1995**, *488*, C13–C14.

Frank, N.; Hanau, K.; Langer, R. *Inorg. Chem.* **2014**, *53*, 11335.

Fulmer, G. R.; Miller, A. J. M.; Sherden, N. H.; Gottlieb, H. E.; Nudelman, A.; Stoltz, B. M.; Bercaw, J. E.; Goldberg, K. I. *Organometallics* **2010**, *29*, 2176–2179.

Gao, D. *J. Chem. Educ.* **2009**, *86*, 864–868.

Goldberg, K. I.; Goldman, A. S. *Acc. Chem. Res.* **2017**, *50*, 620–626.

Goldman, A. S.; Goldberg, K. I. In *Activation and Functionalization of C-H Bonds*; 2004; pp 1–43.

Gopalakrishnan, J. *Appl. Organomet. Chem.* **2009**, *23*, 291–318.

Gorelsky, S. I.; Lapointe, D.; Fagnou, K. *Chem. Lett.* **2010**, *39* (11), 1118.

Griffiths, D. C.; MacTavish, D. I.; Male, N. A. H.; Tocher, D. A.; Young, G. B. *J. Chem. Soc. - Dalt. Trans.* **1997**, *2*, 3373–3385.

Gunsalus, N. J.; Koppaka, A.; Park, S. H.; Bischof, S. M.; Hashiguchi, B. G.; Periana, R. A. *Chem. Rev.* **2017**, *117*, 8521–8573.

Hackett, M.; Ibers, J.; Whitesides, G. *J. Am. Chem. Soc.* **1988**, *110*, 1436.

Halpern, J. *Acc. Chem. Res.* **1970**, *3*, 386–392.

Heinekey, D. M.; Oldham, W. J. *Chem. Rev.* **1993**, *93*, 913–926.

Hill, G. S.; Irwin, M. J.; Levy, C. J.; Rendina, L. M.; Puddephatt, R. J. *Inorg. Synth.* **1998**, *32*, 149–151.

Hinman, J. G.; Baar, C. R.; Jennings, M. C.; Puddephatt, R. J. *Organometallics* **2000**, *19*, 563–570.

Horn, R.; Schlögl, R. *Catal. Letters* **2015**, *145*, 23–39.

Horváth, I. T.; Cook, R. A.; Millar, J. M.; Kiss, G. *Organometallics* **1993**, *12*, 8–10.

How much oil and gas are actually in the Bakken Formation? https://www.usgs.gov/faqs/how-much-oil-and-gas-are-actually-bakken-formation?qt-news_science_products=3#qt-news_science_products (accessed Oct. 25, 2019)

Jamali, S.; Rashidi, M.; Jennings, M. C.; Puddephatt, R. J. *J. Chem. Soc. Dalt. Trans.* **2003**, *3*, 2313–2317.

Janka, M.; Anderson, G. K.; P., R. N. *Organometallics* **2000**, *19*, 5071–5076.

Jenkins, H. A.; Yap, G. P. A.; Puddephatt, R. J. *Organometallics* **1997**, *16*, 1946–1955.

Johansson, L.; Tilset, M.; Labinger, J. A.; Bercaw, J. E. *J. Am. Chem. Soc.* **2000**, *122*, 10846–10855.

Juhasz, M.; Takahashi, S.; Arulmozhiraja, S.; Fujii, T. *J. Struct. Chem.* **2012**, *53*, 443–448.

Kaljurand, I.; Kütt, A.; Sooväli, L.; Rodima, T.; Mäemets, V.; Leito, I.; Koppel, I. A. *J. Org. Chem.* **2005**, *70*, 1019–1028.

Kégl, T. R.; Pálinkás, N.; Kollár, L.; Kégl, T. *Molecules* **2018**, *23*, 1–11.

Khusnutdinova, J. R.; Milstein, D. *Angew. Chem. Int. Ed.* **2015**, *54*, 12236.

Konnick, M. M.; Stahl, S. S. *J. Am. Chem. Soc.* **2008**, *130*, 5753–5762.

Krause, L., Herbst-Irmer, R., Sheldrick, G.M. & Stalke, D. *J. Appl. Cryst.* **2015**, *48*, 3.

Kreutz, J. E.; Shukhaev, A.; Du, W.; Druskin, S.; Daugulis, O.; Ismagilov, R. F. *J. Am. Chem. Soc.* **2010**, *132*, 3128–3132.

Krevor, J. V. Z.; Simonis, U.; Karson, A.; Castro, C.; Aliakbar, M. *Inorg. Chem.* **1992**, *31* , 312–317.

Kua, J.; Xu, X.; Periana, R. A.; Goddard, W. A. *Organometallics* **2002**, *21*, 511–525.

Kubas, G. J. *Proc. Natl. Acad. Sci.* **2007**, *104*, 6901–6907.

Labinger, J. A. In *Alkane C-H Activation by Single-Site Metal Catalysis,*; 2012; pp 17–71.

Labinger, J. A. *Organometallics* **2015**, *34*, 4784–4795.

Labinger, J. A.; Bercaw, J. E. *Nature* **2002**, *417*, 507–514.

Lapointe, D.; Fagnou, K. *Chem. Lett.* **2010**, *39*, 1118

Laporte, C.; Frison, G.; Grützmacher, H.; Hillier, A. C.; Sommer, W.; Nolan, S. P. *Organometallics* **2003**, *22*, 2202–2208.

Lee, D. H.; Patel, B. P.; Clot, E.; Eisenstein, O.; Crabtree, R. H. *Chem. Commun.* **1999**, 3, 297–298.

Lee, W. C.; Sears, J. M.; Enow, R. A.; Eads, K.; Krogstad, D. A.; Frost, B. J. *Inorg. Chem.* **2013**, *52*, 1737–1746.

Lei, A.; Shi, W.; Liu, C.; Zhang, H.; He, C. In *Oxidative Cross-Coupling Reactions*; 2016; pp 49–53.

Lersch, M.; Tilset, M. *Chem. Rev.* **2005**, *105*, 2471–2526.

Liao, C. T.; Chen, H. H.; Hsu, H. F.; Poloek, A.; Yeh, H. H.; Chi, Y.; Wang, K. W.; Lai, C. H.; Lee, G. H.; Shih, C. W.; Chou, P. T. *Chem. - A Eur. J.* **2011**, *17*, 546–556.

Ligands, N.; Rendina, L. M.; Puddephatt, R. J. *Chem. Rev.* **1997**, *97*, 1735–1754.

Lin, M.; Shen, C.; Garcia-zayas, E. A.; Park, U. V; Pennsyl, V.; June, R. V. *J. Am. Chem. Soc.* **2001**, *6*, 1000–1001.

Look, J. L.; Wick, D. D.; Mayer, J. M.; Goldberg, K. I. *Inorg. Chem.* **2009**, *48*, 1356–1369.

Lotz, M. D.; Remy, M. S.; Lao, D. B.; Ariafard, A.; Yates, B. F.; Canty, A. J.; Mayer, J. M.; Sanford, M. S. *J. Am. Chem. Soc.* **2014**, *136*, 8237–8242.

Luedtke, A. T.; Goldberg, K. I. *Inorg. Chem.* **2007**, *46*, 8496–8498.

Luinstra, G. A.; Wang, L.; Stahl, S. S.; Labinger, J. A.; Bercaw, J. E. *J. Organomet. Chem.* **1995**, *504*, 75–91.

MacPherson, J. North Dakota Oil Producers are Wasting Billions of Cubic Feet of Natural Gas. *L.A. Times*. [Online] **2019**, https://www.latimes.com/business/la-fi-north-dakota-natural-gas-flaring-carbon-emissions-20190527-story.html (accessed Oct. 23, 2019).

Madison, B. L.; Thyme, S. B.; Keene, S.; Williams, B. S. *J. Am. Chem. Soc.* **2007**, *129*, 9538–9539.

Mallat, T.; Baiker, A. *Catal. Today* **1994**, *19*, 247–283.

Minghetti, G.; Stoccoro, S.; Cinellu, M. A.; Soro, B.; Zucca, A. *Organometallics* **2003**, *22*, 4770–4777.

Monthly Crude Oil and Natural Gas Production. https://www.eia.gov/petroleum/production/ (accessed Nov 5, 2019)

Moret, M.; Chen, P. *Organometallics* **2008**, *27*, 4903–4916.

NATRUAL GAS INFRASTRUCTURE, Appendix,B: Natural Gas; U.S. Department of Energy, U.S. Government Printing Office: Washington, D.C. 2017.

Natural Gas Monthly; U.S. Energy Information Administration, U.S. Governement Printing Office: Washington, D.C.; 2019.

Negishi, E.; Takahashi, T.; Akiyoshi, K. *J. Organomet. Chem.* **1987**, *334*, 181–194.

Nilsson, P.; Plamper, F.; Wendt, O. F. *Organometallics* **2003**, *22*, 5235–5242.

Niroomand Hosseini, F.; Nabavizadeh, S. M.; Abu-Omar, M. M. *Inorg. Chem.* **2017**, *56*, 14706–14713.

Noyori, R. *Angew. Chem. Int. Ed.* **2002**, *41*, 2008.

Noyori, R.; Ohkuma, T.; Kitamura, M.; Takaya, H.; Sayo, N.; Kumobayashi, H.; Akutagawa, S. *J. Am. Chem. Soc.* **1987**, *109*, 5856–5858.

O'Reilly, S. A.; White, P. S.; Templeton, J. L. *J. Am. Chem. Soc.* **1996**, *118*, 5684–5689.

Oddershede, J.; Geertsen, J.; Scuseria, G. E. *J. Phys. Chem.* **1988**, *92*, 3056–3059.

Oil and Natural Gas Sector Hydraulically Fractured Oil Well Completions and Associated Gas during Ongoing Production; U.S. EPA Office of Air Quality Planning and Standards 2014.

Oil Fields from Space at Night, https://geology.com/articles/oil-fields-from-space/(accessed Oct. 23, 2019).

oldberg, K. I.; Yan, J.; Breitung, E. M. *J. Am. Chem. Soc.* **1995**, *117*, 6889–6896.

Pangborn, A. B.; Giardello, M. A.; Grubbs, R. H.; Rosen, R. K.; Timmers, F. J. *Organometallics* **1996**, *15*, 1518–1520.

Parkins, B. A. W. *Platin. Met. Rev.* **1996**, *40*, 169–174.

Periana, R. A.; Taube, D. J.; Evitt, E. R.; Löffler, D. G.; Wentrcek, P. R.; Voss, G.; Masuda, T. *Science* **1993**, *259*, 340–343.

Polezhaev, A. V; Chen, C.-H.; Losovyj, Y.; Caulton, K. G. *Chem. - A Eur. J.* **2017**, *23* , 8039–8050.

Poverenov, E.; Gandelman, M.; Shimon, L. J. W.; Rozenberg, H.; Ben-David, Y.; Milstein, D. *Organometallics* **2005**, *24*, 1082–1090.

Poverenov, E.; Leitus, G.; Milstein, D. *J. Am. Chem. Soc.* **2006**, *128*, 16450–16451.

Prantner, J. D.; Kaminsky, W.; Goldberg, K. I. *Organometallics* **2014**, *33*, 3227–3230.

Procelewska, J.; Zahl, A.; Liehr, G.; Van Eldik, R.; Smythe, N. A.; Williams, B. S.; Goldberg, K. I. *Inorg. Chem.* **2005**, *44*, 7732–7742.

Prokopchuk, E. M.; Jenkins, H. A.; Puddephatt, R. J. *Organometallics* **1999**, *18*, 2861–2866.

Ritch, J. S.; Chivers, T.; Eisler, D. J.; Tuononen, H. M. *Chem. Eur. J.* **2007**, *13*, 4643–4653.

Rodríguez Vallejo, D. F.; De Klerk, A. *Energy and Fuels* **2013**, *27*, 3137–3147.

Rong, M. K.; Holtrop, F.; Slootweg, J. C.; Lammertsma, K. *Coord. Chem. Rev.* **2019**, *382*, 57–68.

Ruiz-Castillo, P.; Buchwald, S. L. *Chem. Rev.* **2016**, *116*, 12564–12649.

Ruscic, B. *J. Phys. Chem. A* **2015**, *119*, 7810–7837.

Scheuermann, M. L.; Goldberg, K. I. *Chem. - A Eur. J.* **2014**, *20*, 14556–14568.

Scheuermann, M.; Grice, K.; Ruppel, M.; Roselló-merino, M.; Kaminsky, W.; Goldberg, K. I. *Dalton Trans.* **2014**, No. 31, 12018–12025.

Schulz, A. J.; Williams, J. M.; Koetzle, T. F.; Dawoodi, Z.; Green, M. L. H.; Prout, K. *Acta Cryst.* **1984**, *A* (40), C292.

Schwartsburd, L.; Iron, M. A.; Konstantinovski, L.; Ben-ari, E.; Milstein, D. *Organometalics* **2011**, *30*, 2721–2729.

Scott, J. D.; Puddephatt, R. J. *Organometallics* **1986**, *5*, 2522–2529.

Shan, J.; Li, M.; Allard, L. F.; Lee, S.; Flytzani-Stephanopoulos, M. *Nature* **2017**, *551*, 605–608.

Sheldrick, G. . *Acta Cryst.* **2015**, *71*, 3.

Sheldrick, G. M. (1997) SHELXL-97, P. for the refinement of crystal structures. University of Göttingen, Germany.

Sheldrick, G. M. *Acta. Cryst.* **2015**, *A71*, 3.

Shilov, A. E.; Shul, G. B. *Chem. Rev.* **1997**, *2665*, 2879–2932.

Short-Term Energy Outlook (STEO); U.S. Energy Information Administration; U.S. Governement Printing Office: Washington, D.C.; 2018.

Simoes, J. A. M.; Beauchamp, J. L. *Chem. Rev.* **1990**, *90*, 629–688.

Singh, K.; Long, J. R.; Stavropoulos, P. *Inorg. Chem.* **1998**, *37*, 1073.

Souillart, L.; Cramer, N. *Chem. Rev.* **2015**, *115*, 9410–9464.

Stoessel, P.; Joosten, D.; Breuning, E.; Yersin, H.; Monkowius, U. Organic electroluminescent devices employing multinuclear metal complexes and their production using organic vapor

deposition and selected platinum-containing complexes and their preparation, 2010.

Sutcliffe, V. F.; Young, G. B. *Polyhedron* **1984**, *3*, 87–94.

Tang, P.; Zhu, Q.; Wu, Z.; Ma, D. *Energy Environ. Sci.* **2014**, *7*, 2580–2591.

Tao, J.; Sun, F.; Fang, T. *J. Organomet. Chem.* **2012**, *698*, 1–6.

Thomas, J. C.; Peters, J. C. *J. Am. Chem. Soc.* **2003**, *125*, 8870–8888.

Toda, T.; Kuwata, S.; Ikariya, T. *Chem. - A Eur. J.* **2014**, *20*, 9539–9542.

Toda, T.; Saitoh, K.; Yoshinari, A.; Ikariya, T.; Kuwata, S. *Organometallics* **2017**, *36*, 1188–1195.

Tolman, C. A. *Chem. Rev.* **1977**, *77*, 313–348.

United States Natural Gas Industrial Price, https://www.eia.gov/dnav/ng/hist/n3035us3m.htm. (accessed Nov. 1, 2019)

Van Leeuwen, P. W. N. M.; Kamer, P. C. J.; Reek, J. N. H.; Dierkes, P. *Chem. Rev.* **2000**, *100*, 2741–2769.

Vedernikov, A. N.; Binfield, S. A.; Zavalij, P. Y.; Khusnutdinova, J. R. *J. Am. Chem. Soc.* **2006**, *128*, 82–83.

Vedernikov, A. N.; Pink, M.; Caulton, K. G. *Inorg. Chem.* **2004**, *43*, 3642–3646.

Veenboer, R. M. P.; Collado, A.; Dupuy, S.; Lebl, T.; Falivene, L.; Cordes, D. B.; Slawin, A. M. Z.; Cazin, C. S. J.; Nolan, S. P. *Organometallics* **2017**, *36*, 2861–2869.

Vela, J.; Vaddadi, S.; Kingsley, S.; Flaschenriem, C. J.; Lachicotte, R. J.; Cundari, T. R.; Holland, P. L. *Angew. Chem. Int. Ed.* **2006**, *45*, 1607–1611.

Waasmaier, D.; Kirfel, A. *Acta Cryst.* **1995**, *51*, 416.

Wang, Y.; Zheng, B.; Pan, Y.; Pan, C.; He, L.; Huang, K.-W. *Dalt. Trans.* **2015**, *44*, 15111–15115.

Wehman-Ooyevaar, I. C. M.; Grove, D. M.; Kooijman, H.; van der Sluis, P.; Spek, A. L.; van Koten, G. *J. Am. Chem. Soc.* **1992**, *114*, 9916–9924.

Weinberg, D. R.; Labinger, J. A.; Bercaw, J. E. *Organometallics* **2007**, *26*, 167–172.

Weissermel, K.; Arpe, H.-J. *Industrial Organic Chemistry*, 4th ed.; Wiley-VCH: Weinheim; 2003.

Wick, D. D.; Goldberg, K. I. *J. Am. Chem. Soc.* **1997**, 119, 10235–10236.

Wik, B. J.; Lersch, M.; Tilset, M. *J. Am. Chem. Soc.* **2002**, *124*, 12116–12117.

Williams, B. S.; Goldberg, K. I. *J. Am. Chem. Soc.* **2001**, *123*, 2576–2587.

Williams, B. S.; Holland, A. W.; Goldberg, K. I. *J. Am. Chem. Soc.* **1999**, *121*, 252–253.

Xie, J.; Jin, R.; Li, A.; Bi, Y.; Ruan, Q.; Deng, Y.; Zhang, Y.; Yao, S.; Sankar, G.; Ma, D.; Tang, J. *Nat. Catal.* **2018**, *1*, 889–896.

Xing, X.; Xu, C.; Chen, B.; Li, C.; Virgil, S. C.; Grubbs, R. H. *J. Am. Chem. Soc.* **2018**, *140*, 17782–17789.

You, Z. L.; Jiao, Q. Z.; Niu, S. Y.; Chi, J. Y. *Z. Anorg. Allg. Chem.* **2006**, *632*, 2486–2490.

Yu, W. S.; Cheng, C. C.; Cheng, Y. M.; Wu, P. C.; Song, Y. H.; Chi, Y.; Chou, P. T. *J. Am. Chem. Soc.* **2003**, *125*, 10800–10801.

Zeitler, H. E.; Kaminsky, W. A.; Goldberg, K. I. *Organometallics* **2018**, *37*, 3644–3648.

Zeng, M.; Li, L.; Herzon, S. B. *J. Am. Chem. Soc.* **2014**, *136*, 7058–7067.

Vita

Braden A. Zahora was born in 1992 to parents Andy and Ingrid Zahora. He grew up in Charlotte, NC where he graduated high school from Hickory Ridge High School in 2010. He attended the University of North Carolina in Chapel Hill, NC, where he graduated with a Bachelor of Science degree in chemistry in 2014. While at UNC-CH, Braden worked in the research laboratory of Prof. Jillian L. Dempsey on synthesizing a library of quinoline bases for future proton coupled electron transfer reactions. Braden then attended graduate school at the University of Washington in Seattle, WA. There, he worked with Prof. Karen I. Goldberg on synthesizing platinum complexes for C-H activation reactions. He obtained a Doctor of Philosophy degree in inorganic chemistry in 2019.